PHD

Investigating the role of endothelin signalling system in the establishment of adult pigment progenitors in zebrafish development.

Camargo Sosa, Karen

Award date:
2019

Awarding institution:
University of Bath

Investigating the role of endothelin signalling system in the establishment of adult pigment progenitors in zebrafish development.

Karen Camargo Sosa

A thesis submitted for the degree of Doctor of Philosophy

University of Bath
Department of Biology and Biochemistry
September 2018

Declaration of authorship I am the author of this thesis, and the work described therein was carried out by myself personally, with the exception of Chapter 3 where 37.5% of the figures contains data generated by other researchers.

Candidate's signature.....

This thesis may be made available for consultation within the University Library and may be photocopied or lent to other libraries for the purposes of consultation with effect from.....

Signed on behalf of the Faculty of Science of.....

A mamá y Pam por supuesto

AKNOWLEDGMENTS

Academic

I would like to thank Prof. Robert Kelsh for accepting me in his research group, he has always been supportive and a good mentor. I am sincerely grateful for the time invested guiding me throughout the project but also for his career advice. His has been a role model of the kind of supervisor I aspired to become: patient and always willing to encourage people to keep moving forward.

Special thanks to my examiners Prof. David Tosh and Dr. Corinne Houart for their input during my *viva* and suggestions to improve this thesis.

My sincere gratitude to Prof. Christiane Nüsslein-Volhard for the opportunity to work in her lab group at the Max-Plank Institute for Developmental Biology in Tübingen, Germany and for providing the zebrafish CRISPR mutants. To Gurpreet, Anastasia and April for their support and help during my time in Tübingen.

A very special thanks to all my colleagues in the zebramouse lab (Ruqaiya, Jennifer, Deeya, Brigite, Kleio, Yusuke, Tatiana, Kim, Sasi and Valentina) that were always willing to help and that made this journey a great experience. A special thanks to Marc Sheddon for his dedicated work in fish facility. Finally, to Anne Gesell for her dedicated assistance in the microscopy and analysis suite.

I am grateful with the Mexican Council for Science and Technology (CONACyT) for sponsoring my PhD.

Personal

Apologies for the change of language.

No encuentro la elocuencia para expresar lo afortunada que soy de ser tu hija y lo agradecida que estoy por los 28 años de tu vida dedicados a darme tu amor. Mami, encuentra en estas páginas un pedacito de lo que me has ayudado a construir y ten la seguridad de que cada día lejos de ti fue aprovechado no sólo para terminar esta tesis sino para hacer lo que siempre me has pedido que haga, vivir y disfrutar.

Mi Pame, gracias por no dejar de sorprenderme con tu inmensa bondad, pero particularmente por la fortaleza que me transmitiste en los últimos años. Saberte incondicional, cariñosa y paciente me llenó de calma en los tiempos brumosos. También valoro tu ánimo por celebrar mis alegrías y procurarme a la distancia a través de tus detalles. Hermana, gracias.

Al resto de mi familia por recibirme con emoción en cada regreso a mi país.

Gracias a Claudia y Andrés por todo el apoyo, por convertirse en mi familia en Bath, pero particularmente por los muchos buenos momentos.

Gracias a mi amiga Ruqaiya, que a pesar de la extrema diferencia de nuestros orígenes siempre escuchó mis inquietudes y me confió sus rebeldías. Jennifer, gracias por tu entendimiento y por siempre motivarme a ser más valiente, ere un ejemplo de bondad. Muchas gracias a Hannah por la mucha paciencia que me tuvo y su extrema positividad. A Deeya y Ravi por su amistad y confianza.

Rodri, gracias por no fallar en ningún sentido y por siempre ser una inspiración. Especial gratitud a mis amigos Xime y Paco cuyo cariño se manifiesta en la honestidad de sus palabras, en la incondicionalidad de su apoyo sin importar distancia ni tiempo. A Marco gracias por escuchar.

Y finalmente gracias a, Tom Beale, porque nos encontramos justo a tiempo (of course we did). Porque cuando te hablo Amor, la ideas en mi mente encuentran con facilidad un camino claro hacia ti.

ABBREVIATIONS

4-OHT Tetrahydrozytamoxifen
APSC Adult Pigmetn Stem Cells
a.a. Amino acid(s)
BLAST Basic Local Alignment Search Tool
BMP Bone Morphogenetic Protein
bp Base pairs
Cas9 CRISPR associated protein 9dct Dopachrome tautomerase
cDNA Complementary DNA
CRISPR Clustered regularly interspaced short palindromic repeats
DIC Differential interference contrast
DMSO Dimethyl sulfoxide
DNA Deoxyribonucleic acid
DNase Deoxyribonuclease
dNTP Deoxynucleotide Triphosphate
dpf Days post fertilisation
ece endothelin converting enzyme
edn endothelin
ednr endothelin receptor
EDTA Ethylenediaminetetra-acetic acid
ENU N-ethyl-n-nitrosourea
EpiSCs Epiblast stem cells
ESCs Embryonic stem cells
EtOH Ethanol
FACS Fluorescence activated cell sorting
FSC Fordwars Scatter
gch GTP cyclohydrolase
gRNA Guide RNA
HDR Homology-directed repair
hpf Hours post fertilisation
HSC Haematopoietic stem cell
I/M Iridoblast/melanoblast
iPSC Induces pluripotent stem cell
ISC Intestine Stem cell
KOH Potassium hydroxide
LiCl Lithium chloride
LP Lateral patches

1 ltk Leucocyte tyrosine kinase
2 MeOH Methanol
3 $MgCl_2$ Magnesium chloride
4 $MgSO_4$ Magnesium sulfate
5 MI Melanoiridoblast
6 mitf(a) Microphthalmia-associated transcription factor (a)
7 MO Morphant or morpholino
8 MXIG Melano-xantho-irido-glioblast
9 NaCl Sodium Chloride
10 NaOH Sodium hydroxide
11 Nc Notochord
12 NC(C) Neural crest (cell)
13 NCBI National Center for Biotechnology Information
14 NCSCs Neural crest stem cells
15 NHEJ Non-homologous end-joining
16 NPB Neural plate border
17 NT Neural tube
18 NTP Nucleoside triphosphate
19 PAM Photospacer adjacent motif
20 PBS (T) Phosphate buffered saline (containing Tween20)
21 PCR Polymerase chain reaction
22 *pde* parade
23 PTU 1-phenyl-2-thiourea
24 RNase Ribonuclease
25 RPE Retinal pigment epithelium
26 rpm Revolutions per minute
27 RT Reverse transcriptase
28 RTK Receptor tyrosine kinase
29 SNP Single nucleotide polymorphism
30 sox SRY (Sex Determining Region Y)-related HMG box
31 SSC Side Scatter
32 tfec Transcription factor EC
33 tyr Tyrosinase
34 WT Wild-type
35 xdh Xanthine dehydrogenase
36 xod Xanthine oxidase
37 ZFIN Zebrafish Information Network

ABSTRACT

In this work, we present the characterisation of *parade* mutants, which disrupt activity of the Endothelin receptor Aa (EdnrAa), and which exhibit ectopic melanophores and iridophores in the medial trunk, ventral to the dorsal aorta (DA).

Our first studies were based upon the hypothesis of disruption of embryonic pigment development. Using a transgenic line *(sox10:cre/hsp70:lox:dsRed:lox-LYN-GFP*) that labels neural crest (NC)-derived cells, we showed that cell migration is not disrupted. Furthermore, quantification of other NC-derivatives (sensory, sympathetic, nor enteric neurons) revealed similar numbers in WT and *ednraa* mutant siblings, arguing against transdifferentiation to pigment cells. Instead, by immunodetection of Phospho-Histone-H3, we detected proliferation of NC-derived cells restricted to the vicinity of the DA of *ednraa* mutants.

Previously, a small molecule screen of 1396 compounds performed by a former PhD student of the lab showed that an inhibitor of Erb signalling, which is crucial for setting aside adult pigment stem cells (APSCs) in the embryo, rescued the *ednraa* mutant phenotype. Here we further investigate the requirement for Erb signalling in the *ednraa* phenotype. Strikingly, we have demonstrated that Erb signalling is required for the formation of ectopic pigment cells in *ednraa* mutant embryos in the same time-window in which APSCs are set aside. This strongly implicates APSCs as the source of the ectopic pigment cells. Based on these results, we proposed that a novel population of APSCs exists in association with medial blood vessels, and that their quiescence is dependent upon Endothelin-dependent factors expressed by the blood vessels.

In order to identify what other components of the Endothelin signalling pathway contribute to Ednraa's function in the *pde* phenotype, in collaboration with the Nuesslein-Volhard lab we generated null mutants for some of the endothelin system genes (*edn1*, *edn2a edn3a*, *edn3b*, *ednraa, ednrab* and *ece1*) using CRISPR/Cas9 targeted mutagenesis. Our analysis of the pigment phenotype of these mutants identified that *edn1* and *edn2a* have redundant roles in embryonic iridophore development as single mutants of these genes display a strong reduction of iridophores in the dorsal and ventral stripes, while only *edn2a* mutants lack iridophores in the lateral patches. We also confirmed the previously reported phenotype of *edn1* and *edn2a* mutants affecting the formation of ventral craniofacial

cartilages. Furthermore, we determined that no single ligand mutant (*edn1*, *edn2a*, *edn3a* and *edn3b*) phenocopies the *ednraa* mutant, suggesting that more than one ligand is necessary for APSC development. Unexpectedly, we found that double mutants of *ednraa*; *ednrab* rescued the *ednraa* single mutant phenotype (no ectopic pigment cells), suggesting that *ednrab* has a role on APSC biology.

To further test our model, we investigated whether formation of ectopic chromatophores shares other molecular traits with APSC development. Formation of APSCs does not require activity of *mitfa;* similarly, we determined that formation of ectopic cells in *ednraa* mutants does not require the early activity of this gene, supporting our hypothesis that ectopic pigment cells in *ednraa* mutant are derived from a source different to embryonic pigment cells. Secondly, we began to test whether signalling pathways known to regulate stem cells in other models are required in the formation of ectopic pigment cells in *ednraa* mutants. For instance, we showed that the *ednraa* mutant phenotype depends upon Wnt signalling and can be phenocopied by chemical inhibition of Notch signalling.

Our revised model proposes that APSC associated with a niche consisting of the ventral spinal nerve projections, is regulated (indirectly) through *ednraa* signalling from the dorsal aorta. Thus, we have found in the *ednraa* mutant an exciting opportunity for *in vivo* study of adult pigment stem cell biology.

CHAPTER 1

CHAPTER 1 Introduction

As part of the homeostasis of the adult body in humans and many other organisms, the cells of many organs are naturally replaced in a balanced process that involves death of old cells and generation of new ones. We now know that cell renewal is possible because of organ/tissue specific reservoirs of cells known as stem cells, whose natural function is to supply new cells throughout the life span of an organism. For instance, the cells in the inner layer of the gastric tract, all of the cell types that compose the blood, the cells in the skin and even some neurons in the brain, are replaced by cells derived from adult stem cells (Moore & Lemischka 2006).

Stem cells are generally considered as undifferentiated cells with the capacity to generate differentiated cell from one or multiple cell types. The main characteristic of stem cells is their self-renewal capacity, which means that when dividing, at least one of the daughter cells remains undifferentiated. Therefore, there is a constant supply of stem cells. Adult stem cells originate during embryonic development but are kept quiescent - state of a cell in which it does not divide but retains the capacity to re-enter cell division (Coller 2011) - until they are required to supply new cells during adulthood, hence their name. Stem cells are regulated by the environment, the niche, in which they are located. This environment is comprised of molecular signals derived from adjacent cells that control cycles of quiescence and activation of stem cells, in order to produce cell progenitors that proliferate and differentiate into specific cell lineages that depend on the nature of the stem cell (Morrison et al. 1997).

Within the body, stem cells have been identified in many tissues. For instance, in the bone marrow two types of adult stem cells are found, hematopoietic stem cells (HSC) that produce all of the cell types of the lymphoid and myeloid lineages (Dzierzak & Speck 2008), and mesenchymal stem cells (MSC), that produce, chondrocytes, adipocytes and osteocytes (Phinney & Prockop 2007). Intestinal stem cells (ISC), for instance, renew the entire inner lining of the small intestine, that contains absorptive enterocytes, enteroendocrine cells, goblet cells and Paneth cells (Vries et al. 2010). More recently, it was shown that neural stem cells (NSC) in the subventricular zone, dentate gyrus and hippocampus generate new neurons in the adult mammalian brain (Bond et al. 2015). Another example is the skin epidermis, which is comprised of keratinocyte, Langerhans cell, and melanocytes that are replaced with cells derived from multiple niches of stem cells. Keratinocytes for instance, are replaced with cells from a niche of keratinocyte stem cells (KSC) located in the interfollicular epidermis,

while melanocytes derive from a population of melanocyte stem cells (McSC) located in a specific region of the hair follicle known as the bulge (Metral et al. 2018).

Impaired regulation of stem cells can lead to development of pathologies such as cancer, in which the generation of non-functional new cells is exacerbated, leading to the potential invasion of other organs in the body, breaking its homeostasis and becoming lethal (Reya et al. 2001). In many cancer types, such as colorectal cancer, leukaemia, and melanoma, stem cells-like cells have been found to be the cellular origin of the tumours (Lytle et al. 2018).

The study of stem cells is fascinating because of their highly fined-tuned regulation that is vital for normal organ/tissue homeostasis but also because their understanding opens up opportunities for the design of targeted therapies in a pathological context.

In this work, we used the zebrafish *Danio rerio* as a model for the study of pigment development. In particular, the results of the characterisation of a mutant fish called *parade*, lead us to propose a model in which a new niche of adult pigment stem cells (APSC) is located in the ventral medial pathway of the posterior trunk of the fish and that is regulated by signals emanating from the medial blood vessels and which are regulated by EndrA signalling in the blood vessels.

In the following sections, we will first introduce zebrafish as a model for the study of pigment cell development and pigment patterning, followed by the current understanding of adult pigment stem cells in zebrafish. We will also review the specificities of stem cell characteristics and their regulation within different niches.

1.1 Zebrafish as model organism.

Zebrafish (*Danio rerio*) (Fig. 1.1) is a small freshwater fish that reaches about 3 cm of length. Both females and males reach maturity at about 3-months old and are phenotypically distinguishable, females are larger and males more slender and more yellow in colouration. Fertilization of eggs is external (200 eggs approximately per clutch), which allows immediate access to embryos. Embryonic development (Fig. 1.1 A) occurs within 3 days at an incubation temperature of 28 ºC (Kimmel et al. 1995), but can be slowed or accelerated by incubating the embryos at 21ºC or 33ºC correspondingly. Fish are considered larvae (Fig. 1.1 B) from 3-21 days post fertilization (dpf) after which they undergo a process of metamorphosis (Fig. 1.1 C).

(Mcmenamin & Parichy 2017) p. 12 defined that Metamorphpsis in Teleosts, that metamorphosis is considered to be

"*an irreversible developmental and physiological change that affects multiple traits during post-embryonic development and is brought about by one or more systematically acting endocrine mediators, but is independent of sexual maturation, sex-specific modifications, or senescence. May occur multiple times throughout during a life cycle, and may be simultaneous with puberty. The most common type of metamorphosis is larval metamorphosis during which time a teleost transform from larva to juvenile*"

In zebrafish, metamorphosis occurs when the fish starts acquiring adult features, in which several tissue continue their development such as development of the fins, skin, skeleton the gut, kidneys, gonads and the peripheral and central nervous systems, however, sexual maturity is not paired with it (Parichy et al. 2009). The most obvious change at the onset of metamorphosis is the start of the formation of the adult pigment pattern, in which new pigment cells appear in both flanks of the fish.

It is considered a zebrafish adult, when the fish start producing gametes and secondary sexual characteristics (Fig. 1.1 D) (Webb, JF., 1999).

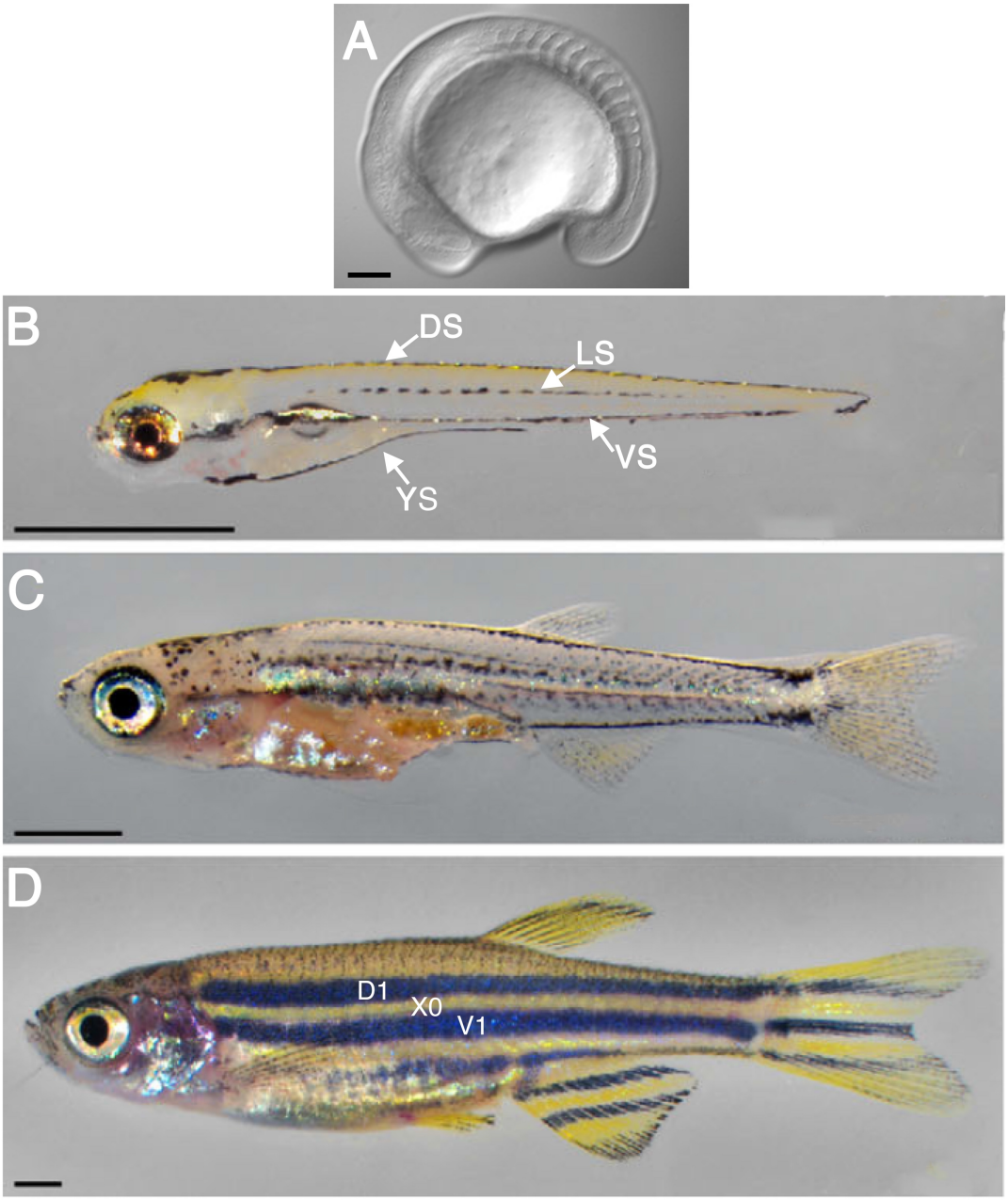

Figure 1.1 *Danio rerio*: The zebrafish. Live imaging of 16 hpf embryo (A), 5 dpf larvae (B), 3 weeks old metamorphic larvae (C) and adult zebrafish(D). Dorsal stripe (DS), lateral stripe (LS), ventral stripe (VS) and yolk sac stripe (YSS) on A and Interstripe (X) on D. Scale bar A= 100 μM, B-D = 1mm. Modified from Parichy, 2016.

1.1.1 Tools for genetic manipulation of zebrafish.

Zebrafish have 25 chromosomes and are diploid, which facilitates genetic analysis (Wixon 2000). Annotation of the *D. rerio* genome identified more than 26,206 protein-coding genes, and approximately 70% of the human genes have at least one orthologue in zebrafish (Howe et al. 2013). Generation of mutants was originally achieved through large-scale chemical mutagenesis with ethylnitrosourea (ENU), a mutagen that induces single base *indel* mutations, followed by the screening of developmental defects (Ransom et al. 1996; Driever et al. 1996). The immediate access to fertilised embryos allows the injection of expression systems based on DNA or RNA and the use of expression vector such as BACs (Krauss et al. 1993; Linney et al. 1999; Yan et al. 1998), directly to into 1-cell stage embryos. Another approach is the transient knock-down of gene function by using morpholino antisense oligonucleotides (Lacroix et al. 2000), or the insertion of transgenes through the injection of Tol2 transposable elements (Linney et al. 1999). For many years, the use of TALEN-mediated targeted gene disruption allowed the generations of *indel* mutations, deletion of large genomic regions, and precise genome modification by homologous recombination (Kühn et al. 2016). More recently the use of the CRISPR/Cas9 targeted mutagenesis system has allowed a faster method for the generation of loss of function (and other) mutants (Ota et al. 2014).

1.2 The study of pigment pattern development.

Almost all animal species display pigmented bodies. Some pigmentation can be as simple as that of an evenly single coloured black cat or display complex multicoloured patterns such as the complex patterns seen in fish. In both cases, colour is given by specialised cells that contain pigments or other material that reflect light in different wave length, these cells are known as chromatophores. The type, number and arrangement of chromatophores generates the wide range of pigment patterns seen in nature. Some of the biological functions of pigmentation include protection of vital organs from sunlight radiation (Brenner & Hearing 2008) and as a communication tool for species recognition, mating and camouflage. In vertebrates, pigment cells, in particular melanocytes, contribute to the process of wound healing (Snell 1963).

Pigment patterning has been used as a model for understanding of the mechanisms behind pattern formation. Patterns are not only found in animals, but all across nature

such as in plants, the formation of snow-flakes or even patterns in social interactions. In all of these example, self-aggregation of the elements that comprise each system result in the formation of a pattern. In a biological context, in addition to pigmentation, patterns are found in the arrangement of cells within tissues and organs, for instance, the pattern of the hexagonal plates of hepatocytes found in the lobules of the liver, the patterning of the autopod in the vertebrate limb or the expression patterns of many genes in development. One of the advantages of studying pigment patterns is that chromatophores are not vital, thus either chemical or molecular ablation of them is not lethal to the organism, allowing the study of patterning in the absence of one or more pigment cells.

Furthermore, in vertebrates, most pigment cells (i.e. not including melanocytes of the pigmented retinal epithelium) derive from the neural crest, an embryonic transitory multipotent population of cells from which a wide range of cell types derive, including pigment cells, several types of neurons and glia, and skeletogenic cell types (Kelsh et al. 2009). Thus, neural crest development and pigment cell development have been used as a model for the study of cell fate choice decision, specification and differentiation.

1.2.1 Zebrafish as a model for the study of pigment pattern development.

In amniotes, pigmentation of feather, hair and skin, is result of keratinocytes that are “coloured” with melanin provided by melanocytes, whereas in teleosts, including zebrafish, pigmentation is due to the presence of different types of chromatophores (Bagnara & Matsumoto 2006). Zebrafish displays two pigment patterns, and embryonic/early larval pattern (Fig. 1.1 A). and the adult zebra-like striped pattern (Fig. 1.1 B). Both patterns are formed by the arrangement of three pigment cells types (Figures 1.2). 1) black melanophores (the homologue of the melanocyte in amniotes), 2) iridescent iridophores and 3) yellow xanthophores. One of the advantages of using zebrafish is that embryos and larvae are transparent, thus the natural colour of pigment cells allows their easy identification, quantification and tracking.

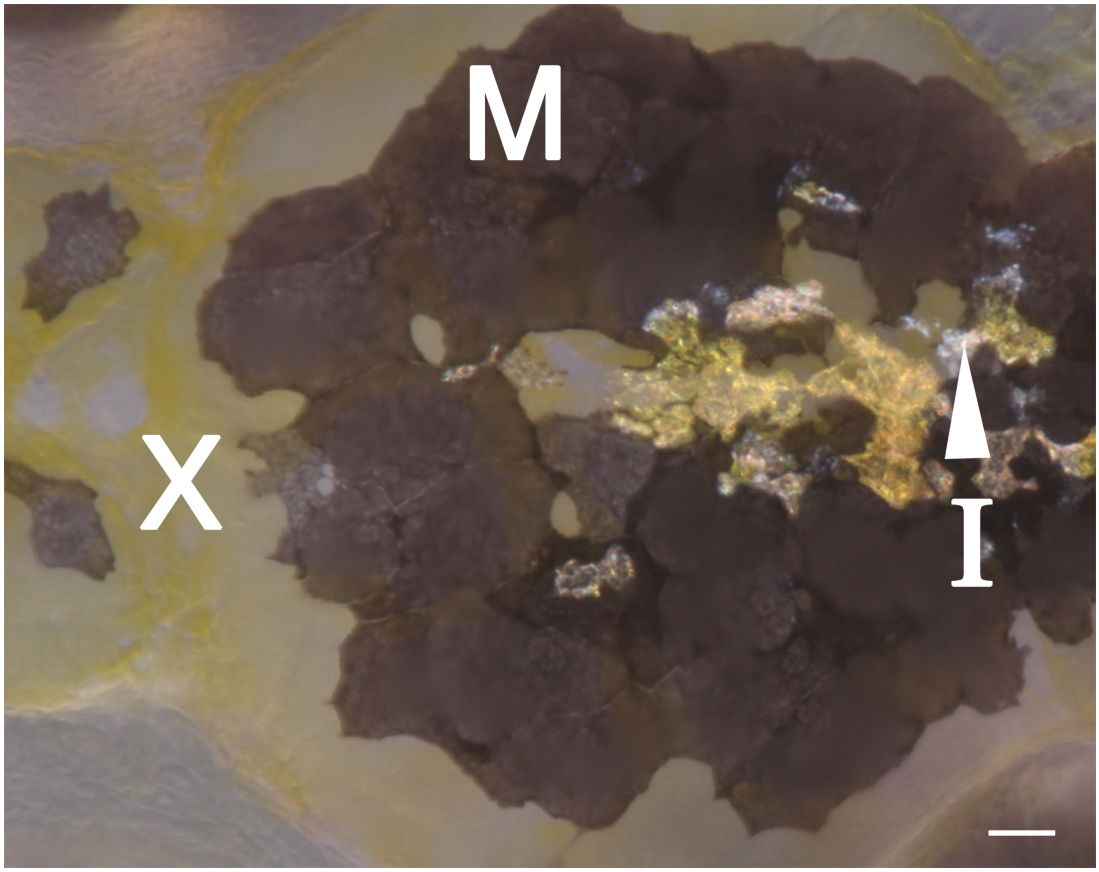

Figure 1.2 Zebrafish pigment cells. Brightfield imaging of dorsal head of 5 dpf WT zebrafish larvae. Indicated are melanophores (M), iridophores (I) and xanthophores (X). Scale bar 50 μm.

1.2.2 Embryonic/early larval pigment pattern.

The embryonic pigment pattern is completely established by 5 dpf (Fig. 1.1 B). Melanophores are arranged into 4 stripes along the anterio-posterior axis. One of the stripes is located dorsal to the embryo, from the top of the head to the tip of the tail, the second stripe is located ventral to the myotomes blocks, between the yolk and yolk sac extensions, the third stripe is located on top of the yolk and the yolk sac extension and finally there are two stripes parallel to each other in the flanks of the fish, at the level of the horizontal myoseptum. The stripes are named according to their position, as dorsal, ventral, yolk sac and lateral stripes. Iridophores are located only in three of the stripes, the dorsal, ventral and yolk sac stripes in very close association with melanophores. Additionally, a region of dense iridophores can be seen above the swim bladder, these are called lateral patches. Xanthophores are spread underneath the epidermis covering the dorsal and lateral flanks of the embryo. This embryonic/early larval pigment pattern remains mostly unaltered until the onset of metamorphosis.

1.2.3 Adult pigment pattern.

The adult pattern (Fig. 1.1 D) consists of five dark stripes intercalated with four light interstripes that run along the flanks of the fish, specifically in the hypodermis and the anal and tail fins (Tu & Johnson 2011). Similar to the embryonic pattern, the adult pattern results from the arrangement of the three previously mentioned chromatophore types. However, some of the pigment type are present in different shapes. While melanophores are found only in one form, iridophores can be either loose or densely packed but also have either an ellipsoidal shape with small reflecting platelets, S-iridophores, or a spindle shape containing large reflecting platelets, L-iridophores (Kasai & Oshima 2006; Hirata et al. 2003). Xanthophores can be either dendritic and lightly coloured or compacted and heavily pigmented. The final pigment pattern results from the layered arrangement of pigment cells in the hypodermis (Hawkes 1974; Kirschbaum 1975; Le Guellec et al. 2004; Rakers et al. 2010). The dark stripes are comprised from the outside to the inside of the body, of dendritic lightly coloured xanthophores, covering a layer of loose blue iridophores, followed by a layer of black melanophores that are above of a layer of L-iridophores. The interstripe consists of dense and heavily pigmented xanthophores covering a layer of densely packed S-iridophores, giving the golden appearance of this lightstripe (Fig. 1.2).

1.2.4 Transition of the embryonic/larval pigment pattern to the adult pigment pattern.

The embryonic/early larval pigment pattern remains mostly unaltered until the onset of metamorphosis at around 21 dpf (see section 1.1; Fig. 1.1 C). The adult pigment pattern is formed by the generation of newly differentiated melanophores, iridophores and xanthophores derived from adult pigment stem cells (Singh et al. 2016), however, xanthophores also derive from proliferation of embryonic xanthophores (McMenamin et al. 2014). The first to be formed is an interstripe (X0) right in the middle of the dorso-ventral axis of each flank, at the level of the horizontal myoseptum. The interstripe starts forming with the appearance of iridophores along the horizontal myoseptum that proliferate and spread on the surface of the skin in the area of the future stripes and interstripes (Singh et al. 2014). Melanophores precursors reach the skin at the sites where the first dorsal (1D) and ventral (1V) stripes will form. Different to iridophores, melanoblast do not proliferate once they reach the skin but achieve a high density and form a continuous layer on the area where stripes will form. Xanthophore proliferation and differentiation is known to be directly triggered by thyroid hormone (at least) at the onset of metamorphosis (McMenamin et al. 2014), covering all the skin surfaces but adopting two different shapes, dendritic and lightly coloured on the stripes and compacted and heavily pigmented in the interstripes (Mahalwar et al. 2014). The interactions between the three cell types is necessary for the establishment of boundaries between stripes and interstripes. The rest of the stripes (D2, V2 and V3) and interstripes (X1D, X1V and X2V) are added cyclically through the same mechanism during the metamorphic process that last around 1 month.

The formation of the adult pigment pattern requires of the activation of adult pigment stem cells that derive from the neural crest but that are kept quiescent until metamorphosis. Thus, zebrafish provide a model for the *in vivo* study of establishment and regulation of adult pigment stem cells. In the following section, we will address the formation of the neural crest, from which both embryonic and adult zebrafish chromatophore lineages derive.

1.3 Neural crest.

The neural crest is an embryonic transitory population of multipotent cells present in all vertebrates (Bronner & LeDouarin 2012). During neurulation, three distinctive areas of the ectoderm becomes specified, the neural ectoderm, the neural plate border and the non-neural ectoderm. In the centre, the neuronal ectoderm is flanked on both sides by the neural plate border, after which the non-neural ectoderm is specified. Neurulation progresses with the folding of the neural plate until both borders of the neural plate reach each other. At their closure, the neural plate forms the neural tube that will form the central nervous system while the non-neuronal ectoderm, now on top of the neural tube, forms the epidermis. Is in the region under the non-neural ectoderm and the dorsal region of the neural tube where neural crest cells emerge (Le Douarin & Kalcheim 1999). Neural crest cells are specified progressively from the most anterior region of the head towards the most posterior part of the embryo (Raible et al. 1992). Once neural crest cells are specified, cells undergo epithelial-to-mesenchymal transition and migrate ventrally and dorsolaterally, through distinctive pathways until reaching their final destination. At this stage, neural crest cells are denominated migratory neural crest cells (Fig. 1.3).

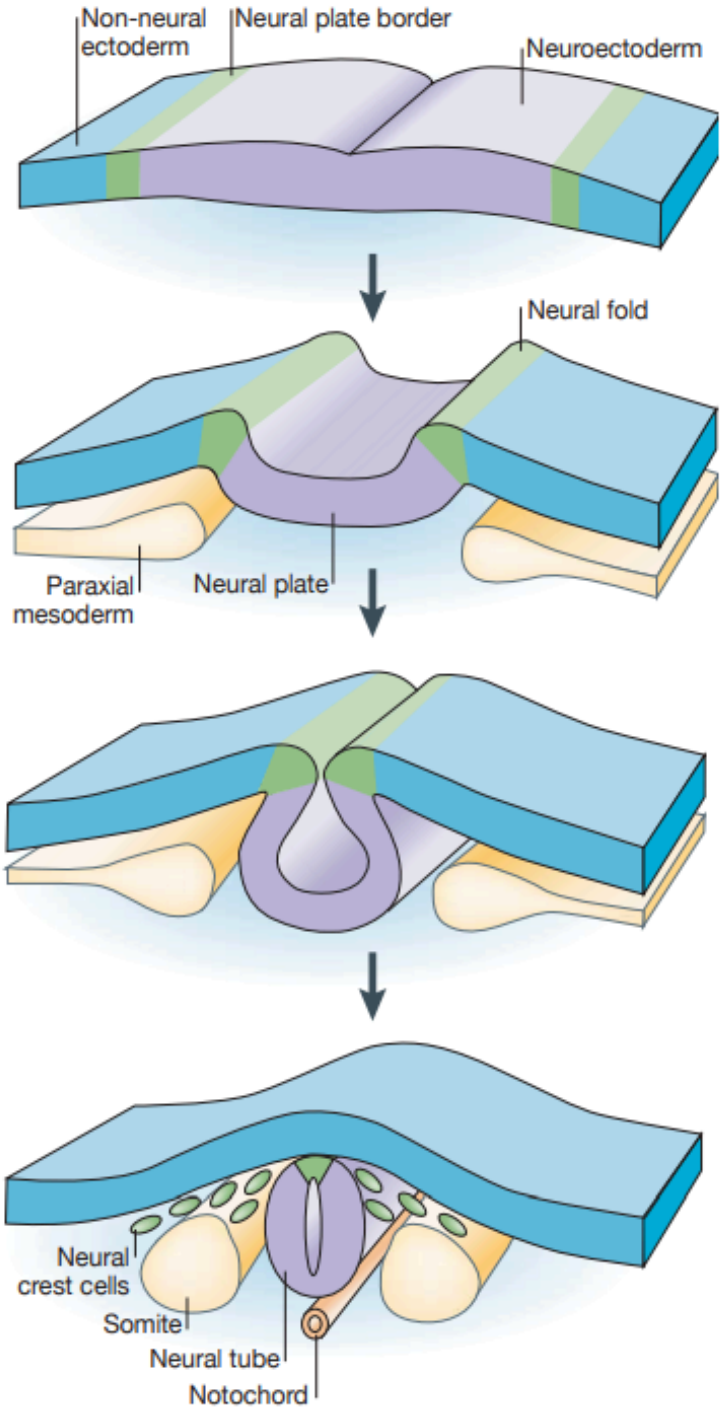

Figure 1.3 Neural crest formation. Scheme shows specification of the neural plate border between the neural (purple) and the non-neural (blue) ectoderm domains. The neural crest domain (green) is specified from the neural plate border. During neurulation, invagination of the neural plate forms the neural tube, bringing both neural plate border together. The neural crest delaminates from the dorsal neural tube (purple) and begin to migrate either between the somites and the epidermis or between the somites and the neural tube. From (Gammill and Bronner-Fraser 2003).

1.3.1 Neural Crest Derivatives.

From the many derivatives formed from the neural crest, two main groups are recognised, ectomesenchymal derivatives that comprise, e.g. osteocytes, chondrocytes and connective tissue, and the non-ectomesenchymal derivatives that include several types of neurons, glia and pigment cells. *In vivo*, the premigratory neural crest generates specific derivatives in 5 distinctive domains along the anterior-posterior axis: the cranial, cardiac, vagal, trunk and sacral neural crest.

The cranial neural crest forms bones, cartilage, connective tissue and peripheral neurons and glia that contribute to craniofacial formation (Kimmel et al. 1995; Lumsden et al. 1991). Interestingly, only embryonic melanophores are also derived from cranial neural crest cells (Schilling & Kimmel 1994). Caudal to the cranial neural crest, the cardiac neural crest, contributes to the formation of the heart and major blood vessels (Stoller & Epstein 2005; Li et al. 2003). The vagal and sacral neural crest generate the entire enteric neurons and glia and are located in two separated domains, In chick and mouse embryos, the vagal domain is located in the region between somites 1-7 and the sacral region is found posterior to the 28thand 25th somites (Le Douarin & Teillet 1973). However, in zebrafish only a vagal domain has been identified and is responsible for the formation of enteric neurons and glia (Kelsh & Eisen 2000; Wang et al. 2011).

Finally, the neural crest in the trunk generates sensory and sympathetic neurons, glial cells, endocrine derivatives and pigment cells, as well as, in zebrafish at least, the adult pigment stem cells from which newly differentiated cells are generated to form the adult pigment pattern (Bronner-Fraser and Fraser 1989; Budi et al. 2008; Dooley et al. 2013; Raible et al., 1994). Because embryonic pigment cells and adult pigment stem cells derive from neural rest cells in the trunk, in the following section we will describe in more detail the neural crest derivatives of this domain.

1.3.2 Derivatives of the neural crest in the trunk and their migratory pathways.

In zebrafish, neural crest cells in the trunk migrate through two distinctive pathways (Fig. 1.4), the dorso-lateral pathway and the ventro-medial pathway, from now on we will refer to them as the lateral and medial migratory pathways. The lateral pathway consists of the space in between the epidermis and the somites/myotomes, while the medial pathway follows the space between the somites/myotomes and the neural tube, the developing notochord and medial blood vessels.

The neural crest cells of the trunk give rise to the satellite glial cells and peripheral sensory neurons that comprise the dorsal root ganglia (DRG). The precursors of both cell types, migrate through the medial migratory pathway and accumulate ventro-lateral to the neural tube (Le Douarin & Kalcheim 1999), once in place, both cell types differentiate. Glial cells wrap around the bodies of the sensory neurons, which innervate the neural tube, skin, muscles and tendons, (Raible & Ungos 2006; Prendergast & Raible 2014). Another type of glial cells, myelinating and non-myelinating Schwann cells associate with the axonal projections that emerge from the DRGs (Woodhoo & Sommer 2008). Similarly, the progenitors of sympathetic neurons migrate through the medial pathway and develop in ganglia ventro-lateral to the dorsal aorta (Raible & Ungos 2006; An et al. 2002).

Finally, pigment progenitors migrate through both pathways, however, iridophore precursors migrate exclusively through the medial pathway, while xanthophores precursors only migrate through the lateral pathway. In contrast, melanophore precursors migrate through both, the lateral and medial pathway (Raible & Eisen 1994)

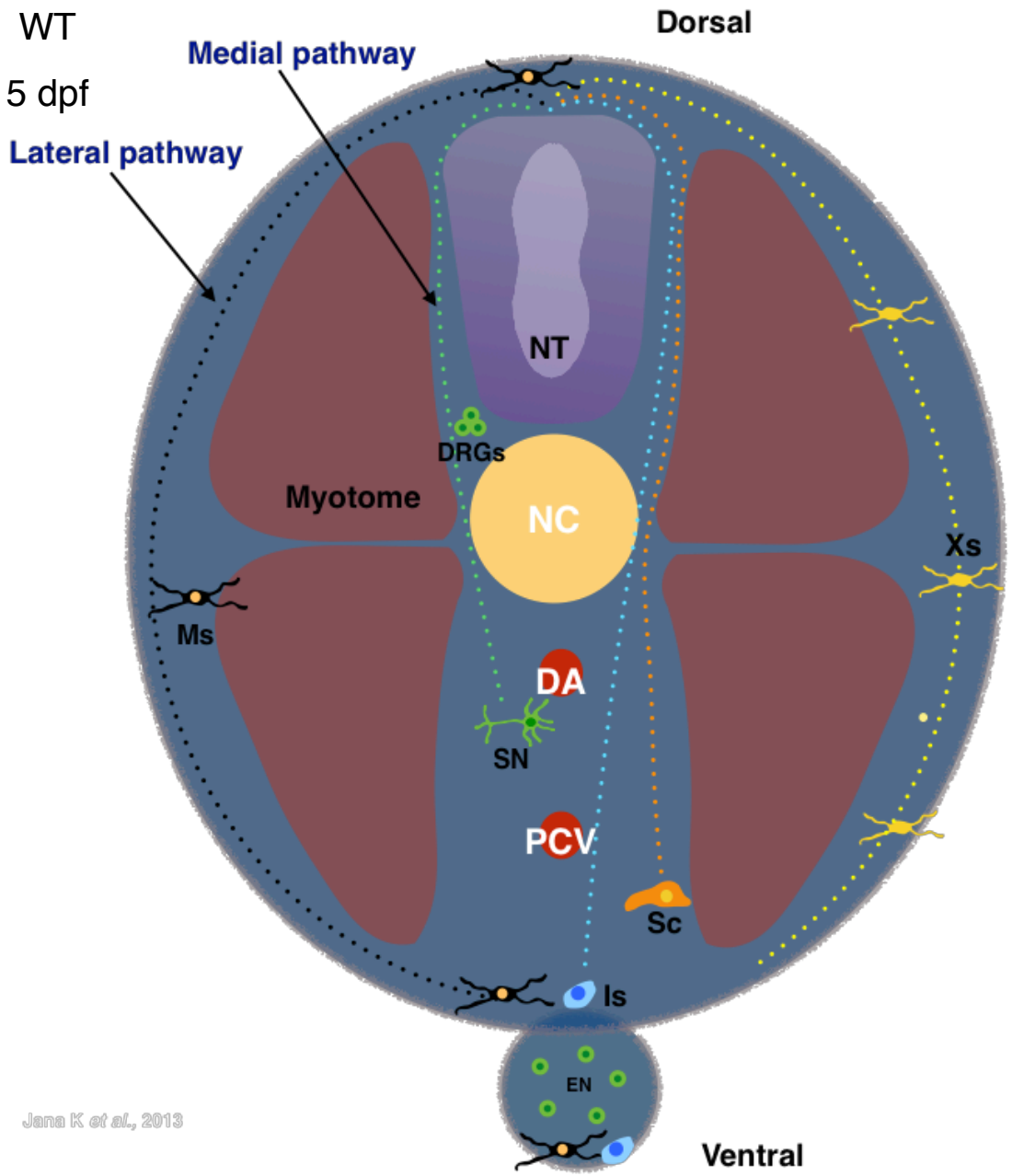

Figure 1.4 Neural crest migratory pathway. Scheme shows transversal view of the posterior trunk of a 5 dpf fish. Neural tube (NT), notochord (NC), dorsal root ganglia (DRG), dorsal aorta (DA), posterior cardinal vein (PCV), enteric neurons (EN), sympathetic neurons (SN), Melanophores (Ms), iridophores (Is) and Xanthophores (Xs). Schwann cells (Sc). Migratory route of each derivative is indicated with doted lines. Melanophores and Xanthophores migrate through the lateral migratory pathway, while DRGs, sympathetic neurons, schwan cells, and iridophores migrate through the medial migratory pathway.

.

1.4 Models for the specification of the neural crest.

Two models for the mechanisms of cell fate choice of neural crest cell have been proposed. One is the direct fate restriction specification model, that proposes that neural crest cells maintain their multipotency until reaching their destination where they are specified by local clues (Bronner-Fraser & Fraser 1989; Bronner-Fraser & Fraser 1991; Collazo et al. 1993; Delfino-Machín et al. 2017). The second model is known as the progressive fate restriction model, in which neural crest cells follow the generation of sequential partially restricted precursors as soon as the neural crest is specified. Migratory neural crest cells then divide producing more restricted precursors along their journey until becoming specified into unipotent precursors, perhaps even prior to reaching their final destination (Weston 1991; Henion & Weston 1997; Le Douarin et al. 2008).

The current understanding of neural crest specification is based on the findings from multiple model organisms with *in vivo* and in *vitro* approaches. So far, the favoured model is the progressive fate restriction model in which some of the neural crest cells in the cranial premigratory domain are partially restricted. Evidence from chick embryos suggest the existence of heterogeneous populations of cells that give rise to several but a limited type of neural crest derivatives favouring the direct fate restriction specification model, however it has been also identified a population of cells that displays a stereotypical progeny, supporting the progressive fate restriction model (Bronner-Fraser & Fraser 1988; Frank & Sanes 1991). Furthermore, previous work suggest that neural crest cells are specified in the premigroatory domain based on their position in respect to the neural tube (Schilling & Kimmel 1994). Cell more distal to the neural tube generate neuronal lineages, medial positioned cells are fated to pigment cell lineages and the more proximal cells to the neural tube make skelletogenic derivatives (Schilling & Kimmel 1994).

1.4.1 Specification of the chromatophore lineage in zebrafish.

During development, the pigment cells that form the embryonic pigment pattern directly differentiate from the neural crest, while the adult pigment pattern is formed mostly by newly differentiated pigment cells that derived from neural crest-derived undifferentiated cell that reside dormant in the body until metamorphosis (Singh et al. 2016), this are known as adult pigment stem cells (APSC) (Budi et al. 2008), while (at

least) part of the adult population of xanthophores is produced from proliferation of embryonic xanthophores (McMenamin et al. 2014). In the following section, we will describe the development of embryonic chromatophores. Establishment of adult pigment stem cells will be discussed later.

In the progressive fate restriction model context, a variety of intermediate precursors have been identified, including precursors for the chromatophore lineage. In chick and mouse embryos, a bipotent precursor for glia and melanocytes has been identified (Thomas & Erickson 2009; Adameyko et al. 2009; Adameyko & Lallemend 2010). In contrast, because of the multiple pigment cells found, zebrafish presents a more interesting model for the study of chromatophore lineage specification. The existence of a common precursor for chromatophores was originally proposed due to the existence of cells with more than one pigment organelle (Bagnara et al. 1979), although direct evidence for a fate-restricted chromatoblast has not yet been published. A bipotent precursor for iridophores and melanophores was first identified, this is known as the melanoiridblast (Curran et al. 2010). Furthermore, data generated from our own group identified a precursor capable of generating the three pigment cell types, melanophores, iridophores and xanthophores (MIX), glia (G) and neurons (N) (Nikaido, M., et al. Unpublished), thus suggesting the existence of a chromatoglioblast (MIXGN). The study of *nacre* mutants led to the conclusion that both iridophores and melanophores may be generated from individual progenitors (Curran et al. 2010).

From the large-scale ENU mutagenesis screening performed in 1996, a variety of mutants affecting pigmentation have been crucial for the understanding of chromatophore specification but also had revealed some of the molecular mechanism behind it (Kelsh et al. 1996). For instance, mutants of the SRY (Sex Determining Region Y)-related HMG box transcription factor 10 (*sox10)*, lack all three chromatophores, glia and peripheral neurons, while mutants of the Microphthalmia-associated transcription factor A (*mitfa)* do not display melanophores in the trunk and have reduced iridophores. Mutant of the Leukocyte tyrosine kinase (*ltk*) shows highly reduced iridophores (Lopes et al. 2008) and more recently a CRISPR/Cas9 mutant of the Transcription factor EC (*tfec)*, displays complete absence of iridophores (Petratou et al. 2018). Phenotypic and molecular characterisation of each of these mutants, has generated evidence of the genetic program that drives chromatophore specification. As a result of the integration of the current data and experimentally validated mathematical modelling, very recent work from our lab has suggested the

gene expression profile of different progenitors of the chromatophore lineage. Briefly a multipotent MXIG (*sox10*$^{+}$*, tfec*$^{+}$*, foxd3*$^{+}$*, ltk*$^{+}$, *mitfa*$^{-}$ and *pnp4a*$^{-}$*)*, generates an (at least) bipotent melanoiridoblast (*sox10*$^{+}$*, tfec*$^{+}$*, foxd3*$^{-}$*, ltk*$^{+}$, *mitfa*$^{+}$ and *pnp4a*$^{+}$*)* that ultimately generates differentiated melanophores (*sox10*$^{-}$*, tfe*$^{-}$*, foxd3*$^{-}$*, ltk*$^{-}$, *mitfa*$^{+}$ and *pnp4a*$^{-}$) and iridophores (*sox10*$^{+}$*, tfec*$^{+}$*, foxd3*$^{+/-}$*, ltk*$^{+}$, *pnp4a*$^{+}$ and *mitfa*$^{-}$) (Petratou, K. Thesis, 2016).

1.4.2 Embryonic pigment cell development in zebrafish.

1.4.2.1. Melanophores

The zebrafish melanophore, is the homologue of the melanocyte in amniotes, thus, melanophores are often referred as melanocytes (Schartl et al. 2016). While in mammals two types of melanin are found, black or dark brown eumelanin and red or yellow pheomelanin (Hearing 2011), melanophores in zebrafish only have one type of melanin. This pigment is synthetized and accumulated in a specialized organelle known as melanosomes. In mammals, melanocytes transfer most of their melanosome to keratinocytes, but melanophores in zebrafish accumulate all of their melanosomes in the cytoplasm.

Although pigmented melanophores can be seen as early as 27 hpf in the dorsal trunk of zebrafish, melanophore precursors, known as melanoblasts are specified even before the start of migration of the neural crest (Kelsh & Eisen 2000). The formation of melanin requires specific enzymes that catalyse melanin production. Some of those enzymes are tyrosinases (Tyr) or domachrome tautomerase (Dct) (Hearing 2011), thus, expression of either of the enzymes can be used a marker for melanophores (Serbedzija et al. 1990; Kelsh et al. 2009; Theveneau & Mayor 2012). Melanoblasts start migrating first through the lateral migratory pathway, followed by migration through the medial pathway. Differentiation of melanophores occurs as they migrate, as pigmented melanophores can be seen in both the lateral and medial pathways. By 3 dpf all melanophores have reached their position at one of the stripes.

1.4.2.2. Iridophores

Differentiated iridophores appear as silver spots that can only be seen under incident light (Fig. 1.2 I) (Kelsh 2004). The silver nature of iridophores come from the structural

colouration (Bagnara et al. 1979) given by staked platelets of purine crystals within specialised organelles known as iridosomes, in which light is reflected and scattered in an effect know as constructive interference (Land 1972; Bagnara et al. 2007).

Embryonic iridophores differentiate as early as 42 hpf in the eye, and by 48 hpf, iridophores are visible in the trunk in close association to melanophores in the dorsal and ventral stripes (Lopes et al. 2008; Kimmel et al. 1995). Dense regions of iridophores are seen in the lateral patches (above the swim bladder) and covering the retinal pigment epithelium (RPE). The progenitor of the iridophore is called the iridoblast, and although these are specified from neural crest cells very early in development, they can be carefully distinguished by the expression of the gene encoding the receptor tyrosine kinase (RTK) the *leukocyte tyrosine kinase* (*ltk*) (Lopes et al. 2008; Petratou et al. 2018). In contrast to melanophores, differentiated iridophores where found to strongly maintain the expression of *sox10* (Petratou et al. 2018). Iridophores migrate exclusively through the medial pathway.

1.4.2.3. Xanthophores

The yellow colour in xanthophores is due to the accumulation of organelles called pterinosomes that contain pigments called pteridines, and carotenoid vesicles that accumulate dietary carotenoids (Obika & Fukuzawa 1993; Ziegler 2003). Catalysis of the biosynthesis of pteridine involves the enzymes encoded by the genes *GTP cyclohydrolase* (*gch*), *xanthine oxidase* (*xod*) and *xanthine dehydrogenase* (*xdh*). The precursors of xanthophores, xanthoblasts, express these genes even before migrating away from neural tube (Kelsh 2004) via the lateral pathway. Differentiated xanthophores are visible from approximately 3 dpf and cover both flanks of the larvae (Mahalwar et al. 2014; Odenthal et al. 1996; Quigley & Parichy 2002; Kelsh et al. 2009).

1.5 Establishment of adult pigment stem cells in zebrafish.

The adult pigment pattern is formed mostly by newly differentiated pigment cells that are derived from neural crest-derived adult pigment stem cells (Singh et al. 2016). Although at least part of the adult population of xanthophores is produced from proliferation of embryonic xanthophores (McMenamin et al. 2014; Mahalwar et al. 2014). The specificities of how adult pigment stem cells in zebrafish are established

are largely unknown, in this section we discuss the current understanding of adult pigment stem cells formation in zebrafish.

After its formation, the embryonic/larval pigment pattern remain unchanged until the onset of metamorphosis, when new pigment cells of all three types appear on the skin of the metamorphic fish. These differentiate *de novo* and in large numbers. Thus suggesting the presence of dormant undifferentiated progenitor/s within the body of the fish. From this observation, many questions arise. What is the nature of this progenitor/s? Are they unipotent progenitors for each pigment cell type or are they bipotent or multipotent progenitors similar to the ones seen during embryonic pigment formations. Where are these pigment progenitors located? How are they kept "dormant" until metamorphosis? What signals trigger their activation?

Studies of a mutant that displays a normal embryonic pigment pattern but that does not form an adult pattern helped to answer some of these questions. This mutant is called *picasso* (Budi et al. 2008), in which the *epidermal growth factor receptor (EGFR)-like tyrosine kinase* gene encoding the protein Erbb3b is affected (loss of function mutant). In zebrafish, *erbb3b* is expressed in the medial pathway in streams that run in a dorso-ventral manner on each somite segment (Langworthy & Appel 2012). It has been described that proliferation and migration of Schwann cells is mediated by ErbB2 and ErbB3 receptor (Lyons et al. 2005), but no function on embryonic pigment development has been noted.

Given that in *erbb3b*/*picasso* mutants the early larval pigment pattern is not affected, it suggests that the disruption to the adult pigment pattern comes from aberrations in the pool of progenitors that generate the adult pigment cells. It has been shown that chemical inhibition of Erb signalling with a specific EGFR inhibitor, AG1478, in WT fish during three stages: 1) embryonic development, 2) pre-metamorphic stages and 3) at metamorphosis showed that only treatment with the Erb inhibitor during embryongenesis (8-72 hpf) phenocopied the *picasso* phenotype, lack of adult pigment pattern, without affecting the embryonic pigment pattern. This suggests that, Erbb3b is only required in an embryonic developmental time-window. Further experiments showed that requirement of Erbb3b is restricted to a shorter time-window that lies within 9-48 hpf, this period is due to the mechanism by which the neural crest is specified. Then eural crest is specified progressively from the most anterior region of the head towards the most posterior part of the embryo (Raible et al. 1992). Thus,

Erb signalling requirement is likely to be shorter on each segment/somite but last 40 hours approximately along the anterior posterior axis.

Erb signalling is also required for the formation of pigment progenitors that generate regenerative melanophores. Embryos in which differentiated embryonic melanophores were chemically ablated by treatment with the melanocytotoxic chemical 4-(4-morpholinobutylthio)phenol (MoTP) from 2-3 dpf, are able to almost completely regenerate melanocphores by 7 dpf. The small molecule MoTP melanocytotoxicity is mediated via the activity of tyrosine kinases that likely convert MoTP to a qunone specie that result toxic. However, embryos treated with the Erb inhibitor AG1478 from 9-48hpf and then with MoTP do not regenerate melanophores (Hultman et al. 2009; Tryon et al. 2011). Thus, Erb signalling is required for the formation of pigment cell progenitors that produce the adult pigment pattern and regenerative melanophores.

Further studies showed that in metamorphic WT fish cells that express neural crest markers (*sox10, mitfa and foxd3*) are abundant within the body , distributed along the nerves that emerge from the DRGs, and project under the hypodermis and within the muscle blocks (Budi et al. 2011). Some of these cells proliferate and differentiate into pigment cells. Interestingly, mutants for *erbb3b* lack these neural crest-like cells.

Work from the Nússlein-Volhard lab, suggested later that these pigment progenitors all derive from single *mitfa:gfp* positive cells that reside within the DRGs. Embryonic melanophores directly differentiate from the neural crest and this process requires of the master regulator of the melanocytic lineage the Microphfthalmia-associated transcription factor a encoded by *mitfa*. Taking advantage of the transient effect of *mitfa*-morpholino injection at 1-cell stage embryos (Mellgren & Johnson 2004), the authors used knock-down of *mitfa* to prevent the formation of embryonic melanophores (before 3 dpf); subsequently, due to dilution of the morpholino, new melanophores were formed by regeneration and restored the pigment pattern. They observed that *mitfa:gfp* positive cells within the DRGs divide at 3 dpf and contribute to the regeneration of melanophores (Dooley et al. 2013). They also showed that more *mitfa:gfp* positive cells appear along the nerve projection that emerge from DRGs prior to the onset of metamorphosis but remain stationary on these nerves.

More recently, clonal cell tracking assays showed the presence of multipotent progenitors within the medial pathway that give rise to adult pigment cells, glia and neurons. These multipotent progenitors appear as early as 16 hpf and remain multipotent at least until metamorphosis. Interestingly, some of these multipotent progenitors are located within the DRGs (Singh et al. 2016). However, this work focused on clones located within the DRGs and did not examine clones located in other positions such as the ventral media pathway.

It has been suggested that these cells in the DRGs are adult pigment stem cells, since they remain dormant/quiescent until required to multipotent contribute to both the adult pigment pattern, and to the regenerating melanophores (Parichy & Spiewak 2015). Thus, there is likely at least one niche of adult pigment stem cells within the DRGs. It is important to note that the self-renewal capacity of this presumptive adult pigment stem cells (APSC) has not yet been tested. However, these data provide the best guide to the *in vivo* properties of the adult pigment progenitors, which we will refer to from now on as APSC.

1.6 Zebrafish *parade/endothelin receptor Aa* mutants as a model of study of adult pigment stem cells.

From the large-scale ENU mutagenesis screening performed in 1996 in Tübingen, a zebrafish mutant called *parade* was isolated (Kelsh et al. 1996). *parade* mutants display a group of ectopic melanophores and iridophores in a very restricted area of ventral medial pathway of the posterior trunk (Fig. 1.5 A), just below the dorsal aorta (Fig. 1.5 B I). In this thesis, I build on the work of two former PhD students to develop an understanding of the cellular and molecular basis for the *parade* mutant phenotype. Previous work of two former PhD students of the lab (Dr. Sarah Colanesi and Dr. Jeanette Müller) identified that the *parade* mutation affects the gene encoding the Endothelin receptor Aa.

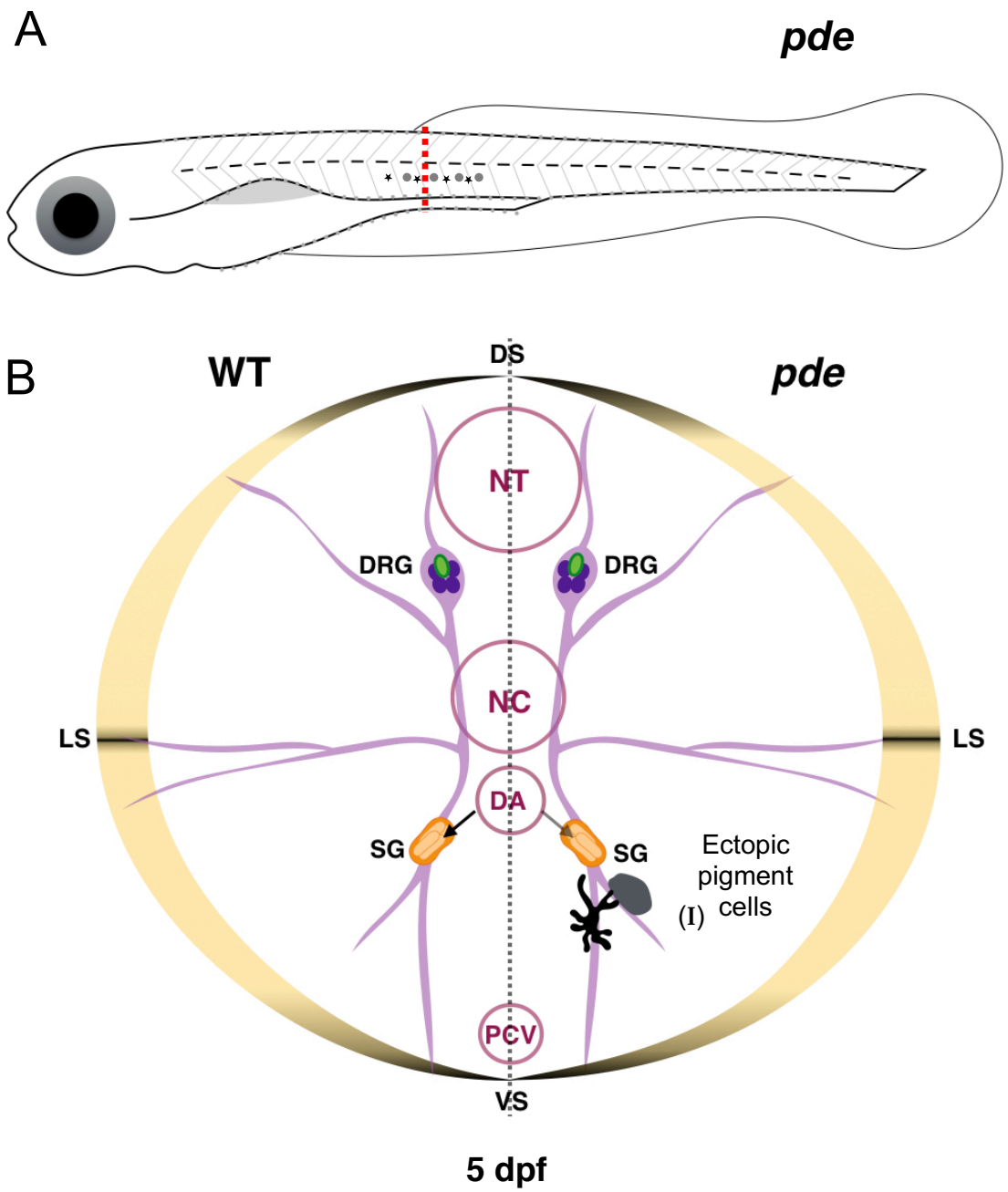

Figure 1.5 *parade* mutants have ectopic pigment cell in the ventral medial pathway. Scheme shows 5 dpf *pde* fish, red dashed line shows the position of the transversal view of scheme represented in B. Scheme shows a transversal view of a 5 dpf zebrafish anterior trunk. The left segment represents the WT context and the right segment the *pde* background. In the most outer layer we indicate the position of the dorsal, lateral and ventral stripes DS, LS, and VS correspondingly. Centrally are indicated the neural tube (NT), notochord (NC), dorsal aorta (DA) and posterior cardinal vein (PCV). Dorsal root ganglia (DRG) and nerve projections are shown in purple while Sympathetic ganglia (SG) are shown in orange. Loss of EdnrAa signalling in *pde* mutants results in formation of ectopic pigment cells (I).

As we previously mentioned, NC cells differentiate into a large number of derivatives (Dupin et al., 2006; Hall, 2008; Le Douarin and Kalcheim, 1999; Le Douarin et al., 2012; Theveneau and Mayor, 2011). From the many derivatives formed from the neural crest, two main groups are recognised, ectomesenchymal derivatives that comprise, e.g. osteocytes, chondrocytes and connective tissue, and the non-ectomesenchymal derivatives that include several types of neurons, glia and pigment cells.

Specification and differentiation of the diverse neural crest derivatives requires of the action of several transcription factors and signalling pathways. The chromatophore lineage requires Wnt/β-catenin pathway and the transcription factor Sox10(Dutton et al. 2001), MITF (Opdecamp et al. 1997) and Kit (Besmer et al. 1993) (Fig. 1.6) and this process occurs from 15 hpf to 72 hpf, in which the pigment cells that form the embryonic pigment pattern directly differentiate from the neural crest, while the adult pigment pattern is formed mostly by newly differentiated pigment cells that derived from neural crest-derived APSC (Raible & Eisen 1994; Budi et al. 2008; Singh et al. 2016). Surprisingly, no role of ET_A, EdnrA nor EdnrAa in pigmentation has been reported.

In the following section we will review the know roles of the endothelin system and ET_A/EdnrA/EdnrAa in *in vivo* and *in vitro* humans and murine models.

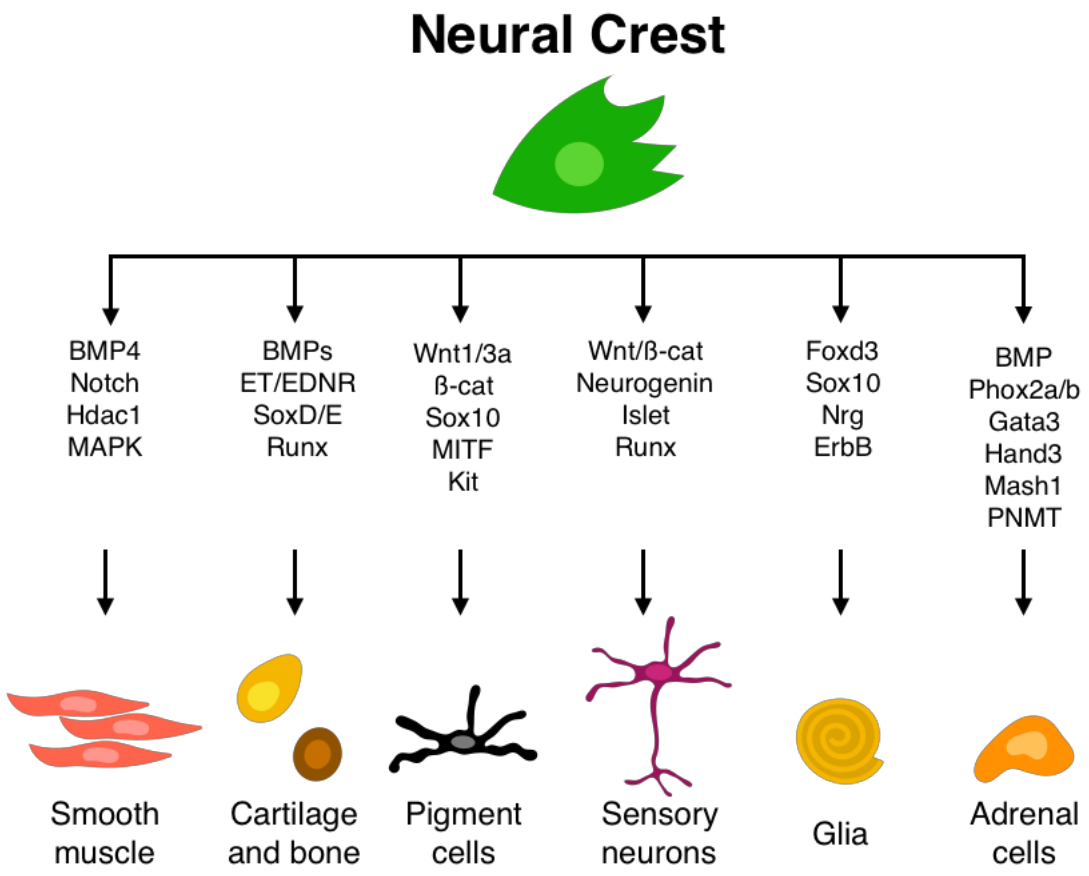

Figure 1.6 Specification and differentiation of neural crest derivatives. Scheme shows some of the known signalling pathways and transcription factors required for the specification and differentiation of neural crest derivatives. Modified from (Theveneau & Mayor 2012)

1.7 The endothelin system.

The endothelin system is comprised of three elements: 1) 21-amino acid ligands known as Endothelins; 2) Endothelin Receptors; and 3) Endothelin converting Enzymes that activate the preligands by proteolytic cleavage.

In mammals, three endothelin (ET) ligands ET-1, ET-2 and ET-3 have been identified. Endothelin-1 was first identified as a vasoconstrictive factor produced by bovine aortic endothelial cells (Hickey et al. 1985). Its first known role was to regulate blood pressure by producing contraction of mammalian blood vessels *in vitro* (Yanagisawa et al. 1988).

Endothelin-1 is a peptide of 21 amino acids with two disulphide bonds in the positions 1-15 and 3-11 (Huggins et al. 1993; Janes et al. 1994; Orry & Wallace 2000). This short peptide derives from a 212-amino acid precursor knows as preproEndothelin-1. A 17-amino acid signal is cleaved by a signal peptidase followed by the removal of 35 and 122 amino acids at the C and N terminals respectively, both removed by furins. This results in a 39-amino acid peptide known as Big endothelin-1 (Big ET-1). Finally, Big ET-1 is cleaved by a type II membrane-bound zinc metalloprotease, the Endothelin converting enzyme-1 (ECE-1) (Yanagisawa, Yanagisawa, et al. 1998), that generates the mature 21 amino acid ET-1. In humans, ET-1 is the most abundant of the endothelins, it is predominantly produced by endothelial cells of blood vessels to maintain normal vascular tone (Haynes & Webb 1994), but it is also produced by epithelial cells of lungs, kidneys, enteric glia cells and certain neurons.

Similar to ET-1, ET-2 is derived from a pre endothelin-2 precursor that is cleaved to a 38-amino acid peptide, Big ET-2 (Yanagisawa, Yanagisawa, et al. 1998), which has been shown *in vitro* to be cleaved by ECE-1 and ECE-2 (Yorimitsu et al. 1992; Shinmi et al. 1993). The resulting 21 amino acid peptide differs from ET-1 by only two amino acids in humans and by three amino acids in rodents. A murine reporter line has shown expression of the endothelin-2 gene (*Edn2*) in the developing hair follicles, ovary, stomach, intestine, corneal epithelium, liver, lung, pituitary, uterus and heart. Its first known role was as a vasoactive intestinal contractor (VIC) in mouse (Ishida et al.,1989), but has also been implicated in ovulation (Meidan & Levy 2007; Ko et al. 2012; Ling et al. 2013) and interestingly, it is over expressed in skin basal cell carcinoma (Tanese et al. 2010) suggesting a role on cancer development.

In mice, *Ece1* is found in many tissues of the body such as the neuroepithelium, liver primordia, ear and gut (Rossi et al. 1995; Davenport et al. 1998; Davenport & Kuc 2000). In humans, *ECE*-1 expression is found increased in breast cancers samples from patients that showed cancer recurrence and the PC-3 prostate cancer cell line (Smollich et al. 2007; Whyteside et al. 2014). On the other hand, in mice, *Ece2* is expressed in development, specifically in the mesenchyme and neural tube, and later in development it is expressed in neurons and the developing heart (Yanagisawa et al. 2000).

In humans, ET-3 differs from ET-1 and ET-2 by six amino acids. It is likely to be processed by ECE-1 as the mouse mutant of this gene showed lower levels of Edn3 (Takeshi et al. 1992)). It has been found to be the most abundant Edn in the rat brain (Giaid et al. 1991) but is also found in other organs such as the heart (Plumpton et al. 1993).

Endothelins are known to activate two receptor subtypes, the endothelin receptor type A (ET_A) and the endothelin receptor type B (ET_B), which are members of the class 1 G protein-coupled family of 7 transmembrane-spanning domains receptors (GPCR). The human ET_A has a 65% sequence similarity to that of the ET_B. In both receptors, the N-terminus tail is the region that has the most differences amongst ET receptors of other species and it is this region that binds to endothelin. The cytoplasmic tail of both receptors undergoes posttranslational modifications that are essential for functional activity and selectivity for coupling with different G proteins in order to activate different signalling pathways (Hashido et al. 1992). ET_A is mainly expressed in the vascular smooth muscle (Regard et al. 2008), lungs and liver, while ET_B is produced in the endothelial cells of the lungs, kidneys and liver and strongly in the brain (Harland et al. 1995).

1.7.1 The endothelin system in zebrafish.

Phylogenetic analysis of endothelins identifies the presence of six endothelin ligands: *edn1, edn2a, edn2b edn3a, edn3b and edn4*, four endothelin receptors: *ednraa* and *ednrab* and *ednrba* and *ednrbb* and three endothelin converting enzymes *ece1, ece2a and ece2b*. (Braasch et al. 2009). For comparison with human an mammals see Table 1.1.

Gene	Human	Mouse	Zebrafish
Ligand	ET1 ET2 ET3	Edn1 Edn2 Edn3	Edn1 Edn2a Edn2b Edn3a Edn3b Edn4
Receptor	ET_A ET_B	Ednra Ednrb	EdnrAa EdnrAb EdnrBa EdnrBb

Table 1 .1 Table shows the endothelin ligands and receptors in humans, mouse and zebrafish (Braasch et al. 2009).

1.7.2 The endothelin receptor type Aa.

The endothelin receptor type Aa is a member of the class 1 G protein-coupled family of 7 transmembrane-spanning domains receptors (GPCR). The cytoplasmic tail of the receptors undergoes posttranslational modifications that are essential for functional activity and selectivity for coupling with different G proteins in order to activate different signalling pathways (Hashido et al. 1992). In mammals, ET_A is mainly expressed in the vascular smooth muscle (Regard et al. 2008), lungs and liver, while ET_B is produced in the endothelial cells of the lungs, kidneys and liver and strongly in the brain (Harland et al. 1995).

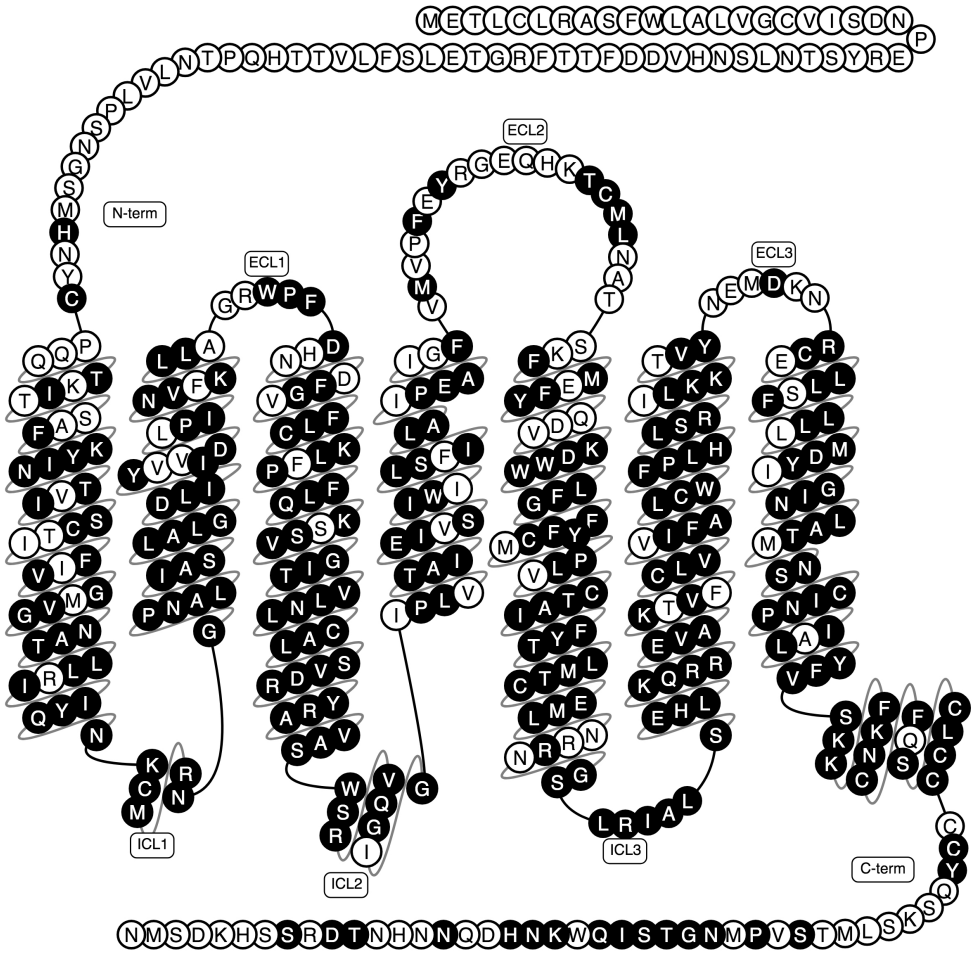

Figure 1.7 Receptor structure of the ET_A. Scheme shows 2D structure of the human ET_A receptor, the identical amino acid of the zebrafish EdnrAa receptor are shown in black. The extracellular domains (ECL) and intracellular domains (ICL) are indicated and numbered accordingly.

Mice homozygous for mutations of *Endothelin 1* (*Edn1*) or *Endothelin receptor type A* (*EdnrA*) receptor (Kurihara et al. 1994; Yanagisawa, Yanagisawa, et al. 1998) exhibit the same craniofacial and cardiac abnormalities as well as impaired thyroid and thymus development, while *Ece1* mutants show the same phenotype as *Edn1*/*Ednra* single mutants, but also display lack of epidermal melanocytes and enteric neurons of the distal gut (Yanagisawa, Hammer, et al. 1998), and are lethal 30 minutes after birth. *Ednra* mutant mice display conversion of lower jaw into similar structures of the upper jaw (Ruest et al. 2004). Thus, in mice, Ece-1, Edn1 and EdnrA work together in dorsoventral patterning of the ventral craniofacial neural crest derived cells, however no pigmentation phenotype has been reported, likely because all of these mutants are lethal at the time of birth.

1.8 Objectives

Our first objective was to elucidate the mechanism behind the *parade* phenotype. previous work of Dr. Sarah Colanesi and Dr. Jeanette Müller, together with my work is presented in the manuscript that forms Chapter 3. Based on our initial characterization of the *parade* mutant we hypothesized that the ectopic pigment cells in the *parade* mutant arise from precocious activation of APSC. We proposed a model in which *pde*/EdnrAa signalling in the dorsal aorta regulates a second niche of APSC in the ventral medial pathway and keeps them in a quiescent state, whereas in *pde* mutants, disruption of EdnrAa allows premature activation of APSC and subsequent differentiation resulting in the *pde* phenotype.

In order to identify what other components of the zebrafish endothelin system interact with EdnrAa to control APSCs, in Chapter 4 we present the assessment of the pigment phenotype of mutants of the zebrafish endothelin system generated through CRISPR/Cas9 targeted mutagenesis.

Finally, in Chapter 5 we tested our model derived from Chapter 3, by investigating the embryonic origin of the ectopic pigment cell in *parade* mutants. We also looked for evidence of a second niche of APSC in a WT background in the ventral medial pathway. And finally, we test whether chemical inhibition of signalling pathways that regulate stem cells in other systems phenocopy the *pde* phenotype.

CHAPTER 2

CHAPTER 2 Materials and methods

This section describes the protocols used to perform the experiments in this thesis as well as the information on the reagents and kits used.

2.1 Fish methods

2.1.1 Fish husbandry

Fish care and procedures were approved by the University of Bath Ethical Review Committee and in full accordance with the Animals (Scientific Procedures) Act 1986, under Home Office Project Licenses 30/2937 and P87C67227.

Individual females and males were set up in mating tanks separated overnight to prevent mating; the next morning, pairs were allowed to mate for only 20 minutes in order to obtain batches of developmentally homogenous embryos. Embryos were collected using a tea strainer and rinsed with fish water and transferred to Petri dishes containing embryo medium with or without methylene blue (see section 2.1.2.1). Fifty embryos per petri dish were sorted paying special care to remove all abnormal, dead or unfertilized eggs. All embryos were allowed to develop at 28.5 ºC for at least 6 hours and then incubated at 23 ºC or 33 ºC to delay or speed their growth as required in each experiment.

When required, embryos were dechorionated with Dumont forceps #5 (Interfocus) and anesthetised with tricaine for examination. For some experiments, melanisation was prevented using 1-phenyl-2-thiourea (PTU). Details on the solutions and treatment conditions are described in the following sections.

2.1.2 Solutions

2.1.2.1 Embryo medium

Fertilized eggs and embryos up to 5 dpf were grown in freshly made embryo medium. To prepare embryo medium a stock of full strength Hank's solution was prepared as follows:

Full Strength Hank's solution

0.137 M NaCl
5.4 mM KCl
0.25 mM Na2H PO4
0.44 mM KH2 PO4
1.3 mM CaCl2
1.0 mM Mg SO4
4.2 mM NaH CO3

The full strength Hank's solution was then diluted 1/10 and 1ml of methylene blue was added. For pharmacological treatments and clonal induction embryo medium without methylene blue was used.

2.1.2.2 Tricaine

To anesthetise embryos and adult fish, a stock 0.4% solution of tricaine (3-amino benzoic methanesulfonate; Sigma-Aldrich, Cat. No. E10521) was prepared by dissolving 400 mg of tricaine powder in 97.9 ml of distilled water and adding 2.1 ml of 8M tris (pH9). The pH and volume were adjusted to 7 and 100 ml, correspondingly. The stock solution was stored protected from light at 4ºC.

2.1.2.3 1-phenyl-2-thiourea (PTU)

A stock solution of PTU (Sigma-Aldrich, Cat. No. CDS004712) 0.03% was prepared in embryo medium without methylene blue. To prevent melanophore pigmentation, embryos were treated at 22 hpf with a 1/10 dilution of PTU stock in embryo medium.

2.1.3 Fish strains

The strains used are listed in Table 2.1, details on their characteristics are described in the in the results text as they are mentioned.

No.	Abbreviation	Allele	Reference
1	WT	*AB*	
2	*pde^{tj262}*	*pde^{tj262}*	(Kelsh et al. 1996)
3	*pde^{tv212}*	*pde^{tv212}*	(Kelsh et al. 1996)
4	*pde^{hu4140}*	*pde^{hu4140}*	HI
5	*fli:EGFP*	*Tg(fli1a:EGFP)^{y1}*	(Lawson & Weinstein 2002)
6	*sox10:cre*	*Tg(-4725sox10:cre)^{ba74}*	(Rodrigues et al. 2012)
7	*sox10:ER^{T2}cre*	*Tg(sox10:ER^{T2}Cre)*	(Mongera et al. 2013)
8	*hsp70:loxp-DsRed-loxp-EGFP*	*Tg(hsp:loxp-dsRed-loxp-EGFP*	(Hans et al. 2009)
9	*β-actin:STOPDsRed*	*Tg(β-actin2:loxPSTOPloxPDsRedexpress)*	(Bertrand et al. 2010)
10	*edn1*	*edn1$^{\Delta 11bp}$*	MPIDB
11	*edn2*	*edn2$^{\Delta 4bp}$*	MPIDB
12	*edn3a*	*edn3a^{+1bp}*	MPIDB
13	*edn3b*	*edn3b$^{\Delta 11bp}$*	MPIDB
14	*ednraa*	*ednraa$^{\Delta 4bp}$*	MPIDB
15	*ednrab*	*ednrab$^{\Delta 4bp}$*	MPIDB
16	*ece1*	*ece1$^{\Delta 11bp}$*	MPIDB
17	*mne*	*moonstone*	(Ransom et al. 1996)

Table 2 .1 Zebrafish strains used in this work. Hubrecht Institute (HI), Max-Plank Institute for developmental Biology (MPIDB),

2.1.4 Anaesthesia procedures for free feeding stage fish.

For embryos between 1 and 5 dpf the stock solution of tricaine was diluted to 0.02% in embryo medium. Fish beyond 5 dpf were anesthetised according Table 2.2.

dpf	Tricaine %	Max. length of anaesthesia
7	0.02	30 min
10	0.02	30 min
15	0.01	30 min
21	0.08	30 min

Table 2 .2 Anaesthesia concentration for free feeding zebrafish larvae

2.1.5 Microinjection of 1-cell stage embryos

Immediately after being laid, embryos were collected as described in section 2.2.1 and placed in a Petri dish covered with 2% v/w agarose in embryos medium. A standard slide for microscopy (VWR; Cat. No. 6310114) was placed on top of the agar and the embryos were carefully aligned against the edge of the slide. Special care was taken to orientate the animal pole exposing it 45º from the agar surface in order to allow injection directly to the animal pole (Fig. 2.1). Glass needles were generated by melting 100 mm glass capillaries (1 mm outer/0.75 mm inner diameter) (World Precision instruments, Inc.) at 63 ºC using a needle puller (PC-10 puller; Narishige Ltd.). The needle was filled with mineral oil and placed in a Drummond Nanoject II Auto-Nanoliter Injector (Drummond Scientific Co.). The morpholino or gRNA+Cas9 mix was then taken with the tip of the needle (Fig. 2.1). Embryos were injected by piercing the chorion of the embryos and the animal pole. After injection embryos were placed in Petri dishes with embryo medium and incubated at 28.5ºC.

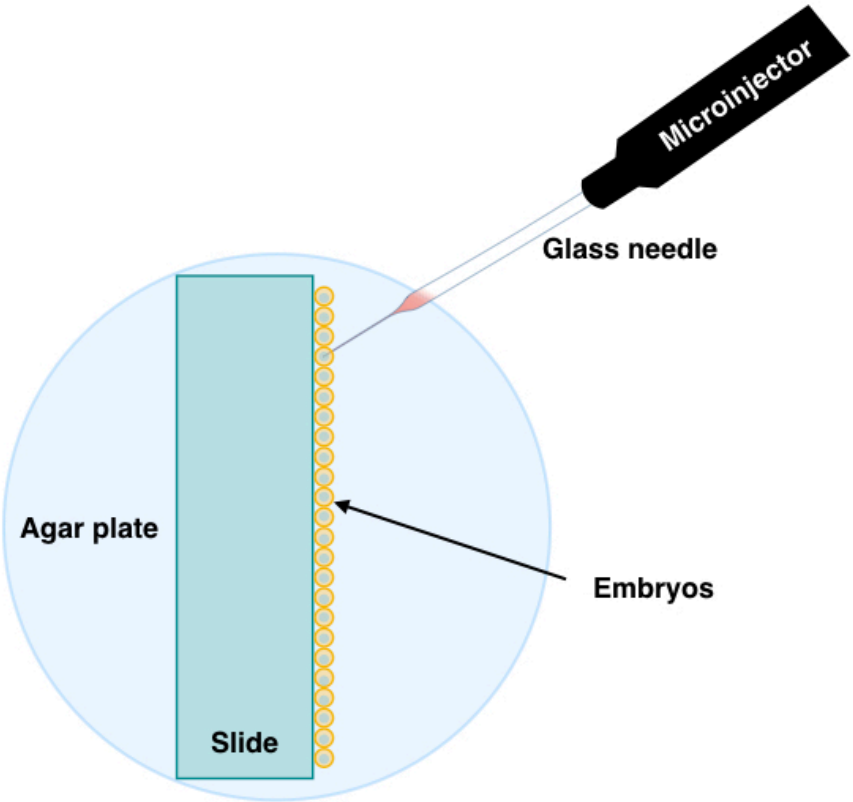

Figure 2.1 Microinjection of 1-cell stage embryos. Scheme shows an agar plate and microscopy slide on top of it. 1-cell stage embryos are aligned against the microscope slide and injected with a fine glass needle attached to a microinjector.

2.2 Molecular methods

2.2.1 Morpholino-mediated Knockdown

Gene expression knock-down was performed using customised morpholinos (Table 3) purchased from Gene Tools LLC. Stock solutions were prepared using molecular graded distilled water to a dilution of 20 µg/µl and stored at -20º C. Prior to dilution morpholinos where heated at 70º C for 5 min and subsequently diluted to a concentration of 2 ng/nl. For injection of *ednrab*-MO and *ednraa*-MO1/2, embryos were injected with 5 nl and the pigment phenotype was assessed at 5 dpf. For melanophores regeneration experiments WT and $pde^{tj262/tj262}$ embryos were injected in the animal pole at the 1-cell stage with 20 ng of morpholino per embryo. Injected embryos were incubated at 28.5º C and screened at 3 dpf for no melanophores phenotype. Individuals with no melanophores were imaged and sorted into 48-well dishes with 1 ml of fresh embryo medium and kept at 28.5 ºC until 5 dpf.

Name	Target	Morpholino sequence (5'-3')
cMO	N/A	CCTCTTACCTCAGTTACAATTTATA
ednrab-MO	Splicing site	AGTGGTGTGTTCACCTGTTTGAGGT
ednraa-MO1	Splicing site	ATCAGACTTTTCTTTACCTGCTTAA
ednraa-MO2	Translation	GCCATTGCAGAACACTGGCCGCTCT
mitfa-MO	Translation	CATGTTCAACTATGTGTTAGCTTC

Table 2 .3 Morpholino sequences

2.2.2 CRISPR/Cas9-mediated targeted mutagenesis

To generate non-functional mutant alleles of the endothelin system genes, the clustered regularly interspaced short palindromic repeats (CRISPR)/ CRISPR-associated 9 (Cas9) system was used to site-directed mutagenesis. This strategy consists of a synthetic guide RNA (gRNA) composed of CRISPR RNA (crRNA) and a transactivated crRNA (tracrRNA) that directs a CRISPR-associated 9 (Cas9) endonuclease to mediated cleavage of a target DNA. The double stranded break is repaired by the non-homologous end-joining (NHEJ) mechanism, which is known to be error-prone, inducing insertions or deletions that can lead to a shift of the reading frame or a creation of a premature stop codon. Details of the crRNA sequences are described in the following sections.

2.2.2.1 gRNAs designs

crRNA had a sequence length of approximately 20 nucleotides that are complementary to the targeted genomic sequence lying immediately 5′ of a protospacer adjacent motif (PAM), a canonical 5′-NGG-3' sequence. crRNAs were manually designed by targeting the first or second exon of each gene when possible, but for genes where no PAM site was found within the first two exons, other locations in the gene were targeted. Customized sequences were purchased from IDT (Integrated DNA Technologies; Table 4.1) together with a generic tracrRNA and a Nuclease-Free-Duplex Buffer.

Alternatively, gRNAs were synthetized using a pDR274 vector that allows T7 RNA polymerase-mediated production of a customizable gRNA containing a 20 nucleotides sequence complementary to the target site of each gene.

CRISPR target sites of the form 5'-$\mathbf{N_{20}}$-NGG-3' were identified (Table 4.1) and oligonucleotides of the form Forward (Fw) 5'-TAGG$\mathbf{N_{20}}$-3 and Reverse (Rv) 5'-AAAC$\mathbf{N_{20}}$-3' were designed ($\mathbf{N_{20}}$=gene specific sequence; both primers are reverse complementary to each other). Oligonucleotides were annealed in order to obtain a double stranded DNA fragment with 4bp overhang that was cloned into the pDR274 vector and subsequently transformed into competent *E. coli* DH5α cells.

Oligonucleotides were annealed as follows:

Reaction:

10x PCR buffer	5 µl
Fw primer 100 µM	5 µl
Rv primer 100 µM	5 µl
H_20	35 µl

Thermocycler conditions:

94 ºC 2 min (ramp rate 1%)
25 ºC 1 min
4 ºC hold

The resulting double stranded DNA fragment was cloned into a linearized pDR274 vector with BsaI.

Reaction conditions:

2x quick ligation buffer	2.4 µl
Annealed oligonucleotides	1.5 µl
Linearized vector (100 ng/µl)	0.5 µl
T4 DNA ligase	0.5 µl

Incubate at room temperature 1-2 hours.

After ligation, plasmid was transformed into E. coli DH5α competent cells by adding to the ligation reaction 50 μl of competent cells and then incubated for 5 minutes on ice. Cells were heat shocked for 60 second at 42ºC in a water bath. After heat shock cells were incubated on ice for 1 minute. 400 μl of 2xTY (Sigma-Aldrich, Cat. No. Y1003) was added to the cells and incubated for 60 minutes at 37ºC in agitation. 100 μl of transformed cells were plated on LB + Kanamycin (100 mg/mL) plates and incubated at 37ºC. At least 3 clones per targeted sequence were inoculated in 2ml of 2xTY + Kanamycin each and incubated on agitation at 37ºC for 8 hours. Plasmid was isolated using a QIAprep Spin Miniprep kit (Cat No. 27104) following the manufactures instructions.

Sequence plasmid for corroboration of successful cloning.

Sequencing reaction:

H_2O	6.0 μl
5x Buffer	2.0 μl
Purified plasmid	1.0 μl
Primer (Tü1193 μM)	0.5 μl
BigDYE ready reaction mix	0.5 μl

Thermocycler reaction:

96 ºC 2 min
96 ºC 20 sec
50 ºC 10 sec
60 ºC 4 min

After labelling reaction, samples were provided to the sequencing facility of the Max-Planck Institute for Developmental Biology. Sequences were compared with original vector to corroborate cloning. A PCR fragment of 122 bp that includes the T7 promotor and the gRNA scaffold was amplified for further *in vitro* transcription.

Reaction:

10x PCR Buffer	5.0 μl
DNA template	1.0 μl
Primer Tü1105	10.0 μl
Primer Tü1134	10.0 μl

dNTP mix 10 mM each	0.5 μl
H_2O	41.0 μl
Taq DNA polymerase	0.5 μl

Thermocycler conditions:

1. 94 ºC 2 min
2. 94 ºC 30 sec
3. 60 ºC 30 sec
4. 72 ºC 30 sec

   repeat step 2- 4 10x

5. 94 ºC 30 sec
6. 56 ºC 30 sec
7. 72 ºC 30 sec

   repeat step 5-7 35 x

8. 72 ºC 5 min
9. 8CºC hold

PCR fragment was purified with a QIAGEN PCR purification Kit (QIAGEN, Cat No. 28104) and yield was quantified with a Nanodrop spectrophotometer. gRNA was transcribed with a MegaScript T7 Kit (Ambions, Cat. No. AM1334).

Reaction:

H_2O	6 μl
ATP 75 mM	2 μl
CTP 75 mM	2μl
GTP 75 mM	2 μl
UTP 75 mM	2 μl
10x Buffer	2 μl
PCR fragment	2 μl
Enzyme Mix	2 μl

Reaction was incubated at 37 ºC for 4 hours. After reaction, 0.5 μl of DNaseI was added to the reaction and incubated at 37 ºC for 20 minutes. gRNA transcription was assessed on a 2% agarose gel.

RNA was precipitated by adding:

H_2O	160 µl
Na OAc	20 µl
2-Propanol	200 µl

Reaction was incubated on ice for 30 minutes. After incubation, reaction was centrifuged at 15,000g for 15 minutes at 4 ºC. Supernatant was removed and RNA was washed with 200 µl of 70% ethanol and centrifuged again. Supernatant was removed and gRNA pellet was air dried for 20 minutes. gRNA was dissolved in 40 µl of nuclease free H_2O. Concentration was measured with a Nanodrop spectrophotometer and stored in 5 µl aliquots at -80 ºC.

2.2.2.2 Injection conditions

For every experiment, 10 µl of the reaction in Table 2.4 was prepared fresh:

Component	Volume
crRNA 100 µM	1 µl
tracrRNA 100 µM	1 µl
Nuclease-Free-Duplex Buffer	8 µl

Table 2 .4 crRNA + tracrRNA reaction.

The reaction in Table 2.5 was incubated at 95ºC and then allowed to cool down at room temperature before adding the Cas9 protein as follows:

Component	Volume
crRNA + tracrRNA reaction	2 µl
Cas9 700 ng/µl	5 µl
Phenol red	1 µl

Table 2 .5 Cas9 protein + crRNA + tracrRNA reaction.

For gRNA, the reaction in Table 2.6 was made.

Component	Volume
gRNA 420 ng/μl	1μl
Cas9 700 ng/μl	9 μl
Phenol red	1 μl

Table 2 .6 Cas9 protein+ gRNA reaction

A volume of 5 nl of either crRNA or gRNA reaction was injected within the first 10 minutes after fertilization directly to the animal pole. After injection embryos were incubated at 28.5ºC until 5 dpf and then raised until adulthood for identification of potential carriers.

2.2.2.3 Identification of mutant carriers

F_0 adults were outcrossed to a wild type strain, from the resulting F_1, DNA was extracted from eight embryos per cross. The targeted region was amplified and sequenced to look for potential mutation carriers. The remaining sibling embryos of those crosses that showed frame shifts or stop codons were grown. The F_1 adults were subsequently genotyped (see section 2.2.3) and identified carriers of the same mutant allele were in crossed. The pigment phenotype of the F3 larvae was assessed, imaged and genotyped at 5 dpf.

2.2.3 Genomic DNA isolation

Genotyping of fish was performed by either swabbing a sample of the external mucus of adult fish or single embryo genotyping. DNA extraction was performed using a NaOH solution or a KAPA Express Extract Kit. The following section describes the specifics of each method.

2.2.3.1 Solutions

KAPA Express Extract lysis solution

- 88 µl of PCR grade H_2O
- 10 µl of 10x KAPA express extract buffer
- 2 µl of KAPA express extract enzyme

NaOH 50 mM

Dissolve 0.01 g of NaOH in 50 ml of distilled water.

Tris 1M pH 8

Dissolve 6.057g Tris (American Bioanalytical, Cat. No. AB14042) in 40 ml distilled water. Adjust pH to 8.0 with the appropriate volume of concentrated HCl. Bring final volume to 50 ml with distilled water.

2.2.3.2 Sample collection

A sample of the external mucus of the fish was take using the tip of a cotton bud (Fig. 2.2 A) and kept in a 1.5 ml conical tube on ice (Fig. 2.2 B) until processing. Alternatively, single embryos or larvae where processed as follows.

2.2.3.3 Sodium hydroxide extraction

After sample collection, 50 µl of NaOH 50mM was added directly to the tip of the cotton bud (Fig. 2.2 B), Samples were heated inside the 1.5 ml conical tube at 75ºC (Fig. 2.2 C) for 15 min. The cotton bud was transferred to a new 1.5 ml conical tube containing a pre cut 500 µl tube and centrifuged for 1 min at 13, 500 rpm (Fig. 2.2 D) to recover the DNA sample to which 5 µl of 1M Tris-HCl pH 8 was added (Fig. 2.2 E). Samples were stored at -20ºC until further use and 1 µl of sample was used for subsequent genotyping.

2.2.3.4 KAPA Express Extract Kit extraction

After sample collection, DNA extraction was performed using the KAPA Express Extract Kit extraction (Kapa Bio Systems, Cat. No. KR0383 – v3.15). 100 µl of KAPA express extract lysis solution was added directly to the tip of the cotton bud (Fig. 2.2 B). Samples were heated inside the 1.5 ml conical tube (Fig. 2.2 C), at 60 ºC for 5

min and then at 90 ºC for 10 min. The cotton bud was transferred to a new 1.5 ml conical tube containing a 500 µl conical tube (Fig. 2.2 D), to which the bottom was previously cut and centrifuged for 1 min at 13, 500 rpm to recover the DNA sample (Fig. 2.2 E). DNA concentration was measured using a Nanodrop 2000 and diluted to a concentration of 10ng/µl. Samples were stored at -20ºC until further use and 1 µl of sample was used for subsequent genotyping.

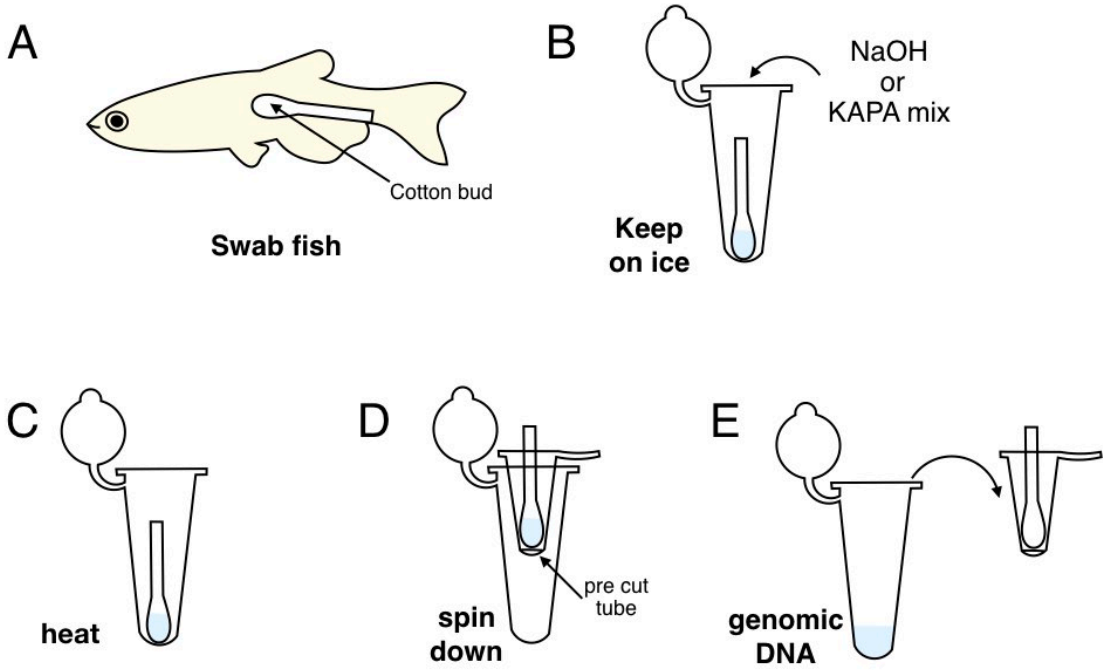

Figure 2.2 DNA extraction from swabbed samples. Fish were swabbed with a cotton bud (A). Samples were kept on 1.5 ml conical tubes on ice (B) until further processing. 50 µl of either NaOH 50 mM or KAPA extraction mix was added to the tip of the cotton bud inside the tube. Afterwards the sample were heated (C; see text for details). The cotton bud was transferred to a new 1.5 ml conical tube containing a pre cut 500 µl conical tube (D) the sample was then spin down to recover the genomic DNA sample (E).

2.2.4 PCR-Based genotyping

To genotype alleles with a 4 bp deletion, primers were designed with the 5' end overlapping the region of the deletion, so that in a WT background, a primer complementary to the wild type sequence would generate a PCR product, but not in a mutant background. Correspondingly, a primer complimentary to the mutant sequence, would produce amplification in a mutant background but not in a wild type background.

Reaction conditions in Table 2.7 were set up according to the manufacturer's instructions adjusting the volume to 15 μl per reaction.

Component	Volume	Final Concentration
10X Buffer	1.50 µl	1 X
25 mM MgSO4	0.90 µl	1.5 mM
dNTPs 2 mM	1.50 µl	0.2 mM
Fw Primer 10 µM	0.45 µl	0.3 µM
Rv Primer 10 µM	0.45 µl	0.3 µM
KOD Hot Start DNA Polymerase (1 U/µl)	0.30 µl	0.02 U/µl
Template DNA	1.00 µl	1.0 μg
PCR Grade Water	8.90 µl	

Table 2 .7 PCR reaction conditions

The reaction was carried out according t the condition on Table 2.8.

Step	Condition
Polymerase activation	95°C for 2 min
Denature	95°C for 20 s
Annealing	Lowest Primer Tm°C for 10 s*
Extension	70°C for 10 s/kb
Hold	4ºC

Table 2 .8 PCR thermocycler conditions

* Specific Tm temperature are listed in appendix A

2.2.5 Sequencing-based genotyping

2.2.5.1 PCR

Amplification of the desired gene region was performed using a REDTaq® ReadyMix™ PCR Reaction Mix (Sigma-Aldrich, Cat. No. R2523). Based on the manufacturer's instructions. The volume of the reaction on Table 2.9 was optimised for a 20 µl reaction.

Component	Volume
REDTaq® ReadyMix™ PCR Reaction Mix	10 µl
Fw Primer 10nM	1 µl
Rv Primer 10nM	1 µl
PCR grade H_2O	7 µl
DNA template	1 µl

Table 2 .9 PCR reaction conditions

The reaction on Table 2.10 was performed for 25 cycles using an Eppendorf Mastercycler S Ep ep Gradient S Thermal Cycler 5341 with the following condition:

Step	Condition
Denature	94°C for 1 m
Annealing	55°C for 2 m*
Extension	72°C for 3 min
Hold	4ºC

Table 2 .10 PCR thermocycler conditions

2.2.5.2 Sequencing labelling

Sequencing was performed in the facilities of the Max-Planck Institute for Developmental Biology. After amplification of the desired gene region, the reaction on Table 2.11 was prepared in a total volume of 10 µl.

Component	Volume
BDT RRMix	0.5 µl
5x Buffer	1.9 µl
PCR template	1.0 µl
Fw or Rv Primer 3.5 µM	1.0 µl
PCR Grade Water	5.6 µl

Table 2 .11 Fluorescent labelling reaction conditions for sequencing. The reaction was performed in an Eppendorf Mastercycler ep Gradient 5341 for 25 cycles.

The above-mentioned reaction was then carried out on the condition described on Table 2.12

Step	Condition
Rapid thermal ramp to	96°C for 20 s
Rapid thermal ramp to	50°C for 10 s
Rapid thermal ramp to	60°C for 4 min
Hold	4ºC

Table 2 .12 Thermocycler conditions for sequencing.

After labelling reaction, samples were handled to the sequencing facility of the Max-Planck Institute for Developmental Biology.

2.2.5.3 Sequence visualisation and alignment

Chromatograms were visualised using the software SeqMan Pro V14.0.0.88, the free version of the software SnapGene Viewer V4.1.0 or the free software ApE- A plasmid editor V2.0.49.10.

2.2.6 Single embryo phenol Chloroform RNA isolation

Single embryos were collected in 1.5 ml conical tubes and rinsed with distilled water 3 times. The sample was homogenised with 20 µl of 24:1 chloroform/isoamyl (Sigma-Aldrich, Cat. No. 2069) and mechanical disruption of the tissue was performed with

a maximum recovery 200p tip. The sample was centrifuged at 12,000g for 15 min at 4ºC. 10 μl of the aqueous layer was recovered into a new 1.5 ml UV sterilised conical tube adding 25 μl of isopropanol and mixed by inversion 3 times. The sample was centrifuged at 12,000g for 10 min at 4ºC. The supernatant was decanted and 50 μl of 75% cold ethanol was added and mixed by inversion 3 times. The sample was centrifuge at 12,000g for 5 min at 4ºC. The supernatant was decanted and the pellet air dried for 10 min. To resuspend the RNA, 20 μl of RNAse free water was added directly to the RNA pellet and left on ice for 5 min to allow the pellet to dissolve.

2.2.6.1 RNeasy Plus Micro Kit RNA isolation

RNA extraction from sorted cells was performed using the RNeasy Plus Micro Kit (QIAGEN, Cat. No.79654). Based on the manufacturer manuals the volumes were adapted to the requirements of the experiment.

2.2.6.2 Solutions

RLT + β-ME buffer

- Add 20 µl β-ME (Sigma-Aldrich, Cat. No. M6250) per 1 ml Buffer RLT Plus. This solution can be kept at room temperature for up to a month.

70% ethanol

- Dilute ethanol 100% (VWR, Cat No. 20821-330) with distilled water.

RPE buffer

- Add 4 volumes of ethanol 100% as indicated on the bottle.

80% ethanol

- Prepare 80% ethanol by mixing 24 ml ethanol 100% and 6 ml RNase-free water supplied in the kit.

2.2.6.3 Procedure

After sorting cells into the RLT + β-ME buffer, the cell lysate was pipetted to a QIAshredder homogenizer (QIAGEN, Cat. No. 79654) and centrifuged for 2 min at full speed. The homogenized lysate was then transferred to a gDNA Eliminator spin column and centrifuged for 30 s at 10,000 rpm. 1 volume of 70% ethanol was added to the flow through and mixed by pipetting.

The sample was transferred to an RNeasy MinElute spin column and centrifuged for 15 s at 10,000 rpm. The flow-through was discarded and the column membrane was washed with 700 µl of buffer RW1 and centrifuged for 15 s at 10,000 rpm, then washed with 500 µl of buffer RPE and centrifuged for 15 s 10,000 rpm and finally washed with 500 µl of 80% ethanol and centrifuged for 2 min at 10,000 rpm. Prior to elution, the RNeasy MinElute spin column was placed in a new 2 ml collection tube with the lid open and centrifuged at full speed for 5 min to dry the spin column membrane.

To elute the sample, the RNeasy MinElute spin column was placed in a new 1.5 ml conical tube and 14 µl of RNase-free water was added directly to the centre of the spin column membrane and centrifuged for 1 min at full speed. RNA concentration was measured using a Nanodrop NanoDrop (Thermo Fisher Scientific, 2000) or Qubit™ 4 Fluorometer (Q33226) and samples were stored at -20ºC until further use.

2.2.7 RNA Quality analysis

RNA concentration was measured using a Qubit RNA HS Assay Kit following the manufactures instructions (Thermo Fisher Scientific, Cat. No. Q32852). The 260/280 ratio was measured using a NanoDrop (Thermo Fisher Scientific, 2000) and RNA integrity was observed in a bleached gel (Aranda et al. 2012). A bleached gel was prepared by adding 1.0% w/v agarose to 1x TAE, 1% v/v commercial bleach and then incubated for 5 min at room temperature. The suspension was heated to melt the agarose and allowed to cool before adding ethidium bromide to a final concentration of 0.5 µg/ml. A minimum of 100 ng of RNA was ran in 1x TAE at 100V for 35 minutes and visualized by UV transillumination.

2.2.8 RT-PCR

Reverse transcription was performed using the iScript cDNA Synthesis Kit (BIO-RAD, Cat. No. 1708890) and cDNA amplification of the desired genes was performed using a KOD Hot Start DNA Polymerase (Merk, Cat. No. 710086).

2.2.8.1 cDNA synthesis

Reverse transcription was performed in 20 µl reactions (Table 2.13) following the manufacturer manuals. The reaction condition are described on Table 2.14.

Component	Volume
5X iScript Reaction Mix	4 µl
iScript Reverse Transcriptase	1 µl
RNA template 100ng/µl	1 µl
Water	14 µl

Table 2 .13 Reverse transcription reaction conditions

Step	Condition
Priming	5 min at 25 ºC
Reverse transcription	20 min at 46 ºC
Reverse transcriptase inactivation	1 min at 90 ºC
Hold	4 ºC

Table 2 .14 Reverse transcription thermocycler conditions

2.2.8.2 PCR

Reaction conditions (Table 2.15). were set up according to the manufacturer adjusting the volume to 15 µl per reaction.

Component	Volume	Final Concentration
10X Buffer	1.50 µl	1 X
25 mM MgSO4	0.90 µl	1.5 mM
dNTPs 2 mM	1.50 µl	0.2 mM
Fw Primer 10 µM	0.45 µl	0.3 µM
Rv Primer 10 µM	0.45 µl	0.3 µM
KOD Hot Start DNA Polymerase (1 U/µl)	0.30 µl	0.02 U/µl
Template DNA	1.00 µl	1.0 µg
PCR Grade Water	8.90 µl	

Table 2 .15 PCR reaction conditions

The above mentioned PCR reaction was carried out with the conditions on Table 2.16.

Step	Condition
Polymerase activation	95°C for 2 min
Denature	95°C for 20 s
Annealing	Lowest Primer Tm°C for 10 s*
Extension	70°C for 10 s/kb
Hold	4ºC

Table 2 .16 PCR thermocycler conditions

* Specific Tm temperature are listed in appendix A

2.3 Immunostaining protocol

2.3.1 Solutions

PBS

1 PBS tablet was dissolved (Gibco, Cat. No. 18912-014) in 500 ml of distilled water and sterilised by autoclaving.

PFA

PFA (Sigma-Aldrich, Cat. No. P6148) powder was dissolved in PBS to a concentration of 4% w/v. Aliquots of 35 ml were stored at -20 ºC and thawed only once and used within two weeks.

PBT

- Triton-X 100 (Sigma-Aldrich, Cat. No. T9284) was diluted in PBS to a 0.5% v/v concentration.

Stop solution

- Goat serum (Vector, Cat, No. S-1000) was diluted in distilled water to a 5% v/v concentration

Blocking Solution

To prepare blocking solution, goat serum and DMSO were diluted in PBT as follows:

- 5% v/v goat serum.
- 1% v/v DMSO (Sigma-Aldrich, Cat. No. D8418).

2.3.2 Fixation

Embryos where anesthetised in tricaine diluted in embryo medium to a concentration of 0.01% v/v and transferred to a 1.5 ml conical tube. The embryo medium was removed as much as possible before adding 1ml of PFA per 25-30 embryos. Fixation was carried out for 3 hours at room temperature with agitation or overnight at 4ºC with agitation. Fixative was washed with 0.5% Triton-X 100/PBS for 4x5 minutes. Embryos where immediately processed or stored in PBS/Sodium azide 5mM (Sigma-Aldrich, Cat. No. S-8032) at 4ºC for up to two weeks.

2.3.3 Permeabilization

All steps were performed using between 25 and 30 embryos in 10 ml glass bottles. Embryos younger than 40 hpf were permeabilized with distilled water 3x1 hour. Embryos older than 40 hpf were permeabilized with 1 ml of proteinase K (Ambion. Cat. No. AM2546) at 37ºC. Concentration and incubation times are shown in the following Table 2.17..

Stage	[PK]	Time
2-3 dpf	5 μg/ml	30 min
4-5 dpf	15 μg/ml	15 min
7 dpf	15 μg/ml	15 min

Table 2 .17 Proteinase K (PK) permeabilization conditions.

To stop permeabilization reaction, the proteinase solution was removed and 1 ml of stop solution was added for 5 min in agitation at room temperature. Subsequently, samples were permeabilized with distilled water 3x1 hour.

2.3.4 Antibody incubation

Prior to antibody incubation embryos were incubated in blocking solution for 3 hours at room temperature. The primary and secondary antibodies were diluted in blocking solution as shown in Table 2.18. The primary antibody was incubated overnight at room temperature with agitation and washed with 0.5% Triton-X 100/PBS 1x5 minutes and 3x1 hours. The secondary antibody was incubated for 3 hours at room

temperature or overnight at 4ºC, both with agitation protected from light. For counterstaining, 2 mg/ml of DAPI (Roche, Cat. No. 10236276001) was added to the secondary dilution in a 1:1000 ratio. The secondary antibody and DAPI were washed 1x5 minutes and 6x30 minutes. Finally, embryos were cleared overnight in 50% glycerol (Fisher. Cat. No. BP229-1)/PBS at 4ºC. For long term storage sample were kept at -20 ºC.

Antibody	Dilution
Mouse α -Hu	1:400
Mouse α -TH	1:200
Rabbit α -Sox10	1:100
Mouse α -PH3	1:500
Rabbit α -PH3	1:500
Mouse α -GFP	1:750
Rabbit α -GFP	1:750
Chicken α -GFP	1:500
Goat α -Mouse AF488	1:750
Goat α -Mouse AF546	1:750
Goat α -Rabbit AF488	1:750
Goat α - Rabbit AF546	1:750
Goat α -Chicken AF 633	1:500

Table 2 .18 Primary and secondary antibody dilution. For details on the antibodies on appendix B.

2.3.5 Sample mounting

Prior to mounting, samples were dissected one at a time in a dark room under a stereoscope using low transmitted light to prevent bleaching of the fluorochromes. For dissection, a single embryos was placed on a clean regular slide with as little glycerol as possible. For larvae between 24-72 hpf, the yolk sac was dissected away (Fig. 2.3 A) using the bevel of a dissecting needle as a blade. For 3-7 dpf larvae the head was removed (Fig. 2.3 B) to prevent the embryo from lying at a tilt. After dissection, the embryo was transferred into clean glycerol:PBS 50% and rinsed to avoid debris from the yolk when imaging.

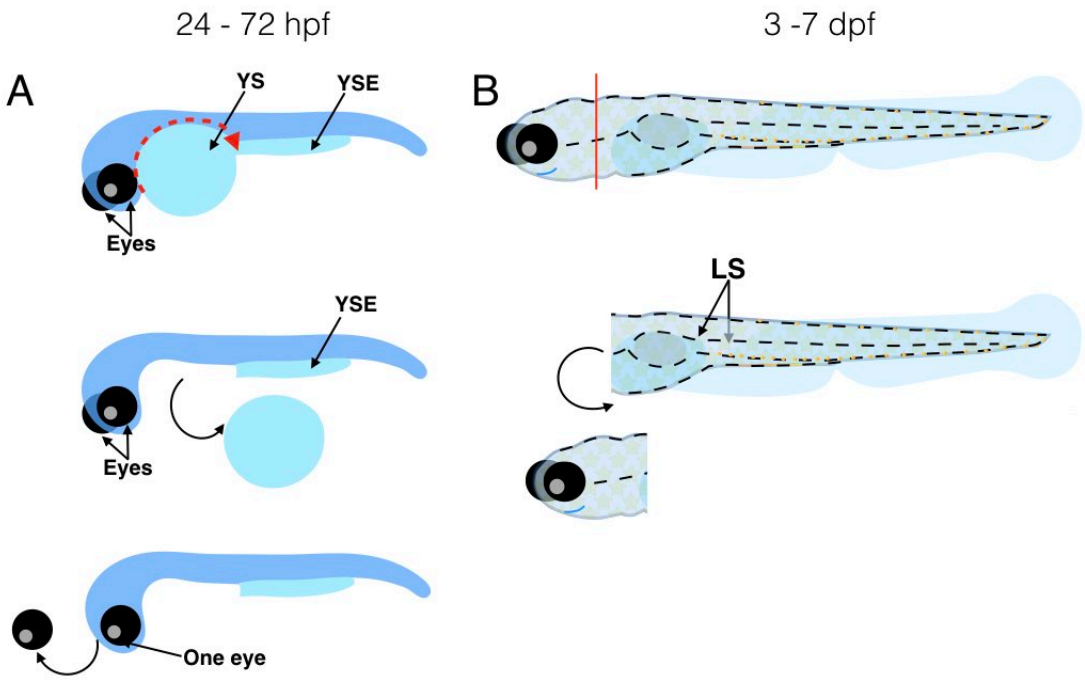

Figure 2.3 Dissection of fixed embryos for mounting. Scheme shows lateral view of dissection method for embryos between 24-72 hpf (A). The yolk sac (YS) was removed by cutting as shown by the red dashed arrow leaving the yolk sac extension (YSE) intact; when necessary, an eye was removed to prevent the head from tilting to one side. For 3-7 dpf the head was removed to prevent the trunk from tilting to one side (B).

For mounting the sample, imaging slides (Figure 2.4 A) prepared by gluing one 22x22 mm coverslip (Disher, Cat. No. FB-58633) in one side of a standard slide (VWK, Cat. No. 1508037). Using a dissecting needle, the sample was placed on the imaging slide approximately 1 cm away from the glued coverslip. Special care was taken to align the embryo laterally with the head towards the glued coverslip. The sample was covered with 5 μl of 50% glycerol before covering with a coverslip. Using forceps, the sample was covered from left to right with a new coverslip by resting the left side of it on the glued coverslip and carefully lowering the new coverslip over the sample. With a glass pipette, the space around the sample was filled with glycerol:PBS 50% to prevent the sample from drying. Using nail polish, the sample was sealed around the edges of the coverslip covering the sample (Fig. 2.4 B).

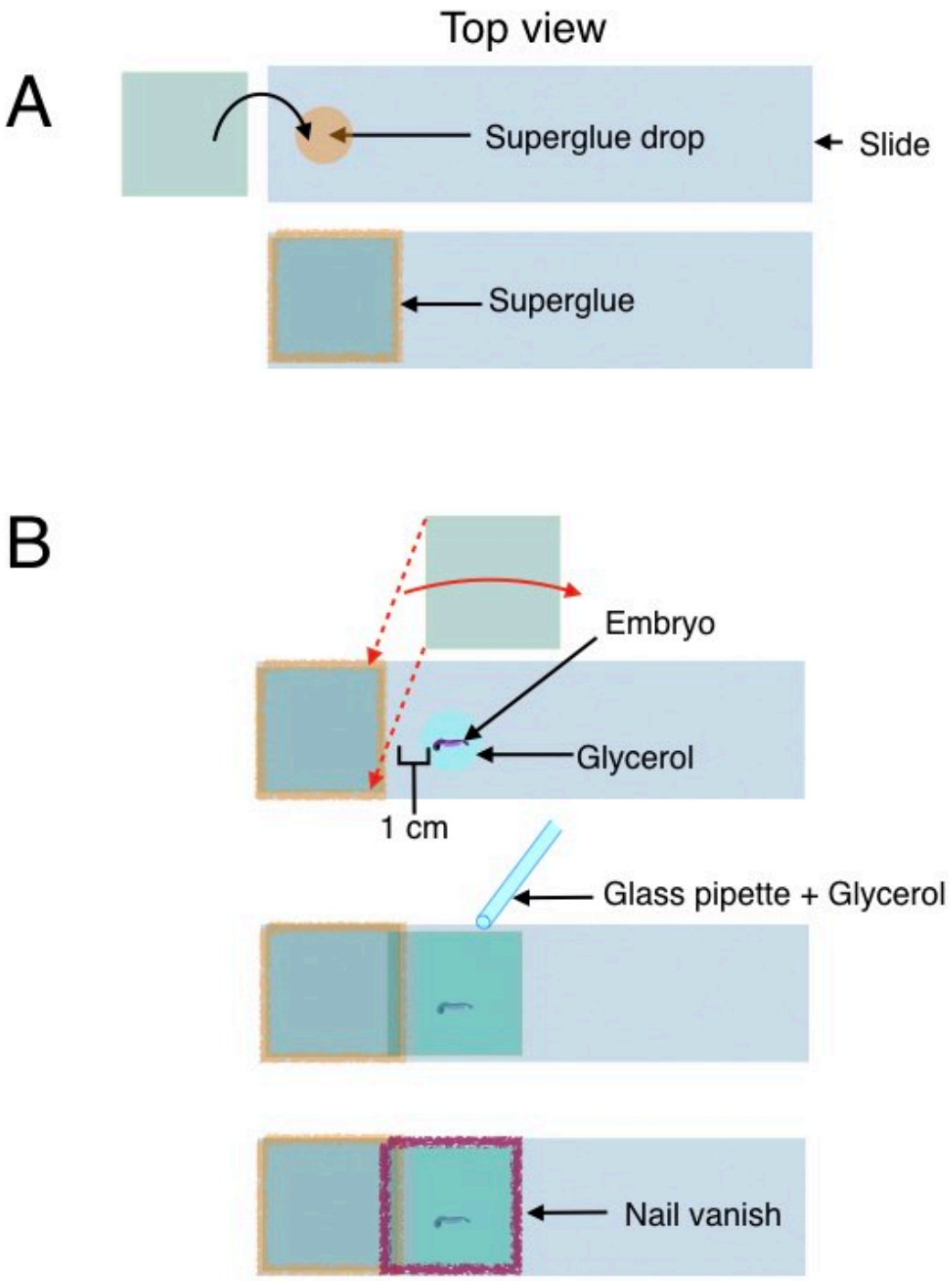

Figure 2.4 Mounting of fixed sample for imaging. (A) Scheme shows preparation of slide for imaging consisting of a standard slide to which a coverslip was attached with super glue. (B) A previously dissected sample was placed 1 cm away from the glued sample and covered with glycerol, the sample was covered with a new coverslip resting one side of it over the glued coverslip. Using a glass pipette, more glycerol was added under the coverslip to prevent the sample from drying. Finally, then mounted sample was sealed with nail vanish (purple line).

2.3.6 Image acquisition

Epifluorescent images were acquired using a Zeiss Axio Vision compound microscope with an Apotome2.0 device. Confocal imaging was performed in a Zeiss LSM880 confocal microscope using a 20X air objective and a 40X oil objectives. For high resolution, images were acquired using the super resolution Airy scan tool. For all images, a stack with the optimal slice distance was acquired using the optimal frame size, an averaging of 4 times with a single acquisition direction and minimum of 12 bit.

2.4 Pharmacological treatments

2.4.1 Stock preparation

All inhibitors were dissolved in DMSO at a concentration of 10 mM and stored at -20ºC protected from light. Details on each inhibitor are listed on appendix C.

2.4.2 Treatment conditions

Treatment was performed in 12-well plates (Nucleon, Cat. No.142475) using 2 ml of working dilution per well and 6 embryos per well were treated. Inhibitors where diluted to the working concentration in 1% DMSO/Embryo medium. As a control, the equivalent volume of DMSO was added instead of inhibitor. Treatment was performed at either 23ºC or 28ºC protected from light. After treatment, embryos were washed three times with fresh embryo medium and incubated at 28ºC until the phenotype was assessed at 4-5 dpf.

2.5 Fluorescence Activated Cell Sorting

2.5.1 Solutions

HBSS 1X

To prepare 50 ml of HBSS 1X, 5 ml of HBSS 10X (Thermo Fisher Scientific, Cat. No. 14185-045) were diluted in 42 ml of distilled water. 235 μl of 7.5% sodium bicarbonate solution (Thermo Fisher Scientific, Cat. No. 25080094) and adjust the pH was

adjusted to 7.0–7.4 as necessary using 1 N HCl or 1 N NaOH. The volume was adjusted to 50 ml with distilled water and the solution was filter and stored at 4 ºC.

HBSS$^{+/+}$

For 50 ml of solution the following reagents were diluted as follows:

Reagent	Amount	Final []
- HBSS 1X	45 ml	1X
- BSA (Sigma-Aldrich, Cat. No. A3059)	125 mg	0.25 %
- HEPES 1M (Thermo Fisher Scientific, Cat. No. 15630-056)	0.5 ml	10 mM

The volume was adjusted to 50 ml with distilled water, filter sterilized and stored at 4 ºC.

Ringer solution (-Ca2^{+}/-Mg)

To prepare 50 ml of ringer solution, the following solutions were mixed as follows:

Reagent	Amount	Final Concentration
- NaCl 5M (Fisher Scientific, Cat. No. S13120/65)	01.160 ml	116 mM
- KCl 1M (Sigma-Aldrich, Cat. No. P-9541)	00.145 ml	2.9 mM
- HEPES 1M	00.250 ml	5 mM
- H_2O	48.445 ml	

The solution was then filter sterilize the solution and store at 4 ºC.

De-yolking buffer

To prepare 10 ml of solution, the following solutions were mixed as follows:

Reagent	Amount	Final []
- Ringer solution	10 ml	
- EDTA 0.5 M (Thermo Fisher Scientific, Cat. No.AM9260G)	20 µl	1 mM

Collagenase/Trypsin

Aliquots of 20 mg of collagenase were kept in 2 ml conical tubes and stored at -20 ºC. For every experiment a fresh solution was prepared as follows:

Reagent	Stock []	Amount	Final []
- Collagenase (Sigma-Aldrich, Cat. No. C8176)		20 mg	20 mg/ml
- Trypsin EDTA (Thermo Fisher Scientific, Cat. No.15400054)	0.05 %	1 ml	0.05 %

Stop solution

For 700 μl of solution, 50 μl of FBS (Thermo Fisher Scientific, Cat. No. A3160801) were diluted in 650 μl of $HBSS^{+/+}$.

$HBSS^{+/+}$/$Hoechst^{Dead}$ (1/10, 000)

For 10 ml of solution, 1μl of $Hoechst^{Dead}$ (Thermo Fisher Scientific, Cat. No. H1399) were dilute in 10 ml of $HBSS^{+/+}$.

2.5.2 Singe cell suspension

WT and *$pde^{tj262/tj262}$* fish with a *$Tg(fli1a:EGFP)^{y1}$ or $Tg(-4725sox10:cre)^{ba74}$*; *Tg(hsp:loxp-dsRed-loxp-EGFP* transgenes were used. The posterior trunk of 150 anesthetised embryos was manually dissected using a dissecting needle and collected in 1.7 ml low binding microcentrifuge tube (Sigma-Aldrich, Cat. No. CLS3207-250EA). 500 μl of de-yolking buffer was added and embryos were rinsed through a P200 tip 5 times and immediately spin down at 500 g at 4ºC. The supernatant was removed and 300-500 μl of collagenase/trypsin solution was added for 10-15 mins at 30°C homogenizing every 3-5 minutes with a P200 maximum recovery tip (Thermo Fisher Scientific, Cat. No.12649535). The reaction was stopped by adding 350μl of stop solution and the dissociated cells were spun down at 500 g for 5 min at 4ºC. The supernatant was discarded and cells were re-suspended in 600 μl of $HBSS^{+/+}$ solution. The cell suspension was passed through a 40 µm cell strainer (Sigma-Aldrich. Cat. No. CLS431750-50EA) to a new 1.7 ml low-binding microcentrifuge tube and centrifuged for 5 minutes at 750g. Lastly the supernatant was removed and cells were finally re-suspend in 400 μl of HBSS+/+;$Hoechst^{Dead}$.

2.5.3 Sample Acquisition

Samples were acquired using a Becton Dickinson FACS Aria III with a 80 μm nozzle. A dot plot of the Forward Scatter (FSC) against the Side Scatter (SSC) was used to gate a main population (P1) of cells (Fig. 2.5 A). The P1 population of cells was then assessed for GFP and Hoechst^{Dead} fluorescence signal. A WT non-transgenic and non-Hoechst^{Dead} stained sample was used to establish the quadrants for negative and positive thresholds in both fluorescent signals (Fig. 2.5 B). The experimental single cell suspension of GFP and Hoechst^{Dead} stained cells was then analysed and a second population of cells (P2) in the positive quadrant for GFP but negative for Hoechst^{Dead} (Fig. 2.5 C) were then sorted using the purity condition. 250,000 cells were sorted directly to a 5 ml polystyrene tube containing 700 μl of RLT+ βME buffer. RNA isolation was performed using a RNEasy Micro Plus kit (see 2.2.7).

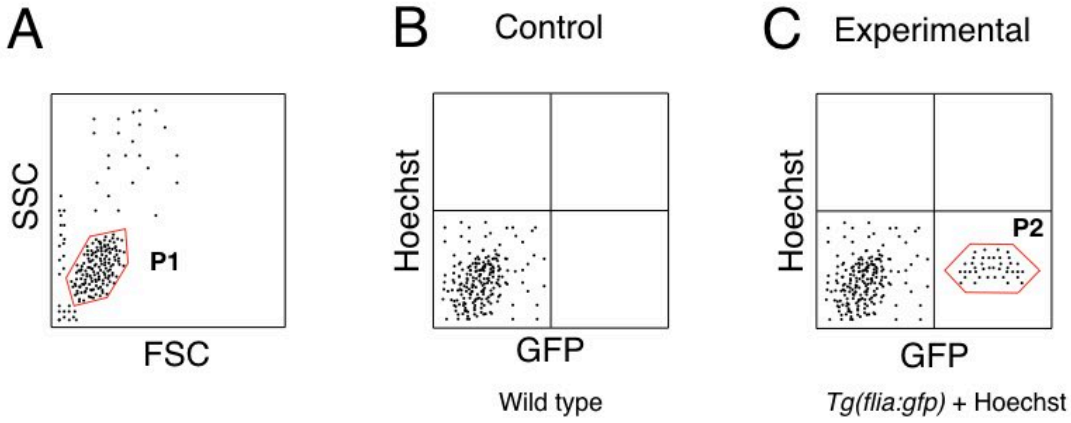

Figure 2.5 Establishment of negative and positive threshold for cell sorting. (A) Shows dot plot of Forward Scatter (FSC) against Side Scatter (SSC). The population 1 (P1) was then assessed for GFP and Hoechst signal (B). Quadrants were stablished using a single cell suspension of a wild type fish strain not stained with Hoechst. Once the thresholds had been established, a single cell suspension from a *Tg(flia:gfp)* or *Tg(-4725sox10:cre)^{ba74}; Tg(hsp:loxp-dsRed-loxp-EGFP* fish strain stained with Hoechst was assessed. Cells positive for GFP and negative for Hoechst were gated as a second population (P2) and sorted.

2.6 Clonal Induction

2.6.1 4-OHT stock preparation

A stock solution of 5mM of 4-hydroxytamoxifen (4-OHT; Sigma-Aldrich, Cat. No. H7904) was prepared by adding 2.58 ml of 100% ethanol to 5 mg of 4-OHT. Aliquots of 250 µl kept at -20ºC protected from light.

2.6.2 4-OHT treatment conditions

Homozygotes for the transgene *sox10:ER*$_{T2}$*Cre* were out-crossed to homozygotes for the transgene *β-actin2:loxPSTOPloxPDsRedexpress*. Embryos laid from a single cross were collected and sorted in batches of 40 embryos per petri dish and grown at 28.5 ºC in embryo medium without methylene blue. At 29 hpf embryos were dechorionated using microforceps and transferred to a new petri dish with a total volume of 1 ml using a plastic Pasteur-pipette. Immediately, 39 ml of fresh embryo medium without methylene blue was added using a measuring cylinder. 40 µl of 5mM of 4-OHT was added to each petri dish and mixed immediately to achieve a final concentration of 5 µM. Embryos were incubated for 1 hour at 28.5 ºC protected from light. After incubation, the embryos were washed three times with fresh embryo medium and kept at 28.5 ºC until screening.

2.6.3 Single clone screening

Expression of the DsRed transgene was allowed overnight before screening. Anesthetised embryos were placed in a 27 mm glass bottomed dish with embryo medium/0.02% tricaine and both sides of each fish were observed in a Zeiss LSM510 Meta confocal microscope using an air 20x objective and a fluorescent lamp. Embryos with single clones were sorted into 48-well dishes with 1 ml of fresh embryo medium and kept at 28.5 ºC until imaging.

2.6.4 Confocal imaging

Fish were imaged at different developmental stages using a Zeiss LSM880 confocal microscope. A 554 nm laser was use for excitation of the DsRed protein with a maximum of 2% of laser power and 1 airy scan unit. Images were acquired with an

20x air objective and 40x oil objectives. For super resolution, images were acquired using the Airy scan tool. For all images, a stack with the optimal slice distance was acquired using the optimal frame size, an averaging of 4 times with a single acquisition direction and minimum of 12 bit.

2.7 Image processing and statistical Analysis

Images were processed using the Zen Blue package or the free software FIJI, the resulting projections were digitally enhanced for contrast and exposure using the software Photoshop CC 2018. Statistical analyses were performed using the package Graph Pad Prism 6 (License).

CHAPTER 3

This declaration concerns the article entitled:									
Endothelin receptor Aa regulates proliferation and differentiation of Erb-dependant pigment progenitors in zebrafish.									
Publication status (tick one)									
draft manuscript		**Submitted**	X	**In review**		**Accepted**		**Published**	
Publication details (reference)	Chapter 3 contains the first manuscript submitted to PlosGenetics.								
Candidate's contribution to the paper (detailed, and also given as a percentage).	The candidate considerably contributed to Formulation of ideas: 25% Design of methodology: 25% Experimental work: 62.5% Presentation of data in journal format: 70%								
Statement from Candidate	This paper reports on original research I conducted during the period of my Higher Degree by Research candidature.								
Signed						**Date**	28/09/18		

CHAPTER 3 Endothelin receptor Aa regulates proliferation and differentiation of Erb-dependant pigment progenitors in zebrafish.

Karen Camargo-Sosa[1], Sarah Colanesi[1], Jeanette Müller[1], Stefan Schulte-Merker[2], Derek Stemple[3], E. Elizabeth Patton[4] and Robert N. Kelsh[1]*

[1]Department of Biology and Biochemistry and Centre for Regenerative Medicine, University of Bath, Claverton Down, Bath BA2 7AY, UK

[2]Hubrecht Institute, Uppsalalaan 8, 3584 CT Utrecht, Netherlands (current address, Institute for Cardiovascular Organogenesis and Regeneration, Faculty of Medicine, WWU Münster, Münster 48149, Germany)

[3]Wellcome Genome Campus, Hinxton, Cambridgeshire, CB10 1SA, UK

[4]MRC Human Genetics Unit, MRC Institute of Genetics and Molecular Medicine, University of Edinburgh, Western General Hospital, Crewe Road, Edinburgh EH4 2XR, UK

*Corresponding author: bssrnk@bath.ac.uk

Abstract

Skin pigment patterns are important, being under strong selection for multiple roles including camouflage and UV protection. Pigment cells underlying these patterns form from adult pigment stem cells (APSCs). In zebrafish, APSCs derive from embryonic neural crest cells, but sit dormant until activated to produce pigment cells during metamorphosis. The APSCs are set-aside in an ErbB signalling dependent manner, but the mechanism maintaining quiescence until metamorphosis remains unknown. Mutants for a pigment pattern gene, *parade*, exhibit ectopic pigment cells localised to the ventral trunk, but also supernumerary cells restricted to the Ventral Stripe. Contrary to expectations, these melanophores and iridophores are discrete cells, but closely apposed. We show that *parade* encodes Endothelin receptor Aa, expressed in the blood vessels, most prominently in the medial blood vessels, consistent with the ventral trunk phenotype. We provide evidence that neuronal fates are not affected in *parade* mutants, arguing against transdifferentiation of sympathetic neurons to pigment cells. Similar to mice, we showthat inhibition of BMP signalling prevents specification of sympathetic neurons, however, inhibition of sympathetic neuron differentiation does not enhance the *parade* phenotype. Instead, we pinpoint ventral trunk-restricted proliferation of neural crest cells as an early feature of the

parade phenotype. Importantly, using a chemical genetic screen for rescue of the ectopic pigment cell phenotype of *parade* mutants (whilst leaving the embryonic pattern untouched), we identify ErbB inhibitors as a key hit. The time-window of sensitivity to these inhibitors mirrors precisely the window defined previously as crucial for the setting aside of APSCs in the embryo, strongly implicating adult pigment stem cells as the source of the ectopic pigment cells. We propose that a novel population of APSCs exists in association with medial blood vessels, and that their quiescence is dependent upon Endothelin-dependent factors expressed by the blood vessels.

3.1 Introduction.

Pattern formation is a crucial aspect of development since it creates the functional arrangements of cell-types that allow an organism to thrive. Pigment pattern formation – the generation of correctly distributed pigments or pigmented cells within the skin or elsewhere in the body – is a case in point, with pigmentation crucial for diverse aspects of an animal's ecology, including avoidance of predators, kin recognition, mate selection, thermal regulation and UV protection.

In vertebrates, all pigment cells except those of the pigmented retinal epithelium, are derived from a transient embryonic tissue called the neural crest. Neural crest cells are multipotent, generating numerous types of neurons, glia, pigment cells and other derivatives. They are also highly migratory, moving from their origin in the dorsal neutral tube to occupy diverse sites throughout the embryo. Thus, correct positioning of the different cell-types is a crucial aspect of their development.

Pigment cells in mammals consist only of melanophores, making (and secreting) black eumelanin or yellow pheomelanin granules. In fish, amphibians and reptiles, pigment cells are much more diverse [1], allowing the generation of the varied and often beautiful pigment patterns these groups display. The zebrafish *Danio rerio* has rapidly become a paradigmatic example for the genetic and cellular study of pigment pattern formation [2-6]. Zebrafish pigment patterns consist of three pigment cells, black melanophores making melanin, yellow xanthophores making pteridines and carotenoids, and iridescent iridophores containing reflecting platelets [1].

Zebrafish, in common with most fish, develop two distinct pigment patterns, an early larval pigment pattern generated in the embryo by direct development of pigment cells

from neural crest cells, and an adult pattern formed during metamorphosis, mostly through the de novo differentiation of pigment cells from adult pigment stem cells (APSCs, also formerly known as melanophores stem cells; [7-9]). The adult pigment pattern consists of prominent stripes consisting of melanophores and associated blue iridophores, alternating with pale stripes (interstripes) consisting of dense silver iridophores and xanthophores. Pigment pattern formation in adults is partially well characterised, with many genes identified that regulate the production of different pigment cell-types from the APSCs or which control their cellular interactions to create the bold horizontal stripe pattern. A key aspect of adult pigment pattern formation that is less well-understood is the generation of the APSCs from neural crest cells. Remarkably, elegant experimental studies from multiple laboratories have established that these are set-aside from the neural crest in a narrow time-window (9-48 hours post-fertilisation (hpf); [10]), with at least some occupying a niche within the dorsal root ganglia (DRGs; [9, 11]) of the peripheral nervous system. They remain quiescent until metamorphosis begins around 20 days post-fertilisation (dpf), when they become activated. The mechanisms controlling their quiescence and their activation are largely unknown.

Pigment pattern formation in embryos is also poorly understood [3]. The embryonic pigment pattern consists principally of four longitudinal stripes of melanophores, with iridophores arranged in a characteristic association with the melanophores in three of these (Dorsal, Ventral and Yolk Sac Stripes), whereas the Lateral Stripe consists only of melanophores; xanthophores then occupy the space under the epidermis between these stripes. Whereas in the adult the stripes are in the dermis, in the embryo they are associated with other structures, including the CNS, horizontal myoseptum of the body muscle blocks, the internal organs and the ventral most yolk sac. One study has investigated the detailed mechanism driving the association of melanophores with the horizontal myoseptum [12]. In general, stripes form through migration of pigment cell precursors down migration pathways used by neural crest. These neural crest migration pathways are known as the dorsal (or dorsolateral) migration pathway, consisting of cells migrating under the epidermis and over the outer face of the somites/developing muscle blocks, and the medial migration pathway, running between the neural tube and notochord and the medial face of the somites/developing muscle blocks [13]. Pigment cell precursors of different fates use distinct migration pathways. Thus, xanthoblasts only use the lateral migration pathway, iridoblasts use only the medial migration pathway, whereas melanoblasts use both [14-17]. Note that migrating pigment cell precursors often show early signs

of pigmentation i.e. they are differentiating as they migrate. During the migration phase, early differentiating melanophores and iridophores can be found in the ventral trunk on the medial migration pathway, but these have disappeared by 72 hpf as those cells migrate into the Ventral and Yolk Sac Stripes [16].

As in adult pigment pattern formation, mutants affecting embryonic pigment pattern offer an exciting entry-point to the study of the mechanisms controlling pigment pattern formation. In a large-scale ENU mutagenesis screen performed in 1996, we identified two zebrafish mutant alleles, *pde*^{tj262} and *pde*^{tv212}, that defined the *parade* (*pde*) gene [18]. These mutants showed ectopic melanophores and iridophores in a well-defined region of the ventral side of the posterior trunk (Fig. 3.1 B and E), in addition to a stripe pattern similar to the wild type (WT) pigment phenotype (Fig 3.1 A and C). The striking coincidence of melanin and reflecting platelet distribution lead us to initially propose that the *pde* mutant phenotype results from differentiation of pigment cells of mixed fate i.e. with both melanin granules and reflecting platelets within the same cell [18]. Here we perform a comprehensive analysis of the *pde* mutant phenotype. We show that the *pde* locus encodes a zebrafish Endothelin receptor A, Ednraa, which in the trunk is expressed only in the developing blood vessels, although in the head it is also expressed in cranial neural crest cells and is associated with craniofacial patterning [21]. Using chemical genetics, coupled with analysis of cell fate studies, we propose that APSCs occupy a niche associated with the medial blood vessels of the trunk, likely to be a second PNS niche within the sympathetic ganglion chain, and that these become precociously activated in *pde*/*ednraa* mutants. Thus, we hypothesise that key components of that blood-vessel niche are Ednraa-dependent factors that promote APSC quiescence.

3.2 Results

3.2.1 Early larval *pde* mutants have supernumerary iridophores in the ventral stripe and ectopic melanophores and iridophores in the posterior medial trunk .

To test our initial working model, that the ectopic cells are cells of mixed melanophores/iridophore fate, we began by asking exactly where the ectopic cells were located, and which pigment cell-types were involved. Whilst WT siblings at 5 dpf (Fig. 3.1 D) show no pigment cells in the ventral trunk between the notochord and the Ventral Stripe, in *pde*^{tj262} mutants (from now on referred to simply as *pde* unless specified otherwise) ectopic chromatophores are located in a medial position, directly beneath the dorsal aorta (DA) and above the posterior cardinal vein (PCV; Fig. 3.1 F). Thus, their location corresponds precisely to the ventral region of the medial neural crest migration pathway.

In zebrafish, pigment cell migration (both as unpigmented progenitors and as pigmenting cells) is pathway specific, with cells of the melanophore and iridophore, but not xanthophore, lineages using the medial pathway [3]. Direct observation clearly shows cells with the pigmentation characteristics of both melanophores and iridophores in this region of *pde* mutants, but detection of xanthophores by their pigmentation is difficult at these stages. Thus, to assess the presence of ectopic xanthophores, we used whole-mount *in situ* hybridisation (WISH) using fate-specific markers. Detection of the melanophore marker *dopachrome tautomerase* (*dct*; Fig. 3.1 J), the *iridoblast marker endothelin receptor ba* (*ednrba*; Fig. 3.1 K) and the xanthophore marker *GTP cyclohydrolase I* (*gch*; Fig. 3.1 L) at 72 hpf, provided clear confirmation that *pde* mutants display ectopic melanophores and iridophores, but importantly revealed the complete absence of ectopic xanthophores in the ventral trunk (Fig. 3.1 L).

Initial observations of *pde* mutants indicated the intriguing possibility that some of the ectopic chromatophores displayed mixed characteristics of both iridophores and melanophores, i.e. both reflecting platelets and melanin-containing melanosomes (Fig. 3.1 E and F; [18]). This suggested that the phenotype might result, at least in part, from a failure of the normal mutual repression of alternative pigment cell fates.

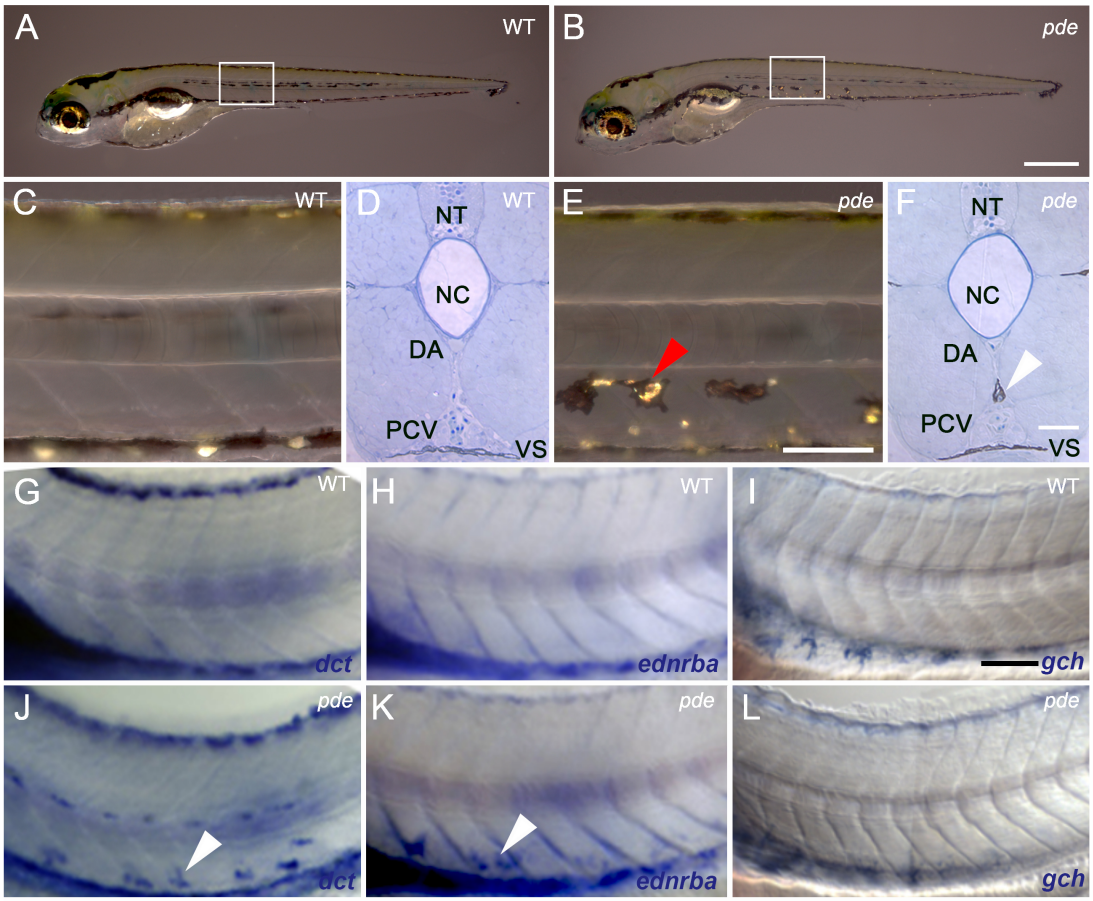

Figure 3.1 *pde* mutants display ectopic melanophores and iridophores, but not xanthophores, in the ventral medial pathway. (A,B) Overview of early larval WT (A) and *pde* (B) pigment phenotype at 5 dpf. (C-F) Anatomical location of ectopic pigment cells in *pde*. Magnification of lateral views (white boxes in A and B) and cross sections of posterior trunks show no pigment cells on the medial migration pathway in the ventral trunk of WT larvae (C and D). Ectopic pigment cells are located in the ventral trunk of *pde* mutants (E; red arrowhead), under the dorsal aorta (DA) and above the posterior cardinal vein (PCV) as shown by cross sections (F, white arrowhead). (G-L) Whole mount in situ hybridization of 3 dpf WT (G-H) and *pde* mutants (J-L) embryos for *dct* (G and J), *ednrba* (H and K), and *gch* (I and L). Ectopic *dct* (J; white arrowhead) and *ednrba* (K; white arrowhead) expression is seen in the ventral trunk of *pde* mutant larvae. Neural tube (NT), notochord (NC) and ventral stripe (VS). Scale bar = 500 μm (A and B) and 100 μm (C and F) and 50 μm (G-L).

To test this, we used transmission electron microscopy to assess the structure of the ectopic cells. Unexpectedly, we consistently saw that melanosomes, the melanin synthesising organelles of melanophores, and the reflecting platelets that contain the reflective crystals in iridophores, formed separate clusters, and were never intermingled (Fig. 3.2 A-C). Furthermore, these clusters were consistently separated from each other by double membranes (Fig. 3.2 A-C), similar to the appearance of melanophores and iridophores in the WT Yolk Sac Stripe (S Fig. 3.1), and consistent with there being separate cells. We conclude that the ectopic pigment cells are not of mixed fate, but instead are tightly associated individual melanophores and iridophores; we note that this arrangement is characteristic of iridophores in their normal locations, where in each of the Dorsal, Ventral and Yolk Sac Stripes iridophores are tightly associated with melanophores.

We hypothesised that the ectopic cells might reflect a defect in pigment cell migration through the ventral pathway, with cells that would normally contribute to the Ventral Stripe becoming stuck during migration. To test this, we quantitated the ectopic pigment cells and the cells of both the Dorsal and Ventral Stripes (Fig. 3.2 D-I). Our model predicted that the counts in the Dorsal Stripe would be unaffected, but that pigment cells in the Ventral Stripe might be reduced, perhaps in proportion to the number of ectopic cells.

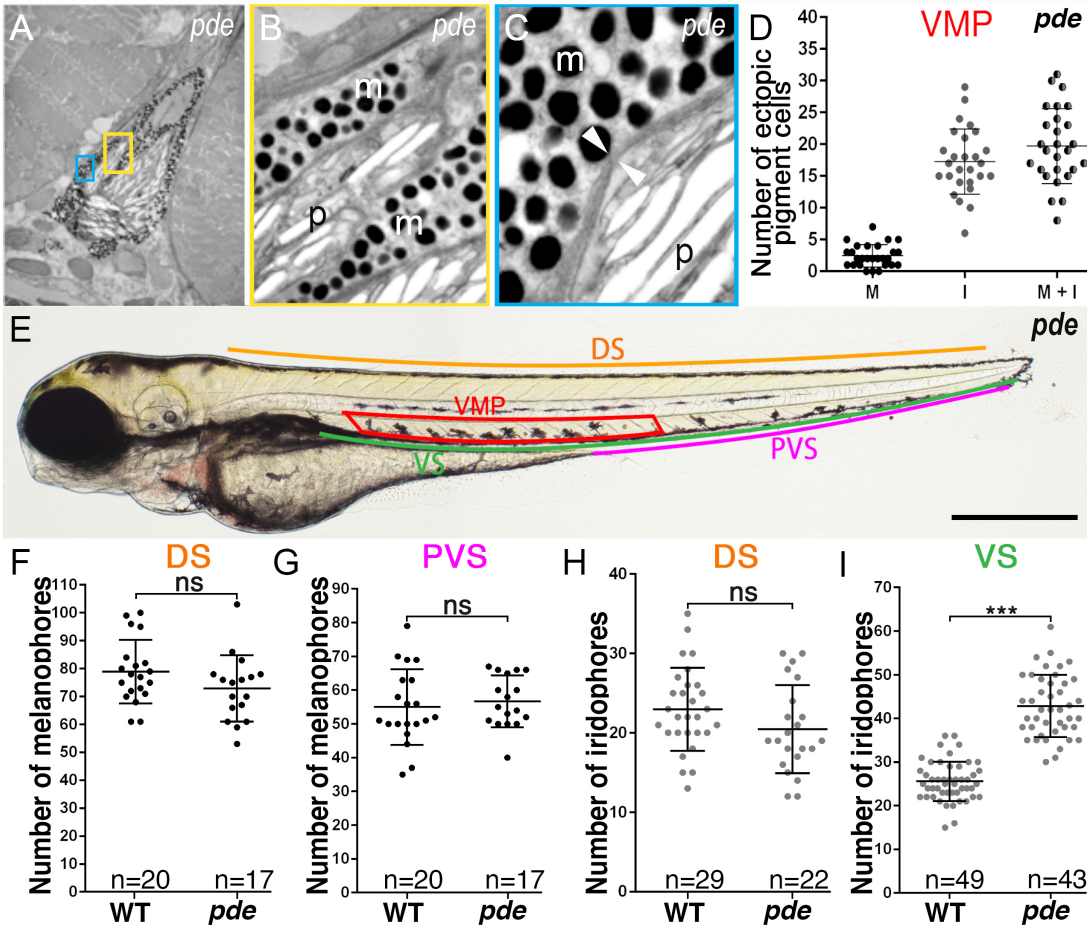

Figure 3.2 *pde* mutants show supernumerary melanophores and iridophores in the Ventral Stripe and nearby medial migration pathway, but not the Dorsal Stripe. (A-C) Transmission electron photomicrographs of ectopic pigment cells in *pde* mutants. Magnifications of yellow (B) and blue (C) boxes show melanosomes (m) and reflecting platelets (p) separated by a double membrane (C; white arrowheads). (D) Dot-plot of quantitation of ectopic melanophores (M), iridophores (I) and overall number of ectopic pigment cells (sum of melanophores and iridophores; M+I) from individual *pde* mutant larva at 4 dpf reveals a variable phenotype, with a consistently larger number of iridophores than melanophores in the ectopic position (iridophores mean + s.e.=17.26±0.99; melanophores mean + s.e.=2.44±0.34, n=27). (E) Regions where number of pigment cells were counted, Dorsal Stripe (DS; orange line), Ventral Stripe (V; green line), posterior Ventral Stripe (PVS; pink line) and ventral medial pathway (VMP, red box). (F-I) Quantitation of number of melanophores in dorsal (F; p>0.05, two-tailed t-test, WT mean + s.e.= 78.8+2.5, n=20 and *pde* m + s.e.=72.8 + 2.8, n=17) and posterior ventral stripes (G; wild-type: mean + s.e. 55.0 + 2.5 n=20; *pde*; 56.6 + 1.8, n=17) show no significant (ns) difference between WT and *pde* mutants. Iridophore quantitation in the DS (H; p>0.05, two tailed t-test, WT mean + s.e. = 22.9 + 0.9, n=29; *pde* mean + s.e. = 20.4 + 1.1, n=22) is not different between WT and

pde mutants while the ventral stripe has a 58% increased number of iridophores compared to WT embryos (I;***, $p<0.0001$, two-tailed t-test; WT mean + s.e. = 25.5 + 0.6, n=49; *pde* mean + s.e. = 42.8 + 1.0, n=43). Scale bar = 500 μm (E).

Quantitation of the ectopic pigment cells (melanophores + iridophores) in the ventral medial pathway revealed a variable phenotype, with a consistently larger number of iridophores than melanophores in the ectopic position (Fig. 3.2 D). The number of melanophores in the Dorsal (Fig. 3.2 F) and Ventral (Fig. 3.2 G) Stripes in *pde* mutants was not statistically different to those of WT siblings. Similarly, there was no significant difference in the number of iridophores in the DS of *pde* mutants and WT siblings (Fig. 3.2 H). Interestingly, and in contradiction to the disrupted migration model, the number of iridophores in the ventral stripe of *pde* mutants shows a 58% increase compared to WT siblings (Fig. 3.2 I). Thus, we reject the disrupted migration hypothesis, and instead note that *pde* mutants display a regionally localised increase in melanophores and iridophores in the ventral trunk, with some as supernumerary cells in the Ventral Stripe, but many in an ectopic position nearby.

3.2.2 *pde* encodes the *endothelin receptor Aa* gene

To identify the mutation that causes the *pde* phenotype we crossed *pde* heterozygotes onto a WIK wild-type background, and mapped the locus of the mutation using two sets of microsatellite markers, G4 and H2 [20]. The *pde* mutation showed strong linkage to markers Z15424 and Z23059 on chromosome 1, ~1.5 cM and ~3.8 cM away from the mutation, respectively (Fig. 3.3 A). Using the 8th version of the zebrafish genome assembly, further analysis showed that the marker P249 in clone BX51149 was only 0.2 cM (4 recombinants in 17959 embryos) away from the mutation, placing the *pde* mutation about 132 kb away in clone CU462997, in which three genes were annotated: 1) *mineralocorticoid receptor* (now renamed *nuclear receptor subfamily 3*, *group C*, *member 2*, *nr3c2*), 2) *Rho GTPase activating protein 10* (*arhgap10*), and 3) *endothelin receptor Aa* (*ednraa*). Of these three candidate genes, *ednraa* has been previously reported to be required in the development and patterning of the neural crest-derived ventral cranial cartilages. Furthermore, *ednraa* is expressed in the developing blood vessels of the posterior trunk [21]. This striking correlation between *ednraa* expression and the region with ectopic pigment cells in *pde* mutants made *ednraa* a strong candidate. Previous studies had not reported a

pigment phenotype during morpholino-mediated knockdown, but the focus in that work had been on craniofacial development, reflecting another region of *ednraa* expression [21].

To test the possible role of *ednraa* in pigment development, we used morpholino-mediated knockdown by injection of 1-2-cell stage wild-type embryos using the previously validated splice-blocking *ednraa*-morpholino (*ednraa*-MO1; Table 3.1 and Fig 3.3 B; [21]). As controls, we used injection of a random-sequence morpholino (cMO; standard control provided by Genetools) and the *ednrab* morpholino (*ednrab*-MO; S1 Table; [21]), neither of which resulted in ectopic pigment cells, nor any other disruption to the early larval pigment pattern (Fig 3.3 C). In contrast, after injection of *ednraa*-MO1 we saw ectopic melanophores and iridophores in the ventral medial pathway in a *pde*-like phenotype (Fig 3.3D). As a further test, we designed a new translation blocking morpholino against *ednraa* (*ednraa*-MO2, Table 3.1); injection of this morpholino phenocopied the *pde* mutant pigment phenotype, but also was prone to non-specific deformations, such as curved trunks, likely due to off-target effects (Colanesi, S. 2011). Together, these data strongly support the hypothesis that the *pde* mutants disrupt *ednraa* function.

Name	Target	Morpholino sequence (5'-3')
cMO	N/A	CCTCTTACCTCAGTTACAATTTATA
***ednrab*-MO**	splicing site	AGTGGTGTGTTCACCTGTTTGAGGT
***ednraa*-MO1**	splicing site	ATCAGACTTTTCTTTACCTGCTTAA
ednraa-MO2	translation	GCCATTGCAGAACACTGGCCGCTCT

Table 4 .1 Morpholino sequences. A random sequence morpholino (cMO) provided by Gen Tools and a splice-blocking morpholino against *ednrab* (*ednrab*-MO) were used as control. *ednraa* was targeted with either a splice-blocking morpholino (*ednraa-MO1*) or a translation-blocking *ednraa* morpholino (*ednraa-MO2*).

To assess directly the link between *pde* mutations and disruption of *ednraa* function we amplified *ednraa* cDNAs from *pde* mutant alleles to examine mRNA sequence and structure from mutants. In addition to the two original alleles, pde^{tj262} and pde^{tv212}, we also analysed pde^{hu4140}, a third mutation identified in an independent screen at the Hubrecht Institute which showed a phenotype indistinguishable from the original alleles, and which failed to complement those original alleles (S Fig. 3.2). This cDNA sequencing showed that pde^{hu4140} has a single base transition mutation in the 3' region of exon 5 (bp 847; AGA > TGA; Fig. 3.3 B), which is predicted to result in a premature translation stop in Ednraa. The pde^{tj262} and pde^{tv212} alleles each showed deletions, of 103 bp and 135 bp respectively. cDNA sequence alignment indicates a deletion of exon 7 and a couple of extra bases, predicted to cause a frame shift of translation in exon 8 in pde^{tj262}, while pde^{tv212} has a deletion of exon 6 and a couple of extra bases which results in a frame shift of translation in exon 7 and 8 of Ednraa (Fig. 3.3 B). Given that the pde^{tj262} and pde^{tv212} alleles were isolated from an ENU-mutagenesis screen and hence are likely to result from induced point mutations, we propose that the mutations in pde^{tj262} and pde^{tv212} are likely to affect key bases involved in *ednraa* splicing.

The Ednraa protein is a member of the rhodopsin-like G-protein coupled receptor family (GPCR, class A), and as such is characterised by seven transmembrane domains. In silico translation (S Fig. 3.5 A) and structural predictions (Fig. 3.3 C) for the *ednraa* alleles indicate that the N-terminus and the early transmembrane domains are likely to be intact, but that the other transmembrane domains and the C-terminus are absent. Our three *ednraa* mutant alleles show indistinguishable phenotypes, consistent with the similar predicted molecular effects of the mutations, and strongly indicating that the receptor is not functional. Consequently, we propose that these alleles are all likely null mutants, although formal proof of this will require generation of an N-terminal truncation allele. We used an *in situ* hybridization time-course between 6 and 72 hpf to assess the domain of *ednraa* expression, and in particular, whether it was detectable in neural crest or pigment cells. Our data was fully consistent with the earlier demonstration of *ednraa* expression in the developing blood vessels, but we saw no evidence of neural crest expression in the trunk (Fig. 3.3 E-H).

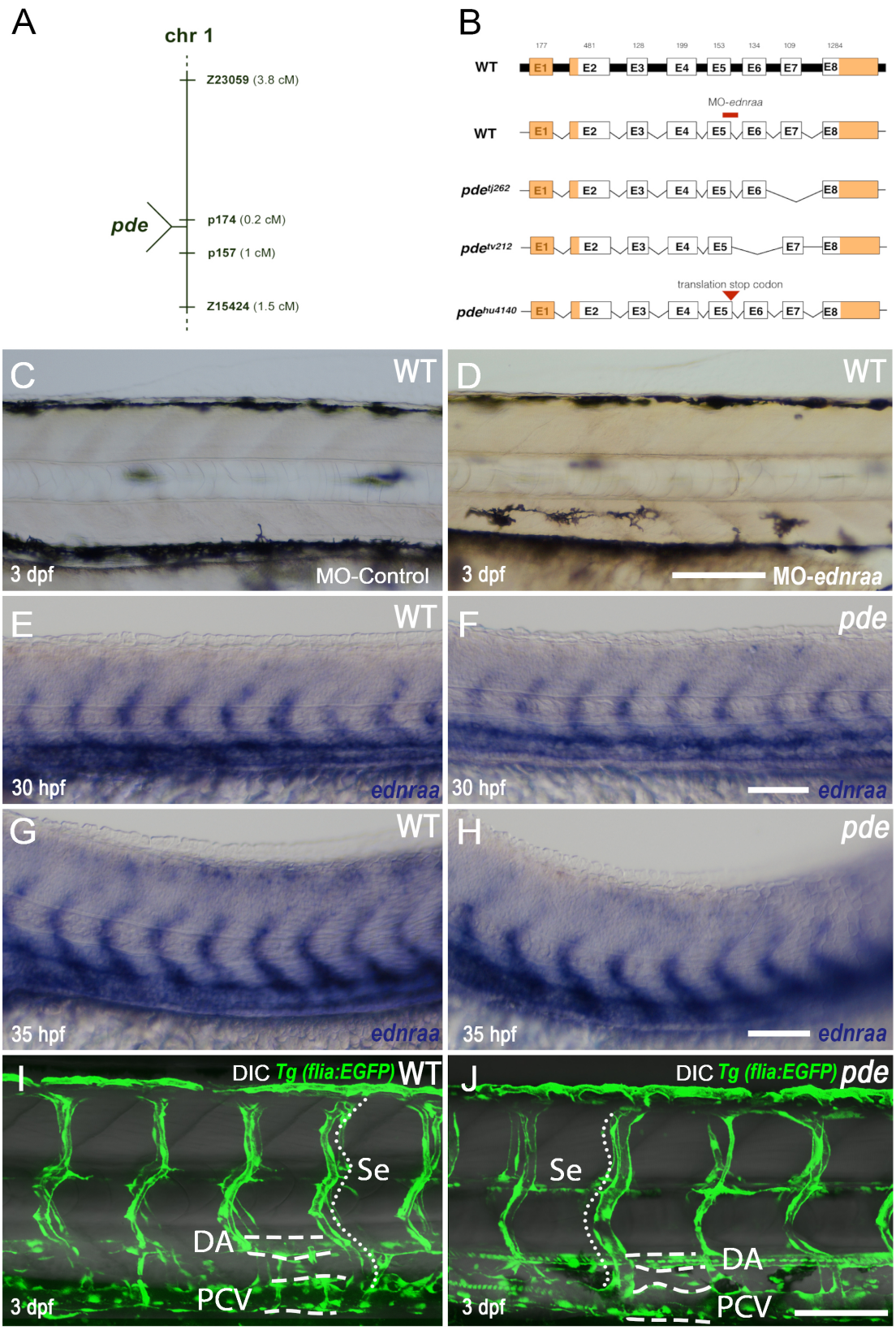

Figure 3.3 *pde* mutations affect *ednraa*, but not blood vessel formation and patterning. (A) *pde* map position on chromosome 1. (B) Schematic of predicted mRNA structure based upon sequencing of cDNA from pdetj262, pdetv212 and pdehu4140 mutants. cDNA of pdetj262 mutants lack exon 7, pdetv212 lack exon 6

and pdehu4140 have a transition mutation (AGA847TGA) that causes a premature translation stop (triangle) in the 3' region of exon 5. The location of the *ednraa* splice-blocking morpholino (*MO-ednraa*) is indicated (red bar). (C-D) Injection of *ednraa* morpholino into WT embryos phenocopies *pde* mutant pigment phenotype. (C) WT embryos injected with a control morpholino (MO-control) display a normal phenotype. (D) WT sibling injected with *MO-ednraa* display ectopic pigment cells in the ventral medial pathway. (E-H) Close up of posterior trunk of whole mount in situ hybridization of *ednraa* at 30 hpf and 35 hpf is restricted to the developing blood vessels, and is indistinguishable between *pde* mutants (F and H) and their WT siblings. (I-J) Imaging of blood vessels in the posterior trunk using the transgenic reporter *flia:GFP* shows no difference in blood vessel morphology between WT siblings (I) and *pde* mutants (J). DA, Dorsal Aorta; PCV, Posterior Cardinal Vein; Se, Segmental Vessels. Scale bar = 100 μm (C,D, E and J) and 25 μm (E-H).

We then tested whether blood vessels morphology was affected in *pde* mutants, which we will refer to as *ednraa* mutants from now on. One possible explanation for the pigment cells might be that blood vessel morphology might be disrupted in *ednraa* mutants, resulting in misplaced pigment cells. However, neither in situ hybridisation for *ednraa* (Fig. 3.3 E-H), nor examination of trunk blood vessel morphology using the transgenic line *Tg(flia:GFP)* (Fig. 3.3 I and J) showed differences between WT and *ednraa* mutant embryos. We conclude that gross morphology of blood vessels is not affected in the *ednraa* mutants, but that the supernumerary and ectopic pigment cells in the *ednraa* mutants result from a non-cell autonomous effect of endothelin signalling in the blood vessels.

3.2.3 The *ednraa* phenotype does not result from neural crest cell transdifferentiation in the ventral trunk.

The location of the ectopic pigment cells on the ventral medial pathway corresponds with the location of the nascent sympathetic ganglia, which form on the medial neural crest migration pathway in the vicinity of the dorsal aorta. We considered a transdifferentiation model in which neural crest cells fated to form sympathetic neurons switch to generating pigment cells, predicting that sympathetic neuron numbers would be reduced in *ednraa* mutants. However, immuno-detection of the early neuronal marker Elav1 (Hu neuronal RNA-binding protein) showed no

differences in the number of sympathetic neurons between phenotypically WT embryos and their *ednraa* mutant siblings (Fig. 3. 4 A, B and K). Furthermore, we also tested whether other neural crest-derived neurons are affected in the trunk, but neither DRG sensory neuron nor enteric neuron numbers differed between *ednraa* mutants and their WT siblings. Thus, trunk DRGs contained around 3 neurons per ganglion (Fig. 3.4 C, D and L;), while the posterior gut contained around 125 enteric neurons (Fig. 3.4 E, F and M).

As a further test of the sympathetic neuron transfating hypothesis, we reasoned that if a key signal driving sympathetic neuron specification was reduced, this might result in enhanced numbers of ectopic pigment cells. In mammals and birds, secreted BMP signals from the dorsal aorta have been shown to induce sympathetic neurons [22-24], but it is not known if this mechanism is conserved in zebrafish. To test this, we treated zebrafish embryos with Dorsomorphin (2.5 μM), a well characterised BMP signalling inhibitor [25]. Given the well-known roles for BMP signalling in early patterning in the embryo, we chose a treatment window from 1-4 days post fertilisation (dpf). Although this treatment left the larvae looking morphologically normal, immunofluorescent detection of Elav1 showed that treated larvae had a strong reduction the number of sympathetic neurons compared to DMSO carrier-treated controls (Fig. 3.4 G, H and N).

Having shown that zebrafish sympathetic neurons were BMP-dependent, we then asked whether ectopic pigment cells in *ednraa* mutants were increased if sympathetic neuron specification was inhibited; using the same treatment conditions, we saw no enhancement of ectopic pigment cells in *ednraa* mutants treated with dorsomorphin compared to DMSO-treated controls (Fig. 3.4 I, J and O). Thus, although we provide the first evidence to our knowledge that specification of zebrafish sympathetic neurons is BMP-dependent, we discount the hypothesis that the ectopic pigment cells in *ednraa* mutants result from transfating of sympathetic neurons.

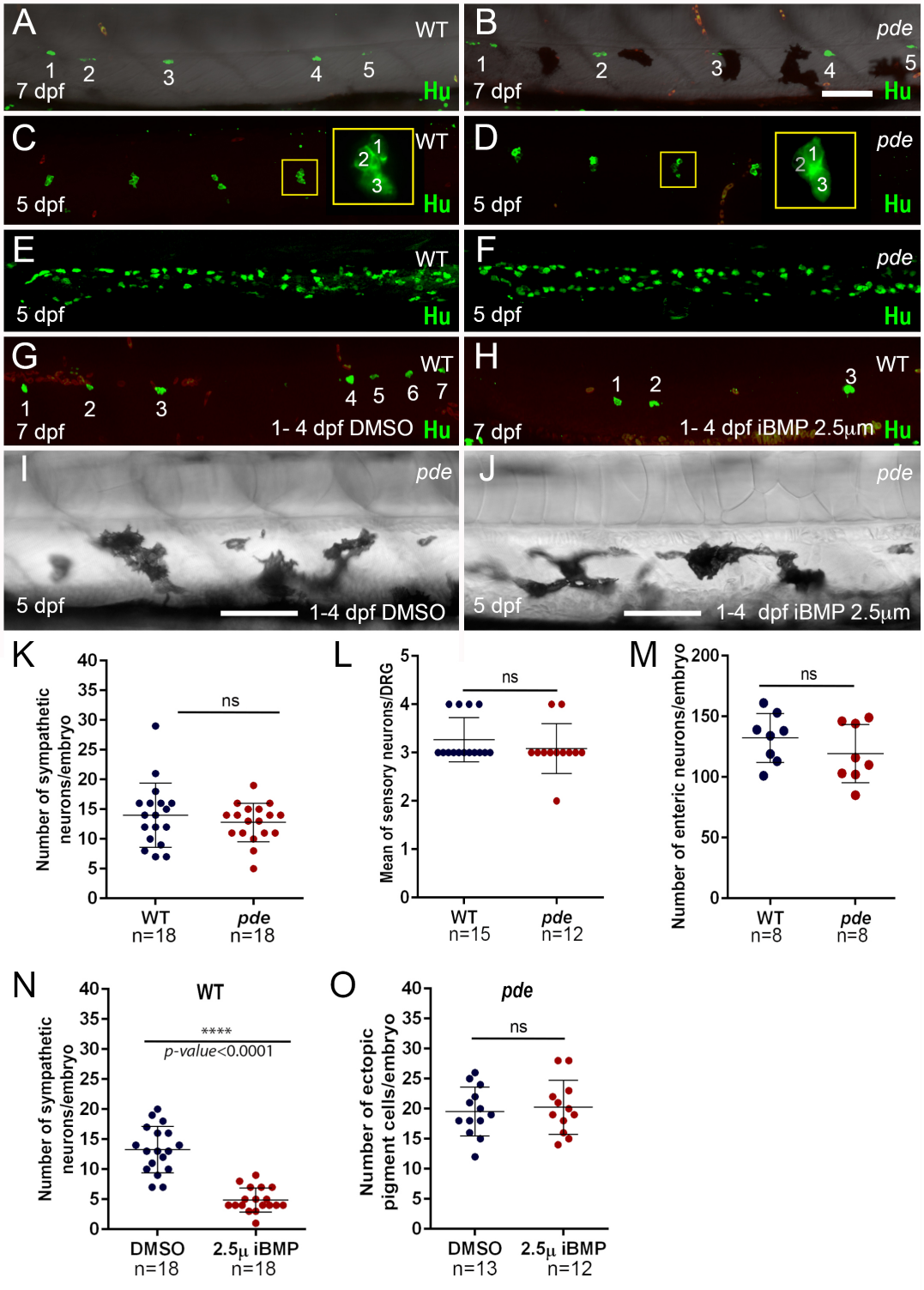

Figure 3.4 Neural crest-derived peripheral neurons are not reduced in *pde* mutants, but a role for BMP signaling in sympathetic neuron specification is conserved in zebrafish. Immunodetection of the neuronal marker Hu in 7 dpf WT embryos (A) and *pde* mutant siblings (B), shows no significant difference (ns) in the number of sympathetic neurons (K; WT mean+s.e.=14.0+1.27, n=18 and pde=12.78+0.76,

n=18, n=18; p>0.05, two-tailed t-test). (C-F) Immunodetection of the neuronal marker Hu in 5 dpf WT embryos (C and E) and pde mutant siblings (D and F) shows no significant (ns) difference in the number of sensory neurons per dorsal root ganglion (DRG; C and D; WT=3.26+0.11, n=15 and *pde* =3.08+0.14, n=12; >0.05, two-tailed t-test) nor in enteric neurons in the posterior gut (E, F and M; WT =132.3+7.14, n=8 and *pde* =119.4+8.49, n=8; p>0.05, two-tailed t-test). (G-J) Chemical inhibition of BMP signalling with dorsomorphin (iBMP 2.5 μM; 1-4 dpf treatment). Treatment of WT embryos shows a 63.25% reduction in the number of sympathetic neurons in comparison with 1% DMSO-treated controls (G, H and N; DMSO =13.28+0.91, n=18 and dorsomorphin=4.88+0.47, n=18; p<0.0001, two-tailed t-test). Quantification of the number of ectopic pigment cells in *pde* mutants treated with DMSO (I) or dorsomorphin (iBMP 2.5 μM; 1- 4 dpf; J) shows no significant (ns) difference (O; DMSO mean+s.e.=19.54+1.12, n=13 and *pde* =20.25+1.30, n=12; p>0.05, two-tailed t-test). Weak red fluorescence in the fluorescent images result from autofluorescence of red blood cells. Scale bar = 100 μm (A-J).

3.2.4 The *ednraa* phenotype results from localised increased neural crest cell proliferation in the ventral trunk, in the vicinity of the medial blood vessels

In order to identify the earliest stage at which ectopic pigment cells appear in the ventral trunk of *ednraa* mutants, we performed in situ hybridization with the melanophore marker *dct* and the iridoblast marker *ltk*. Comparison of gene expression between WT and *ednraa* mutant embryos at 24, 30 and 35 hpf showed that ectopic/supernumerary expression of both *dct* and *ltk* is detected in the ventral trunk from 35 hpf (Fig. 3.5 A-D).

We tested whether this production of extra pigment cells correlated with an increased proliferation of NC-derived cells in *ednraa* mutants. Given that ectopic and supernumerary pigment cells appear in the ventral trunk of *ednraa* mutants between 30 and 35 hpf, this indicates that enhanced proliferation might be expected to be detectable during this time-window. We used our *Tg(sox10:cre)* driver [26] combined with a *Tg(hsp70:loxP-dsRed-loxp-lyn-egfp)* red-green switch reporter to label all neural crest cells with membrane tagged GFP, in conjunction with expression of the proliferation marker phosphohistone H3 (pH3) by immunofluorescent labelling. GFP expression in the neural crest-derived cells was induced by brief heat shock at 28 hpf.

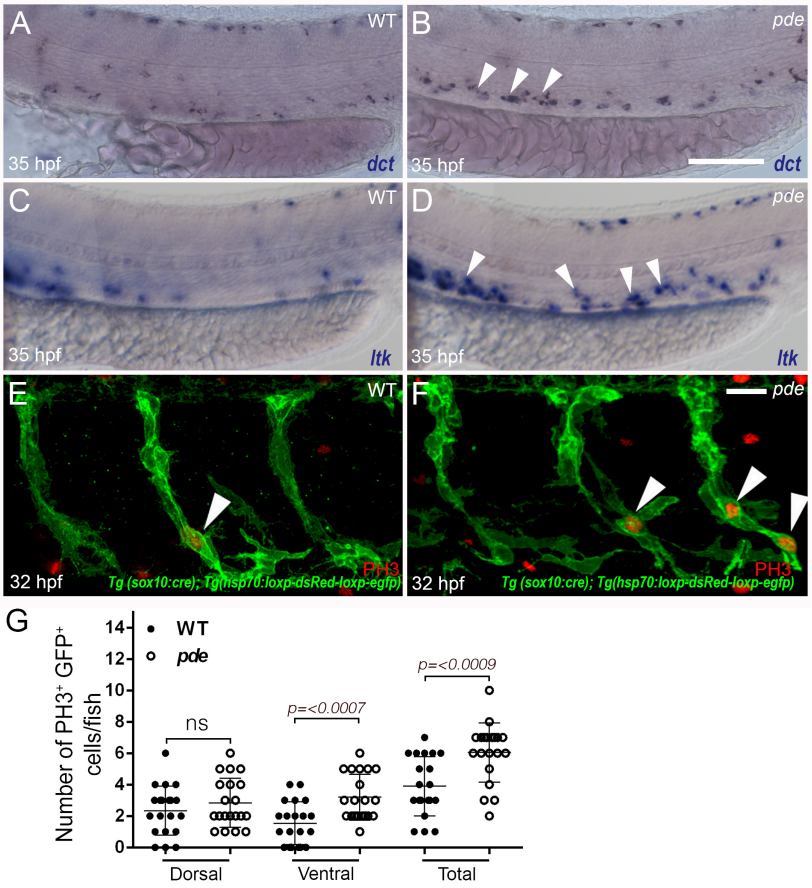

Figure 3.5 Ectopic pigment cells in *pde* mutants are detectable by 35 hpf, and generated by localised increased proliferation of neural crest-derived cells. (A-D) Whole mount in situ hybridization of 35 hpf WT (A and C) and *pde* mutant (B and D) embryos shows ectopic expression in *pde* mutants (white arrowheads in D) of melanophores marker *dct* (A and B) and the iridophore marker *ltk* (C and D). (E-G) Immunodetection of the proliferation marker phosphohistone 3 (PH3) in neural crest derived cells (labelled with membrane –tethered GFP due to Tg(-4725sox10:cre)ba74; Tg(hsp:loxp-dsRed-loxp-LYN-EGFP)) of 32 hpf WT (E; white arrowhead) and *pde* mutant (F, white arrowheads) sibling embryos. Quantification of double positive GFP+ PH3+ cells in medial migratory pathway, shows a significant increase in *pde* mutants compared to WT siblings (Total; WT mean+s.e.=3.9+0.42, n=20 and *pde* =6.05+0.41, n=20; p<0.0009, two-tailed t-test). Subdividing this quantification of GFP+ PH3+ cells in the medial migratory pathway into those dorsal and ventral to the notochord shows that this increase is not detected on the dorsal medial pathway (dorsal double positive cells, WT=2.35+0.35, n=20 and *pde* =2.85+0.35, n=20; p<0.3188, two-tailed t-test), but is significantly increased on the ventral medial pathway WT=1.55+0.30, n=20 and *pde* =3.2+0.32, n=20; p<0.0007, two-tailed t-test). Scale bar = 30 μm (A-D) 15 μm (E-F).

Subsequent double labelling of GFP and pH3 at 32 hpf showed a 55% overall increase in NC-derived proliferating cells in *ednraa* mutants compared with WT siblings, albeit over a very low basal rate (Fig. 3.5 E, F and G). Furthermore, over-proliferation of neural crest cells was detectable only in the ventral region of the medial pathway (Fig. 3.5 G). Our results show that ectopic pigment cells in *ednraa* mutants result from overproliferation of NC-derived cells in a localised region of the medial pathway in the vicinity of the dorsal aorta, coinciding with the region of *ednraa* expression.

During the proliferation assays, we noted that the ventral proliferation of neural crest-derived cells was often clustered at the ventral end of the migrating streams (arrowheads, Fig. 3.5 F). Furthermore, this association was true also of the ectopic pigment cells themselves, as shown by imaging of all NC-derived cells using the same transgenic line *(Tg(-4725sox10:cre)ba74; Tg(hsp:loxp-dsRed-loxp-EGFP*)) (S Fig. 3.3). This imaging confirmed the widespread ventral migration of neural crest-derived cells in *ednraa* mutants, comparable to that in WT siblings, at 35 hpf (S Fig. 3.3 A and B), reinforcing the conclusion from our WISH studies (Fig. 3.1 and 5). At 5 dpf, this imaging readily showed the ectopic pigment cells, but clearly revealed that their location is ventral to the notochord, in close proximity to the dorsal aorta and associated with the sympathetic ganglia chain, and also near the ventral projections of the spinal nerves (S Fig. 3.3 C-F).

3.2.5 The formation of ectopic pigment cells in *ednraa* mutants requires ErbB signalling.

In order to identify possible mechanisms involved in the formation of the *ednraa* phenotype, we performed a small molecule screen of 1396 compounds using three different libraries: 1) the Sigma LOPAC library, which contains 1280 small organic ligands including marketed drugs and pharmaceutically relevant structures; 2) the Screen-WellTM Kinase Inhibitor Library that comprises 80 known kinase inhibitors; and 3) the Screen-WellTM Phosphatase Inhibitor Library, containing 33 phosphatase inhibitors of well-characterised activity. Screening was performed using the methodology of our previous screen for pigmentation modifiers [27]; we took advantage of the adult viability of the *ednraa* mutants, to perform the screen on *ednraa* mutant embryos. In order to cover most developmental procecess, *ednraa* mutant embryos were treated from 4 hpf to 96 hpf at a standard concentration of 10 μM and rescue or enhancement of *ednraa* mutant phenotype was systematically

assessed at 4 dpf. After rescreening, we identified 23 compounds able to rescue the *ednraa* mutant phenotype, as well as 3 that enhance the phenotype (Table 3.2). Of these hits, four (Tyrphostin AG 1478, U0126, PD 98059 and PD325901) target the MAPK/ERK pathway: Tyrphostin AG-1478 is an inhibitor of the Epidermal Growth Factor Receptor (EGFR) [28] while U0126, PD98059 and PD325901 are highly selective inhibitors of MEK1/2 signalling [29-31]. Our previous work has shown that MEK inhibitors interfere with production of regenerative melanophores, whilst not affecting direct developing pigment cells forming the early larval pattern in zebrafish [32, 33]. Treatment of *ednraa* mutants with each of two of the latter compounds shows a clear dose-response in the degree of rescue of the *ednraa* phenotype (S Fig. 4).

The identification of Tyrphostin AG-1478 and the more specific EGFR inhibitor, PD158780, have been shown to affect APSC biology, but not embryonic pigment cells (except a small population contributing to the Lateral Stripe), in zebrafish [10]. Similarly, mutants for the *epidermal growth factor receptor (EGFR)-like tyrosine kinase erbb3b* (*picasso*), despite developing a normal embryonic/larval pigment pattern, fail to develop a normal adult pigment pattern and are unable to regenerate melanophores after embryonic melanophores ablation due to a lack of APSCs [10]. Thus, inhibition of Erb signalling by either AG-1478 or PD158780 selectively affects the biology of NC-derived APSCs that give rise to adult and regenerative melanophores. This is shown by the fact that treatment of embryos with both inhibitors do not affect embryonic pigment pattern formation but instead affects the adult pigment pattern. Rescue of the *ednraa* mutant by treatment with the Erb inhibitors suggested the exciting hypothesis that the ectopic cells in the *ednraa* mutants might result, not from embryonic pigment cells, but by precocious differentiation of APSCs. Interestingly, this role for ErbB signaling shows a tightly constrained time window, since inhibition of ErbB signalling with AG-1478 and PD158780 during window 9-48 hpf of embryonic development is sufficient for these effects [10]. Moreover, after melanophores ablation throughout 24-72 hpf, melanophores regeneration normally occurs by 5 dpf, but this is prevented when embryos are treated with AG-1478 during a 9-30 hpf window [7].

	Compound	Effect	Target
Cell signaling	**CCG-4886**	D	Rho/SRF pathway inhibitor
	CinnGEL	D	Protein tyrosine phosphatase 1B inhibitor
	Cyclosporin A	D	Inhibitor of protein calcineurin phosphatase 2B.
	Fenvalerate	D	Inhibitor of calcineurin (protein phosphatase 2B).
	Genistein	D	Tyrosine kinase inhibitor
	GW 9662	D	Irreversible PPARγ antagonist.
	PQ 401	D	Insulin-like growth factor receptor (IGF1R) inhibitor
	Rac-2-ethoxy-3-hexadecamino-1-propyl phosphocholine	E	Selective inhibitor of the VEGFR2 receptor kinase, Flk-1
	Rapamycin	D	mTOR inhibitor
	SU 1498	D	Inhibitor of the VEGFR2
	Tyrphostin AG-126	D	Block the production of tumor necrosis factor-alpha (TNF-alpha)
	Tyrphostin AG-1478	D	EGF receptor (EGFR) inhibitor
	PD98059	D	MEK inhibitor
	PD325901	D	MEK inhibitor
	U-0126	D	MEK inhibitor
Synaptic signaling	**CGP-13501**	D	Positive allosteric modulator of GABAB receptors.
	CPCCOEt	D	Non-competitive metabotropic glutamate receptor mGluR1 antagonist
	(-)-Eseroline fumarate	D	Anti-acetylcholinesterase and opiate agonist activities
	Fusaric acid	D	Dopamine β-hydroxylase inhibitor.
	GR 89696	E	Selective κ2 opioid receptor agonist.
Ion channel blocker	**Clotrimazole**	D	Specific inhibitor of Ca^{2+}-activated K^+ channels
	Felodipine	D	L-type calcium channel blocker
Hormon signaling		D	Non-steroidal anti-androgen
Anti-inflammatory	**L-Canavanine**	D	Selective inhibitor of inducible nitric oxide synthase (iNOS).
	Nalidixic acid sodium salt	D	Inhibits bacterial DNA gyrase
	4-Chloromercuribenzoic acid	E	Cysteine active site modifier

Table 4 .2 Screening of small molecules in *pde* mutants. Name and known targets of small molecules that enhance (E) or rescue (R) the *pde* phenotype.

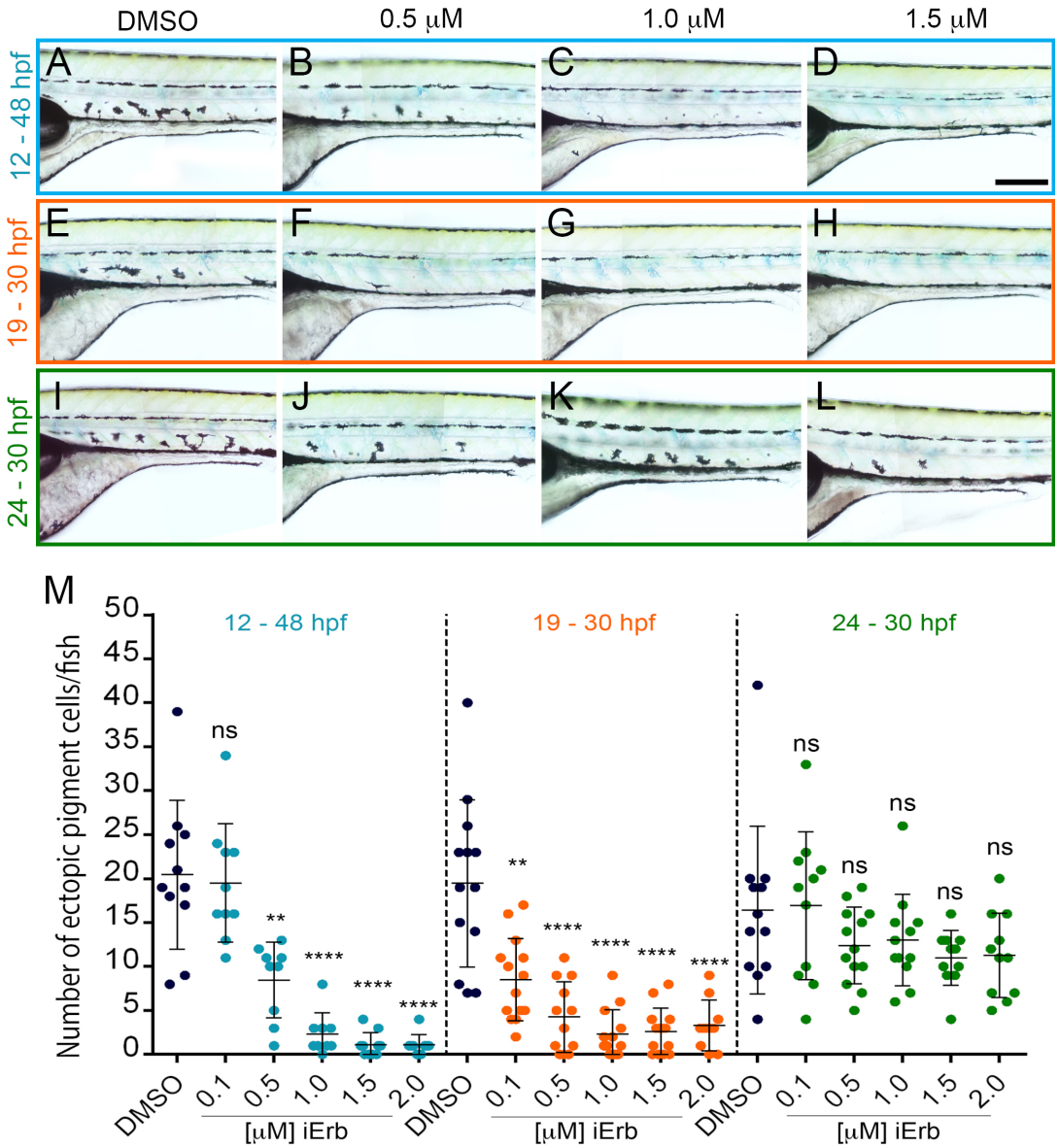

Figure 3.6 Chemical inhibition of Erb signalling rescues the *pde* phenotype. (A-H) Treatment of *pde* embryos with increasing concentrations of Erb inhibitor PD158780 (iErb; 0.5- 2.0 μM) or DMSO carrier control from 12-48 hpf (A-D), 19-30 hpf (E-H) and 24-30 hpf (I-L) hpf. Quantification of the number of ectopic pigment cells in the ventral medial pathway showed a decrease in the number of ectopic cells when embryos were treated from 12-48 hpf or just from 18-30 hpf, but not in a later 24-30 hpf time-window (M). Scale bar = 200 μm (A-L).

Thus, our hypothesis makes the testable prediction that rescue of the ectopic pigment cells in *ednraa* mutants would share the very specific temporal window known to

regulate APSCs development. We treated *ednraa* mutant embryos with a range of concentrations (0.1 – 2.0 μM) of PD158780 from 12-48 hpf (Fig. 3.6 A-D). Quantification of the number of ectopic pigment cells showed that *ednraa* mutant embryos treated with PD158780 have a significant dose dependant-reduction in the number of ectopic cells compared to DMSO treated embryos (Fig. 3.6 M).

Moreover, shorter treatment with PD158780 revealed that the *ednraa* phenotype is effectively rescued when treatment is restricted to a 19-30 hpf window (Fig. 3.6 E-H and M,), showing a striking match to the critical period for establishment of APSCs, while treatment after this window (24-30 hpf) does not rescue the *ednraa* phenotype (Fig. 3.6 I-M). This data strongly supports the hypothesis that the source of ectopic pigment cells in *ednraa* mutants is likely to be APSCs and not embryonic pigment cells.

3.3 Discussion

In this study, we show that *ednraa* encodes one of two zebrafish Ednra orthologues, Ednraa. In mammals, the EdnrA receptor binds selectively to Edn1 and Edn2, mediates vasoconstriction, and is overexpressed in many cancers [34]). In contrast, loss of function in mouse results in homeotic transformation of the lower jaw towards an upper jaw morphology, and in humans underlies Auriculocondylar syndrome (ACS [35-38]. These studies did not identify pigmentation phenotypes, although an Ednra lacZ knock-in mouse strain shows prominent expression in the hair follicles [35]. In contrast, Ednrb and Edn3 mutants, as well as mutations in the Edn-processing enzyme Ece1, lack neural crest-derived melanophores [39-41].

Analysis of the zebrafish genome identifies eleven components of endothelin signalling system: Four ligands, Edn1, Edn2, Edn3a and Edn3b; three Endothelin Converting Enzymes, Ece1, Ece2a, Ece2b that activate the ligands; and four receptors, Ednraa, Ednrab, Ednrba and Ednrbb [42]. In adult zebrafish, *ednrba* and *ece2b* loss-of-function mutants have all been shown to display reduced iridophores and broken stripes, indicating their coordinated role in iridophore development and pigment patterning, but no effect on embryonic pigment pattern [43, 44]. In contrast, *edn1* mutants and *ednraa* and *ednrab* morphants revealed disruption of the lower jaw, similar to the mammalian role in dorsoventral patterning, but did not examine pigmentation [21].

Here we identify a novel function for Ednraa signalling in pigment cell development. Our experimental studies assess in turn a series of hypotheses regarding the embryonic basis of the ectopic pigment cell phenotype, initially exploring disrupted biology of embryonic (direct developing) pigment cells, before coming to the conclusion that the phenotype must result from disruption of APSC biology. The *ednraa* mutant phenotype is restricted to supernumerary and ectopic pigment cells in the ventral trunk and anterior tail; this spatial localization had been perplexing, but identification of the gene as *ednraa*, which is consistently expressed strongly in developing blood vessels (but not in the trunk NC) from well before the onset of detectable ectopic cells, helps to explain the restricted phenotype of *ednraa* mutants. We find no evidence that neural crest migration is disrupted, since not only is blood vessel morphology normal, but neural crest cell migration and patterning is normal except for the ectopic pigment cells themselves, and pigment cells are abundant in the Ventral and Yolk Sac Stripes. Similarly, we disprove the ‘mixed-fate’ hypothesis

by showing using TEM that the ectopic cells are indistinguishable from those melanophores and iridophores in the Yolk Sac Stripe where these two cell-types are consistently found in tight apposition. Instead, we conclude that the close association of the two cell-types reflects the natural tendency for iridophores to adhere to melanophores (as seen in all locations in the early larval pattern). Finally, we find no evidence that the ectopic cells derive from transfating of sympathetic neurons, since neurons are unaffected in *ednraa* mutants and even when sympathetic neuron specification is inhibited using a BMP inhibitor, ectopic pigment cell number is unchanged.

However, these studies were unable to address the possible role of glial or progenitor cells in the ventral trunk. We reasoned that the supernumerary and ectopic cells were likely to be associated with increased proliferation of a subset of neural crest cells. Strikingly, we found that enhanced proliferation of neural crest did characterise the *ednraa* mutants, but that this proliferation was specifically associated with neural crest cells in ventral regions i.e. near the dorsal aorta, at around the time (35 hpf) that ectopic pigment cells begin to be identifiable. This is before the sympathetic ganglia show detectable differentiation and suggested that a subset of NC-derived cells undergoes ectopic or precocious proliferation. A key insight into the identity of these cells came from the observation that both ErbB inhibitors rescued the homozygous phenotype. Inhibition of Erb signalling within a defined embryonic time window by either AG-1478 or PD158780 selectively affects the biology of NC-derived APSCs that give rise to adult and regenerative melanophores [7, 10]. We show that *ednraa* mutants are rescued by ErbB inhibitors in a dose- and time-dependent manner, and with a time-window overlapping that known to regulate APSC development. We conclude that the ectopic pigment cells in *ednraa* mutants result from precocious differentiation of pigment cells from APSCs, cells that would normally be quiescent until metamorphosis.

APSCs give rise to the numerous melanophores and iridophores of the adult skin [11]. Our model would be consistent with the lack of ectopic xanthophores, since the evidence to date is that the majority of adult xanthophores derive from embryonic xanthophores and not from APSCs, although a small contribution from the stem cells is indicated by clonal analyses [11, 45]. Finally, the localised increase in neural crest cell proliferation that we document is also consistent with the activation of otherwise quiescent stem cells. APSCs in zebrafish have been closely-linked to the developing peripheral nervous system. One intriguing aspect of our data is that this proliferation

is exclusively localised to the ventral trunk, consistent with the idea that the blood vessels form a key aspect of the stem cell niche, but surprising in that to date APSCs have been exclusively associated with the DRGs [9, 46]. We note that homozygous *ednraa* mutants are adult viable, but have no visible skin pigment pattern defect.

Our data are consistent with a second source of APSCs, associated with the peripheral nervous system in the ventral trunk, likely the sympathetic ganglia. We propose a model in which these APSCs reside in a novel niche in close proximity to the medial blood vessels, which provide signals holding them in a quiescent state. In the *ednraa* mutants, these signals are reduced or absent, such that the APSCs become precociously activated. They then undergo proliferation and differentiate as melanophores and iridophores. Many of these move into the Ventral Stripe location, but the excess cannot be accommodated in this stripe and remain ectopically located in the ventral trunk near the sympathetic ganglia (Fig. 3.7). It is somewhat surprising that homozygous *ednraa* mutants show no disruption of the adult pigment pattern, but we propose several hypotheses, none mutually exclusive, to explain this observation: 1) although as we have shown APSCs are precociously activated in *ednraa* mutants, APSC renewal may be unaffected so that the stem cells are not exhausted; 2) ventral APSCs may primarily populate internal, rather than skin, pigment cell populations; 3) APSCs localised in DRGs may compensate for the effects on the more ventral APSCs.

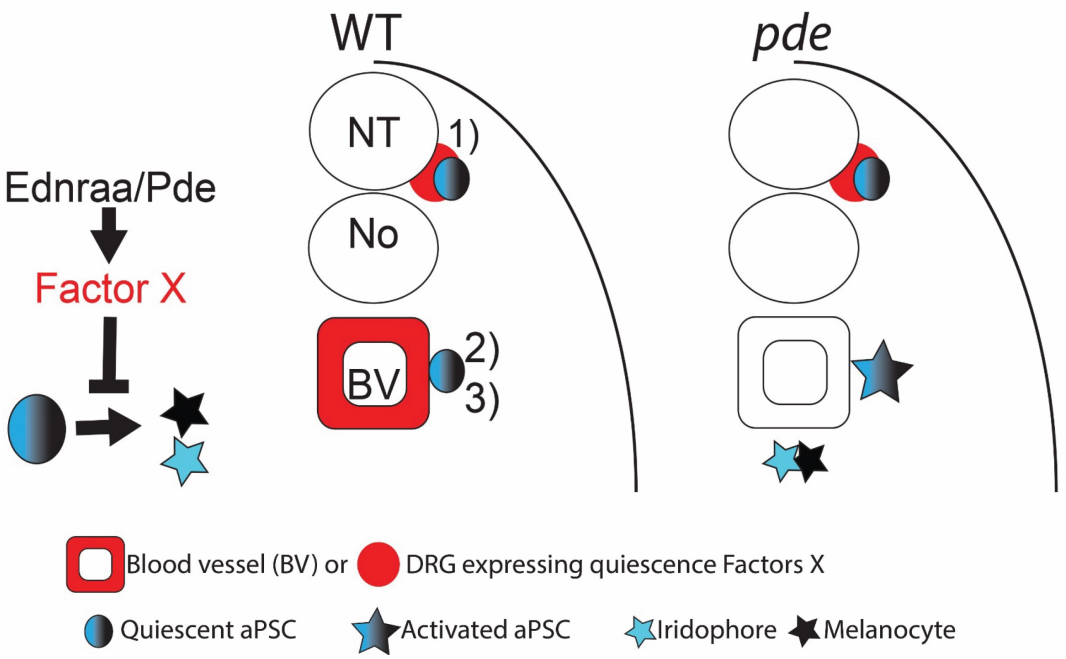

Figure 3.7 A second source of APSCs is held in a quiescent state by Ednraa-dependent factors from the blood vessels. Figure shows a model integrating our observations with current knowledge. 1) Dorsal root ganglia associated APSCs (APSC) are maintained in a quiescent state by local factors (red); 2) we propose a second source of APSCs in the vicinity of the medial blood vessels. Ednraa/*pde* activity in the blood vessels results in signals that hold this novel population in a quiescent state. In the *pde* mutants, these factors (red) are lost locally from the blood vessels and the APSCs become precociously activated, generating melanophores and iridophores in their vicinity.

Although novel in the context of APSCs, blood vessels form an important part of adult stem cell niches in other contexts, especially that of adult Neural Stem Cells (NSCs) [47]. Indeed, in the case of NSCs in the subependymal zone of mouse, blood vessel-mediated signals play a role in maintaining quiescence [47], although other sources for these quiescence signals have also been identified in the neurepithelial component of this niche [48-51]. In these studies of NSCs, notch signaling has been shown to be important in maintenance of quiescence, so it will be fascinating to compare the molecular signals derived from the vasculature that regulate APSC quiescence in the zebrafish. Our discovery of a second niche for APSCs and identification of the key role for blood vessels in controlling their behaviour provides an entry point for uncovering an important but currently understudied aspect of zebrafish pigment pattern formation.

Our work may also have implications for human disease. For example, Phakomatosis pigmentovascularis (PPV) is a rare mosaic disorder defined as the simultaneous occurrence of a widespread vascular nevus and an extensive pigmentary nevus, and associated with activating mutations of $G\alpha\beta\gamma$ subunits of heterotrimeric G proteins [52]. It is currently unknown if there is a common progenitor that gains an oncogenic mutation and leads to both large nevi and vascular proliferations, or if changes in one cell type impact upon another. Our study provides evidence that melanophores can expand/differentiate in association with a modified blood vessel niche, making it conceivable that, for instance, oncogenic activation in blood vessels might result in non-cell autonomous activation of melanophore stem cells in the niche to generate a nevus.

3.4 Materials and Methods.

3.4.1 Fish husbandry.

All fish strains were maintained in accordance with local and national guidelines on animal welfare. This study was performed with the approval of the University of Bath ethics committee and in full accordance with the Animals (Scientific Procedures) Act 1986, under Home Office Project Licenses 30/2937 and P87C67227. Animal experiments were approved by the Animal Experimentation Committee (DEC) of the Royal Netherlands Academy of Arts and Sciences. AB, *pde*^{tj262}, *pde*^{tv212} and *pde*^{hu4140}, *Tg(flia:GFP)* and *Tg(-4725sox10:cre)ba74; Tg(hsp:loxp-dsRed-loxp-EGFP).*

3.4.2 Genetic mapping.

3.4.2.1. Mapping panels

Two specific sets of microsatellite markers, the G4 and H2 panels (Geisler et al., 2007) were used for bulk segregant analysis of *parade*, placing the mutation on linkage group 1. We subsequently used a consolidated meiotic map of the zebrafish genome, ZMAP, which is available on ZFIN (http://zfin.org/cgi-bin/webdriver?MIval=aa-crossview.apg&OID=ZDB-REFCROSS- 010114-1; Sprague et al., 2006; Geisler et al., 2007).

3.4.2.2. Reference zebrafish line

The standard mapping wild-type line WIK was crossed with mutant *parade*^{tj262} carriers (in AB wild-type background). This founder generation F0 was in crossed to produce heterozygous F1. Eight pairs of F1 fish were in crossed to produce the F2 generation. In total 1796 F2 embryos at 5 dpf were sorted into two groups, those that display the mutant phenotype and those with a normal wild- type pigment phenotype. These were transferred into 96-well plates where the extraction of genomic DNA was performed and stored. Additionally, genomic extracts of 10 homozygous *parade*^{tj262} and 10 wild-type sibling embryos of each of the 8 parent pairs were pooled for identification of new SSLP markers.

3.4.2.3. Mapping procedure

The *pde* locus was mapped to linkage group 1 (LN 1) by bulked segregant analysis using pooled genomic DNA of 48 wild-type siblings and 48 *parade*^{tj262} mutant embryos of the F2 generation obtained from F1 Pair 2. For fine mapping we designed new mapping primers using the Primer3 online software tool (http://frodo.wi.mit.edu/primer3/, default settings plus 1 primer pair per 300–400 bp. Primer pairs were designed to generate PCR products of 300-400 bp, which if generating polymorphic PCR amplicons, were then tested on the 1796 single F2 embryos to determine the frequency of recombination.

PCR protocol

2 µl of individual or pooled DNA were added to 13 µl of PCR mix (1.5 µl 10 x buffer for KOD Hot Start DNA Polymerase; 1.5 µl dNTP's with 0.2 mM for each nucleotide; 1 µl primer mix with 10 mM forward and 10 mM reverse primer; 0.3 µl DMSO; 0.6 µl 25 mM MgSO4; 8.3 µl MiliQ water; 0.3 µl KOD polymerase (Novagen)). PCR's were run in a GStorm thermal cycler (Gene Technologies Ltd) (program: 2 min 94° C; then 35 x (30 sec 94° C, 30 sec 60° C, 30 sec 72° C); then 5 min 72° C; then stored at 10° C). The PCR products were then analysed by electrophoresis.

Morpholino injection

Custom morpholinos were purchased from Gene Tools LLC (Philomath, USA) and resuspended in autoclaved MilliQ water to a stock dilution of 20 µg/µl. Stock solutions were stored at -20° C to prevent evaporation and heated at 70° C for 5 min prior to dilution to eliminate precipitates. Wild-type embryos were injected into the yolk at the 1-cell stage with 5 ng/nl dilutions. Phenotypes were observed under the microscope at 3 dpf and 4 dpf. Volumes varied between 5 and 10 nl per embryo. Sequences of morpholino oligos can be found in S1 Table.

Whole mount in situ hybridization

Our protocol for whole-mount in situ hybridization is based on (Thisse et al., 1993). All solutions were prepared with DEPC-treated autoclaved MiliQ water or PBS. All probes for in situ hybridization were synthesized using the Dig RNA Labeling Kit (Boehringer). Depending on the orientation of the gene and choice of plasmid, we

have chosen either T3, T4 or SP6 RNA polymerases for creating the antisense RNA probe.

Briefly, embryos between 5 and 120 hpf were euthanized with a lethal overdose of tricaine and fixed overnight (4 % PFA in PBS). Embryos older than 18 hpf were dechorionated with forceps before fixation, younger embryos were dechorionated with flamed forceps after fixation. All following steps were carried out in 1.5 ml microfuge tubes with 1 ml liquid volumes; up to 40 embryos were processed per tube. The fixative was rinsed out with PBTween (DEPC-treated PBS plus 0.1 % Tween). Embryos were then gradually dehydrated on ice with 25, 50, 75 and 100 % methanol. For the ISH procedure, embryos were rehydrated on ice using 5 min washes with 75, 50, 25 % methanol followed by 3 x 5 min washes with PBTween at room temperature. To improve permeability, embryos between 30 – 48 hpf were treated for 10 min with 0.01 mg/ml proteinase K/PBTween, embryos; older than 50 hpf were treated for up to 20 min. The proteinase K was removed by washing samples for 3 x 5 min with PBTween followed by a brief re-fixation step with 4% PFA for 20 min at room temperature. The fixative was then washed out with 3 x 5 min PBTween. To prepare the samples for optimal binding conditions, embryos were pre-hybridized with hybridization mix (formamide, 20 x SSC, heparine, tRNA, Tween20, citric acid; stored at -20° C) in a water bath at 65° C for 4 h. The hybridization of the RNA probe (diluted 1:400) was done over night at 65° C in 200 µl hybridization mix. The samples were washed with decreasing concentrations of hybridization mix (100 % hyb mix; 75 % hyb mix/25 % 2x SSCT; 50 % hyb mix/50 % 2x SSCT; 25 % hyb mix/75 % 2x SSCT; 100 % 2x SSCT), each for 10 min, followed by 2 x 30 min washing with 0.2x SSCT. All steps were carried out in a water bath at 65° C. Samples were then infiltrated for 3 x 5 min with MABT (from 5 x MAB stock solution plus 0.1 % Tween) at room temperature. Samples were blocked for 3 h in MABTween with 5 % sheep serum at room temperature under gentle shaking. Antibody binding reaction was performed over night at 4° C using 200 µl of 1:5000 diluted anti - dioxigenin alkaline phosphatase conjugated antiserum in blocking solution. Samples were then washed for 6 x 15 min in MABT, then prepared for signal detection reaction by infiltrating for 3 x 5 min with NBT/BCIP buffer (100 mM Tris HCl pH 9.5, 50 mM MgCl2, 100 mM NaCl, 0.1 % Tween). The embryos were transferred into 9-well glass dishes to observe the staining reaction under the dissecting microscope. 300 µl of BMPurple substrate solution were added per well and the development of the reaction regularly monitored. Signal development was stopped by washing with PBTween.

3.4.3 Chemical screening

3.4.3.1. Compounds used

The compounds used in this investigation originated from the 1280 compounds from the LOPAC library (Sigma LO1280), 80 compounds from a kinase inhibitor library (Biomol 2832) and 33 compounds from a phosphatase inhibitor library (Biomol 2834A). The compound libraries were stored at -80C and plates thawed at room temperature prior to use. For screening, potential effects on developing zebrafish embryos compounds were diluted to 10uM in E3 embryo medium.

For drug treatments, six embryos were placed in each well of 24 well plates. Chemical treatments were prepared in 10μM doses in 1ml E3 medium. To ensure that compounds did not precipitate, the plates containing small molecule treatments were placed on The Belly Dancer (Sorval) for a minimum of 20 minutes. When embryos reached 8hpf E3 medium was removed and 1ml of E3 containing 10 μM of compound was added to each well. Wells containing E3 only and 10 μM DMSO were used in each chemical treatment as controls. Plates containing treated embryos were incubated at 28 ºC until the embryos reached 5 dpf.

Detailed observations were recorded daily and any dead embryos removed to avoid contamination of the medium. At day 5 embryos were anaesthetised with a small dose of tricaine to enable easy manipulation for accurate detailing of pigment phenotype. Pigment cell phenotypes and rescue of the *parade* mutant phenotype were recorded as well as additional phenotypes such as developmental abnormalities (e.g. shortening of the tail or cardiac edema).

Re-screening of important chemical ‘hits’

Once molecules of specific interest to pigment cell development were identified the treatment was repeated on embryos at different developmental time points and across a concentration gradient in order to identify the developmental time point of greatest phenotypic significance and the optimal small molecule concentration.

3.4.4 Wholemount immunostaining.

Antibody staining was largely performed as described in [19]. Prior to primary antibody incubation, embryos were permeabilized with 1 ml of 5 μg/ml of proteinase K/distilled water during 30 minutes at 37 ºC, then rinsed with 5% of goat serum/distilled water at RT for 5 minutes and washed 3x1 hour with distilled water at RT. The antibodies used were Hu (1:500,) and Alexa Fluor 488 goat-mouse IgG (1:750, Molecular Probes, Cat. # A11001).

3.4.1 Image acquisition and processing.

For in vivo microscopy, embryos were mounted at the Leica Fluo III or Zeiss Axiovision dissection microscope in 0.6 % agarose or 3 % methyl cellulose. For anaesthesia, 0.02 % Tricaine was added freshly to the mounting medium. The embryos were transferred to a microscope slide or to a glass-bottomed Petri dish. For immunofluorescence, embryos were visualized with a Nikon Eclipse E800 or Zeise M2 Imager compound microscope under bright field, incident light or epifluorescence illumination, mainly using a 10x, 20x and 63x objective for magnification. Images were taken with a DS-U1 (Nikon) or Orca and color 546 camera (Zeiss). Confocal fluorescence imaging was performed on an inverted Zeiss LSM 510 Meta or LSM 880 confocal microscope with 20x and 40x objectives. Incident light was provided by installing an additional antler lamp (Leica) around the microscope to allow visualisation of iridophores. NIS-Elements D2.30, Zen blue, Fiji and/or Adobe Photoshop 7 were used to adjust white balance and exposure and to assemble the images to figures.

3.5 Acknowledgments.

We gratefully acknowledge funding support that enabled this research, specifically University of Bath Studentships (SC and JM), Consejo Nacional de Ciencia y Tecnología grant 329640/384511 (KCS), and Biotechnology and Biological Sciences Research Council (BBSRC) grant BB/L00769X/1 and Medical Research Council (MRC) grant MR/J001457/1 (RNK), and MRC Human Genetics Unit Programme (MC_PC_U127585840), European Research Council (ZF-MEL-CHEMBIO-648489) and L'Oreal-Melanoma Research Alliance (401181)(EEP). We thank Anne Gesell for technical assistance with confocal microscopy, and Kerstin Howe and Mario

Caccamo (Wellcome Trust Genome Campus) for their expert assistance in interpreting the zebrafish genome during the mapping.

3.6 References.

1. Schartl M, Larue L, Goda M, Bosenberg MW, Hashimoto H, Kelsh RN. What is a vertebrate pigment cell? Pigment Cell Melanoma Res. 2016;29(1):8-14. doi: 10.1111/pcmr.12409. PubMed PMID: 26247887.

2. Irion U, Singh AP, Nusslein-Volhard C. The Developmental Genetics of Vertebrate Color Pattern Formation: Lessons from Zebrafish. Curr Top Dev Biol. 2016;117:141-69. doi: 10.1016/bs.ctdb.2015.12.012. PubMed PMID: 26969976.

3. Kelsh RN. Genetics and evolution of pigment patterns in fish. Pigment Cell Res. 2004;17(4):326-36. PubMed PMID: 15250934.

4. Kelsh RN, Harris ML, Colanesi S, Erickson CA. Stripes and belly-spots -- a review of pigment cell morphogenesis in vertebrates. Semin Cell Dev Biol. 2009;20(1):90-104. Epub 2008/11/04. doi: 10.1016/j.semcdb.2008.10.001 S1084-9521(08)00096-7 [pii]. PubMed PMID: 18977309; PubMed Central PMCID: PMC2744437.

5. Parichy DM. Animal pigment pattern: an integrative model system for studying the development, evolution, and regeneration of form. Semin Cell Dev Biol. 2009;20(1):63-4. Epub 2009/01/17. doi: S1084-9521(08)00155-9 [pii] 10.1016/j.semcdb.2008.12.010. PubMed PMID: 19146966.

6. Singh AP, Nusslein-Volhard C. Zebrafish stripes as a model for vertebrate colour pattern formation. Curr Biol. 2015;25(2):R81-92. doi: 10.1016/j.cub.2014.11.013. PubMed PMID: 25602311.

7. Hultman KA, Budi EH, Teasley DC, Gottlieb AY, Parichy DM, Johnson SL. Defects in ErbB-dependent establishment of adult melanocyte stem cells reveal independent origins for embryonic and regeneration melanocytes. PLoS Genet. 2009;5(7):e1000544. Epub 2009/07/07. doi: 10.1371/journal.pgen.1000544. PubMed PMID: 19578401; PubMed Central PMCID: PMC2699538.

8. Johnson SL, Nguyen AN, Lister JA. mitfa is required at multiple stages of melanocyte differentiation but not to establish the melanocyte stem cell. Dev Biol. 2011;350(2):405-13. Epub 2010/12/15. doi: S0012-1606(10)01245-5 [pii] 10.1016/j.ydbio.2010.12.004. PubMed PMID: 21146516; PubMed Central PMCID: PMC3040983.

9. Dooley CM, Mongera A, Walderich B, Nusslein-Volhard C. On the embryonic origin of adult melanophores: the role of ErbB and Kit signalling in establishing

melanophore stem cells in zebrafish. Development. 2013;140(5):1003-13. Epub 2013/02/01. doi: 10.1242/dev.087007
dev.087007 [pii]. PubMed PMID: 23364329.
10. Budi EH, Patterson LB, Parichy DM. Embryonic requirements for ErbB signaling in neural crest development and adult pigment pattern formation. Development. 2008;135(15):2603-14. Epub 2008/05/30. doi: dev.019299 [pii]
10.1242/dev.019299. PubMed PMID: 18508863.
11. Singh AP, Dinwiddie A, Mahalwar P, Schach U, Linker C, Irion U, et al. Pigment Cell Progenitors in Zebrafish Remain Multipotent through Metamorphosis. Dev Cell. 2016. doi: 10.1016/j.devcel.2016.06.020. PubMed PMID: 27453500.
12. Svetic V, Hollway GE, Elworthy S, Chipperfield TR, Davison C, Adams RJ, et al. Sdf1a patterns zebrafish melanophores and links the somite and melanophore pattern defects in choker mutants. Development. 2007;134(5):1011-22. PubMed PMID: 17267445.
13. Raible DW, Wood A, Hodsdon W, Henion PD, Weston JA, Eisen JS. Segregation and early dispersal of neural crest cells in the embryonic zebrafish. Dev Dyn. 1992;195(1):29-42.
14. Kelsh RN, Schmid B, Eisen JS. Genetic analysis of melanophore development in zebrafish embryos. Dev Biol. 2000;225(2):277-93. PubMed PMID: 10985850.
15. Lister JA, Robertson CP, Lepage T, Johnson SL, Raible DW. nacre encodes a zebrafish microphthalmia-related protein that regulates neural-crest-derived pigment cell fate. Development. 1999;126(17):3757-67. PubMed PMID: 10433906.
16. Lopes SS, Yang X, Muller J, Carney TJ, McAdow AR, Rauch GJ, et al. Leukocyte tyrosine kinase functions in pigment cell development. PLoS Genet. 2008;4(3):e1000026. Epub 2008/03/29. doi: 10.1371/journal.pgen.1000026. PubMed PMID: 18369445.
17. Minchin JE, Hughes SM. Sequential actions of Pax3 and Pax7 drive xanthophore development in zebrafish neural crest. Dev Biol. 2008;317(2):508-22. Epub 2008/04/18. doi: S0012-1606(08)00177-2 [pii]
10.1016/j.ydbio.2008.02.058. PubMed PMID: 18417109.
18. Kelsh RN, Brand M, Jiang YJ, Heisenberg CP, Lin S, Haffter P, et al. Zebrafish pigmentation mutations and the processes of neural crest development. Development. 1996;123:369-89.
19. Petratou K, Camargo-Sosa K, Al Jabri R, Nagao Y, Kelsh RN. Transcript and protein detection methodologies for neural crest research on whole mount zebrafish

and medaka. In: Schwarz Q, Wiszniak S, editors. Methods relevant to Neural Crest Cell research. Methods in Molecular Biology Springer; in press.

20. Geisler R, Rauch GJ, Geiger-Rudolph S, Albrecht A, van Bebber F, Berger A, et al. Large-scale mapping of mutations affecting zebrafish development. BMC Genomics. 2007;8:11. Epub 2007/01/11. doi: 1471-2164-8-11 [pii] 10.1186/1471-2164-8-11. PubMed PMID: 17212827; PubMed Central PMCID: PMC1781435.

21. Nair S, Li W, Cornell R, Schilling TF. Requirements for Endothelin type-A receptors and Endothelin-1 signaling in the facial ectoderm for the patterning of skeletogenic neural crest cells in zebrafish. Development. 2007;134(2):335-45. doi: 10.1242/dev.02704. PubMed PMID: 17166927.

22. Reissmann E, Ernsberger U, Francis-West P, Rueger D, Brickell P, Rohrer H. Involvement of bone morphogenetic protein-4 and bone morphogenetic protein-7 in the differentiation of the adrenergic phenotype in developing sympathetic neurons. Development. 1996;122(7):2079-88.

23. Schneider C, Wicht H, Enderich J, Wegner M, Rohrer H. Bone morphogenetic proteins are required in vivo for the generation of sympathetic neurons. Neuron. 1999;24(4):861-70.

24. Saito D, Takahashi Y. Sympatho-adrenal morphogenesis regulated by the dorsal aorta. Mech Dev. 2015;138 Pt 1:2-7. doi: 10.1016/j.mod.2015.07.011. PubMed PMID: 26235279.

25. Yu PB, Hong CC, Sachidanandan C, Babitt JL, Deng DY, Hoyng SA, et al. Dorsomorphin inhibits BMP signals required for embryogenesis and iron metabolism. Nat Chem Biol. 2008;4(1):33-41. Epub 2007/11/21. doi: nchembio.2007.54 [pii] 10.1038/nchembio.2007.54. PubMed PMID: 18026094; PubMed Central PMCID: PMC2727650.

26. Rodrigues FS, Doughton G, Yang B, Kelsh RN. A novel transgenic line using the Cre-lox system to allow permanent lineage-labeling of the zebrafish neural crest. Genesis. 2012;50(10):750-7. Epub 2012/04/24. doi: 10.1002/dvg.22033. PubMed PMID: 22522888.

27. Colanesi S, Taylor KL, Temperley ND, Lundegaard PR, Liu D, North TE, et al. Small molecule screening identifies targetable zebrafish pigmentation pathways. Pigment Cell Melanoma Res. 2012;25(2):131-43. Epub 2012/01/19. doi: 10.1111/j.1755-148X.2012.00977.x. PubMed PMID: 22252091.

28. Levitzki A, Gazit A. Tyrosine kinase inhibition: an approach to drug development. Science. 1995;267(5205):1782-8. PubMed PMID: 7892601.

29. Barrett SD, Bridges AJ, Dudley DT, Saltiel AR, Fergus JH, Flamme CM, et al. The discovery of the benzhydroxamate MEK inhibitors CI-1040 and PD 0325901. Bioorg Med Chem Lett. 2008;18(24):6501-4. doi: 10.1016/j.bmcl.2008.10.054. PubMed PMID: 18952427.

30. Dudley DT, Pang L, Decker SJ, Bridges AJ, Saltiel AR. A synthetic inhibitor of the mitogen-activated protein kinase cascade. Proc Natl Acad Sci U S A. 1995;92(17):7686-9. PubMed PMID: 7644477; PubMed Central PMCID: PMCPMC41210.

31. Favata MF, Horiuchi KY, Manos EJ, Daulerio AJ, Stradley DA, Feeser WS, et al. Identification of a novel inhibitor of mitogen-activated protein kinase kinase. J Biol Chem. 1998;273(29):18623-32. PubMed PMID: 9660836.

32. Anastasaki C, Estep AL, Marais R, Rauen KA, Patton EE. Kinase-activating and kinase-impaired cardio-facio-cutaneous syndrome alleles have activity during zebrafish development and are sensitive to small molecule inhibitors. Hum Mol Genet. 2009;18(14):2543-54. Epub 2009/04/21. doi: ddp186 [pii]
10.1093/hmg/ddp186. PubMed PMID: 19376813; PubMed Central PMCID: PMC2701326.

33. Grzmil M, Whiting D, Maule J, Anastasaki C, Amatruda JF, Kelsh RN, et al. The INT6 Cancer Gene and MEK Signaling Pathways Converge during Zebrafish Development. PLoS ONE. 2007;2(9):e959. Epub 2007/09/27. doi: 10.1371/journal.pone.0000959. PubMed PMID: 17895999.

34. Cong N, Li Z, Shao W, Li J, Yu S. Activation of ETA Receptor by Endothelin-1 Induces Hepatocellular Carcinoma Cell Migration and Invasion via ERK1/2 and AKT Signaling Pathways. J Membr Biol. 2016;249(1-2):119-28. doi: 10.1007/s00232-015-9854-1. PubMed PMID: 26501871.

35. Gordon CT, Petit F, Kroisel PM, Jakobsen L, Zechi-Ceide RM, Oufadem M, et al. Mutations in endothelin 1 cause recessive auriculocondylar syndrome and dominant isolated question-mark ears. Am J Hum Genet. 2013;93(6):1118-25. doi: 10.1016/j.ajhg.2013.10.023. PubMed PMID: 24268655; PubMed Central PMCID: PMCPMC3853412.

36. Miller CT, Schilling TF, Lee K, Parker J, Kimmel CB. sucker encodes a zebrafish Endothelin-1 required for ventral pharyngeal arch development. Development. 2000;127(17):3815-28. PubMed PMID: 10934026.

37. Sato T, Kurihara Y, Asai R, Kawamura Y, Tonami K, Uchijima Y, et al. An endothelin-1 switch specifies maxillomandibular identity. Proc Natl Acad Sci U S A. 2008;105(48):18806-11. doi: 10.1073/pnas.0807345105. PubMed PMID: 19017795; PubMed Central PMCID: PMCPMC2596216.

38. Clouthier DE, Garcia E, Schilling TF. Regulation of facial morphogenesis by endothelin signaling: insights from mice and fish. Am J Med Genet A. 2010;152A(12):2962-73. doi: 10.1002/ajmg.a.33568. PubMed PMID: 20684004; PubMed Central PMCID: PMCPMC2974943.

39. Baynash AG, Hosoda K, Giaid A, Richardson JA, Emoto N, Hammer RE, et al. Interaction of endothelin-3 with endothelin-B receptor is essential for development of epidermal melanocytes and enteric neurons. Cell. 1994;79(7):1277-85.

40. Hosoda K, Hammer RE, Richardson JA, Baynash AG, Cheung JC, Giaid A, et al. Targeted and natural (piebald-lethal) mutations of endothelin-B receptor gene produce megacolon associated with spotted coat color in mice. Cell. 1994;79(7):1267-76.

41. Yanagisawa H, Yanagisawa M, Kapur RP, Richardson JA, Williams SC, Clouthier DE, et al. Dual genetic pathways of endothelin-mediated intercellular signaling revealed by targeted disruption of endothelin converting enzyme-1 gene. Development. 1998;125(5):825-36. PubMed PMID: 98119793.

42. Braasch I, Volff JN, Schartl M. The endothelin system: evolution of vertebrate-specific ligand-receptor interactions by three rounds of genome duplication. Mol Biol Evol. 2009;26(4):783-99. Epub 2009/01/29. doi: msp015 [pii] 10.1093/molbev/msp015. PubMed PMID: 19174480.

43. Krauss J, Astrinidis P, Frohnhofer HG, Walderich B, Nusslein-Volhard C. transparent, a gene affecting stripe formation in Zebrafish, encodes the mitochondrial protein Mpv17 that is required for iridophore survival. Biology open. 2013;2(7):703-10. doi: 10.1242/bio.20135132. PubMed PMID: 23862018; PubMed Central PMCID: PMCPMC3711038.

44. Parichy DM, Mellgren EM, Rawls JF, Lopes SS, Kelsh RN, Johnson SL. Mutational analysis of endothelin receptor b1 (rose) during neural crest and pigment pattern development in the zebrafish Danio rerio. Dev Biol. 2000;227(2):294-306. doi: 10.1006/dbio.2000.9899. PubMed PMID: 11071756.

45. McMenamin SK, Bain EJ, McCann AE, Patterson LB, Eom DS, Waller ZP, et al. Thyroid hormone-dependent adult pigment cell lineage and pattern in zebrafish. Science. 2014;345(6202):1358-61. doi: 10.1126/science.1256251. PubMed PMID: 25170046; PubMed Central PMCID: PMCPMC4211621.

46. Singh AP, Schach U, Nusslein-Volhard C. Proliferation, dispersal and patterned aggregation of iridophores in the skin prefigure striped colouration of zebrafish. Nat Cell Biol. 2014;16(6):607-14. Epub 2014/04/30. doi: 10.1038/ncb2955. PubMed PMID: 24776884.

47. Ottone C, Krusche B, Whitby A, Clements M, Quadrato G, Pitulescu ME, et al. Direct cell-cell contact with the vascular niche maintains quiescent neural stem cells. Nat Cell Biol. 2014;16(11):1045-56. doi: 10.1038/ncb3045. PubMed PMID: 25283993; PubMed Central PMCID: PMCPMC4298702.

48. Kawai H, Kawaguchi D, Kuebrich BD, Kitamoto T, Yamaguchi M, Gotoh Y, et al. Area-Specific Regulation of Quiescent Neural Stem Cells by Notch3 in the Adult Mouse Subependymal Zone. J Neurosci. 2017;37(49):11867-80. doi: 10.1523/JNEUROSCI.0001-17.2017. PubMed PMID: 29101245.

49. Engler A, Rolando C, Giachino C, Saotome I, Erni A, Brien C, et al. Notch2 Signaling Maintains NSC Quiescence in the Murine Ventricular-Subventricular Zone. Cell Rep. 2018;22(4):992-1002. doi: 10.1016/j.celrep.2017.12.094. PubMed PMID: 29386140.

50. Alunni A, Krecsmarik M, Bosco A, Galant S, Pan L, Moens CB, et al. Notch3 signaling gates cell cycle entry and limits neural stem cell amplification in the adult pallium. Development. 2013;140(16):3335-47. doi: 10.1242/dev.095018. PubMed PMID: 23863484; PubMed Central PMCID: PMCPMC3737716.

51. Chapouton P, Skupien P, Hesl B, Coolen M, Moore JC, Madelaine R, et al. Notch activity levels control the balance between quiescence and recruitment of adult neural stem cells. J Neurosci. 2010;30(23):7961-74. doi: 10.1523/JNEUROSCI.6170-09.2010. PubMed PMID: 20534844.

52. Thomas AC, Zeng Z, Riviere JB, O'Shaughnessy R, Al-Olabi L, St-Onge J, et al. Mosaic Activating Mutations in GNA11 and GNAQ Are Associated with Phakomatosis Pigmentovascularis and Extensive Dermal Melanocytosis. J Invest Dermatol. 2016;136(4):770-8. doi: 10.1016/j.jid.2015.11.027. PubMed PMID: 26778290; PubMed Central PMCID: PMCPMC4803466.

3.7 Supplementary figures.

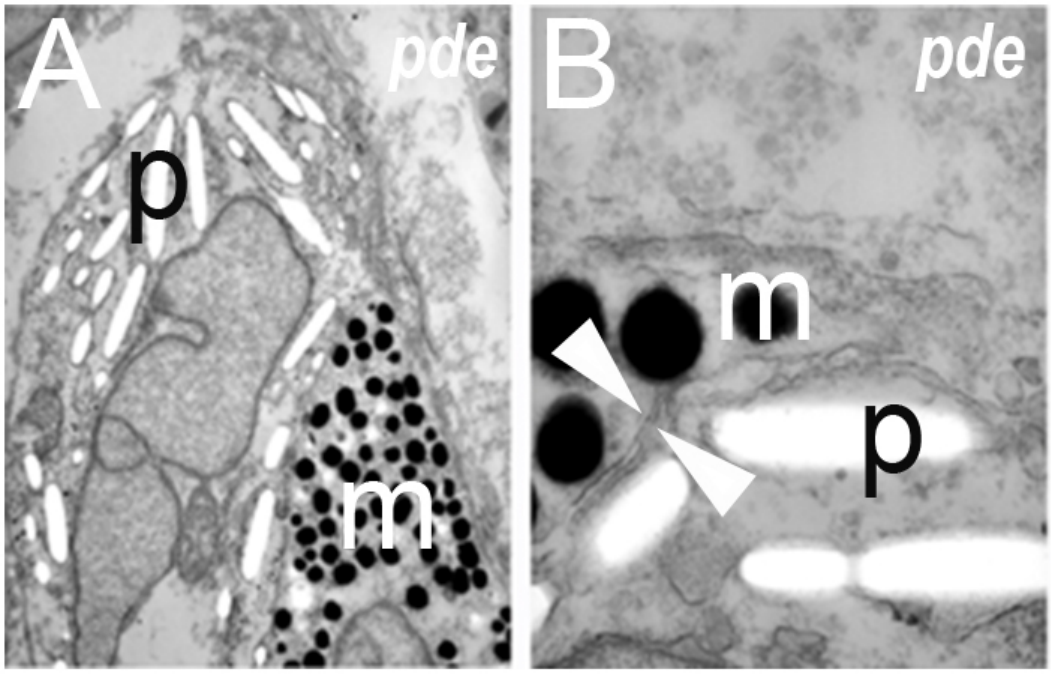

S Figure 3.1 Figure Melanophores and iridophores in the WT yolk sac stripe are consistently separated from each other by double membranes. Transmission electron photomicrographs of melanophores and iridophores in the WT yolk sac stripe ectopic pigment cells in *pde* mutants. A and B show two examples of melanosomes (m) and reflecting. platelets (p) separated by a double membrane (white arrowheads).

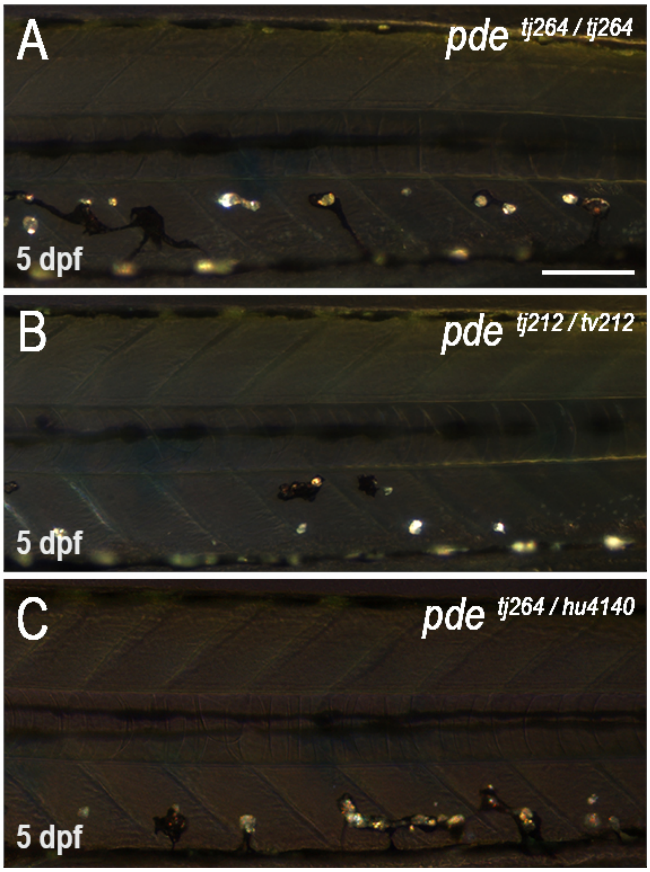

S Figure 3.2 Figure Complementation assay of the *pde* alleles. Overview of early larval pigment phenotype at 5 dpf of *pde*$^{tj262/tj262}$ (A), *pde*$^{tj262/tv212}$ and *pde*$^{tj262/hu4140}$. All three allele combinations show ectopic melanophores and iridophores in the ventral medial pathway of the posterior trunk. Scale bar = 100 μm (A-C).

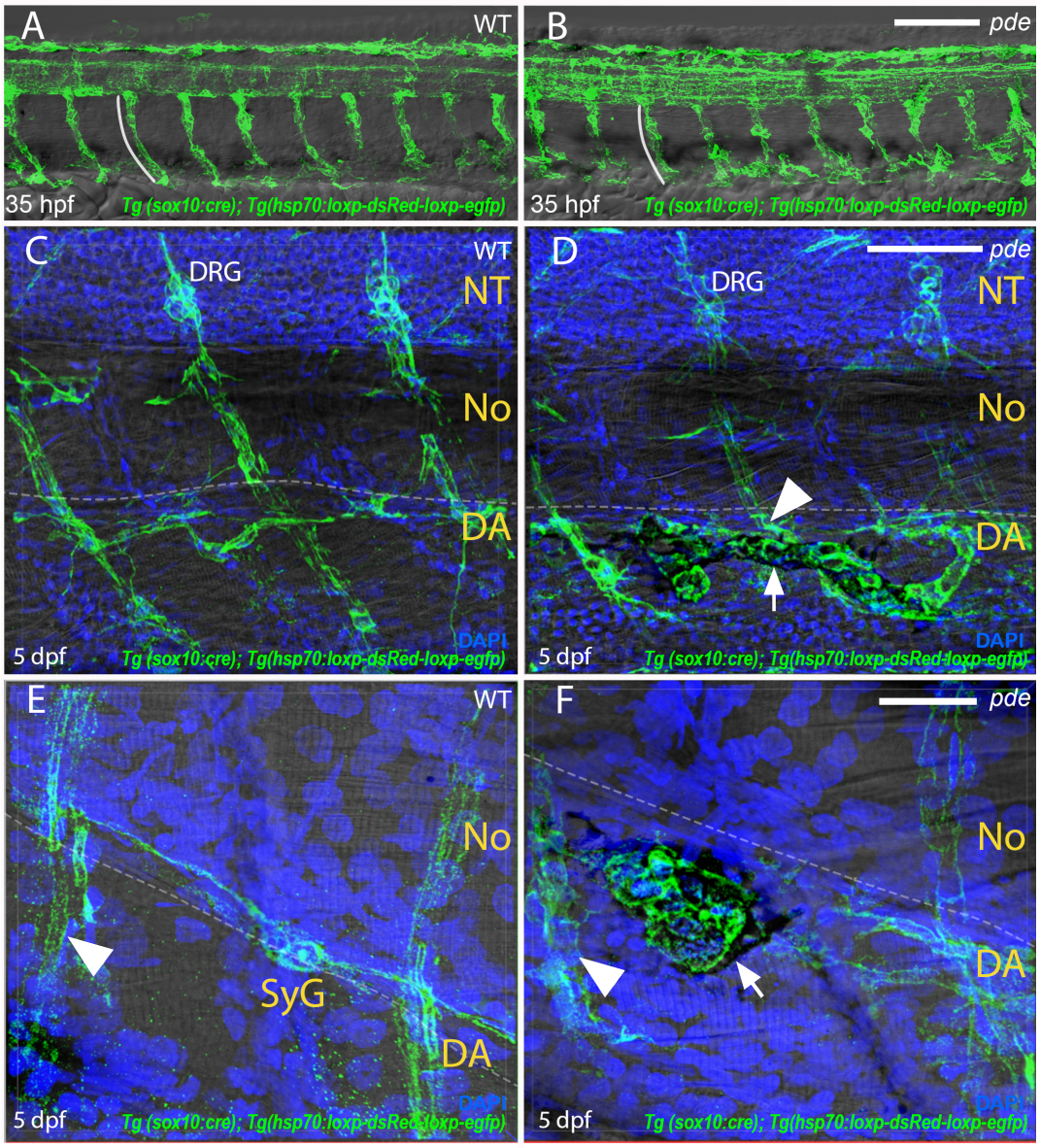

S Figure 3.3 Migration of neural crest cells through the medial migratory pathway. Labelling of neural crest derivatives with GFP using the transgenic line *Tg(-4725sox10:cre)ba74; Tg(hsp:loxp-dsRed-loxp-LYN-EGFP)* shows no difference between 35 hpf WT fish (A) and *pde* mutants (B), neural crest cells migrate ventrally in a intersegmental arrangement (white line in A and B). 5 dpf *pde* mutant larvae show ectopic pigment cells (white arrow in D) associated with the spinal nerve projections (arrowheads in D) that emerge from the dorsal root ganglia (DRG). Ectopic pigment cells (white arrows) are also associated with the sympathetic ganglion (SyG), chain that forms perpendicular to the spinal nerve projections (white arrowhead in E and F) and ventral to the notochord (No). Guided by DIC image, dorsal edge of the dorsal aorta (DA) is highlighted with a dashed white line in C-F. Neural tube (NT). DAPI labels nuclei (blue). Scale bar = 25 μm (A and B), 50 μm (C and D) and 15 μm (E-F).

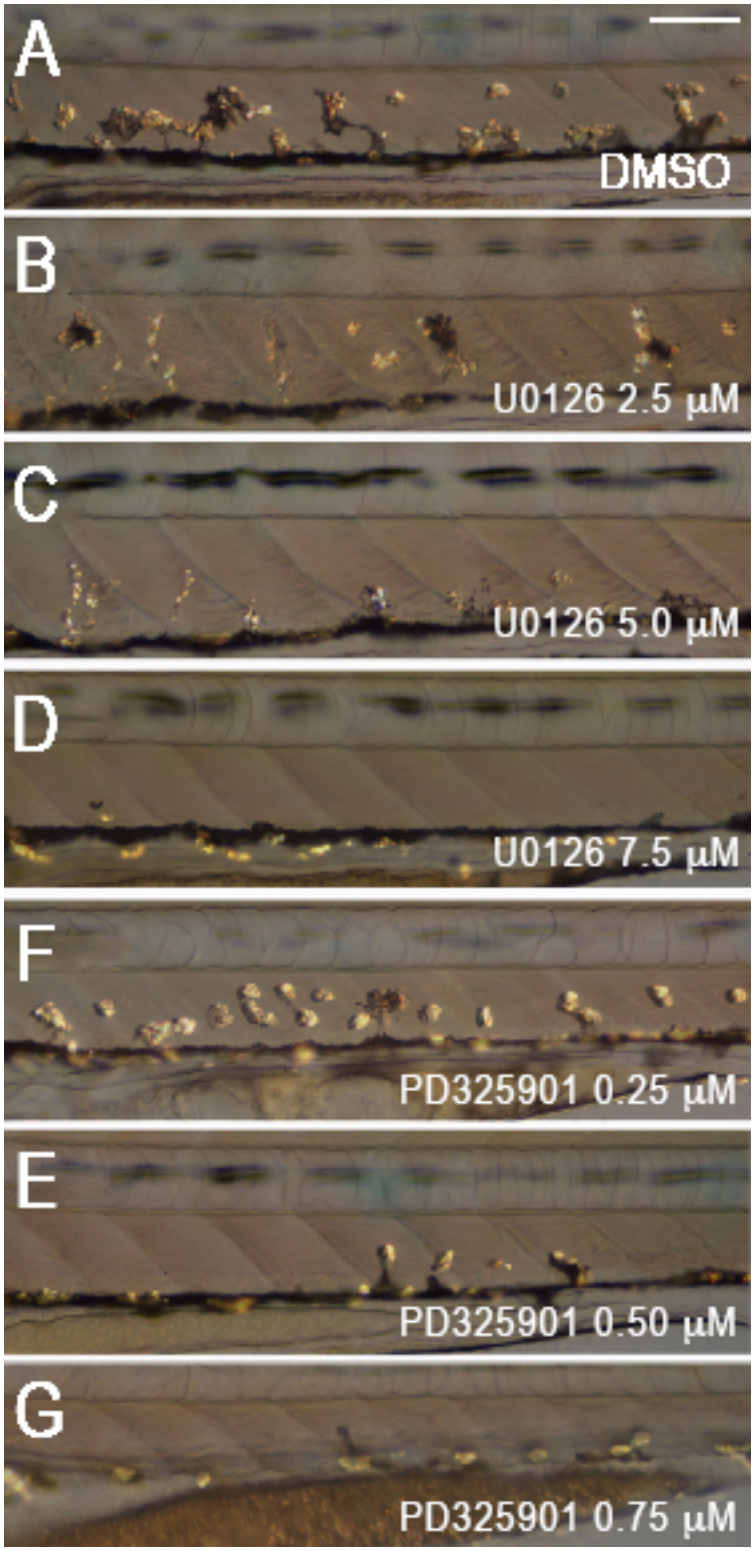

S Figure 3.4 Inhibition of MEK rescues the *pde* phenotype. Treatment with increasing concentrations of the MEK inhibitors U0126 (2.5-7.6 µM) and PD 325901 (0.25 -0.75µM), from 6 – 96 hpf, shows increasing rescue of the ectopic pigment cells. Scale bar = 100 µm (A-G).

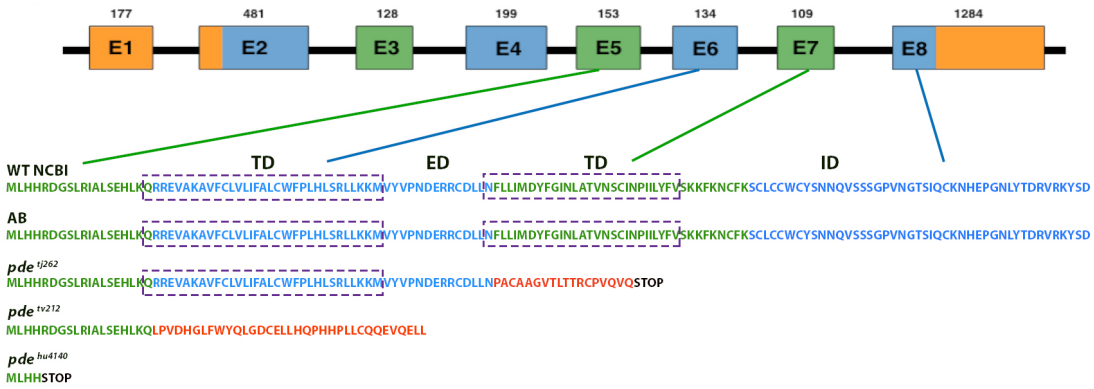

S Figure 3.5 In-silico translation and structural prediction for the *pde* alleles. Schematic representation of the WT ednraa gene. Solid black line corresponds to intronic regions, but these are not shown to scale. Exons are numbered and shown in boxes. 5' and 3' UTRs are shown in orange, while coding exons are shown in alternating blue and yellow colour for visualisation purpose. Single letter a.a. sequence is shown. From top to bottom, the amino acid sequence provided by NCBI, and deduced sequences from in-silico translation of our sequenced cDNAs from AB, *pde*^{tj262}, *pde*^{tv212} and *pde*^{hu4140} alleles. Solid green and blue lines link the corresponding exon to the amino acid sequence. Transmembrane domains (TD) are shown in dashed purple boxes and the extracellular domain (ED) and intracellular domains (ID) are labelled accordingly.

CHAPTER 4

CHAPTER 4 Characterisation of zebrafish endothelin signalling system mutants.

4.1 Introduction.

We have identified a mutant of the endothelin receptor Aa (Ednraa), *parade*, which in addition to the normal embryonic pigment pattern, shows a group of ectopic and supernumerary melanophores and iridophores restricted to the ventral medial pathway and that are closely associated with the ventral nerve projections of the DRGs and sympathetic ganglia. We determined that these ectopic pigment cells arise from over proliferation of NC-derived cells near the dorsal aorta and that these cells are dependent on Erb signalling, which is required for the establishment of adult pigment stem cells. We have also shown that neither disrupted migration nor transdifferentiation of other neural crest derivatives are the source of the ectopic cells.

Based on these results, we hypothesized that the disrupted function of Endraa in *pde* mutants, modifies the environment (niche) provided by the blood vessels. Thus, in a WT context, *ednraa* usually keeps adult pigment stem cells in a quiescent state, but in mutant context, lack of function of *ednraa* causes a premature activation (proliferation and differentiation) of the adult progenitor/stem cells, resulting on the *ednraa* mutant phenotype. However, a major gap in our understanding is what other components of the Endothelin signalling pathway contribute to Ednraa's function in pigment cell development. Particularly it remains unknown what is the endothelin ligand of the endothelin receptor Aa in zebrafish and what other components are involved in the mechanism of the *ednraa* mutant.

In the following section, we will address the current understanding of the endothelin system in zebrafish as review the phenotype mammalian and zebrafish mutants.

4.1.1 The endothelin system in zebrafish.

Phylogenetic analysis of endothelins identifies the presence of four endothelin family members (*edn1, edn2, edn3 and edn4*) in bony vertebrates, of which *edn4* family is exclusive of teleost genomes, whereas in tetrapods, only three family members are found. In zebrafish, additionally two co-orthologous copies of *endothelin*-2 (*edn2*) and *endothelin*-3 (*edn3*) have been identified, thus giving a total of six endothelin genes: *edn1*, *edn2a*, *edn2b*, *edn3a*, *edn3b* and *edn4* (Braasch et al. 2009). In human and mouse genomes, there are only two endothelin receptor genes (*EDNR*/*ednr*), *Ednra* and *Ednrb* respectively; Arai et al. 1990; Sakurai et al. 1990), whereas zebrafish possess two orthologues of each endothelin receptor gene (*ednr*): *ednraa* and *ednrab* and *ednrba* and *ednrbb*. Similarly, one of the two endothelin converting enzymes genes identified in zebrafish has two orthologues: *ece1, ece2a and ece2b*.

4.1.2 Mammalian endothelin system mutant models.

Mice homozygous for mutations of *Endothelin 1* (*Edn1*) or *Endothelin receptor type A* (*EdnrA*) receptor (Kurihara et al. 1994; Yanagisawa, Yanagisawa, et al. 1998) exhibit the same craniofacial and cardiac abnormalities as well as impaired thyroid and thymus development, while *Ece1* mutants show the same phenotype as *Edn1*/*Ednra* single mutants, but also display lack of epidermal melanocytes and enteric neurons of the distal gut (Yanagisawa, Hammer, et al. 1998), and are lethal 30 minutes after birth. *Ednra* mutant mice display conversion of lower jaw into similar structures of the upper jaw (Ruest et al. 2004). Thus, in mice, Ece-1, Edn1 and EdnrA work together in dorsoventral patterning of the ventral craniofacial neural crest derived cells. However, likely because all of these mutants are lethal at the time of birth, no pigmentation phenotype has been reported. Mouse homozygous mutant for *Ece2* display a normal phenotype, but the double *Ece1*/*Ece2* homozygote mutants have more sever cardiac abnormalities, thus revealing that ECE-2 contributes or can partially compensate, although to a lower extent and locally (the heart), to the maturation of Edn1.

Interestingly, mice mutant for *Edn3* or *Ednrb* display identical phenotypes, in which the enteric nervous system precursors do not colonize the intestine and neural crest-derived epidermal melanoblasts fail to colonize the skin (Kurihara et al. 1999), a phenotype similar to that of *Ece1* mouse mutants(Yanagisawa, Yanagisawa, et al.

1998). This suggests that in the mouse, ECE-1 contributes to the cleavage of both ET-1 and ET-3. Mutants of *Edn3* had a survival rate of 21 days after birth, although the cause of death is not yet determined (Kuwaki et al. 2002). Regarding the pigmentation phenotype, *Edn3* and *Ednrb* mutants, both in a black coat background, develop a white coat in the body, mainly retaining the black pigmentation of the head.

Mouse homozygote mutants of *Edn2* display growth retardation, reduced blood glucose although normal insulin levels. Additionally, this mutant presents lower temperature level and abnormal lungs (Chang et al. 2013). Surprisingly, although *Edn2* was found to be expressed in the developing hair follicles in a reporter transgenic line (Cacioppo et al. 2015), no pigmentation phenotype has been reported.

A number of studies have shown that *Edn3* is necessary for *in vitro* melanocyte development (Reid et al. 1996) and that inducible tissue specific over expression of *Edn3* promotes skin pigmentation in a mouse model (Garcia et al. 2008).

4.1.3 Endothelin system mutants and morphants in zebrafish.

4.1.3.1 *endothelin* 1 (*sucker*) mutant and *endothelin receptor aa* and ab morphants.

Previous work showed that a zebrafish mutant of e*dn1* called *sucker*, displayed abnormal formation of the ventral craniofacial cartilages, specifically, formation of the lower jaw is completely disrupted (Nair et al. 2007), a phenotype similar to that of *Edn1*/*EdnrA* mice mutants, which suggests that, similar to human and mouse, Edn1 signals through the zebrafish ET_A paralogs, EdnrAa and EdnrAb. Single morphants of *ednraa* and *ednrab* revealed abnormal patterning of the lower jaw, with the former displaying a larger Meckel's cartilage and the latter a shorter one. Interestingly, the double *ednraa*; *ednrab* morphant phenocopies the *edn1* mutant, which confirms the Edn1-EdnrA/EdnrB interaction. In this published study, the pigment phenotype was not examined.

4.1.3.2 *endothelin receptor ba (rose)* mutant.

In adult zebrafish (Fig. 4.1 A), *ednrba* loss of function mutants display reduced iridophores and melanophores and the characteristic striped pattern is disrupted. Instead, the few melanophores that are generated form one stripe in dorsal trunk of the fish and spots in the central stripe (Fig. 4.1 B). In contrast, the ventral trunk has almost no melanophores, nor stripes. In zebrafish, the formation of the adult patterning starts at the onset of metamorphosis, in which newly differentiated pigment cells are mostly generated *de novo*. In *ednrba* mutants, new melanophores are generated in early metamorphosis, however at late metamorphosis fewer melanophores are produced in comparison to WT fish (Parichy et al. 2000). Surprisingly, the embryonic pigment phenotype of this mutant is indistinguishable from that of WT embryos, which suggests that in zebrafish there is an age specific redundancy with one or more of the other endothelin receptors (*ednraa*, *ednrab* or *ednrba*). In contrast, mouse studies have shown that Edn3/EdnrB is required during embryogenesis for the establishment of melanophore precursors in the hair follicle, and for enteric neurons in the distal colon (Hosoda et al. 1994). The latter phenotype has not been assessed in zebrafish *ednrba* mutants.

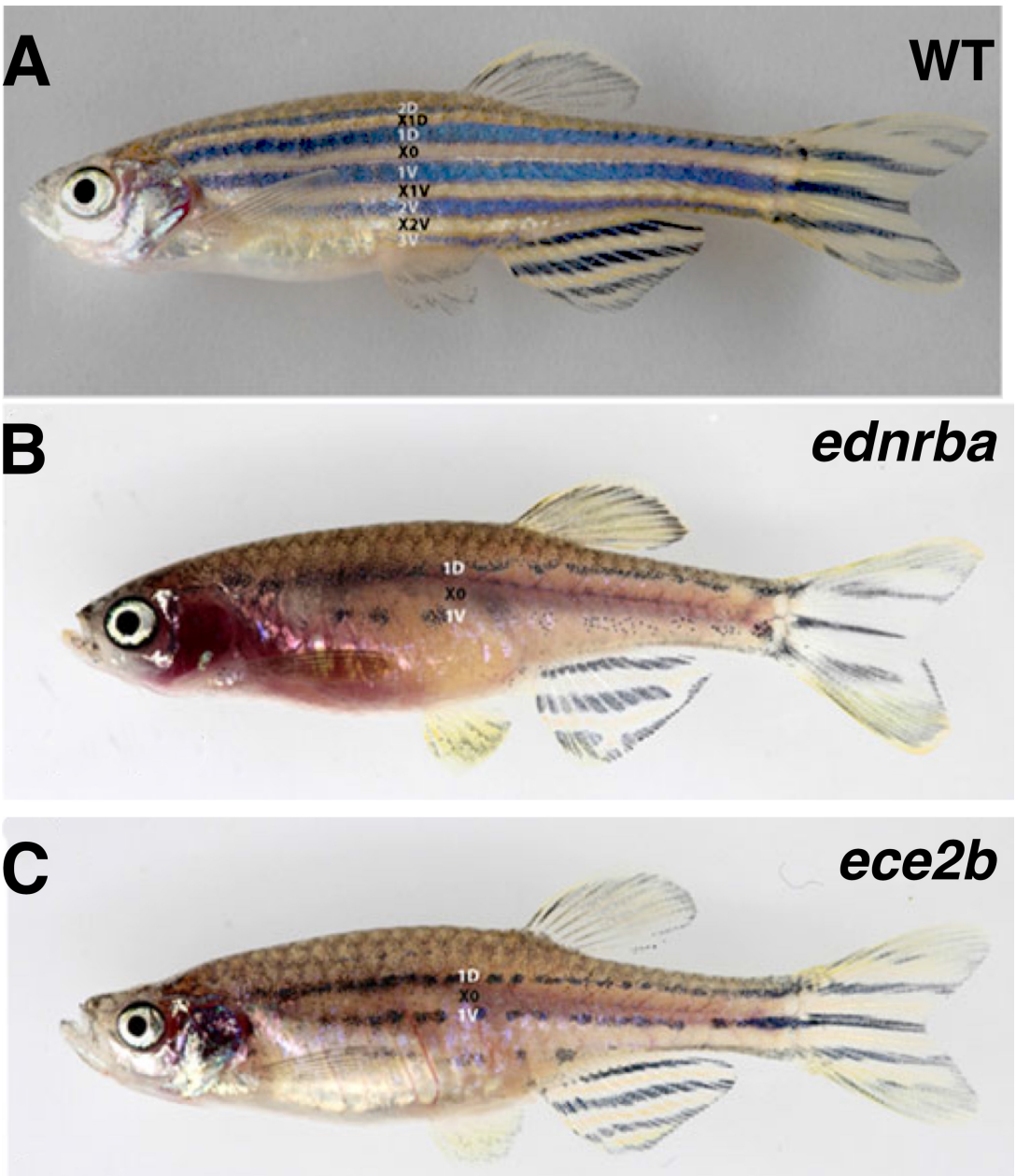

Figure 4.1 *ednrba* and *ece2b* loss of function mutants display reduced melanophores and iridophores and broken stripes. Adult pigment phenotype of WT (A), *ednrba* (B) and *ece2b* (C) mutants. Black stripes are labelled 1V, 1D, 2V, 2D; light interstripes labelled X0, X1D, X1V, X2V from the centre outwards. Adult WT (A) fish display the characteristic striped pattern, while *ednrab* (B) and *ece2b* (C) both display the same phenotype, broken stripes and reduced melanophores and iridophores. Modified from Krauss et al, 2014.

4.1.3.3 *endothelin converting enzyme 2b (karneol)* mutant.

In a ENU mutagenesis screening, the Nüsslein-Volhard research group identified a loss of function mutant of the *endothelin converting enzyme 2b (ece2b)* gene. Adult homozygous mutants display a strong reduction of iridophores and melanophores and a broken-stripes phenotype, resembling the *ednrba* mutant phenotype (Fig.4.1C). Similarly, *ece2b* mutants have a normal embryonic pigment phenotype, suggesting no requirement of *ece2b* in embryonic pigmentation (Krauss et al. 2014). Therefore, in zebrafish, *ece2b* is likely to be the major ECE cleaving the ligand that binds to *ednrab*. In this work, morpholino knock down of *edn3b* revealed strong reduction of embryonic iridophores only, while embryonic melanophores are completely unaffected. This data suggests that in zebrafish *edn3* may have a role in embryonic and conceivably in adult iridophore development.

4.1.4 Embryonic expression pattern of *endothelin* genes in zebrafish.

Expression of *edn1* is detected in the branchial arches and lateral patches at 18, 24 and 48 hpf (Fig. 4.2 A-C). In addition to the branchial arches, at 48 hpf (Fig. 4.2 C and F) the head shows a broader expression of *edn1*. This agrees with the craniofacial phenotype observed in *edn1* mutants in which patterning and formation of the ventral cartilages are disrupted. The posterior trunk also shows *edn1* expression throughout development. At 18 hpf (Fig. 4.2 A) *edn1* is strongly expressed dorsally in the premigratory neural crest domain, then at 24 hpf expression is detected across the dorso-ventral axis with a slightly higher expression on the ventral region of the anterior trunk, specifically above the yolk sac and yolk sac extension, a region that accumulates a high density of iridophores known as lateral patches, and the dorsal side of the tail (Fig. 4.2 B). Expression of *edn1* at 48 hpf is not detected in the posterior trunk nor tail (Thisse & Thisse 2005). Early expression of *edn1* in the premigratory neural crest domain, and across the trunk and tail, suggest a role for *edn1* in early specification and patterning of neural crest derivatives. Expression in the region of the lateral patches recalls that of various iridophore markers, and suggests a possible role in iridophore patterning or maintenance. *In situ* hybridization of *edn3a* and *edn3b* at 48 hpf show that *edn3a* is not detected (Fig. 4.2 D), while *edn3b* expression is strongly detected in the epidermis (Fig. 4.2 E D) (Krauss et al. 2014).

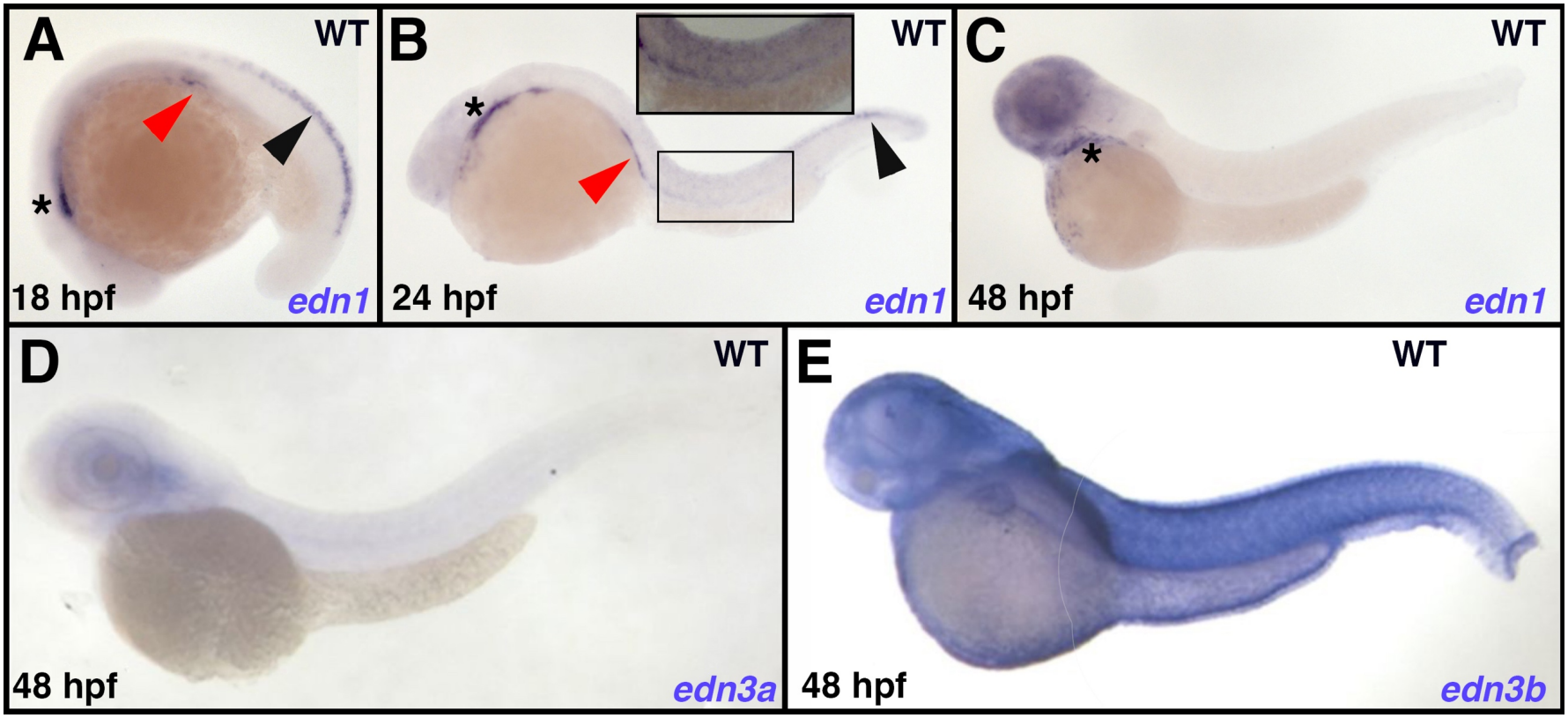

Figure 4.2 Embryonic expression *of edn1*, *edn3a and edn3b*. *In situ* hybridization of *edn1*, 18, 24 and 48 hpf (A-C). *edn3a* (D) and *edn3b* (E) expression at 48 hpf. Branchial arches (*), lateral patches (red arrowheads), premigratory neural crest domain (black arrowheads). Inset represents enlargement of region of posterior trunk in black box (B). Panels A-C from Thisse, B., Thisse, C. (2004). ZFIN Direct Data Submission, panels D and E modified from Krauss et al, 2014.

4.1.5 Embryonic expression pattern of *endothelin receptor* genes.

Expression of *ednraa* is mainly detected in the developing vasculature. At 19 somites stage (Fig. 4.3 A), lateral view shows expression in the region of the anterior and posterior lateral mesoderm, in ventral region of the head, matching the location of the formation of the midcerebral vein. At 22 hpf (Fig. 4.3 B) *ednraa* expression is strongly detected in cranial vasculature, specifically in the mid cerebral vein and the midbrain channel. Expression is also detected in the ventral side of the posterior trunk just above the yolk sac, matching the formation of the nascent dorsal aorta, the posterior cardinal vein and primitive erythroid progenitors within the caudal vein. Higher magnification of the head at 24 hpf shows clear expression in the branchial arches (Fig. 4.4 C) (Nair et al. 2007). This is consistent with the reported morphant phenotypes in which *ednraa*-MO wild type embryos display larger jaws. At 30 hpf and 48 hpf (Fig. 4.3 D and E) the expression of *ednraa* in the trunk matches the characteristic pattern of the major trunk vessels, dorsal aorta and the intersegmental vessels. Note that *ednraa* expressing cells are detected in the dorsal trunk, these could be confused with neural crest cells, however, according to our preliminary data on figure 6.5., expression of *ednraa* by RT-PCR of FACS sorted fluorescently labelled neural crest derived cells is not detected, for which we concluded that expression of *ednraa* in the neural crest in trunk is not observed. Thus, it becomes very intriguing that a gene expressed in the developing vasculature has an effect on pigment cells.

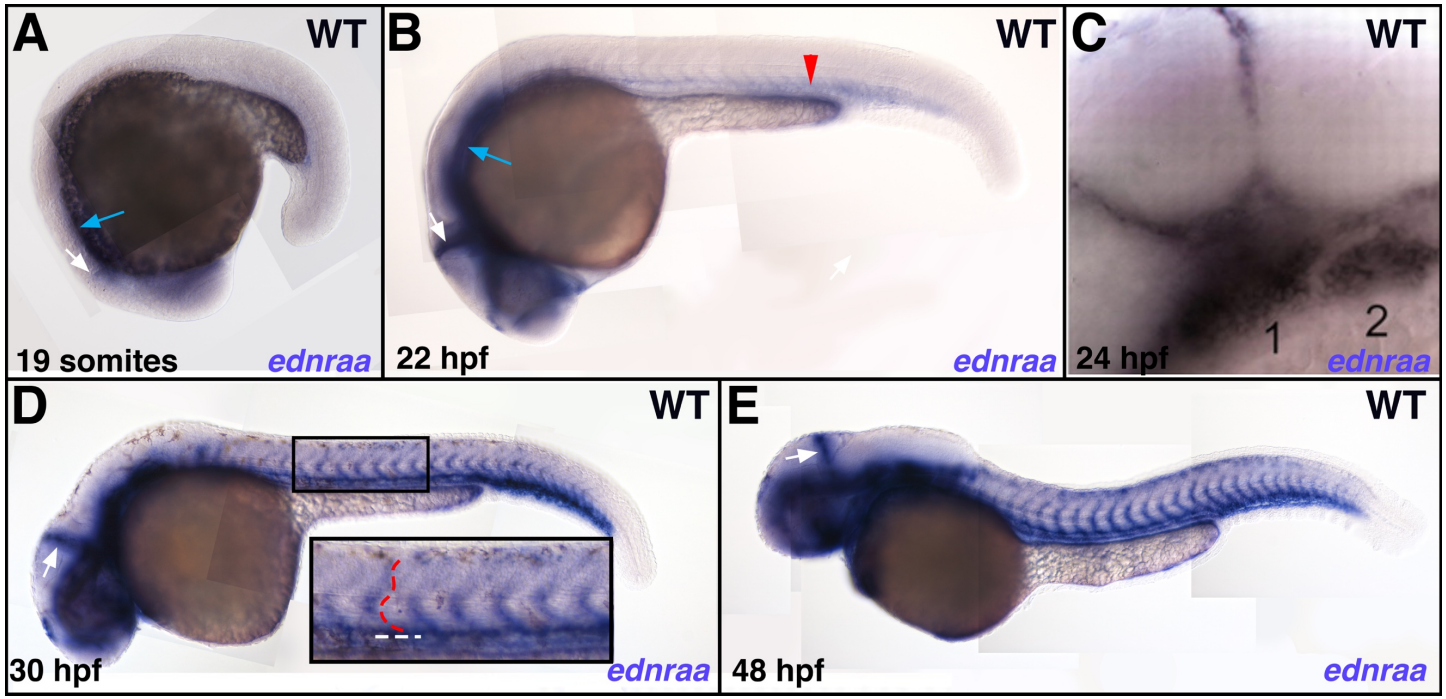

Figure 4.3 Embryonic expression of *ednraa*. *In situ* hybridization of *ednraa* at 19 somites (A), 22 hpf (B), 24 hpf (C), 30 hpf (D) and 48 hpf (E). Midcerebral vein (white arrow; A, B, D and E), lateral mesoderm (blue arrow; A and B). Branchial arches one (1) and (2; C). Magnification of anterior trunk is shown in black box (D), ventral edge of dorsal aorta (white dashed line), intersegmental vessels (red dashed line). Modified from (Camargo-Sosa, K., et al, submitted and Nair et al. 2007).

Expression of *ednrab* at 12 somites stage (Fig. 4.4 A and B) is strongly detected in the migrating neural crest on the head and the premigratory neural crest domain of the anterior trunk. At 19 hpf (Fig. 4.4 B) *ednrba* is expressed in the brachial arches in concordance with its role in craniofacial patterning. In the trunk, *ednrba* it is also detected in the migrating neural crest. At 27 hpf (Fig. 4.4 C), *ednrab* expression is detected in an intersegmental pattern corresponding to neural crest cells migrating through the medial pathway (Thisse & Thisse 2005). Note that expression of *ednrab* in the trunk at 30 hpf seems to overlap with *ednraa* expression. However, *ednrab* is expressed intersegmentally, while ednraa expression is located at the border of each somite segment. On the other hand, overlapping of *ednraa* and *ednrab* expression in the branchial arches is consistent with the craniofacial phenotype observed in the single and double mutants (Nair et al. 2007)

Pigment progenitors migrate from the dorsal side of the neural tube, down towards the ventral region of the embryos through two migratory pathways, the lateral migratory pathway and the medial migratory pathway. Xanthophores, migrate exclusively through the lateral pathway, melanophores, migrate through the lateral and medial pathway and iridophores migrate only through the medial pathway. Because *ednrab* is expressed in the medial pathway, we predict that *ednrab* has a role on iridophores and melanophores development but not in xanthophores.

Expression of *ednrba* at 24 hpf (Fig. 4.4. D) is detected in migratory NC in the head, whereas in the trunk expression is detected in both the premigratory and the migrating neural crest. At 30 hpf (Fig. 4.4 E), a broader expression of *ednrba* is detected, in what seems to be migrating neural crest cells. Previous works have identified that *ednrba* is expressed by neural crest-derived cells that generate both melanophores and xanthophores (Parichy et al. 2000) and very interestingly, late in development, expression of *ednrba* becomes restricted to iridophores (Fig. 4.4 F). Thus, it remains very intriguing that despite being expressed so broadly in the neural crest, *ednrba* mutants do not display an embryonic pigment phenotype.

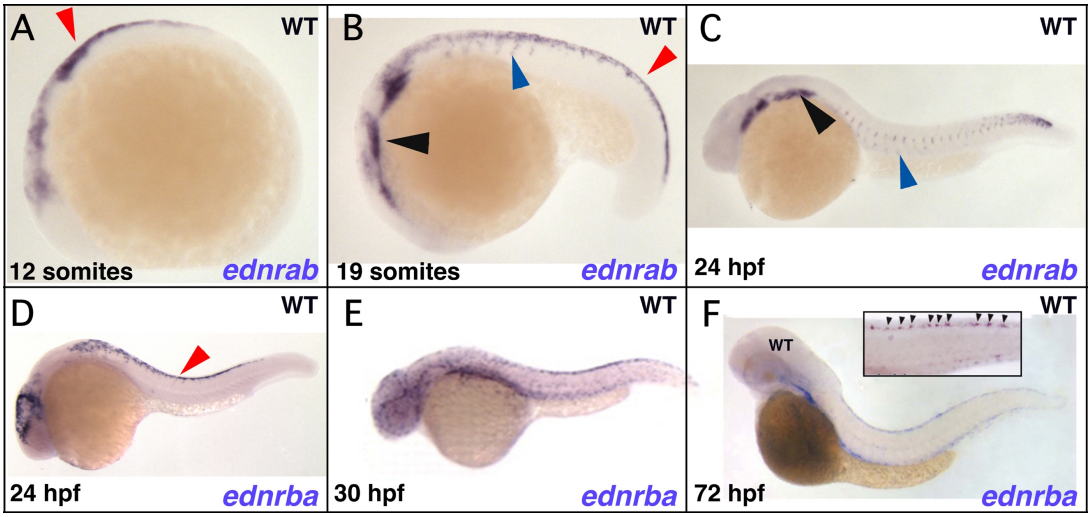

Figure 4.4 Embryonic expression of *ednrab* and *ednrba*. *In situ* hybridization of *ednrab* at 12 and 19 somites and 24 hpf (A-C) and *ednrba* at 24, 30 and 72 hpf (D-F). Premigratory domain (red arrowheads), branchial arches (black arrow heads) and migrating neural crest cells (blue arrow heads.). Black box in F shows *ednra* expression in iridophores. Panels A-C modified from (Thisse & Thisse 2005). Panel D (Arduini et al. 2009), panel E (Lang et al. 2009) and panel F (Krauss et al. 2014).

Zebrafish endothelin mutants such as *ednrba* and *ece2b* mutants, have shown a deficiency in adult pigment pattern development. In mouse, Edn3 signals through EdnrB, thus, potentially, *edn3b* could have a role in iridophore development via *ednrba*. In the embryo, only a craniofacial phenotype has been reported in *edn1* mutants and *ednraa* and *ednrab* morphants, but no pigment phenotype has been noted. Thus, *pde* (*ednraa*) mutants are the only mutants of the endothelin system that display an embryonic pigment phenotype. Furthermore, one in which instead of having decrease pigment cells, more cells are found and these in ectopic places. Because *edn1* is expressed broadly in the posterior trunk and it is known to interact with ET_A/EdnrA in human and mouse, we hypothesize that in the trunk, *edn1* interacts with *ednraa*, and that both are involved in the mechanism of the *parade* phenotype.

In order to address our hypothesis, in collaboration with Prof. Christiane Nüsslein-Volhard, that as part of her ongoing research in adult pigment pattern formation has generate mutant of some of the endothelin system genes (*edn1*, *edn3a*, *edn3b*, *ednraa, ednrab* and *ece1*), using CRISPR/Cas9 targeted mutagenesis. Injection of gRNA/Cas9 into one-cell stage embryos (Dr. Uwe Irion), identification of mutant carriers and establishment of lines was performed in the Max-Plank Institute for Developmental Biology (MPIDB) by the Nüsslein-Volhard lab. Screening and identification of *ece1*. *edn1* and *ednrab* mutants was performed by myself. Additionally, I generated double mutants of *ednraa*; *ednrab* as well as a mutant of the *edn2a* ligand. Initial analysis of the embryonic pigment pattern of all mutants was performed at the MPIDB. Embryos of single mutants for *edn1*, *edn2a*, *edn3a*, *edn3b*, and double mutants for *ednraa* and *ednrab* were shipped to the fish facility of the University of Bath for further examination.

4.2 Results

4.2.1 Generation of mutants with CRISPR/Cas9 targeted mutagenesis.

For the generation of mutants of *edn1*, *ednraa*, *ednrab*, *ednrba* and *ece1*, customised gRNA (Fig. 4.5 A, C-E) were designed and synthetized in the Max-Plank Institute for Developmental Biology using a pDR274 vector (Figure 4.6 A) that allows T7 RNA polymerase-mediated production of a customizable gRNA containing a 20 nucleotides sequence complementary to the target site of each gene. CRISPR target sites of the nature 5'-$\mathbf{N_{20}}$-NGG-3' were identified (Table 4.1), where 5′-NGG-3' is the canonical sequence knows as protospacer adjacent motif (PAM) necessary for Cas9 recognition and cleavage of the target site.

Name	CRISPR target site + PAM
edn1 gRNA	GGAGACGCCGGGCGGCCGTTTGG
edn1 gRNA	GGTTTAAAGCAGCGTCAGACAGG
ednraa gRNA	GGTGGATTATGTCTGATAAATGG
ednrab gRNA	AGGTCGCGCACGCAGGTCAGAGG
ece1 gRNA	CACCTCGCAGAAAATGATGGAGG
edn2a crRNA 1	GCAATCCACCTGCTCACAAACGG
edn2a crRNA 2	AACGCTGTTCCTGTAGTAGCTGG

Table 6 .1 Sequence of CRISPR target sites + PAM sites are shown from 5'-3' PAM sites are underlined.

A forward (Fw) 5'-TAGG$\mathbf{N_{20}}$-3'and a reverse (Rv) 5'-AAAC$\mathbf{N_{20}}$-3' oligonucleotide was designed and purchased from Sigma-Aldrich ($\mathbf{N_{20}}$=gene specific sequence; Fw and Rv primers are reverse complementary to each other; Table 4.2). Oligonucleotides were annealed in order to obtain a double stranded DNA fragment with 4bp overhang that was cloned into the pDR274 vector (Figure 4.6) and subsequently transformed into competent *E. coli* DH5α cells. At least 3 clones of each CRISPR target site were sequenced to corroborate successful cloning and correct sequence. A PCR fragment of 122 base pairs that included the T7 promotor and the gRNA scaffold was amplified for further *in vitro* transcription followed of precipitation of the gRNA (see details on section 2.2.2.1).

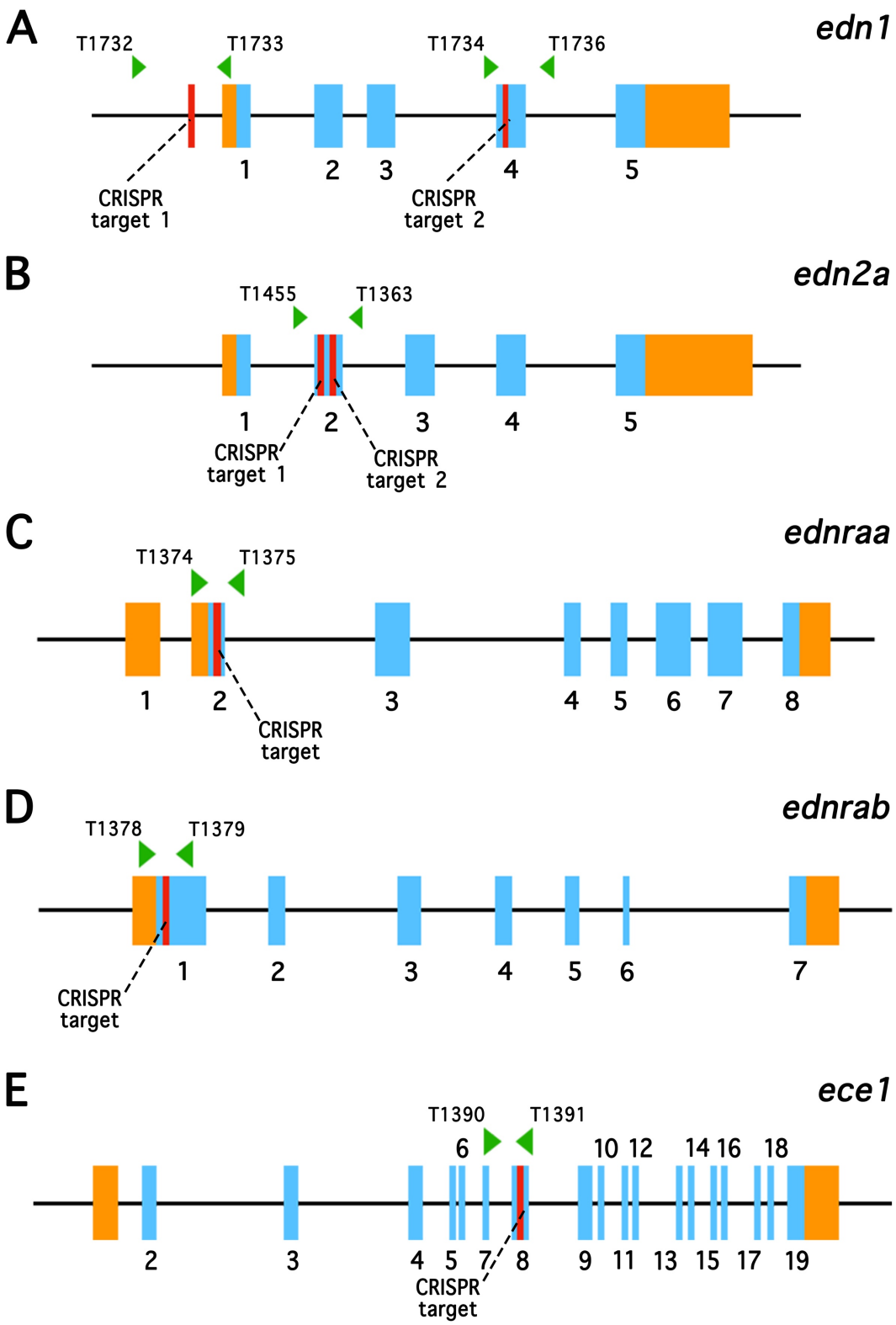

Figure 4.5 CRISPR target sites. Scheme shows gene structure of *edn1* (A), *edn2* (B), *ednraa* (C), *ednrab* (D) and *ece1* (E). Exons (blue boxes) are numbered, UTRs (orange boxes; 5'-3'). CRISPR targets (red lines) and primers (green arrowheads) are annotated above.

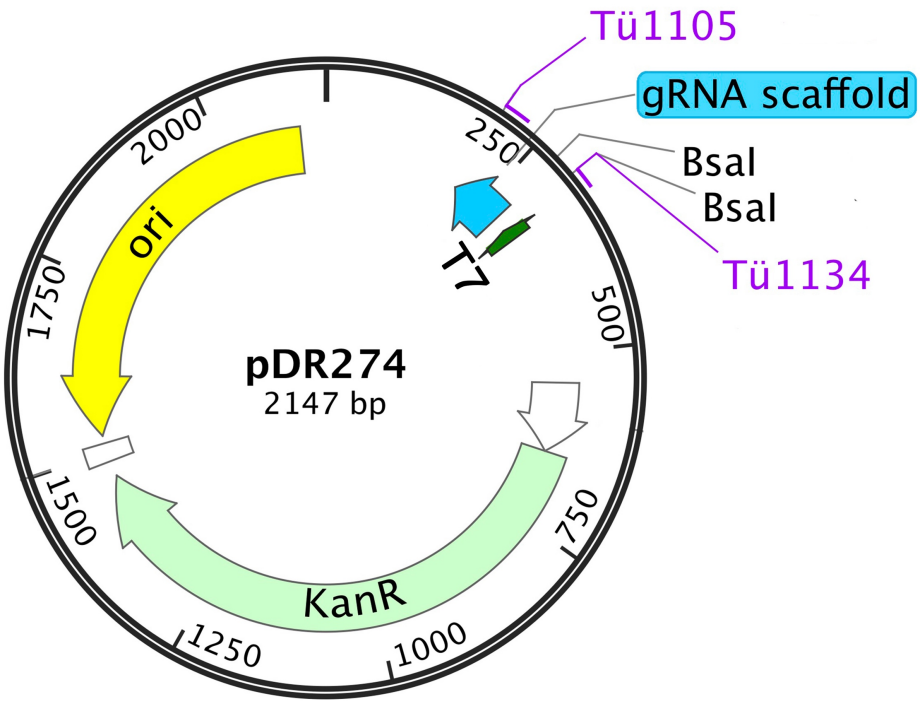

Figure 4.6 pDR247 vector. Map of plasmid pDR247. T7 promotor (green), gRNA scaffold (blue), restriction sites for cloning (BsaI), primers for amplification of T7 promotor + gRNA (Tü1105 and Tü1134).

Name	Forward oligonucleotide	Revers oligonucleotide
edn1 gRNA	TAGGGGAGACGCCGGGCGGCCGTT	AAACAACGGCCGCCCGGCGTCTCC
edn1 gRNA	TAGGGGTTTAAAGCAGCGTCAGAC	TAGGGTCTGACGCTGCTTTAAACC
ednraa gRNA	TAGGGGTGGATTATGTCTGATAAA	TAGGTTTATCAGACATAATCCACC
ednrab gRNA	TAGGAGGTCGCGCACGCAGGTCAG	TAGGCTGACCTGCGTGCGCGACCT
ece1 gRNA	TAGGCACCTCGCAGAAAATGATGG	TAGGCCATCATTTTCTGCGAGGTG

Table 6 .2 Sequence of self-complementary oligonucleotides for cloning into pDR274. 5'-3'.

edn2a mutants were generated using crRNAs and a generic transactivated crRNA (tracrRNA) purchased from Integrated DNA Technologies (see details in section 2.2.2.1). crRNAs had a sequence length of 20 nucleotides complementary to the targeted genomic sequence adjacent to a PAM site.

edn2a crRNA 1	GCAATCCACCTGCTCACAAACGG
edn2a crRNA 2	AACGCTGTTCCTGTAGTAGCTGG

Table 6 .3 Sequence of CRISPR target sites + PAM sites are shown from 5'-3' PAM sites are underlined.

Either the purified gRNAs (35 ng/μl) or the purchased crRNAs (10 μM) were used together with Cas9 protein (700 pg/μl) for injection of approximately 200 1-cell stage wild type embryos (see section 2.2.2.2). Dead and abnormal embryos were discarded and 50 injected embryos of normal morphology were incubated at 28ºC in a single petri dish. At 24 hpf, DNA of 16 normally developing embryos was extracted for sequencing of the targeted region in order to look for chimeric alleles in the chromatograms; an example for the generation of *edn2a* mutants is shown in Fig. 4.7.

After sequencing, sibling of embryos whose sequence showed high percentage of chimeric alleles (>80%) were grown until adulthood as these are likely to have germline transmission of *indel* mutations of the corresponding targeted gene. The F_0 adults were incrossed to look for embryos with a pigment phenotype (decreased or increased number of pigment cells and presence of ectopic pigment cells). Couples of fish that showed embryos with a pigmentation phenotypes were individually outcrossed to a wild type line and the progeny (F_1) was raised until adulthood. F_1 fish were expected to possess either WT homozygous alleles or mutant heterozygous alleles of the targeted gene, however, we expected multiple mutant alleles within each cross as the germline could carry eggs with different mutant alleles. The adult F_1 mutants were genotyped (see section 2.2.3) and mutant carriers of the same allele where in crossed. The phenotype of the resulting progeny (F_2) was assessed, imaged and the region of the corresponding targeted gene was sequenced to corroborate the genotype. Assessment of the phenotype of each mutant is described in the following section.

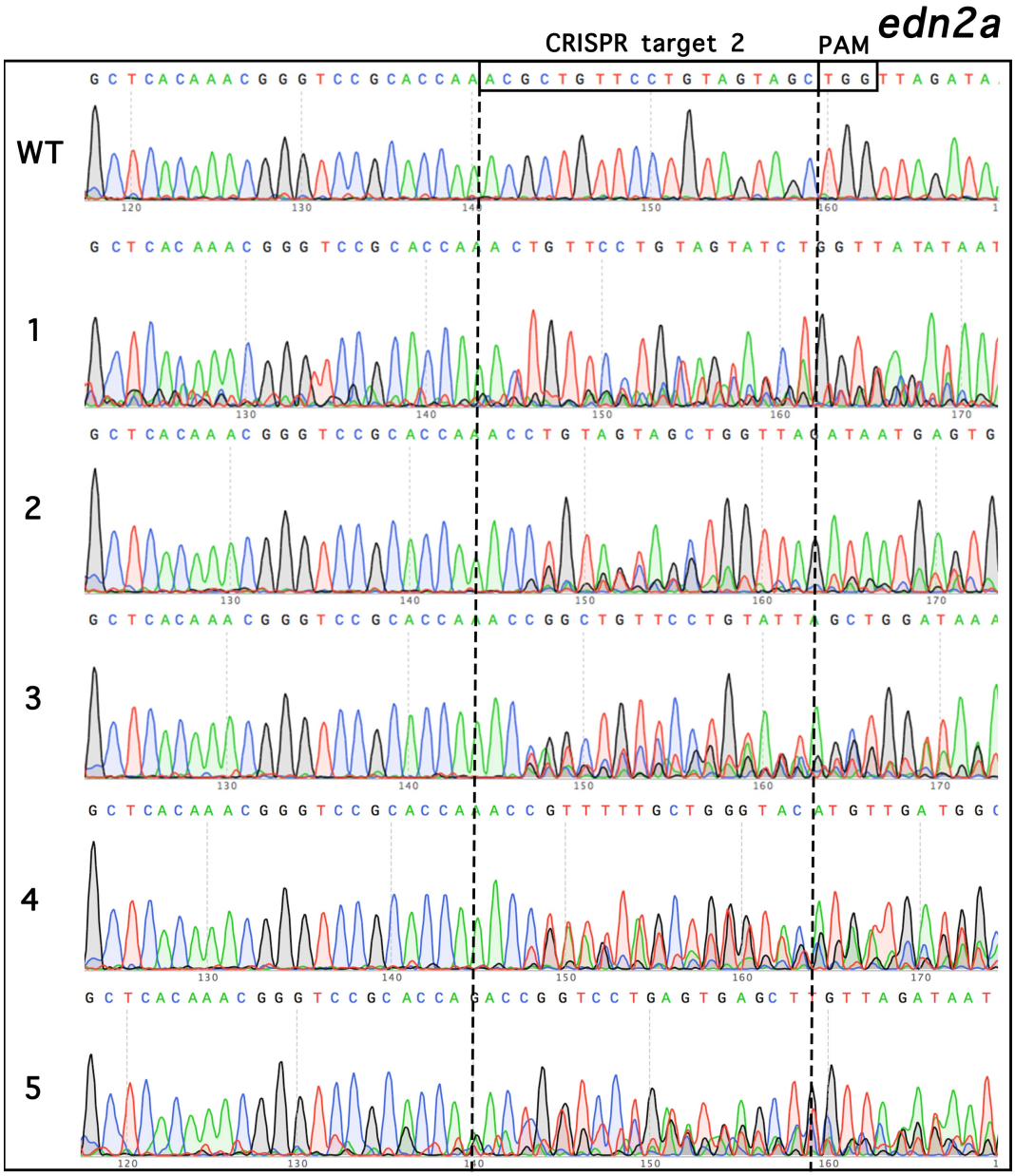

Figure 4.7 Cleavage efficiency. Chromatograms of sequences of individual embryos are shown. Uninjected sibling (A) shows a wildtype sequence, injected embryos (1-7) with the *edn2a* crRNA 1 show chromatograms bearing mixed alleles at the 3' end of the CRISPR target site (box with black dotted lines).

4.2.2 Analysis of the embryonic pigment phenotype of endothelin system mutants. Generation of mutants with CRISPR/Cas9 targeted mutagenesis.

Pairs of genotyped adult mutant carries or homozygotes of each gene were allowed to mate for 20 minutes in order to obtain batches of homogenously developing embryos. Rate of dead and abnormal embryos were recorded; dead embryos were discarded and abnormal embryos were fixed and stored in PBS/Sodium Azide 5mM (see section 2.3.2) for further genotyping. No more than 50 normally developing embryos per petri dish were incubated at 28 ºC in embryo medium with methylene blue (see section 2.1.2.1). For better observation of iridophores embryos were treated with PTU at 22 hpf to prevent melanisation (see section 2.1.2.3). Pigment phenotype (Fig. 4.8) was assessed for presence or absence of melanophores in the dorsal, lateral and ventral stripes (Fig. 4.8 A); iridophores in the dorsal and ventral stripes (Fig. 4.8 B-D), the lateral patches and the eyes (Fig. 4.8 D) or ectopic pigment cells in the ventral medial pathway. Images were acquired between 4 and 5 dpf.

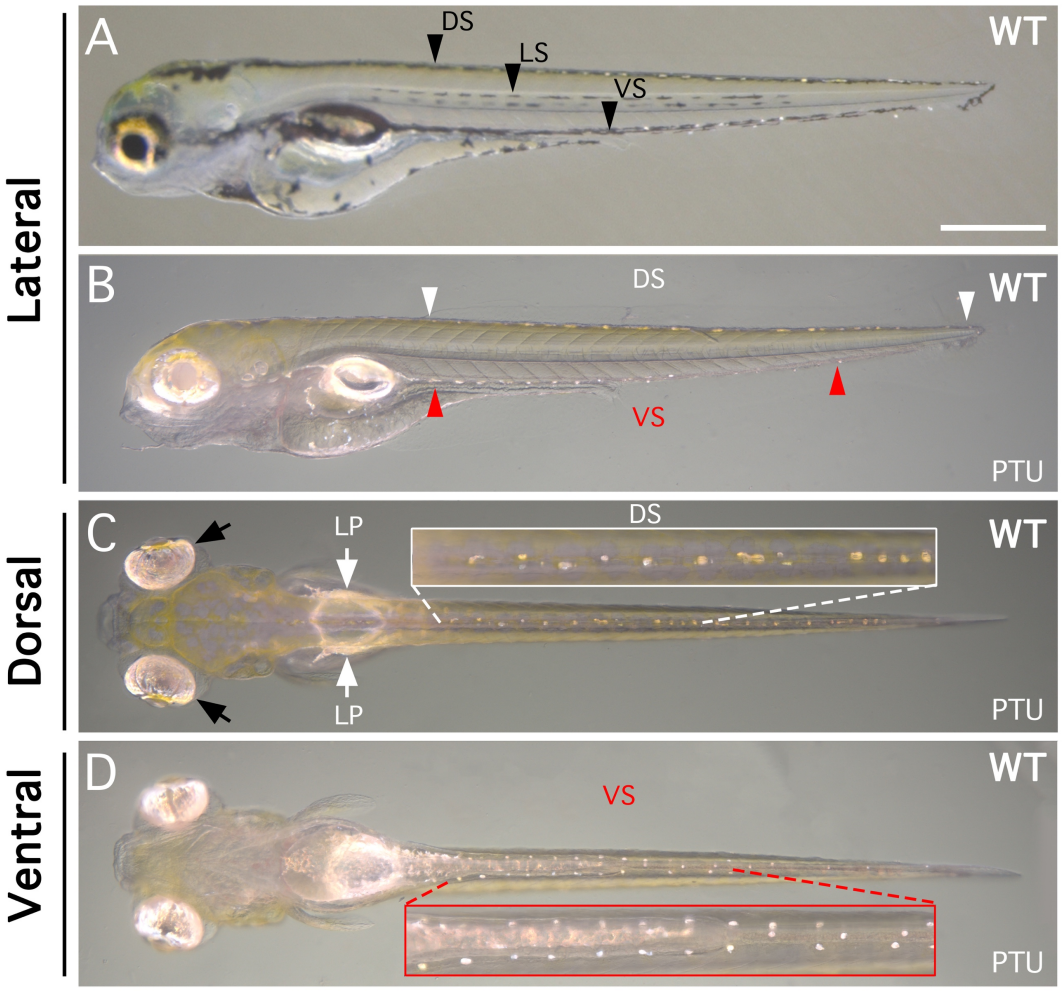

Figure 4.8 Areas of assessment of pigment phenotype. Pigment phenotype of 5 dpf WT larvae. Lateral view (A) shows melanophores (black arrowheads) in the lateral, dorsal and ventral stripes (DS, LS and VS correspondingly). PTU treated larvae under reflected light (B-D). Lateral view (B) shows iridophores in the dorsal (white arrow heads) and ventral (red arrowheads) stripes (B). Dorsal (C) and ventral (D) views allow better examination and quantification of iridophores in the dorsal stripe (white box in C) and ventral stripe (red box in D). Presence of iridophores in the lateral patches (LP and white arrows) and eyes (black arrows; C). Scale bar 500 μm.

4.2.2.1 *endothelin* mutants.

In mammals, the interaction of Edn1 with Ednra is well known, thus the zebrafish orthologue *edn1* is the natural candidate for the ligand of the receptor encoded by *ednraa*. Furthermore, its expression in the posterior trunk suggested a role additional to the patterning of the craniofacial cartilages reported by Nair et al. 2007.

From the two sites targeted for mutagenesis, mutant carriers of 4 base pairs deletion (Δ4) in exon 2 was identified. Incross of genotyped heterozygote *edn1*$^{+/\Delta 4}$ mutant carriers, revealed that 100% of the embryos display a normal pattern of melanophores, (Fig. 4.9 A and B), however 25% of the embryos showed disruption of the iridophore embryonic pattern (Fig. 4.9 C and D). The dorsal stripe shows almost no iridophores except for occasional single iridophores (Fig. 4.9 D), the ventral stripe also showed a reduction of iridophores although more iridophores are seen in the ventral stripe than in the dorsal stripe. Interestingly, the lateral patches and the eyes showed a normal iridophore phenotype. Xanthophores were unaffected. Additionally, all fish that had reduced iridophores did not develop a jaw (Fig. 4.9 H), a phenotype consistent with the previously reported by Nair et al. 2007, in which ventral craniofacial cartilages are not present. Surprisingly, no ectopic pigment cells were found in the ventral medial pathway. Due to the lack of jaw, *edn1* homozygote mutants were not raised beyond the free feeding stage, thus the adult pigment phenotype remains unknown.

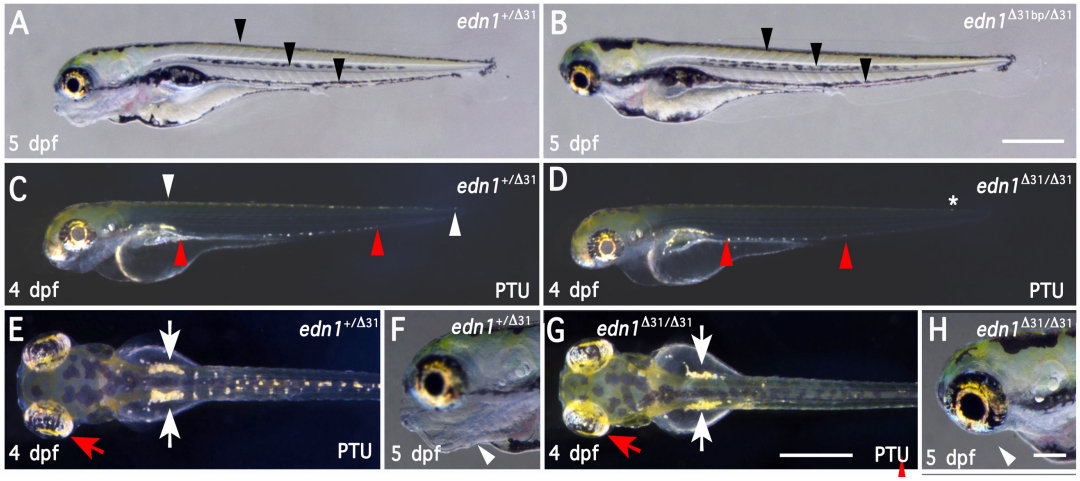

Figure 4.9 *edn1*$^{\Delta 31/\Delta 31}$ mutants have reduced iridophores and no jaw. Pigment phenotype of 5 dpf WT (A, C, E and F) and *edn1* mutant larvae (B, D, G, and H). Melanophores and patterning (black arrowheads) in WT (A) and mutant fish (B). WT (C) 4 dpf larvae treated with PTU display iridophores in the dorsal stripe (white arrowheads) and ventral stripes (read arrowheads). Homozygous mutants (D) have no iridophores in the dorsal stripe except for occasional escapers (*) and reduced number of iridophores in the ventral stripe (red arrow heads; D). Both WT and mutant larvae have iridophores in the lateral patches (white arrows) and eyes (red arrows in E and G correspondingly). Jaw formation in WT fish is normal while in mutant fish is absent (white arrowhead in F and G correspondingly). Scale bar 500 μm (A-D), 400 μm (E and G) and 200 μm (F and H).

Because *edn1* mutants did not show a *parade* phenotype, we next generated *edn2a* mutants. From embryos derived from the F_0 injected with the CRISPR target 2, we identified a mutant carrier of a 4 base pairs deletion (Δ4) in exon 2. Similar to *edn1*$^{\Delta 4/\Delta 4}$ mutants, embryos from an in cross of two *edn2a*$^{+/4\Delta}$ mutant carriers display a normal patterning of melanophores (Fig. 4.10 A-B), 25% of the embryos do not form a jaw (Fig. 4.10 C and D) and lack iridophores in the dorsal and ventral stripes (Fig. 4. 10 E-H). In contrast to *edn1* mutants, *edn2a* mutants also did not show iridophores in the lateral patches (Fig. 4. 10 C and D). Unexpectedly, *edn2a* mutants did not show any ectopic pigment cells in the ventral media pathway of the posterior trunk. Homozygote mutants were not grown beyond 5 dpf, therefore it remains unknown whether *edn2* has a role in adult pigment pattern formation.

In mammals, *in vitro* and *in vivo* studies have shown that Edn3 is necessary for melanophore development through Ednrb. In zebrafish, morpholino knock-down of *edn3b* has suggested its function on embryonic iridophore development. In contrast, the function for *edn3a* is not known. We then examined the embryonic pigment phenotype of mutants of *edn3a* and *edn3b*. A mutant allele of *edn3a* with an insertion of 1 base pair (+1) was identified. Embryos from genotyped heterozygote mutants of *edn3a* were collected and incubated at 28 ºC. The pigment phenotype was assessed at 4 dpf and no differences were found. Previous work from the Nüsslein-Volhard lab determined that genotyping of twenty embryos from cross of genotyped heterozygote mutants of *edn3a* did not show homozygote mutants. Which suggest that homozygote mutants are not viable. Adult heterozygote mutants of *edn3a* showed a wild type pigment phenotype.

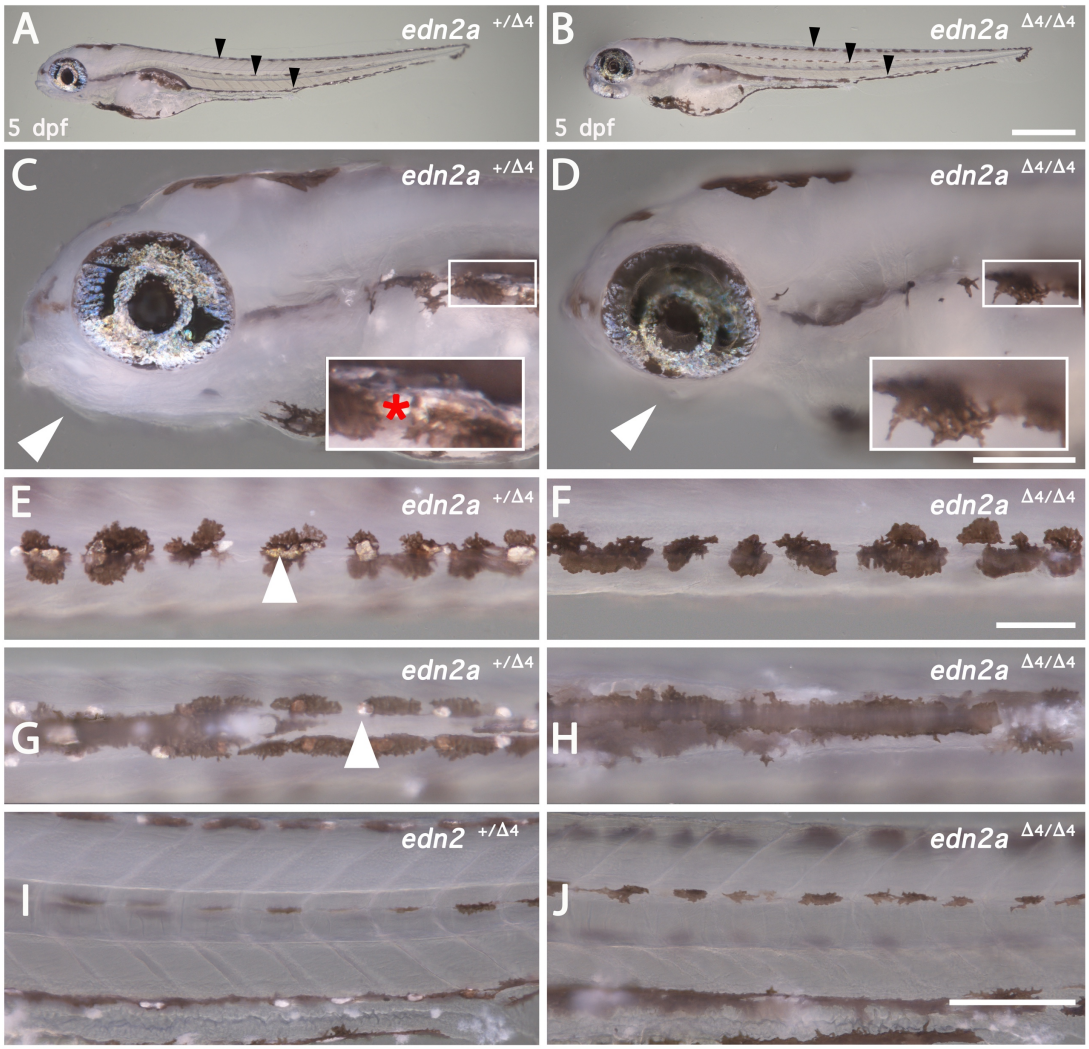

Figure 4.10 *edn2a*$^{\Delta}$mutants have reduced iridophores and no jaw. Pigment phenotype of 5 dpf WT (A, C, E, G and I) and *edn2* mutant larvae (B, D, F, H and J). Melanophore patterning (black arrowheads) is shown unaffected in both WT (A) and mutant fish (B). Normal formation of jaw is shown in WT larvae but is completely absent in *edn2a* homozygous mutants (arrowheads in C and D correspondingly). Iridophores in the lateral patches (red asterisks) are normal in WT embryos but absent in *edn2a* mutants (white boxes show magnification of area). (E and F) Iridophores (arrowhead) in the dorsal (G) and ventral (I) stripes are normal WT fish but absent in both stripes in mutant fish. Lateral view of anterior trunk showing no ectopic pigment cells in the ventral trunk of both WT and mutant fish (I and J respectively). Scale bar = 500 μm (A-B), 200 μm (C and F; I-J) and 100 μm (E and H).

We then examined the pigment phenotype of embryos from an in cross of genotyped adult homozygote mutants of *edn3b* bearing a 11 base pair deletion (Δ11) in exon 2, 165 base pare after the 5' UTR. At 4 dpf, all fish showed normal melanophore pattern (Fig. 4.11 A), while PTU treated embryos show normal iridophores in the dorsal and ventral stripes (Fig. 4.11 B) as well as in the eye and the lateral patches (Fig. 14.11 A). This result differs from the morphant phenotype previously reported in which knock-down of *edn3b* decreases the number of iridophores (Krauss et al. 2014). No ectopic pigment cells were found in the ventral medial pathway of the posterior trunk. Interestingly, adult *edn3* homozygote mutants have a strong reduction of melanophores and iridophores and no stripes are formed, this phenotype resembles the one of *rose* (*ednrba*) and *karneol* (*ece2b*) mutants, confirming that Edn3b is the major ligand of EdnrBa and that this ligand is cleaved by Ece2b.

We also assessed the pigment phenotype of double mutants of *edn3a*$^{+/+1}$ (het); *edn3b*$^{\Delta 11/\Delta 11}$ (homo), but no double homozygote mutants were identified by genotyping and all embryos displayed a normal embryonic pigment phenotype. Adult *edn3a*$^{+/+1}$; *edn3b*$^{\Delta 11/\Delta 11}$ mutants do not display a phenotype different to the single *edn3b*$^{\Delta 11/\Delta 11}$ homozygote mutant.

4.2.2.2 *endothelin converting enzyme 1*.

In order to identify if *Ece1* cleaves the ligand of *pde/ednrAa*, an *ece1* mutant was generated. We identified adult mutants carriers for a 11 base pair deletion (Δ11) on exon 8 of the *ece1* gene (Fig. 4.12 A). 100% of the embryos (n=16) from genotyped heterozygote adult mutants of *ece1* displayed a normal melanophore pigment phenotype with no apparent lack of iridophores or ectopic cells in the ventral medial pathway of the posterior trunk (Fig. 4.12 B). Sequencing of the *ece1* gene showed the expected Mendelian distribution (1:2:1; 4:9:3) of WT (Fig. 4.12 C), heterozygotes (Fig. 4.12 D), and homozygote mutants (Fig. 4.12. E). Adult mutants did not show any pigment phenotype.

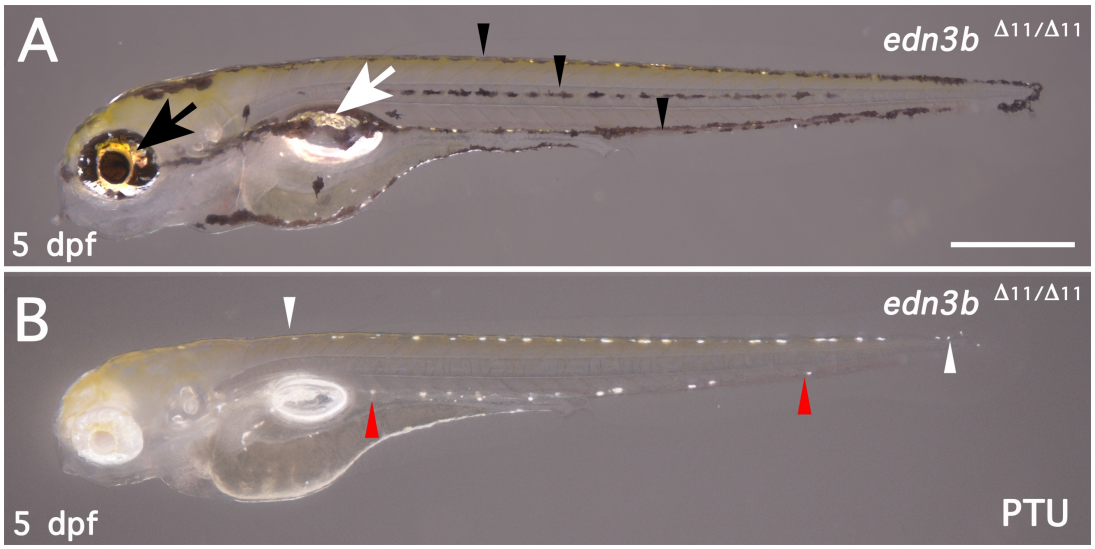

Figure 4.11 *edn3b*$^{\Delta 11/\Delta 11}$ mutants have normal pigment phenotypes. Pigment phenotype of 4 dpf homozygote mutants show normal melanophores formation in all three, dorsal, lateral and ventral, stripes and yolk sac (black arrow heads; A). PTU treated larvae show normal iridophore patterning (B) in the dorsal (white arrowheads) and ventral (red arrowheads). The eyes (black arrow) and lateral patches (white arrow) have normal iridophores (A). Scale bar = 500 μm (A and B).

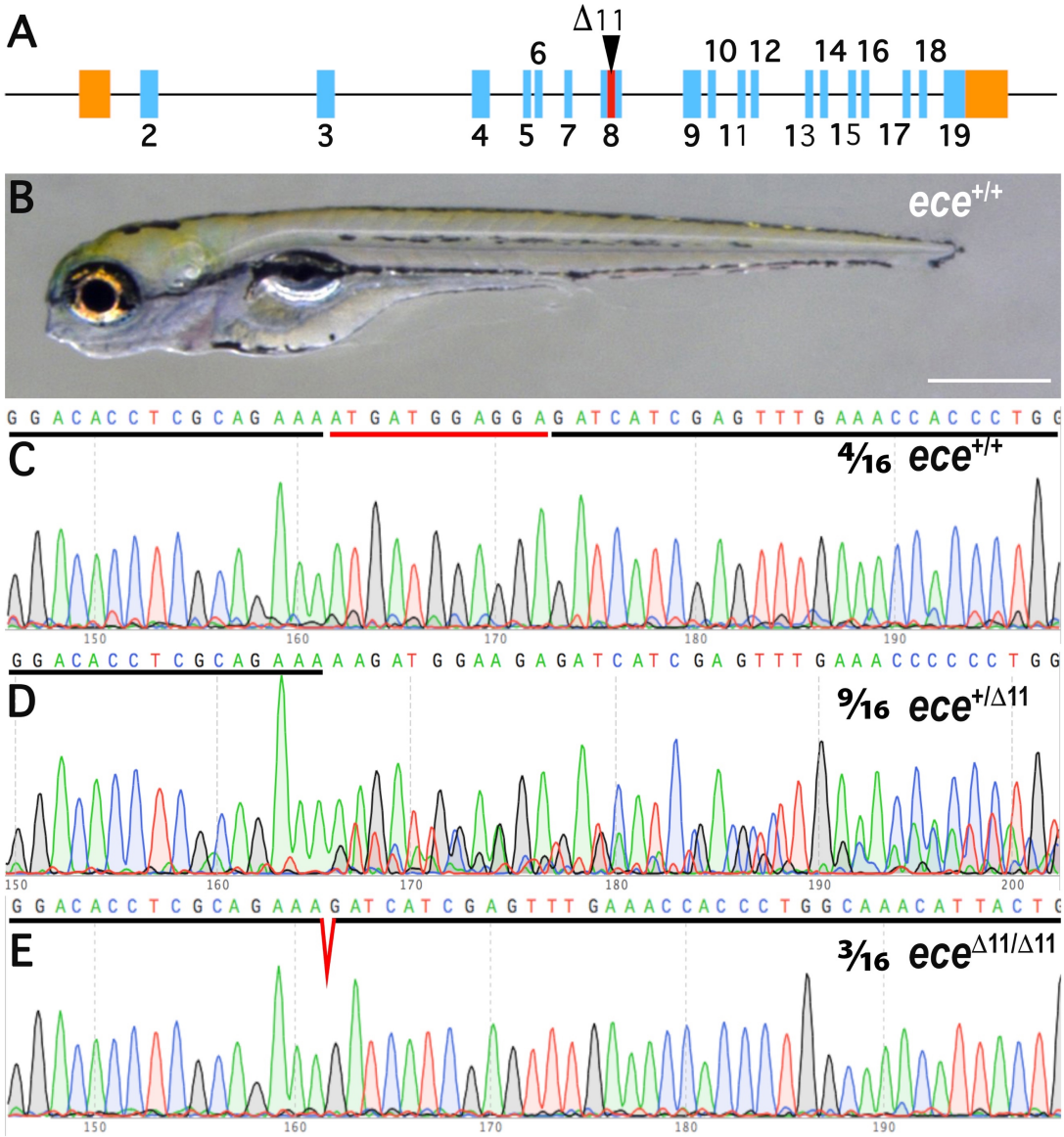

Figure 4.12 *ece1* $^{\Delta 11/\Delta 11}$ mutants have a normal phenotype. Gene structure of *ece1* (A), 5' and 3' UTR are show in orange colour, exons are shown in blue boxes and introns are represented by black lines. A 11 base pair deletion (Δ 11) is localised in exon 8 (black arrow head). Pigment phenotype of all fish at 5 dpf was normal. Chromatograms of sequenced fish shows a proportion of 4 WT sequence (C), 9 heterozygous sequence (D) and 3 mutant homozygous sequence (E). In panel C, black lines shows WT sequence, and red line underlines the 11 nucleotide that are missing in mutants. Similarly, in panel D and E black lines show WT sequence, but in panel E red v- shape line represent gap of the 11 deleted nucleotides. (E). Scale bar = 500 μm (B).

4.2.2.3 Mutants of *endothelin receptor Aa* display ectopic melanophores and iridophores in the ventral medial pathway.

We have previously shown that homozygote carriers of three mutant alleles of the *ednraa* gene (*pde*^{tj262}, *pde*^{tv212} and *pde*^{hu4140}) display ectopic and supernumerary melanophores and iridophores. However, we were not able to identify the nature of the mutation of two of the alleles, *pde*^{tv212} and *pde*^{tj262}. Both showed a wild type genomic sequence, but analysis of their cDNA revealed a lack of exon 6 and 7 correspondingly (Figure 4.13), and a downstream frame shift after the missing exon suggesting that the mutation is placed in a regulatory splicing site. On the other hand, sequencing of the allele *pde*^{hu4140} identified a premature stop codon in exon 5. *In silico* translation of all three alleles predicts the formation of a wildtype protein encoded by exons 2-4, followed by 18 (*pde*^{tj262}) and 35 (*pde*^{tv212}) amino acids product of the frame shift, and a premature stop codon. (Figure 4.13).

We performed a protein alignment of the human ET_A and zebrafish EdnrAa receptors to identify conserved identical amino acids, shown on a scheme of a 2D reconstruction of the crystallized human ET_A receptor (Figure 4.14 B) (Pándy-Szekeres et al. 2018). From the receptor structure, we observe that the *pde*^{tj262} allele could produce a protein that lacks the seventh transmembrane domain and the intracellular domain. The receptor product of the *pde*^{tv212} and *pde*^{hu414} alleles lacks the sixth and seventh transmembrane domains and the intracellular domain. Thus, the extracellular domain in all mutant alleles is unaffected, while the transduction segment of the receptor is not present. The extracellular region and the first four transmembrane loops is where the ligand binds to the receptor, therefore, ligand binding to EdnrAa could then still be possible.

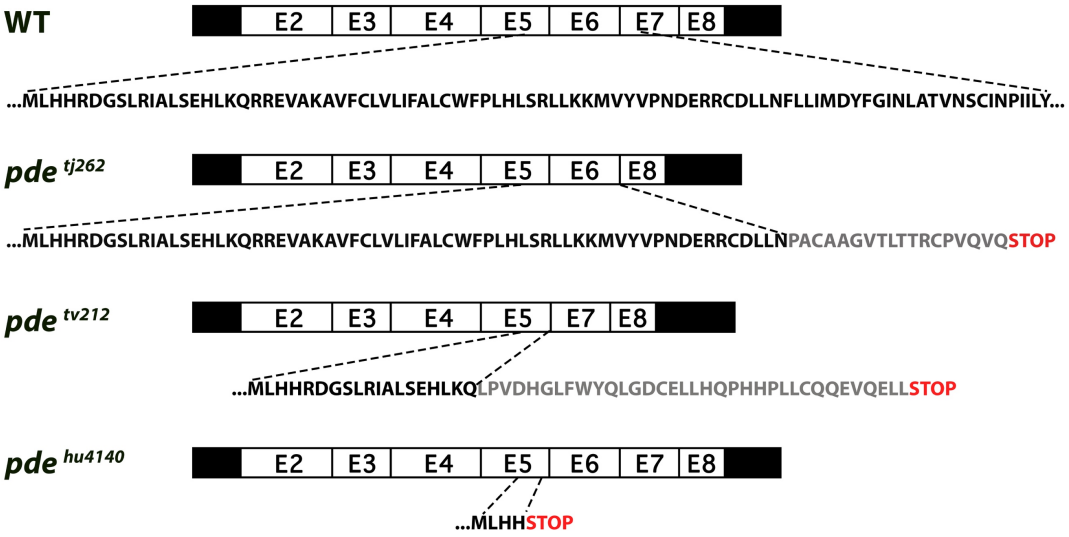

Figure 4.13 *In silico* translation of mutant alleles *pde* ^{tj262}, *pde*^{tv212} and *pde*^{hu4140}. Scheme shows cDNA structure of WT, *pde* ^{tj262}, *pde*^{tv212} and *pde*^{hu4140} alleles. Exons are numbered and UTRs (5'-3-') are shown in black boxes. Region corresponding to the amino acid sequence are indicated with dashed lines. Amino acids in black correspond to the WT sequence and amino acids product of a shift in the reading frame as shown in grey.

In order to corroborate that the *pde* phenotype is result of the loss of function of EdnrAa, we generated a new null mutant of *ednraa* using the CRISPR/Cas9 technology, a mutant of *ednraa* was generated targeting the second exon of the gene, just 72 base pairs downstream the 5' UTR. A 4 bp deletion (Δ4) (Fig. 4. 15 A) allele was identified and outcrossed to a wild type strain. Genotyped adult mutant carriers were incrossed and their progeny raised. Adult homozygote mutants fish were identified and incrossed, simultaneously adult wildtype fish were in crossed to compare and examine the pigment phenotype of the larvae at 5 dpf. At 5 dpf, the pigment phenotypes of wild type and homozygote mutant larvae was examined. Similar to the previously identified alleles (pde^{tj262}, pde^{tv212} and pde^{hu4140}), $ednraa^{\Delta 4/\Delta 4}$ mutants display ectopic melanophores and iridophores in the ventral medial pathway of the posterior trunk (Fig. 4.15 C and F), whereas wild type fish does not show ectopic cells (Fig. 4.15 B and D). Both wild type and mutant embryos were genotyped by sequencing of the region targeted for mutagenesis. Chromatograms showed a wildtype sequence in the control embryos (Fig. 4.15 E) and a 4 base pair deletion in the homozygote mutants (Fig. 4.15 G). As a result of the 4 base pair deletion, *in silico* translation predicts a peptide that contains the first 22 amino acids of the EdnrAa receptor after which a shift of the reading frame of translation leads to the addition of 37 different amino acids followed by a premature ºstop codon (Fig. 4.15 H). Therefore, the phenotype observed in *parade* mutants is due to a loss of function of the receptor, and is essentially a null phenotype.

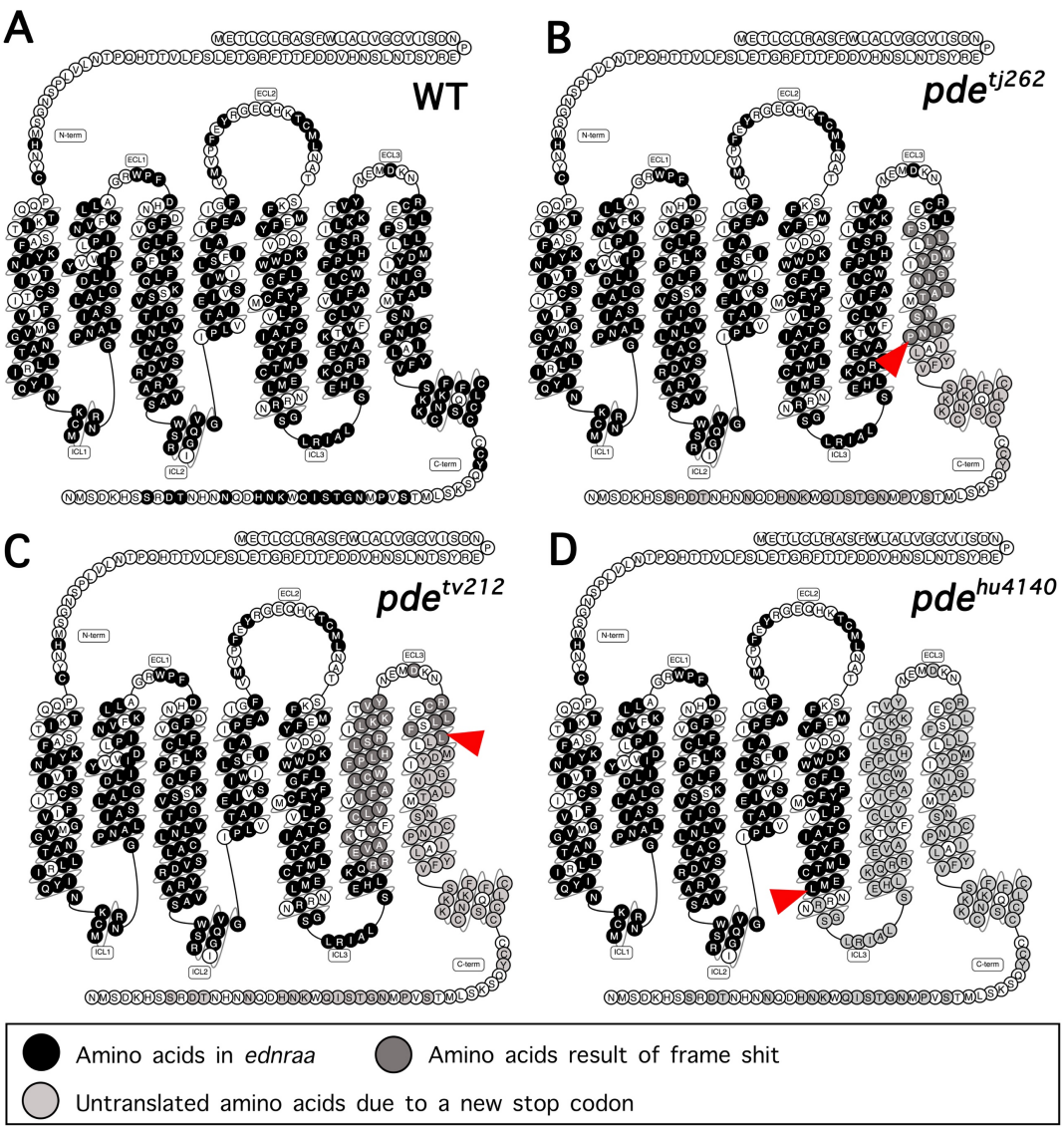

Figure 4.14 Receptor structure of the *pde* ^{tj262}, *pde*^{tv212} and *pde*^{hu4140} alleles. Scheme shows 2D structure of the human ET_A receptor, the identical amino acid of the zebrafish EdnrAa receptor are shown in black for the WT allele (A), *pde* ^{tj262} (B), *pde*^{tv212} (C) and *pde*^{hu4140}(D). Amino acids product of a shift in the reading frame as shown in dark grey and missing amino acids after stop codon (red arrowheads) are shown in light grey.

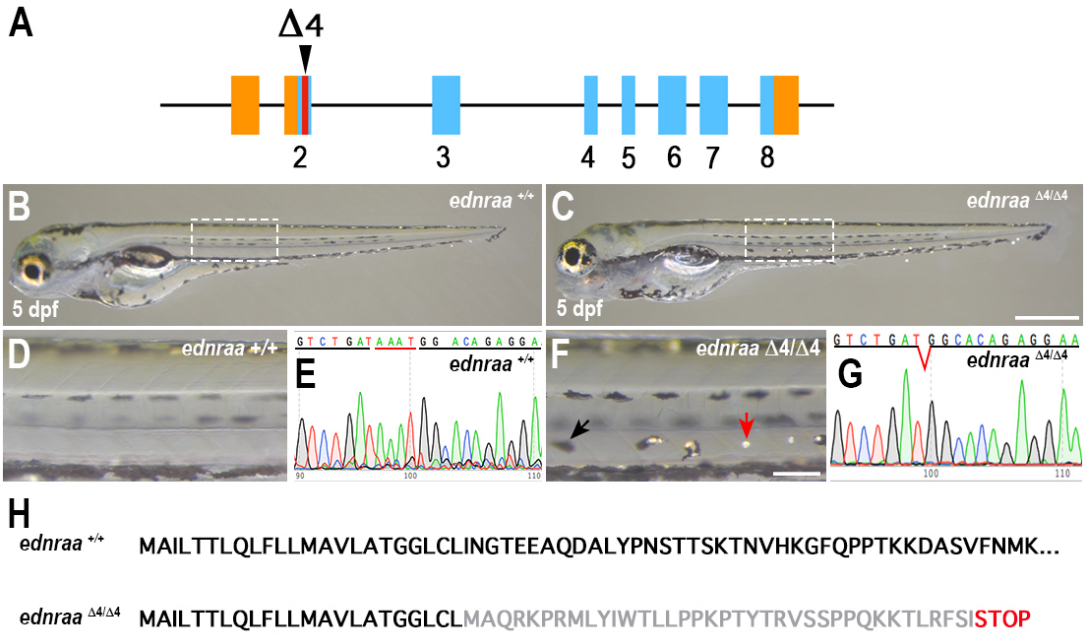

Figure 4.15 Loss of function of *ednraa* generates the *pde* phenotype. Structure of *ednraa* gene shows location of a 4 base pair deletion (Δ4) mutation in exon 2 (A). Exons are numbered and shown in blue boxes, UTRs (5'-3') in orange boxes, intronic regions are correspond to the black line. Pigment phenotype of 5 dpf WT fish (B) and *ednraa* $^{\Delta 4/\Delta 4}$ homozygote mutants (B). Close up of anterior trunk shows a normal pigment pattern in WT larvae (D) but ectopic melanophores (black arrow) and iridophores (red arrow) on mutant fish (F). Chromatogram sequence of exon 2 from fish in panel B shows a WT sequence (E) while fish in panel C is homozygous for a 4 base pair deletion (G). In panel E, black line shows WT sequence, and red line underlines the 4 nucleotide that are missing in mutants. Similarly, in panel G black lines show WT sequence and red "v- shape line represent gap of the 4 deleted nucleotides. *In silico* translation (I) of mutant transcript predicts a 23 amino acid N-terminal peptide shared with the WT sequence (black amino acids) but a shift of the translational reading frame (grey amino acids) and a premature stop codon (red STOP). Scale bar = 500 μm (B and C) and 100 μm (D and F).

4.2.2.4 *endothelin receptor ab* mutant.

To test whether *ednrab* has a role in the mechanism of the *parade* phenotype, we assessed the pigment phenotype of *ednrab* mutants. A mutant allele of the *ednrab* gene was identified, this allele has a 4 base pair (Δ4) deletion in exon 2, just 143 base pairs after the 5' UTR (Fig. 4.16 A). Adult heterozygotous mutants were identified and incrossed. At 4 dpf all of the larvae displayed a normal embryonic patterning of melanophores and xanthophores (Fig. 4.16 A and B). In order to observe the iridophore phenotype better, embryos were treated with PTU to prevent melanisation. 75% of the larvae showed a normal iridophore pattern (Fig. 4.16 D) but surprisingly, similar to *edn1* and *edn2a* mutants, the other 25% of the embryos displayed a complete absence of iridophores in the dorsal stripe and strong reduction in the ventral stripe (Fig. 4.16 E). In contrast to *edn2a* mutants, the lateral patches of all embryos are present (Fig. 4.16 F and G). Unexpectedly, the formation of the jaw was normal in all embryos, which differs from the morphant phenotype reported by Nair et al. 2007. A very elegant study showed that mutants and morphant phenotypes can differ due to activation of compensatory mechanisms in mutants that rescue the morphant phenotype, and that are not activated in morphants. Thus, deleterious mutations activate compensatory gene programmes not observed in translational or transcriptional knockdown (Rossi et al. 2015). This could explain the difference in the craniofacial phenotypes of *ednraa* and *ednrab*. Chromatograms of the sequence of exon 1 shows a WT sequence (Fig. 4.16 H) and a deletion of 4 base pairs in fish with no iridophores (Fig. 4.16 H). *In silico* translation of the mutant sequence (Fig. 4.16 J) reveals a shift in the reading frame and a premature stop codon resulting in a peptide consisting of 47 wild type amino acids followed by 8 amino acids different to the Ednrab. We have not determined whether *ednrab* mutant affect only embryonic iridophores, as the adult phenotype of *ednrab* homozygote mutants has not been assessed.

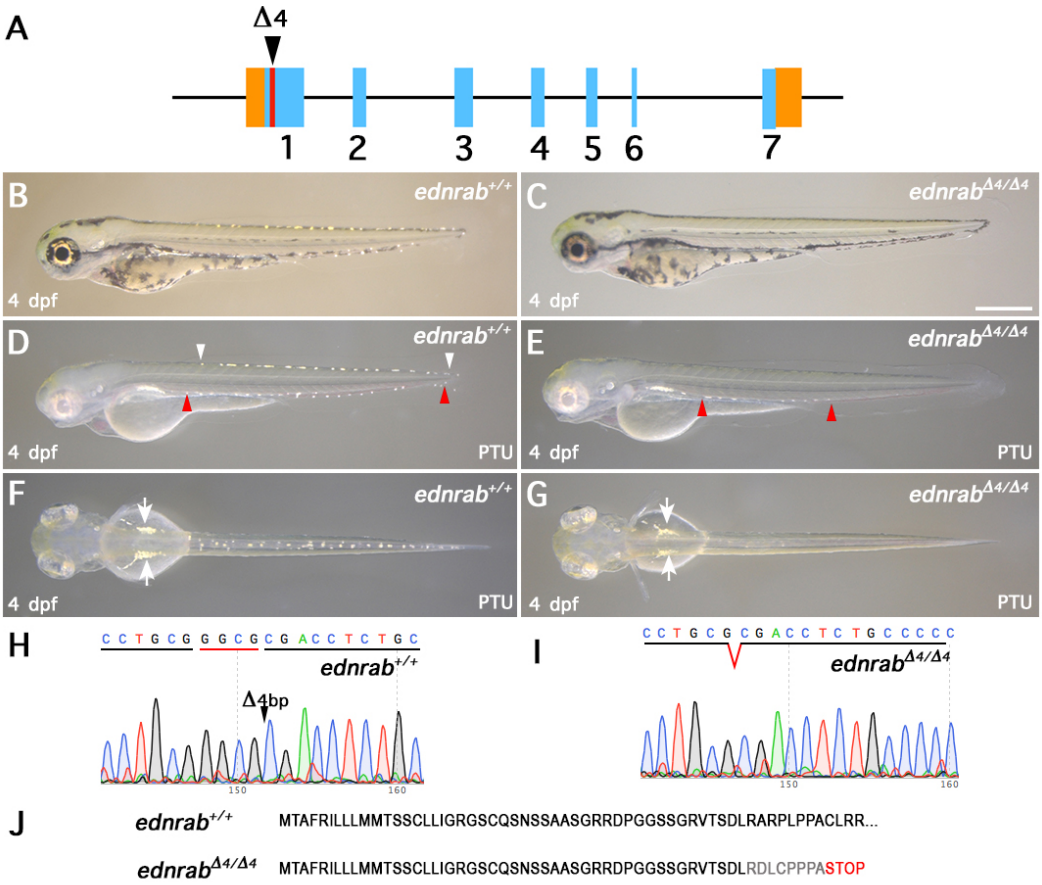

Figure 4.16 *ednrab*$^{\Delta 4/\Delta 4}$ mutants have reduced iridophores. Schematic representation of *ednrab* gene shows location of a 4 base pair deletion (Δ4) mutation in exon one (A). Exons are numbered and shown in blue boxes, UTRs (5'-3') in orange boxes, intronic regions correspond to the black line. Pigment phenotype of 4 dpf WT (B) and mutant (C) larvae show normal melanophore patterning in both backgrounds. Reflected light on PTU-treated WT (D and F) and mutant (E and G) larvae shows normal iridophore formation in the dorsal and ventral stripes of WT fish (white and red arrow heads in C correspondingly), but absence of iridophores in the dorsal stripe, and strong reduction of iridophores in the ventral stripe (red arrowheads in E). Iridophores in the lateral patches (white arrows) are present in both WT (F) and mutant fish (G). Chromatograms of the sequence of exon one from fish in panel F shows a WT sequence (H) while fish from panel G is homozygous for a 4 base pair deletion (Δ4 bp; I). In panel H, black line shows WT sequence, and red line underlines the 4 nucleotide that are missing in the mutant sequence. Similarly, in panel I, black lines show WT sequence and red v- shape line represent gap of the 4 nucleotides missing in mutant fish. *In silico* translation of mutant transcript (J) predicts a 47 amino acid peptide with the WT sequence (black amino acids) and 8 mutant amino acids (grey amino acids) followed by a premature stop codon (red STOP). Scale bar = 500 μm (B -G).

4.2.2.5 *endothelin receptor aa*; *endothelin receptor ab* double mutant.

To test whether EdnrAa and EdnrAb work together in the mechanism of the *parade* phenotype we generated double mutants of *ednraa* and *ednrab. ednraa*$^{\Delta 4/\Delta 4}$; *ednrab*$^{+/\Delta 4}$ fish were incrossed for examination of the larval pigment phenotype and compared to WT larvae (Fig. 4.17 A-D). From the in cross of the double mutant *ednraa*$^{\Delta 4/\Delta 4}$; *ednrab*$^{+/\Delta 4}$, two types of gametes are expected: aB and ab, where a=*ednraa*$^{\Delta 4}$, B=*ednrab*$^{+}$ and b=*ednrab*$^{\Delta 4}$ (Table 4.1). Embryos with three genetic combinations, aaBB, aaBb and aabb, in the ration 1:2:1 are expected. Given that the heterozygote mutants of both genes *ednraa* and *ednrab* do not display a pigment phenotype, the individuals of the nature aaBB and aaBb are expected to display a *parade* phenotype only, while the phenotype of the homozygous individuals (aabb) would reveal whether EdnrAb is involved in the mechanism of the parade phenotype.

	aB	**ab**
aB	**aaBB**	**aaBb**
ab	**aaBb**	**aabb**

Table 6 .4 Expected genotypes from an in cross of *ednraa*$^{\Delta 4/\Delta 4}$; *ednrab*$^{+/\Delta 4}$ double mutants. Genotypes in blue are expected to have a *parade* phenotype. The phenotype of the double homozygote mutant in red will be assessed.

Examination of the pigment phenotype of embryos from an in cross of *ednraa*$^{\Delta 4/\Delta 4}$; *ednrab*$^{+/\Delta 4}$ at 5 dpf, revealed that as expected, ¾ of the larvae have ectopic melanophores and iridophores in the ventral medial pathway of the posterior trunk (Fig. 4.17 E and F) and normal iridophores in the dorsal (Fig. 4.17 G) and ventral stripes. All of these fish displayed a smaller jaw (Fig. 4.17 H) compared to WT fish (Fig. 4.17 D). Unexpectedly, the other ¼ of the fish did not develop ectopic pigment cells (Fig. 4.17 I and J), had reduced iridophores in the dorsal (Fig. 4.17 K) and ventral stripes. In agreement to the previously reported phenotype of the the double morphant of *ednraa*; *ednrab*, all of the embryos that did not form ectopic pigment cells, did not develop a jaw. Due to the lack of jaw, the double homozygote mutants were not raised beyond the free feeding stage, thus the adult pigment phenotype remains unknown. This result shows that the formation of both ectopic melanophores and iridophores in the ventral medial pathway of the posterior trunk in *ednraa* mutants is dependent on *ednrab* function.

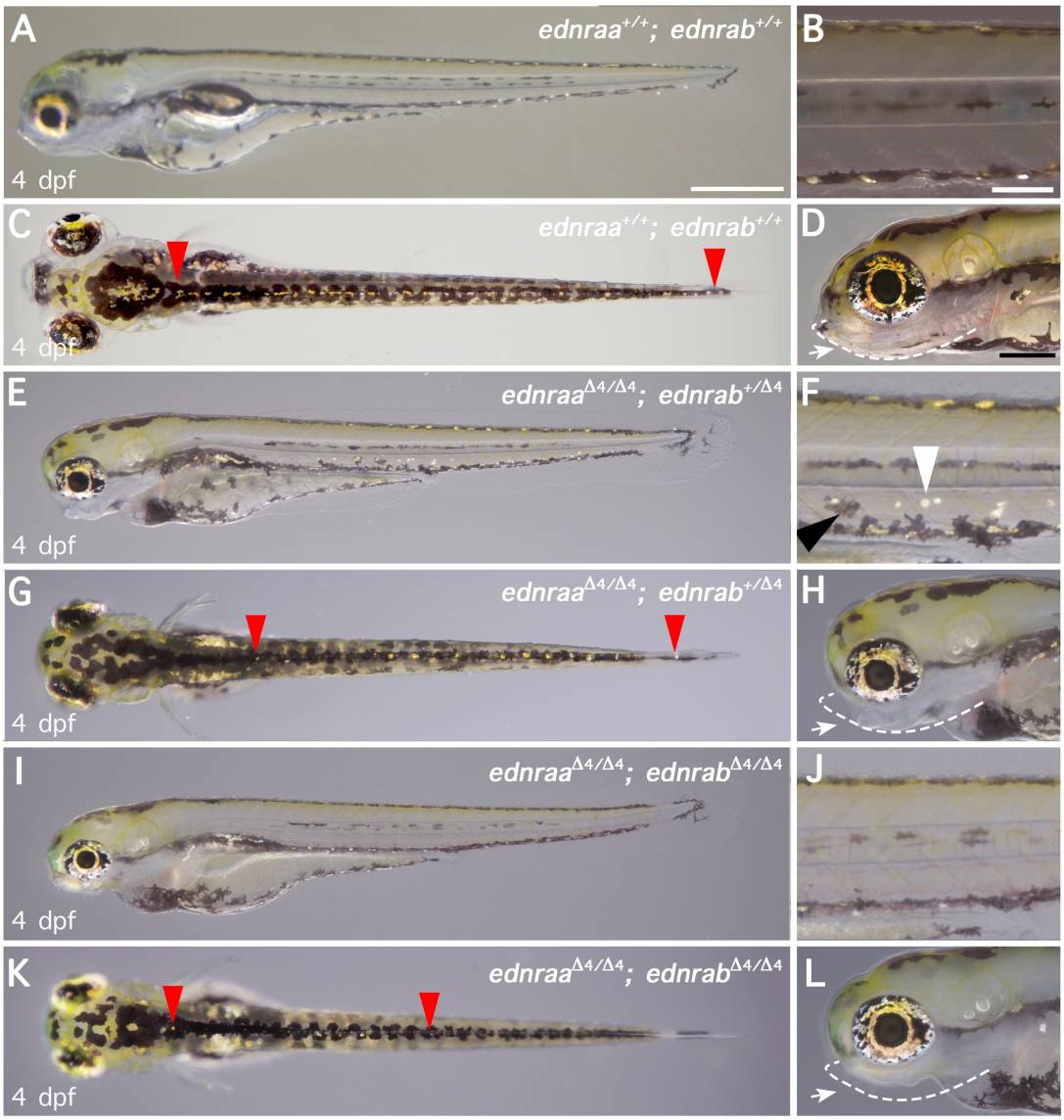

Figure 4.17 Double homozygote mutants of *ednraa*; *ednrab* mutant rescue the parade phenotype. Pigment phenotypes of 5 dpf WT (A-D), *ednraa*$^{\Delta 4/\Delta 4}$; *ednrab*$^{+/\Delta 4}$ (E-H) and *ednraa*$^{\Delta 4/\Delta 4}$; *ednrab*$^{\Delta 4/\Delta 4}$ (I-L) larvae. Lateral view (A, E and I), dorsal view (C, G and K), close up of head (B, F and J) and trunk (D, H and L) of each corresponding fish. Red arrowheads indicate iridophores in ventral stripe (C, G and K). Jaw (white dashed line) or absence of it is pointed with white arrows (B, F and J). Ectopic melanophores (black arrowhead) and iridophores (white arrowhead) in ventral trunk (H) of *ednraa*$^{\Delta 4/\Delta 4}$; *ednrab*$^{+/\Delta 4}$ fish. Scale bar = 500 μm (A, C, E, G, I and K), 200 μm (B, F and J) and 100 μm (D, H and L).

4.3 Discussion

Endothelins were first broadly studied for their potent vasoconstrictor effect in the human cardiovascular system. However more recently, some of the endothelin components have been shown to have a role in craniofacial and pigment pattern formation in mammals (Hosoda et al. 1994; Garcia et al. 2008; Reid et al. 1996; Baynash et al. 1994). Here we examined their roles in zebrafish, assessing to what extent these roles are conserved, and whether they might also have other novel roles.

Analysis of the zebrafish genome identifies twelve genes that encode the elements of the endothelin signalling system: six ligands, Edn1, Edn2a, Edn2b Edn3a, Edn3b and Edn4; four receptors, Ednraa, Ednrab, Ednrba and Ednrbb); and three Endothelin Converting Enzymes, Ece1, Ece2a, Ece2b that activate the ligands (Braasch et al. 2009). Previous studies showed that loss of function of *ednrba* (Parichy et al. 2000) and *ece2b* (Krauss et al. 2014), produces a phenotype in which both adult melanophores and iridophores are reduced and that the formation of the adult pigment pattern is disrupted. In contrast, mutants of *ednraa* display a unique embryonic phenotype in which more melanophores and iridophores are formed, but more strikingly, these extra cells are exclusively located in the ventral medial pathway of the posterior trunk (Kelsh et al. 1996; Camargo-Sosa et. al, 2018 in press), a region of the larvae that in a wild type context lacks pigment cells until the metamorphic stage (Parichy et al. 2009), when adult pigment stem cells are activated to produce the pigment cells that will form the adult pigment pattern (Dooley et al. 2013; Mahalwar et al. 2014; Singh et al. 2016).

In order to study comprehensively the role of the endothelin system in the regulation of pigment progenitors in zebrafish, we worked in collaboration with the research group of Prof. Christiane Nüsslein-Volhard to generate and characterise loss of function mutants of *edn1*, *edn2a*, *edn3a*, *edn3b*, *ece1*, and both single and double mutants for *ednraa* and *ednrab* using CRISPR/Cas9 targeted mutagenesis. Specifically, we wanted to identify the ligand of the EdnrAa receptor, but also which Ece cleaves the ligand and whether other endothelin receptors are involved in the mechanism of the *parade* phenotype. We examined the embryonic pigment phenotype of all mutants looking for the presence of ectopic pigment cells in the ventral medial pathway.

Of the four mutants of the *endothelin* genes (*edn1*, *edn2a*, *edn3a*, *edn3b*) that were generated, none of them phenocopied the *parade* mutant. Thus, we have not been able to identify the ligand of EdnrAa. The most likely explanation is that there is significant redundancy between two or more endothelins. To test this, we are currently breeding double mutants for *edn1* and *edn2a* and if required a triple mutant with *edn3b*. However, we cannot discard Edn2b and Edn4 as a ligand of EdnrAa or to be redundant, thus generation of both *edn2b* and *edn4* mutants is necessary to corroborate its function.

On the other hand, we identified new roles for both *edn1* and *edn2a* in zebrafish pigment development. Previous work has shown that a mutant of *edn1*, *sucker*, (Nair et al. 2007) failed to form the jaw. Similarly, the CRISPR mutant of *edn1* does not develop a jaw. However, we also observed an absence of iridophores in the dorsal stripe and very few in the ventral stripe, something not noted in the previous publication; whether this reflects allele-specific differences, or simply a lack of explicit examination of the iridophores will require further examination. Interestingly, the pigment phenotype we observed for *edn1* resembles that of *ednrab* mutants, strongly suggesting that Edn1 signalling is mediated through Ednrab. To our surprise, in our study *edrnab* mutants did not display a jaw phenotype; although we did not perform an alcian blue staining for cartilage, the phenotypes that was published from *ednrab* morphants is a strong phenotype and would be expected to result in a phenotype that is readily observed morphologically. More likely, we feel, that this reflects a genuine difference between mutant and morphant phenotypes that has been observed in other contexts (Rossi et al. 2015), and warrants further study. Furthermore, it will be really important to assess the pigment phenotype of adult *ednrab* homozygote mutants. Unfortunately, from the batch of mutants embryos that we were sent from Germany, after three months only males reached adulthood, thus, we out crossed them to a wild type background and we are waiting for them to reach adulthood, after which we will genotype them and cross them again, in order to obtain *ednrab* homozygotes larvae that we will grow to assess the adult pigment pattern.

Strikingly, *edn2a*, revealed a phenotype almost identical to *edn1*, but in addition to the lack of jaw, it has a complete absence of iridophores in both the dorsal and ventral stripes but also in the lateral patches, just above the swim bladder. This indicates that both Edn1 and Edn2a are required for some aspect of iridophore development.

Over all, we observed a spatially overlapping function of *edn1* and *edn2a* that suggests that both are necessary for iridophore development in the trunk, and that loss of any of them is sufficient to disrupt iridophore formation, while Edn2 on its own regulates formation of iridophores in the lateral patches. One explanation could be that both Edn1 and Edn2 bind to homodimers of EdnrAb in the trunk to regulate embryonic iridophore formation. Homodimerization and heterodimerization of ET_A and ET_B has been shown in *in vitro* and *in vivo* studies, (Evans & Walker 2008), so it is possible that a combination of Edn1 and Edn2 ligands work together in the trunk for the formation, proliferation, or maintenance of embryonic iridophores via EdnrAb. We could test the effect on iridophores development by analysing the expression pattern of early and late iridophores markers in this mutants in *edn1* and *edn2* mutants. Because of the lack of jaw, embryos were not allowed to grow beyond 5 dpf; hence, we could not asses the adult pigment phenotype of the *edn1* and *edn2a* mutants. Thus, it remains unknown whether *edn1* and or *edn2a* have a role in adult pigment pattern formation or the establishment of adult pigment stem cells/progenitors.

We could also confirm that the *parade* phenotype is due to a loss of function of EdnrAa, rather than some gain-of-function effect of the truncated protein. Previously, it was reported that the N-terminus tail and the first fourth transmembrane domains are required for ligand binding of ET_A (Miyamoto et al. 1996; Bourgeois et al. 1997; Zhang et al. 1998). *In silico* translation of the cDNA of our previously identified mutant alleles of *ednraa* showed that all of the alleles could produce a WT protein sequence of 344 (*tj262*), 297 (*tv212*) and 280 (*hu4140*) amino acids, corresponding to a protein up to the beginning of the seventh, the sixth and the end of the fifth transmembrane domains. Thus, ligand binding could still be possible in all three alleles, although without signal transduction.

One hypothetical role of EdnrAa, considered that this receptor controls the availability of ligand in the ventral side of the trunk. In this context ligand binding could still be possible. However, the new CRISPR mutant produces a peptide of only 22 wild type amino acids. This short peptide corresponds to just a small fragment of the extracellular domain of the receptor and therefore, ligand binding is not possible, confirming that the *parade* phenotypes is due to a loss of function of the EdnrAa.

The double mutant of *ednraa*; *ednrab* confirmed the previously reported morphant phenotype in which knock-down of both receptors prevents the formation of the jaw.

This supports the proposal made by Nair and colleagues that EdnrAa and EdnrAb work together in the patterning of the ventral craniofacial cartilages.

One of the most surprising findings was the pigment phenotype of the double homozygotes for *ednraa*; *ednrab*. We expected a lack of jaw, just as the double morphant had previously shown, but we did not expect the *parade* phenotype to be rescued by the loss of function of *ednrab*. This suggest that formation of ectopic pigment cells is dependent on *ednrab*. Interestingly, our observations for *ednrab* single mutants argues that this gene is not required for embryonic melanophore development, although it has a clear role in embryonic iridophore development. Based on our model that the *parade* phenotype is generated by precocious activation for APSCs, we would predict rescue of the *parade/ednraa* phenotype if Ednrab was required for the formation of adult pigment progenitors or in the differentiation of M and I from them. This will be tested only by assessing the adult phenotype of *ednrab homozygotes.* If *ednrab* has a role only on the development of embryonic iridophores we expect adult homozygotes to have a WT phenotype. On the other hand, if *ednrab* is also involved in the formation of adult pigment progenitors or their differentiation, we expect adult homozygote mutants to have a disrupted pigment pattern. From the reported expression pattern of *ednrab* in the trunk at 24 hpf (Fig. 4.4 C), it can be seen that *ednrab* is expressed in a broad population of migrating neural crest derived cells, consistent with a role beyond embryonic iridophore formation. In this context, we note too that adult *ednrba* (*rose*) mutants, do not display complete absence of iridophores and melanophores, so that redundancy with other Ednrs in melanophores and iridophores formation would be worth exploring.

The adult pigment phenotype of *edn3b*, *ednrba* and *ece2b* (decreased melanophores in the trunk) matches that of the *Edn3* and *Ednrab* mouse homozygote mutants, i.e. reduced melanophores in the trunk. However, in addition to the pigmentation phenotype, both mouse mutants have a reduction of enteric neurons and a survival rate of 21 days after birth. In contrast, all of the homozygote mutants of *edn3b*, *ednrba* and *ece2b* have a normal life span rate, perhaps suggesting that the enteric nervous system remains normal, although note that no enteric neuron quantification has been done yet. Another possibility is that in zebrafish ligands redundant in enteric neuron development.

Unexpectedly, the *ece1* homozygote mutant did not show a pigment phenotype, which suggests redundancy between *ece1*, *ece2a* and or *ece2b*, for which the

generation of a *ece2a* mutant and subsequently breeding double and triple mutants will be necessary to elucidate their role.

Knock-down of gene expression through the injection of morpholinos has been a very useful tool for the identification of gene function. However, the limitations of morpholinos are 1) the off-target phenotypes, making difficult the assessment of the gene function 2) the progressive dilution of morpholinos, allowing just a short window of time to observe a phenotype, 3) full penetrance of gene expression knock down, producing a high degree of variation in the morphants phenotypes and 4) activation of compensatory gene expression. Generation of endothelin mutants through CRISPR/Cas9 targeted mutagenesis has allowed us to confirm the roles of previously reported morphants, but also to identify novel genetic functions of the endothelin system in zebrafish pigment cell development. One of the major difficulties that we encounter has been gene duplication within the different elements of the endothelin system. However, the mutagenesis efficiency of the CRISPR/Cas9 system facilitates the generation of mutants, and in some cases the mutant phenotype can be observed in the injected F_0 with the crRNA, thus facilitating the screening of potential mutant carriers.

In this chapter, we described the pigment phenotype of new mutants of seven of the twelve genes of the endothelin system (*edn1*, *edn2a*, *edn3a*, *edn3b*, *ednraa*, *ednrab*, and *ece1*); together with the previously described mutants *ednrab* and *ece2b*, a total of nine mutants are now available for its study. This collection of mutants represents a powerful source to elucidate the function of each endothelin element not only in pigment development but in craniofacial patterning, enteric neuron colonization, and more recently their role in behaviour.

CHAPTER 5

CHAPTER 5 Investigating the mechanism of the *pde* mutant phenotype.

5.1 Introduction

Zebrafish display two pigment patterns. An embryonic/larval pigment pattern (Fig. 5.1 A) that remains unaltered until metamorphosis, when activation of adult pigment stem cells (APSC) produces newly differentiated pigment cells that form the second pigment pattern, the characteristic striped adult pigment pattern (Fig.5.1 B). Establishment of APSC occurs in development, but they remain quiescent until metamorphosis. Previous work has shown that formation of APSC requires the action of the *epidermal growth factor receptor (EGFR)-like tyrosine kinase* Erbb3b during embryonic development.

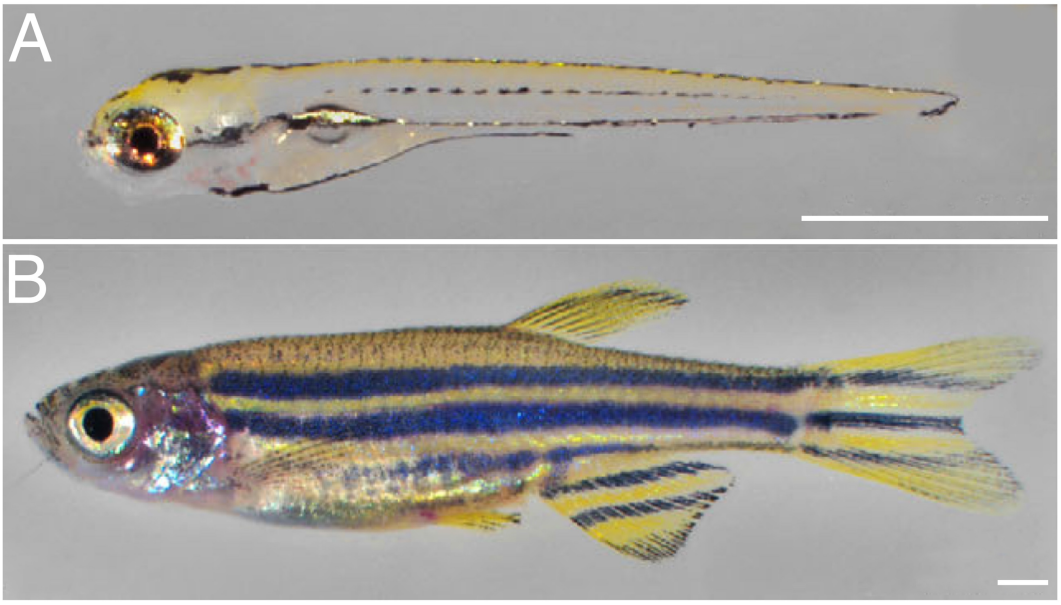

Figure 5.1 Zebrafish display two pigment patterns. Live imaging of a 5 dpf larvae (A) and 2 months old adult (B) shows larval and adult wild type pigment pattern. Modified from (Parichy & Spiewak 2015)

In Chapter 3, we described that in the mutant for the Endothelin receptor Aa (Ednraa), *parade*, the ectopic and supernumerary melanophores and iridophores restricted to the ventral medial pathway (Kelsh et al. 1996) do not result from disrupted neural

crest migration as both embryonic iridophores and melanophores reach the ventral stripe. Instead we identified that these ectopic pigment cells arise from over proliferation of NC-derived cells near the dorsal aorta and that are dependent on Erb signalling.

This data suggests that the ectopic pigment cells in *pde* mutants are not misplaced embryonic chromatophores but instead suggests that they are pigment cells derived from the Erb-dependant population of APSC. We have hypothesized that the disrupted function of Endraa in *pde* mutants, modifies the environment of a niche of APSC provided by the blood vessels that usually keeps APSC in a quiescent state and instead allows their premature activation resulting on the *parade* mutant phenotype. In this chapter, we will investigate whether APSC are the source of the ectopic pigment cells in *parade* mutants and what other signalling pathways contribute to the regulation of the *pde* phenotype.

In the following section, we will review the definition of stem cells, the stem cells niche and examples of characterised stem cells niches. We will then address the current understanding on the mechanism by which APSC in zebrafish are established and the signalling pathways that have been reported to be involved in the control of melanocytes stem cells and other models.

5.1.1 Stem Cells

Stem cells are generally considered as undifferentiated cells with the capacity to generate differentiated cells from one or multiple cell types. The main characteristic of stem cells is their self-renewal capacity, which means that when dividing, at least one of the daughter cells remains undifferentiated. Therefore, there is a constant supply of stem cells.

Based on these characteristics a variety of populations of cell have been classified as stem cells. *In vivo* we can distinguish two main groups. Embryonic stem cells (ESC) and adult stem cells (ASC). ESC, are referred to the cells of the inner cell mass of the blastocyst, they are considered as pluripotent cells that give rise to all of the cell types of the embryo. *In vivo*, they proliferate transitorily before segregating into the different germ layers, while *in vitro* ESC showed high self-renewal capacity (Evans & Kaufman 1981). During development, some embryonic populations are

often referred as stem cells because of their potential to generate multiple cell types. For instance, neural crest cells are often referred as neural crest stem cells because of their multipotency, however, as we described before, neural crest are fate restricted very shortly after the neural crest is specified. However, *in vitro* studies have shown that some cells in the neural crest have clonal expansion capacity (self-renewal) and are capable of generating several cell types (Stemple' et al. 1992).

Many cells isolated from different sources show *in vitro* a clonogenic pluripotency, some examples are embryonic germ cells (GSC) (Donovan & de Miguel 2003), epiblast-derived stem cells (epSC) (Tesar et al. 2007; Brons et al. 2007) and induced pluripotent stem cells (iPSC) (Takahashi & Yamanaka 2006).

Adult stem cells (ASC), also referred as tissue specific stem cells, show a wider variety of differentiation potential. ASC display a unique feature tightly related to their natural function, which is to supply the adult body with new cells to compensate the natural cell waste of specific tissues/organs. ASC are formed during development, but (usually) remain *quiescent* until they are required in the post-embryonic development. Quiescence is defined as the state of a cell in which it does not divide but retains the capacity to re-enter cell division (Coller 2011). ASC undergo cycles of quiescence and activation in which they divide generating one stem cell and a progenitor cell that proliferates, thus, amplifying the population of progenitor before differentiating. Thus, these proliferating cells are called transit amplifying (TA) cells.

The best characterised population of adult stem cells are hematopoietic stem cells (HSC), which give rise to all of the cell types of the lymphoid and myeloid lineages (Till & McCulloch 1980). *In vivo,* HSC exhibit cycles of quiescence and activation. HSC were first referred to as long-term HSC, while the transitory amplifiers were identified as short-term HSC; both can produce all of the lymphoid and myeloid lineages, however, when transplanted to irradiated SCID mice, only long-term-HSC are capable to reconstitute permanently the hematopoietic lineage (Till & McCulloch 1961). Similarly, many other stem cell populations exhibit transient amplifying progenitors, including intestinal stem cells (ISC) in the gut crypts (Vries et al. 2010), neural stem cells (NSC) in the subventricular zone, dentate gyrus and hippocampus (Bond et al. 2015) and keratinocyte stem cells (KSC) in the interfollicular epidermis (Metral et al. 2018).

5.1.2 Stem cell niches

The length of the quiescence/activation cycles depends on the demand for new cells within each tissue and is regulated by the niche where stem cells reside. The term niche was introduced (Schofield 1978) to explain the variation of HSC self-renewal capacity after being transplanted into irradiated SCID mice. Schofield, proposed that the self-renew capacity of a HSC is due to the microenvironment provided by adjacent cells (non-HSC). Currently, it is known that the key components of the niche of a stem cell are the interactions with the neighbouring cells and secreted factors surrounding a given stem cell. Interestingly, many of these niches are closely associated with blood vessels, suggesting a common role of blood vessels in the maintenance/regulation of the stem cells niche. In the following section we will review some of the characterised stem cell niches.

5.1.2.1 The hematopoietic stem cell niche.

Hematopoietic stem cells (Crane et al. 2017) are proposed to reside in a perivascular niche, as the majority of HSC are found adjacent to sinusoidal blood vessels in the bone marrow. In the same position, perivascular stromal cells and endothelial cells produce CXCL12 and stem cell factor (Scf), both crucial for the maintenance of HSC. Additionally, nerve projection, Schwann cells associated with nerve projections, immune cells such as megakaryocytes, macrophages and osteoclasts also regulate HSC maintenance, as their depletion results in the loss of HSC population, however, the mechanism behind their regulation is yet to be determined. The transforming growth factor-β (TGFβ), is known to promote HSC quiescence and self-renewal in vivo.

5.1.2.2 TThe neural stem cell niche.

In a similar example, neural stem cells (NSC), also knowns as Radial glia-like neural stem cells (B cells), maintain direct contact with blood vessels which are proposed to release factors that contribute to the regulation of NSC. Although the ventricular space is lined by ependymal cells, the NSCs occupy a position within the subventricular zone, and extend in between ependymal cells to extend a single cilium

along the ventricular space (Mirzadeh et al. 2008).. NSCs produce transient amplifying cells that ultimately generate neuroblasts that will migrate through the rostral migratory stream, towards the olfactory bulb where they differentiate into olfactory bulb neurons. Other components of the NSC niche include astrocytes and microglia. Some molecular signals which contribute to the maintenance of the NSCs have been identified, including BMPs, SHH, Wnts, and Notch, and growth factors like VEGF, IGF, and EGF (Basak et al. 2012; Than-Trong et al. 2018). Recent studies have shown that a key signalling pathway to maintain NSC in a quiescent state is the Notch pathway, in particular *Notch2*, as loss of function of it results on activation of quiescent NSC, accelerated neurogenesis and early exhaustion of the NSC reservoir. Notch signalling has been identified in many biological systems as a key regulator of the differentiation state of progenitor cells that are adjacent to each other (Kumano et al. 2008), intestinal stem cells maintenance (van Es et al. 2005) and hematopoietic stem cells (Suzuki & Chiba 2005).

5.1.2.3 intestinal stem cells niche.

The current understanding of ISC, considers the existence of two populations of ISC, slow cycling cells +4 and Lrg5+ cycling cells (Barker et al. 2007) Both populations are located within the intestinal crypts and are responsible for the generation of unspecified cells that proliferate towards the tip of the crypts and eventually differentiate into the many cell lineages found in the intestine, during homeostasis or after injury. It has been described that Paneth cells lay immediately next to ISC, and support their maintenance through the secretion of Wnt3a. On the other hand Wnt2b secreted by subepithelial mesenchymal cells are responsible for sustaining ISC self-renewal (Valenta et al. 2016) and prevention of their proliferation (Kabiri et al. 2018) and terminal differentiation (Korinek et al. 1998; Fevr et al. 2007)

5.1.2.4 The melanocytes stem cells niche.

In mammals, the hair is naturally replaced by cells derived from two types of stem cells within the hair follicle, epithelial stem cells and melanocyte stem cells. While epithelial stem cells (EpSC) give rise to keratinocyte and follicular cells, melanocyte stem cells (McSC) give rise only to melanocytes. Both stem cells populations reside in a distinctive area of the hair follicle called the bulge located on the basal membrane

(Nishimura et al. 2002) and undergo repeated coordinated cycles of quiescence and activation paired to the hair cycle. *In vivo* studies have shown activation of the TGF-β signalling pathway via Smad2 when McSC enter the quiescent state, while *in vitro* studies have shown that TGF-β1 prevents melanocyte maturation by downregulating MITF (Nishimura et al. 2010). Activation of McSC in the bulge is regulated by intrinsic and extrinsic sources of Wnt ligand (Rabbani et al. 2011). Furthermore, this study showed that constitutive Wnt signalling in EpSC promotes proliferation and differentiation of McSC via Edn1/EdnrB. In addition, and similar to NSC, Notch signalling also has a role in McSC regulation. Disruption of Notch signalling has been shown to prevent self-renewal of McSC as chemical inhibition of Notch signalling causes irreversible loss of hair pigmentation, and simultaneous loss of function of *Notch1* and *Notch2* results in premature loss of hair pigmentation in mouse (Kumano et al. 2008).

Stem cells have a vital physiological role in the maintenance of the homeostasis of the body. Their study is crucial to understand the mechanism by which homeostasis is finely regulated. Additionally, their differentiation potential makes them ideal for tissue regeneration therapies. Furthermore, they are a potential tool for generating tissue for the design of target therapies in a pathological context.

5.1.3 Adult pigment stem cells in zebrafish

During development, the pigment cells that form the embryonic pigment pattern directly differentiate from the neural crest, while the adult pigment pattern is formed mostly by newly differentiated pigment cells that derived from neural crest-derived APSC (Raible & Eisen 1994; Budi et al. 2008; Singh et al. 2016), while (at least) part of the adult population of xanthophores is produced from proliferation of embryonic xanthophores (McMenamin et al. 2014). Formation of newly differentiated pigment cells requires of activation of APSC that proliferate and differentiate into the pigment cells that will form the adult pigment pattern (Fig. 5.2 A and B). The process of APSC formation last approximately 40 hours, from 9-48 hpf, along the antero-posterior axis. However, establishment of APSC on each segment is likely to be shorter but it has not being determined for each specific segment.

Formation of APSC requires the *epidermal growth factor receptor (EGFR)-like tyrosine kinase* Erbb3b, as previous work has shown that null mutants of *erbb3b* (*picasso*) (Budi et al. 2008) are unable to form the adult pigment pattern (Fig. 5; Fig. 5.2 C and D). The *epidermal growth factor receptor (EGFR)-like tyrosine kinase* gene encoding the protein Erbb3b is affected (loss of function mutant). In zebrafish, *erbb3b* is expressed in the medial pathway in streams that run in a dorso-ventral manner on each somite segment (Langworthy & Appel 2012). It has been described that proliferation and migration of Schwann cells is mediated by the ErbB2 and ErbB3 receptor s(Lyons et al. 2005), but no function on embryonic pigment development has been noted.

Interestingly, treatment with the specific EGFR inhibitors, AG1478 or PD158780 from 9-48 hpf phenocopies the *picasso* mutants (Fig. 5.2 E and F). Strikingly, both *picasso* mutant larvae (Fig. 5.2 C) and larvae treated with Erb inhibitor (Fig. 5.2 E) display a normal embryonic pigment pattern. Thus, although both, embryonic pigment cells and APSC derive from the neural crest, formation of embryonic pigment cells and establishment of APSC are independent from each other. In addition to formation of the adult pigment pattern, it has been shown that APSC support regeneration of melanophores (Hultman et al. 2009; Yang & Johnson 2006; Tryon et al. 2011), as ablation of differentiated embryonic melanophores by treatment with the melanocytotoxic chemical 4-(4-morpholinobutylthio)phenol (MoTP) from 2-3 dpf does not prevent their full regeneration by 7 dpf (Fig. 5.2 G and H). However, larvae treated with the Erb inhibitor AG1478 from 9-48 hpf and then with MoTP do not regenerate melanophores (Fig. 5.2 I and J) (Hultman et al. 2009).

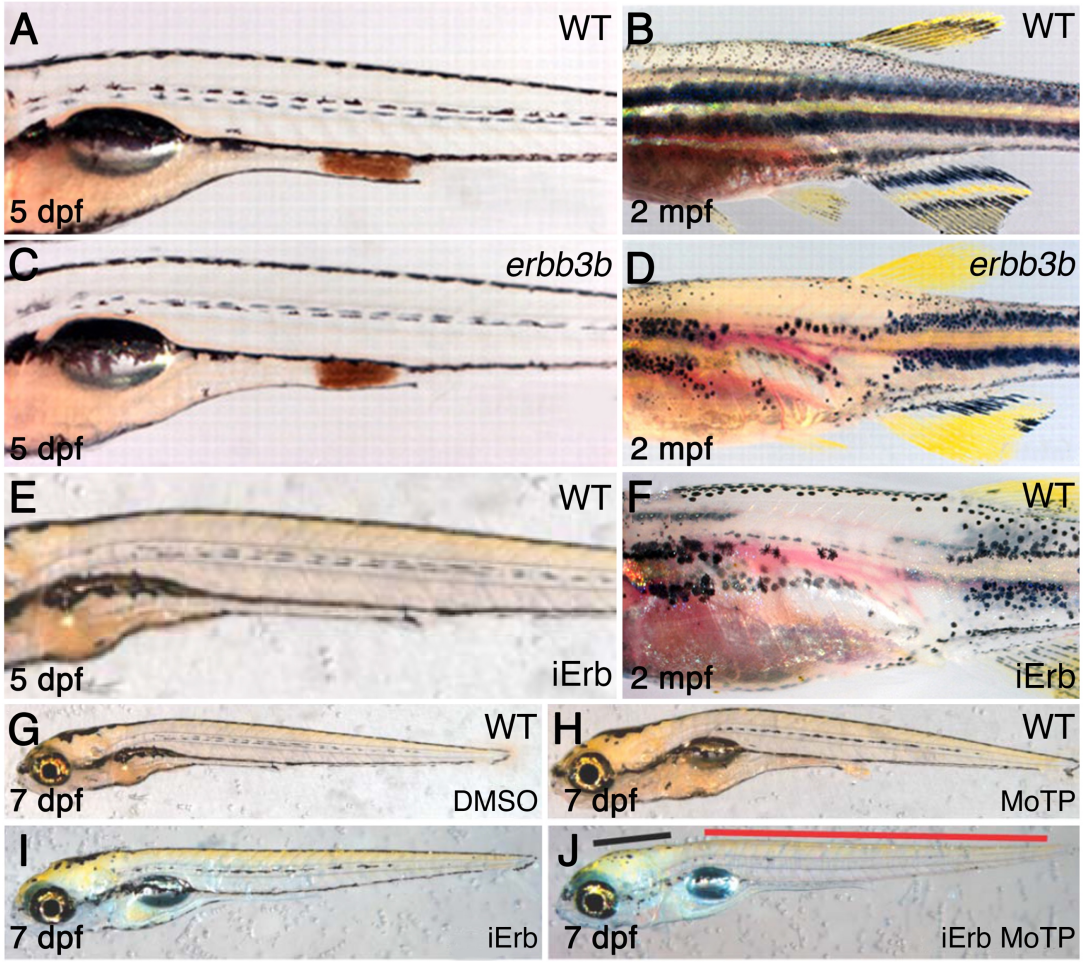

Figure 5.2 Formation of APSC requires of Erb signalling. Live imaging of 5 dpf (A, C and E) and 2 mpf (B, D and F) fish of WT (A and B), *erbb3b* mutants (C and D) and WT fish treated with Erb inhibitor AG1478 (during 9-48hpf timewindow only; E and F). Melanophore regeneration experiments shows 7 dpf WT fish (G-J) treated with DMSO (G) the melanocytotoxic chemical 4-(4-morpholinobutylthio)phenol (MoTP; H), Erb inhibitor (iErb) AG1478 (I) and iErb + MoTP (J). Panels A-F modified from Budi et al 2008, and panels G-J modified from Hultman et al, 2009.

Embryonic melanophores directly differentiate from the neural crest and this process requires the master regulator of the melanocytic lineage the Microphfthalmia-associated transcription factor a encoded by *mitfa*. In contrast, establishment of APSC does not requires embryonic *mitfa* expression, as previous work has shown that morpholino-mediated knock down of *mitfa* ablates embryonic melanophores (Mellgren & Johnson 2004) but that these are regenerated at 5 dpf through the activation of APSC that proliferate and differentiate to melanophores (Dooley et al. 2013). The latter studies also showed that unpigmented *mitfa:gfp* positive cells located in the DRGs contribute to the regeneration of melanophores, suggesting the existence of at least one source of APSC within the DRG.

More recently, fluorescent clonal cell tracking assays have shown the presence of multipotent progenitors within the medial pathway that give rise to adult pigment cells, glia and neurons. This multipotent progenitor appears as early as 16 hpf and remain multipotent at least until metamorphosis. Interestingly, some of these multipotent progenitors are located within the DRGs (Mongera et al. 2013), supporting the idea of a niche of APSC within the DRGs. However, this work focuses on clones located within the DRGs and did not examine clones located in other positions.

The majority of the characterised mutants that affect pigment pattern formation show a reduction of pigment cells. In contrast, few examples of supernumerary or ectopic pigment cells have been reported. For example, a dominant hyperactive allele of the *leukocyte tyrosine kinase* (*ltk*) *moonstone* (*mne*) was recently characterised (Fadeev et al. 2016). Larvae of *mne* mutant display supernumerary and ectopic iridophores in the medial migratory pathway of the trunk and increased number of iridophores on scales and fins of adult fish. Interestingly, in the *mne* larvae mutants, the ectopic iridophores are located in two positions, one in the dorsal medial migratory pathway and the other in the ventral medial migratory pathway, the latter resembling the location of cells in *pde* mutants. This suggests the possibility that there are pigment progenitors in both dorsal and ventral regions of the medial pathway and that hyperactivation of *ltk* promotes their premature differentiation, revealing at the same time the position of the pigment progenitors.

5.1.3.1 Regulation of adult pigment stem cells.

Regulation of APSC in zebrafish is largely unknown, however, one of the best characterised pigment stem cell niches is that of melanophore stem cells (MSC) in the mouse hair follicle. The hair is naturally replaced by cells derived from two types of stem cells within the hair follicle, epithelial stem cells and melanophore stem cells. While epithelial stem cells (EpSC) give rise to keratinocyte and follicular cells, melanophore stem cells (McSC) give rise only to melanophores. Both stem cells populations reside in a distinctive area of the hair follicle called the bulge located on the basal membrane (Nishimura et al. 2002) and undergo repeated coordinated cycles of quiescence and activation paired to the hair cycle. Transcriptional profiling of stem cells in the bulge revealed upregulation of TGF-β induced factors in comparison with keratinocytes (Tumbar et al. 2014). Additionally, i*n vivo* studies showed activation of the transforming growth factor β (TGF- β) signalling pathway via Smad2 when McSC enter the quiescent state, while *in vitro* studies have shown that TGF- β1 prevents melanophore maturation by downregulating MITF (Nishimura et al. 2010). Interestingly, *in vivo* studies have shown that activation of McSC in the bulge is regulated by intrinsic and extrinsic sources of Wnt ligand (Lim et al. 2016; Lowry et al. 2005). Furthermore, this study showed that constitutive Wnt signalling in EpSC promotes proliferation and differentiation McSC via Edn1/EdnrB (Takeo et al. 2016). In addition to TGF-β and Wnt signalling, disruption of Notch signalling has been shown to prevent self-renewal of McSC as chemical inhibition of Notch signalling causes irreversible loss of hair pigmentation. Furthermore, simultaneous loss of function of *Notch1* and *Notch2* results in premature loss of hair pigmentation in mouse (Kumano et al. 2008).

The role of Wnt signalling in stem cell regulation was first characterised in the maintenance of intestinal stem cells (ISC), as depletion of Wnt signalling resulted in neonatal gut epithelium with non-proliferative completely differentiated cells (Muncan et al. 2006). The current understanding of ISC, considers the existence of two populations of ISC, +4 slow cycling cells (Qiu et al. 1994) and Lrg5+ cycling cells (Barker et al. 2007). Both populations are located within the intestinal crypts (Hans et al. 2009) and are responsible for the generation of unspecified cells that proliferate towards the tip of the crypts and eventually differentiate into the many cell lineages found in the intestine, during homeostasis or after injury. On the other hand Wnt2b secreted by subepithelial mesenchymal cells are responsible of sustaining ISC self-

renewal (Valenta et al. 2016) and prevention of their proliferation (Kabiri et al. 2018) and terminal differentiation (Korinek et al. 1998; Fevr et al. 2007).

Another very interesting example in which Notch signalling controls stem cell quiescence is in the niche of the neural stem cells (NSC) in the ventricular-subventricular zone of the mouse brain. Here, NSC have been described to be in direct contact with blood vessels (Mirzadeh et al. 2008). Recent studies have shown that a key signalling pathway to maintain NSC in a quiescent state is the Notch pathway, in particular *Notch2*, as loss of function of it results on activation of quiescent NSC, accelerated neurogenesis and early exhaustion of the NSC reservoir. Notch signalling has been identified in many biological systems as a key regulator of the differentiation state of progenitor cells that are adjacent to each other (Kumano et al. 2008), intestinal stem cells maintenance (van Es et al. 2005) and hematopoietic stem cells (Suzuki & Chiba 2005).

After reviewing the regulation of some stem cell niches, some signalling pathways are found to have a role in one or more stem cell niche. For instance, TGF-β (Nishimura et al. 2010), Wnt/β-catenin (Rabbani et al. 2011) and Notch signalling have a role on maintenance of melanocyte stem cells by promoting self-renewal (Kumano et al. 2008). However, in the gut, in addition to promoting self-renewal and quiescence, Wnt signalling also promotes proliferation of transient amplifiers progenitors (Barker et al. 2007). While notch signalling has been also reported to have a role on keeping NSC in a quiescent state (Than-Trong et al. 2018).

Our model on the mechanism of the *parade* phenotype proposes that APSC are premature activated. Thus, we decided to investigate whether these signalling pathways contribute to the regulation of the *pde* phenotype. We hypothesised that inhibition of one or more of these signalling pathways in a wild type background, would promote APSC differentiation at the expense of APSC self-renewal.

5.1.4 Working model.

The prevalent location of the ectopic cells in *pde* and *mne* mutants indicated two defined positions medial pathway in which pigment progenitors reside, one dorsal and likely corresponding to the DRG, and one ventral in the vicinity of the ventral spinal

nerves or the sympathetic ganglia. The restricted location of ectopic pigment cells in *pde* mutants suggests that EdnrAa has a role in the regulation of the differentiation of the pigment progenitors specifically located ventrally in the medial migratory pathway. Thus, we propose that there is a second niche of APSC in the ventral region of the medial pathway that is normally regulated by signals provided by the blood vessels; and that these signals are somehow dependent upon EdnrAa signalling. Hence, the disruption of Endraa function in *pde* mutants, modifies the environment of the APSC that usually keeps them in a quiescent state and instead causes their premature activation resulting in the ectopic production of pigment cells characteristic of the *parade* mutant phenotype.

Here, we test our hypothesis of a second niche of APSC in the ventral region of the medial pathway. We first investigate whether ectopic pigment cells in *parade* mutants, in particular melanophores, are derived from embryonic melanophores or APSC by ablating embryonic melanophores through *mitfa* morpholino-mediated knock-down. We then test whether EdnrAa disruption has a specific effect on the ventral pigment progenitors by disrupting *ednraa* function in *mne* mutants through *ednraa* gRNA + Cas9 protein injection. Finally, we assess whether pharmacological inhibition of TGF-β, Wnt/β-catenin or Notch signalling allows activation of stem cells resulting in the formation of ectopic pigment cells in a wild type background.

5.2 Results

5.2.1 Formation of ectopic melanophores in *pde* mutants does not depend on early activity of *mitfa.*

In order to investigate if ectopic melanophores in *parade* mutants are derived from embryonic melanophores or APSC, we tested whether ectopic melanophores in *parade* mutants are formed independently of early activity of *mitfa* in the neural crest. To do this we took advantage of the transient effects of morpholino-mediated knock down of *mitfa* ((Dooley et al. 2013). By injecting this morpholino into *parade* mutants, we asked whether ectopic pigment cells (but not the normal embryonic pattern of melanophores) would be generated despite the early inhibiton of *mitfa* activity. In wild-type fish, at 72 hpf, most embryonic melanophores have reached their final position at the dorsal, lateral, ventral and yolk sac stripes, although it is common to find few migrating melanophores in the ventral medial pathway of the trunk and tail. This makes distinguishing *pde* mutants more difficult at 72 hpf. The most reliable stage to assess the *pde* phenotype is at 4 or 5 dpf. We reasoned that if ectopic melanophores derive from embryonic melanophores, knock-down of *mitfa* would ablate both embryonic and ectopic melanophores in *parade* mutants. However, if formation of ectopic melanophores is independent of *mitfa*, morpholino-mediated knock-down of *mitfa* would not ablate ectopic melanophores in *parade* mutants. For all tests, three independent experiments using batches of embryos from different adult pairs were independently injected (section 2.4). Images from embryos and dot plots correspond to a representative experiment.

To assess the efficiency of the *mitfa*-morpholino, we first injected increasing amounts of a previously reported *mitfa* morpholino (*mitfa*-MO) (Mellgren & Johnson 2004) to one-cell stage wild type embryos. We injected 5 ng, 10 ng and 20 ng of *mitfa*-MO and at 60 hpf we categorized the degree of absence of melanophores into five groups (Fig. 5.3): embryos with no melanophores (0 M, Fig. 5.3 A), embryos with melanophores in the dorsal stripe (DS; Fig. 5.3 B), embryos with melanophores in the dorsal and ventral stripe (DVS; Fig. 5.3 C), embryos with melanophores in the dorsal, ventral, lateral and yolk sac strips (DVLYS; Fig. 5.3 D) and embryos with a wild type melanophore pattern (WT; Fig. 5.3 E).

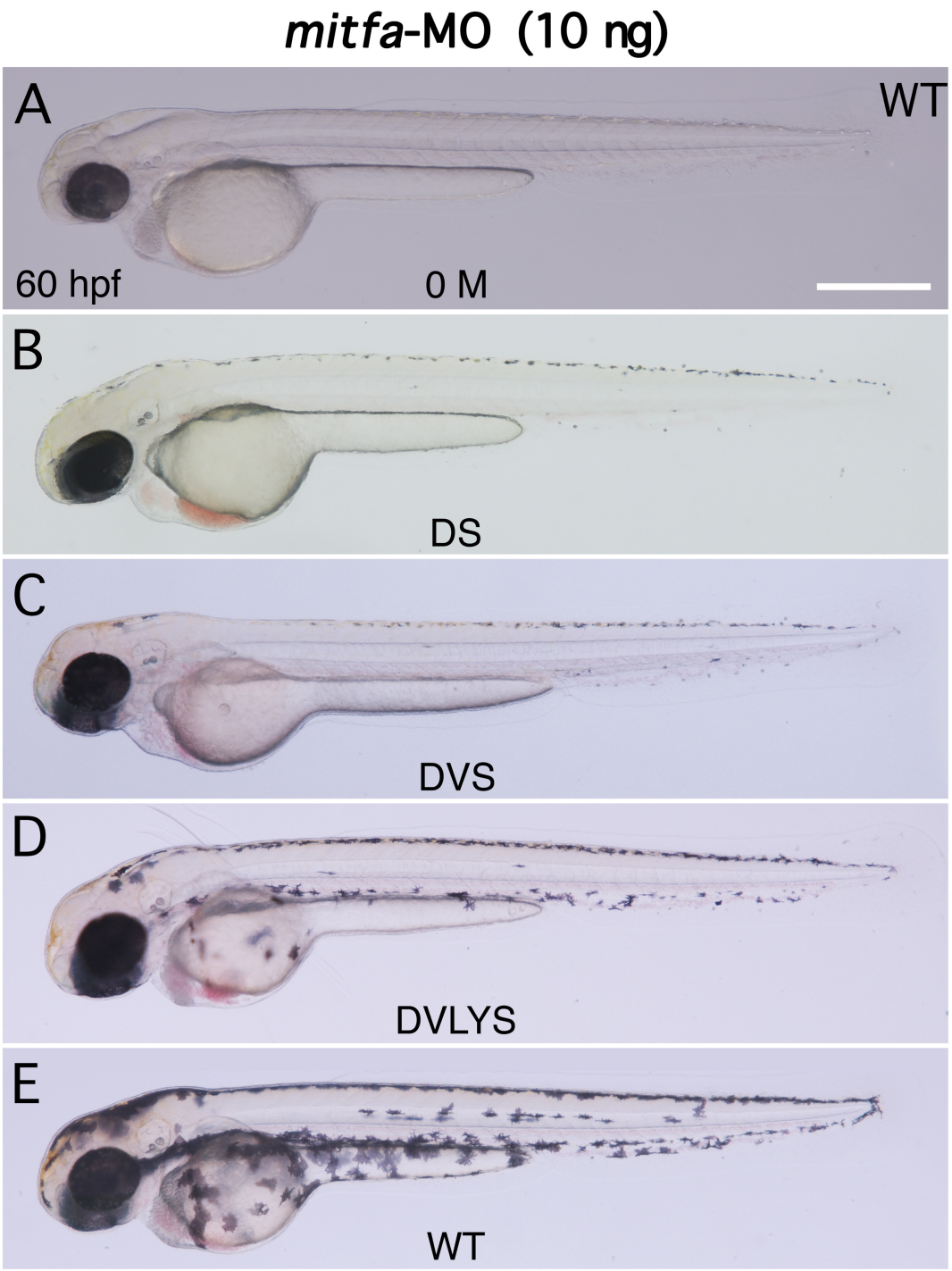

Figure 5.3 *mitfa* morpholino-mediated knock down. Live bright field imaging of 60 hpf WT larvae injected with 10 ng of *mitfa*-MO at one-cell stage. Embryos were scored according the severity of melanophore absence. Embryos with no melanophores (0 M; A), embryos with melanophores in the dorsal stripe (DS; B), dorsal and ventral stripes (DVS; C), dorsal, ventral, lateral and yolk sac stripes (DVLYS; D) and embryos with a WT phenotype (WT; E). Scale bar = 500 μm (A-E).

We carefully screened for embryos with no melanophores at 2 dpf, but we only found embryos with no melanophores in the batches of embryos injected with 10 ng and 20 ng of *mitfa*-MO (Fig. 5.4). Previous work has assessed melanophore regeneration at 7 dpf (Hultman et al. 2009), but on our experiments we did not allow the injected larvae to grow beyond 5 dpf. All of the embryos with no melanophores (Fig. 5.5 B) regenerated most of the larval melanophore pattern by 5 dpf (Fig. 5.5 D, F and H compared to uninjected larvae A, C, E and G). We found that embryos injected with 20 ng presented less regenerated melanophores by 5 dpf than embryos injected with 10 ng (data not shown), probably due to the residual effect of the morpholino, thus we decided to use an amount of 10 ng of morpholino for our further experiments.

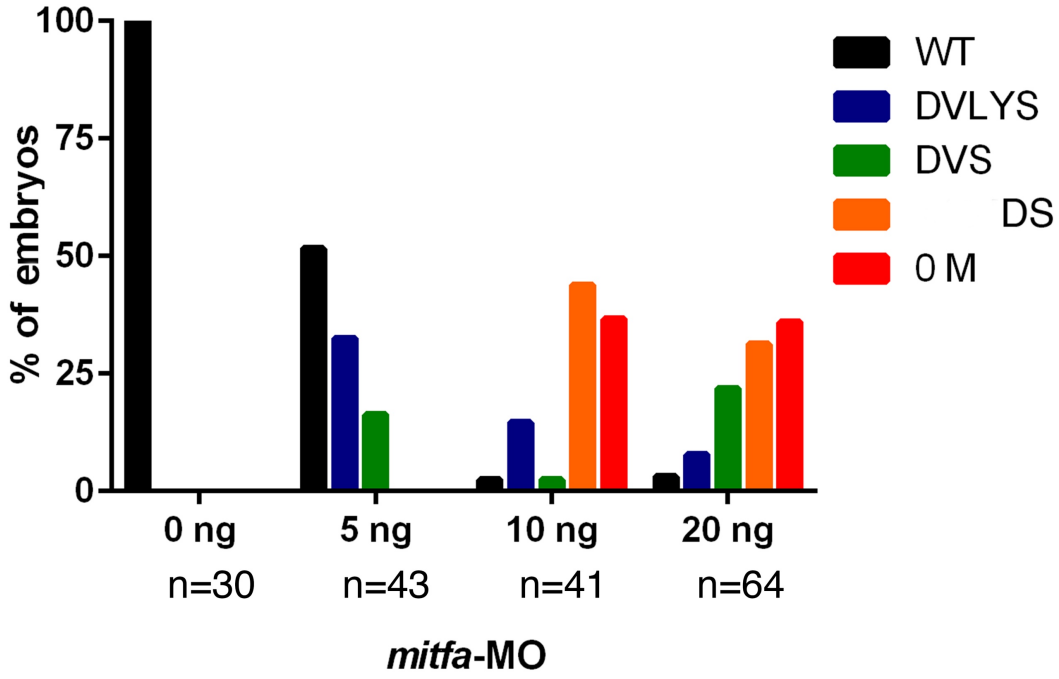

Figure 5.4 Dose-response of *mitfa* knockdown efficiency. Bar chart shows percentage of embryos within the categories 0M, DS, DVS, DVLYS and WT in batches of WT embryos injected with different amounts of *mitfa*-MO (0, 5, 10 and 20 ng).

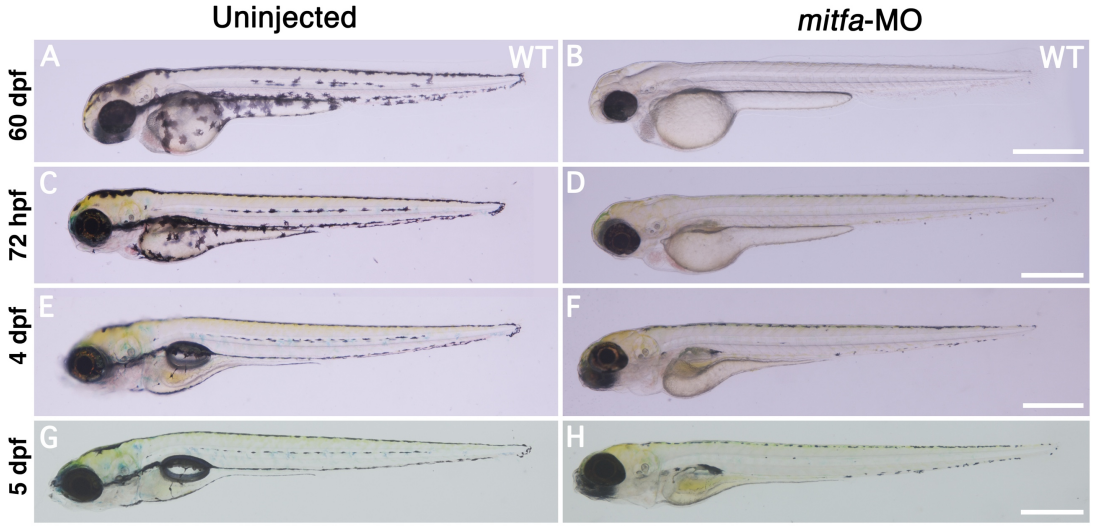

Figure 5.5 Regeneration of melanophores after *mitfa* knock down. Live bright field imaging of uninjected WT larvae (A, C, E and G) and injected WT larva with 10 ng of *mitfa*-MO (B, D, F, and H), at 60 hpf (A and B), 72 hpf (C and D), 4 dpf (E and F) and 5 dpf (G and H). Scale bar = 500 μm (A-H).

We then injected 10 ng of *mitfa*-MO into one-cell stage *pde* embryos and screened for embryos with no melanophores at 60 hpf. We found that $^{15}/_{41}$ embryos had no melanophores (Fig. 5.6 B), we kept these embryos at 28º C and assessed the pigment phenotypes again at 5 dpf, from which $^{9}/_{15}$ presented ectopic melanophores in the ventral medial pathway (Fig. 5.6 B), in addition to the regenerating wild type pattern. Statistical analysis between the mean number of ectopic melanophores in uninjected *pde* embryos and the mean number of ectopic melanophores in the *mitfa*-MO injected embryos that presented ectopic melanophores cells showed no significant difference (tow-tails unpaired t-test; *pde* uninjected m=2.667 ± 0.3727, n=9; *pde* + *mitfa*-MO m=1.778 ± 0.3643, n=9; p-value 0.1074; Fig. 5.6 E).

Thus, if early morpholino knock-down of *mitfa* does not ablates prevents the formation of ectopic melanocytes, these results suggest that formation of ectopic melanophores in *pde* mutants does not depend on early activity of *mitfa* as embryonic melanocytes do. Therefore, supporting the hypothesis that ectopic pigment cells in *pde* mutants do not derive from embryonic pigment cells but from adult pigment stem cells.

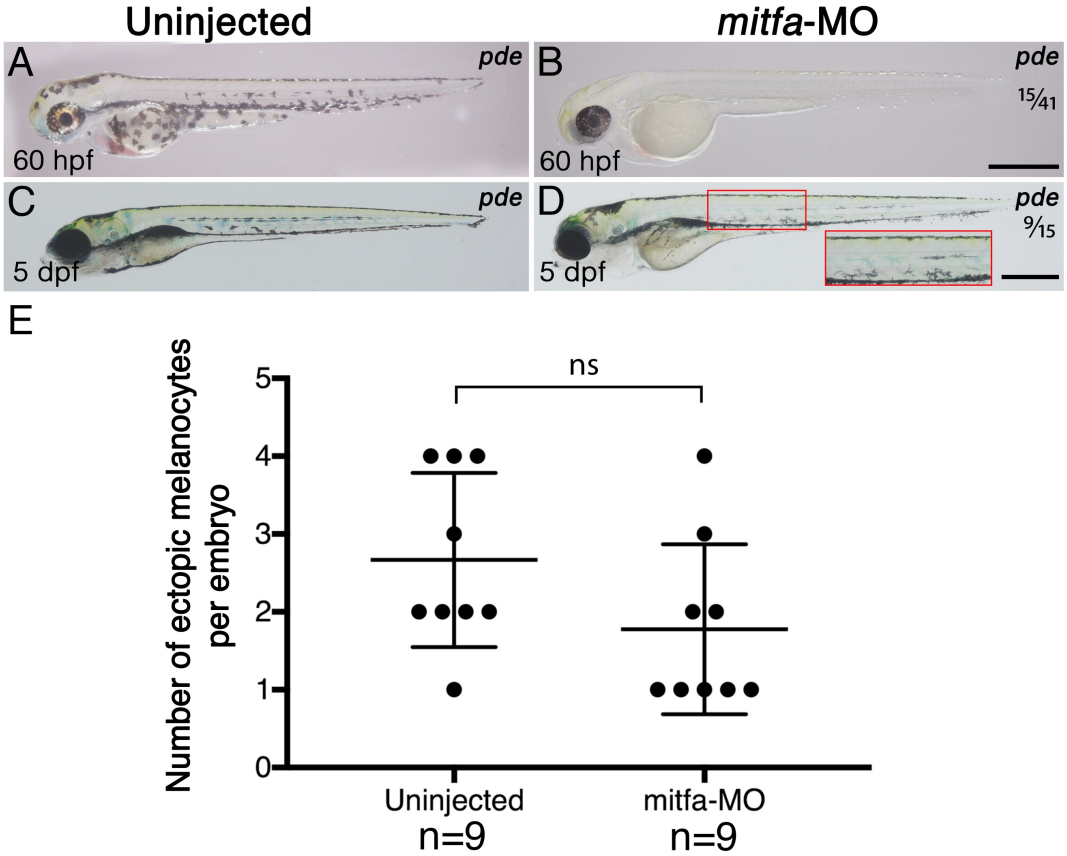

Figure 5.6 Knock down of *mitfa* in *pde* mutants does not ablate ectopic melanophores in the ventral medial pathway. Live bright field imaging of uninjected *pde* larvae (A and C) and sibling larvae injected with 10 ng of *mitfa*-MO (B and D), at 60 hpf (A and B) and 5 dpf (C and D). Scale bar 500 μM (A-C). Dot plot shows number of ectopic pigment cells in ventral medial pathway in WT and *pde* uninjected and injected embryos. Each dot corresponds to one embryo.

5.2.2 Ectopic pigment cells are found in stereotypical locations.

A simple explanation for the *ednraa* mutant /*parade* phenotype could be random miss localization of embryonic pigment cells. However, we have found other mutant context in which ectopic pigment cells are produced and located in the ventral medial pathway but also in the dorsal medial pathway. This mutant is called *moonstone (mne)*, which presents a mutation in the gene that encodes the Leukocyte tyrosine kinase receptor Ltk. The *ltk*^{moonstone} allele, from now on referred only as *mne*, results on a hyperactivated form of the LTK receptor. The characterisation of *mne* revealed that one source of the overproductions of iridophores are *sox10:RFP* expressing cell within the DRG's, however this work did not investigate the source of the ventral ectopic iridophores. Thus, it is possible that in the ventral medial pathway, perhaps in the sympathetic ganglia, there is a second population of pigment progenitor with the potential to form iridophores (at least), and that his second source is regulated by ednraa.

5.2.2.1 Disruption of *ednraa* in *ltk*^{moonstone} mutants strongly enhances the formation of ectopic iridophores in the ventral medial pathway.

In order to investigate whether EdnrAa has a specific effect on the ventral pigment progenitors we tested whether disruption of *ednraa* function in *moonstone (mne)* mutants has a specific effect on the ventral pigment progenitors. To do this, we injected *ednraa* gRNA + Cas9 protein into one-cell stage heterozygote *mne*$^{+/-}$ mutants. We expected that if the role of EdnrAa is specific to the ventral progenitors, embryos injected with the *ednraa* gRNA will show extra iridophores only in the ventral side of the medial pathway. However, if the effect is generic to the medial pathway, increase of iridophores of injected *ednraa* gRNA embryos would be in both the dorsal and ventral medial pathway.

We first tested the efficiency of the gRNA in generating embryos with ectopic pigment cells in wild type embryos. We injected 5 nl of *ednraa* gRNA (35 ng/μl) + Cas9 protein (700 pg/μl; see details in section 2.2.2.1) directly into the one-cell stage within the first 10 minutes after fertilization. Injected embryos and uninjected control siblings were grown in parallel at 28 ºC and the pigment phenotype was examined at 5 dpf. The wild type strain (Fig. 5.7 A and C) used in this experiment is known as Tübingen WT; as shown, in this strain we found sporadic single ectopic cells in the ventral medial

pathway but never more than two. In contrast, 84.5% of the injected embryos ($^{60}/_{71}$; Fig. 5.7 B and D) had between 4 and 22 ectopic pigment cells, 7.05% of the embryos had 1 or 2 ectopic cells and 8.45% had no ectopic pigment cells. The mean number of ectopic pigment cells between the uninjected control embryos and injected embryos is statistically different (two-tailed Welch's unpaired t-test; number of melanophores and iridophores (M+I); WT uninjected m=0.25 ± 0.099, n=20; WT + *ednraa* gRNA/Cas9 m= 7.94 ± 0.6173, n=71; p-value <0.0001; Fig. 5.7 E).

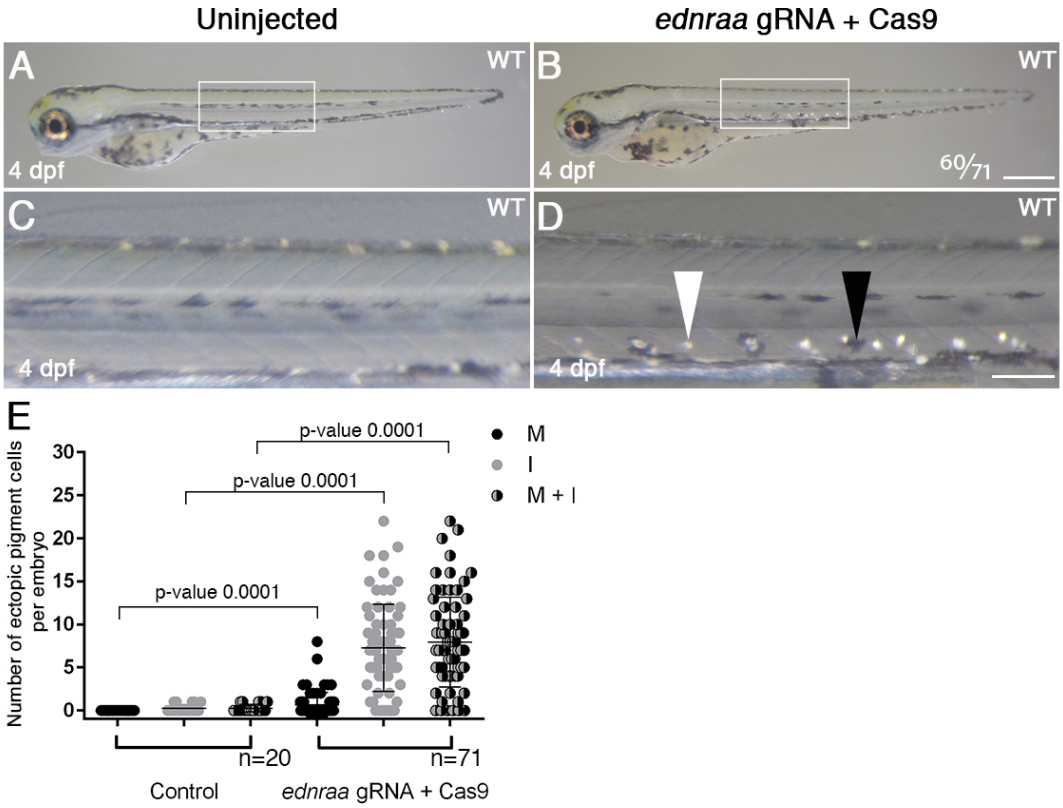

Figure 5.7 Injection of *ednraa* gRNA into WT embryos generates ectopic melanophores and iridophores in the ventral medial pathway. Live imaging of 4 dpf WT uninjected larvae (A and C) and WT larvae injected (B and D) with *ednraa* gRNA + Cas9 protein at 1-cell stage. Dot plot shows number of ectopic melanophores and iridophores (E). Each dot corresponds to one embryo. Scale bar = 500 μm (A and B) and 100 μm (C and D). Injected embryos (B and D) show sticking formation of ectopic iridophores and melanophores in the ventral medial pathway.

We then injected *lt* ^{moonstone} heterozygous, now refered as *mne*$^{+/-}$,embryos with *ednraa* gRNA using the same conditions as described above. Examination of the pigment phenotype at 5 dpf of uninjected *mne*$^{+/-}$ embryos (Fig. 5.8 A and C) and *mne*$^{+/-}$ embryos injected with *ednraa* gRNA (Fig. 5.8 B and D), revealed a striking overproduction of iridophores in the injected embryos (Fig. 5.8 B), particularly in the ventral medial pathway (Fig. 5.8 D). Confocal imaging of *mne*$^{+/-}$ *Tg(sox10:RFP)* injected (Fig. 5.8 E) and uninjected embryos (Fig. 5.8 F) at 5 dpf shows labelled glia and iridophores. Uninjected *mne*$^{+/-}$ embryos show a spaced series of ectopic iridophores in the ventral medial pathway. In contrast, embryos injected with *ednraa* gRNA displayed a continuous chain of iridophores just below the dorsal aorta and around the ventral nerve projections that emerge from the DRGs.

Quantification of clusters of iridophores showed a significant difference between the uninjected and injected *mne*$^{+/-}$ embryos in both the dorsal and ventral medial pathway (tow-tailed Welch's unpaired t-test; number of clusters of iridophores in the dorsal medial pathway; *mne*$^{+/-}$ uninjected m=5.875 ± 0.5154, n=8; *mne*$^{+/-}$ + *ednraa* gRNA/Cas9 m= 11.75 ± 1.887, n=4; p-value=0.0481; tow-tails Welch's unpaired t-test; number of clusters of iridophores in the ventral medial pathway; *mne*$^{+/-}$ uninjected m=11.25 ± 0.8183, n=8; *mne*$^{+/-}$ + *ednraa* gRNA/Cas9 m= 39.5 ± 5.867, n=4; p-value=0.0160; Fig. 5.9 E). However, the mean number of clusters of iridophores in the ventral medial pathway of injected *mne*$^{+/-}$ embryos (m=39.5), was more than 3 folds the mean number of clusters of iridophores in the dorsal medial pathway (m=11.75). Injected embryos also exhibited a few ectopic melanophores (Fig. 5.8 D). Thus, the repeated location of the ectopic cells in *pde* and *mne* mutants supports the idea of the presence of pigment progenitors in a defined position of *both* the dorsal and ventral medial pathway.

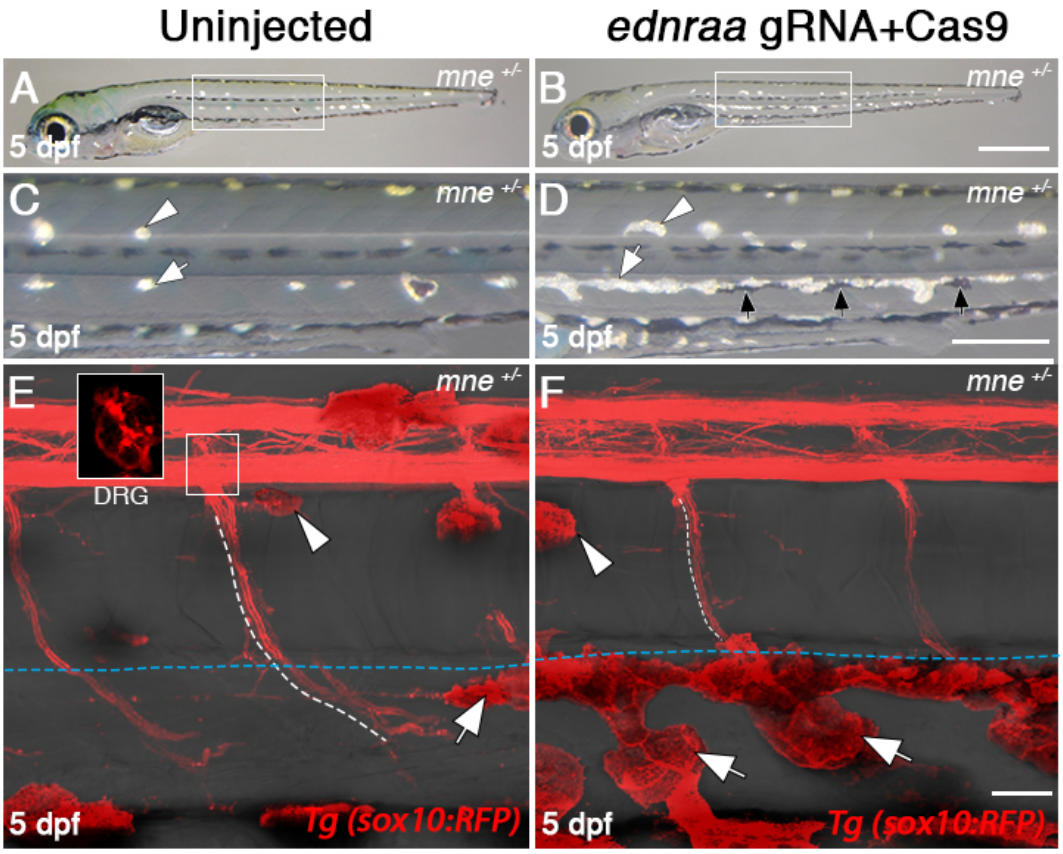

Figure 5.8 Injection of *ednraa* gRNA into heterozygote double *mne*$^{+/-}$ mutants produces ectopic iridophores and melanophores in the medial pathway. Live imaging of 5 dpf heterozygote mutants for *mne*$^{+/-}$ uninjected (A, C and E) and injected (B, D and F) with *ednraa* gRNA + Cas9 protein at 1-cell stage. Close up of posterior trunk of uninjected larvae (C) shows scattered clusters of ectopic iridophores in the dorsal (white arrowhead) and ventral (white arrow) medial pathway. Close up of posterior trunk of injected larvae (D) shows scattered clusters of ectopic iridophores in the dorsal medial pathway (white arrowhead), a continuous chain of iridophores in the ventral medial pathway (white arrow) and melanophores (black arrows). Confocal imaging of *mne*$^{+/-}$ *Tg(sox10:RFP)* at 5 dpf (E and F) shows fluorescently labelled glia (white dashed line) and iridophores (white arrowhead). Uninjected larvae (E) shows ectopic cluster of iridophores close to DRG (white box) and the ventral medial pathway (white arrow), close to the DA. Injected larvae (F) show ectopic continuous clusters of iridophores in the medial pathway (white arrows), just below the dorsal aorta (blue dashed line shows ventral edge of DA). Scale bar = 500 μm (A and B) and 100 μm (C and D) and 50 μm (E-F).

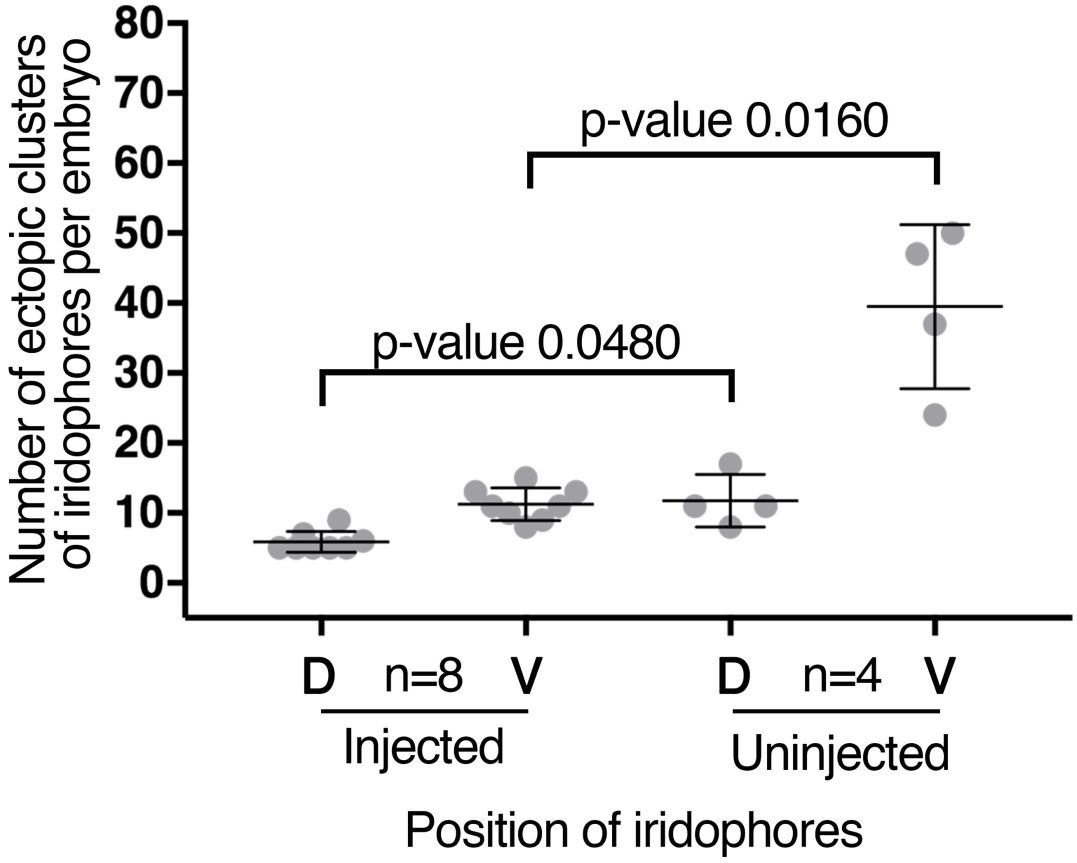

Figure 5.9 Depletion of EdnrAa activity increases number of ectopic clusters of iridophores in *mne*$^{+/-}$ embryos. Dot plot shows number of ectopic iridophores (I) per embryo in the dorsal (D) and ventral V) medial migratory pathway, in uninjected larvae and in larvae injected with *ednraa* gRNA + Cas9 protein.

Another observation provides further support for this conclusion. In a collaboration with the research group of Dr David W. McCauley, a member of our lab, Dr Deeya, R. Ballim, performed an experiment to test the capability of the lamprey *Petromyzon marinus sox10* orthologue *PmSoxE2* to rescue the pigment and enteric phenotype in zebrafish *sox10 colourless* (*cls*^{m618}) mutants. Homozygous mutants of this allele lack the three pigment cell types, glia, sympathetic, enteric and (most) sensory neurons. In that study, embryos from heterozygote *cls* carriers were injected with a pCS2(*CMV:PmSoxE2)* expression vector and mRNA of the Tol2 transposase. In control embryos, 25% of the larvae showed the mutant phenotype, but in the injected embryos, the pigment and enteric phenotype was rescued in the homozygote mutants (Lee et al. 2016).

During the examination of the injected larvae, we noticed that heterozygote *cls*$^{+/-}$ mutants displayed ectopic melanophores and iridophores in the lateral and medial migratory pathway (DB, data not shown). This exciting finding lead us to test whether the pCS2(*CMV: PmSoxE2)* could induce formation of ectopic pigment cells in a wild type background. Thus, we injected 100 pg per embryo of the plasmid + Tol2 mRNA into one-cell stage wild type embryos. Uninjected control siblings were incubated in parallel with injected embryos for further examination.

At 5 dpf all control embryos showed a normal pigment pattern (not shown), however, the injected embryos displayed numerous ectopic melanophores and iridophores. Interestingly, injected embryos displayed ectopic pigment cells in both the lateral and the medial pathway (Fig. 5.10 A) and both melanophores and iridophores in the medial pathway (Fig. 5.10 B). The ectopic pigment cells in the medial pathway were located in three positions, above the neural tube (NT); dorsolateral to the neural tube and above the notochord (Nc), similar to the position of DRGs; and ventral to the dorsal aorta (DA) like in *pde* mutants. Immunodetection of early neuronal marker Elav1 (Hu neuronal RNA-binding protein) revealed that some, but not all, of the melanophores are close to the DRGs, and similarly, in the ventral medial pathway some, but not all, of the ectopic melanophores are close to the sympathetic neurons. Quantification of the number of ectopic pigment cells is shown in the dot plot of Fig. 5.11. We did not asses other neural crest derivatives.

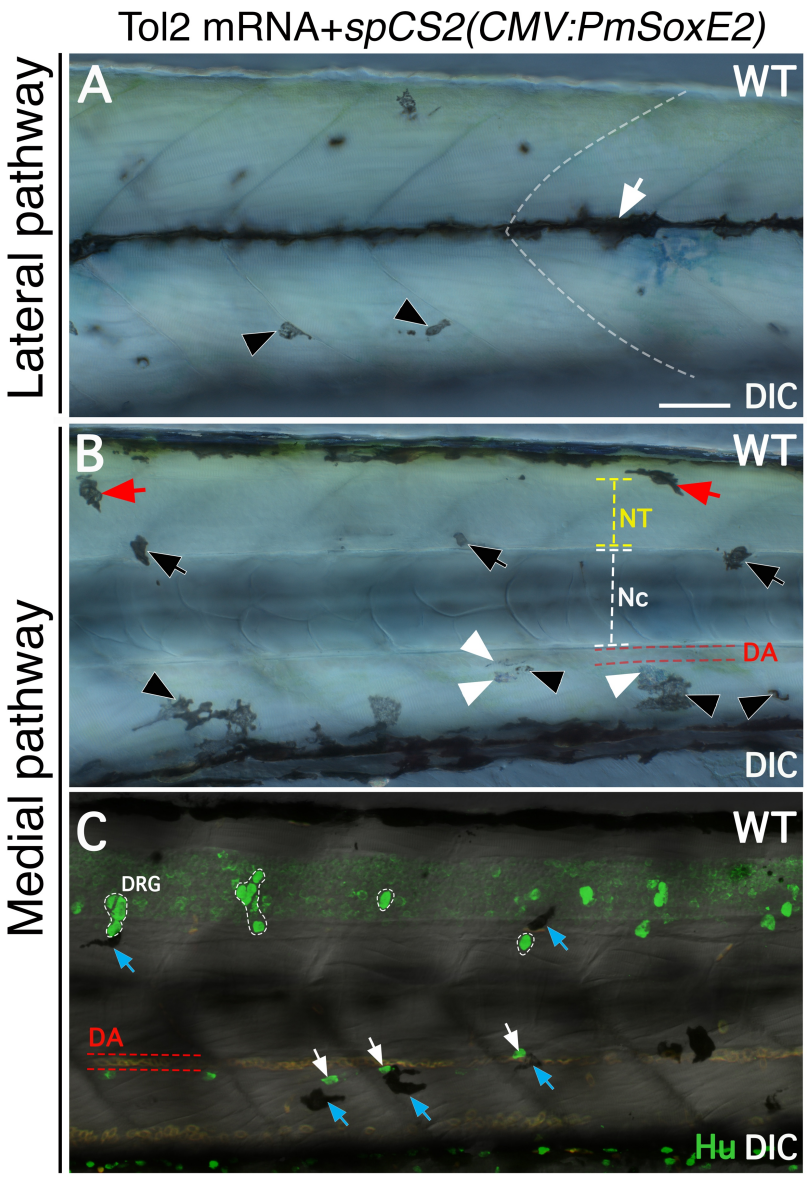

Figure 5.10 Over expression of soxE2 in zebrafish produces ectopic pigment cells in the lateral and medial pathway. Live DIC imaging of lateral (A) and medial (B) migratory pathways of the posterior trunk of 5 dpf WT larvae injected with the expression vector pCS2+*CMV*:*soxE2* and Tol2 mRNA. Border of a muscle segment is outlined with a white dashed line and the lateral stripe is indicated with a white arrow (A), ectopic melanophores are indicated with black arrowhead. In panel B: Neural tube (NT; yellow dashed line), notochord (Nc; white dashed line) and dorsal aorta (DA; red dashed lines). Ventral ectopic iridophores (white arrowheads) and melanophores (black arrowheads), dorsal melanophores (black arrows), melanophores dorsal to the neural tube (red arrows). Immuno detection of Hu (C) shows melanophores (blue arrows) next to DRGs (shape in dashed white line) and sympathetic neurons (white arrows). Dorsal Aorta (DA) is underlined with red dashed lines. Scale bar = 50 μm (A-C).

Although the injected gene was the lamprey *sox10* orthologue *soxE2*, again we see that the formation of ectopic pigment cells is not randomly distributed, but instead is associated with specific positions on the medial pathway.

These positions correspond to the DRG and sympathetic ganglia, which supports the hypothesis of the presence of pigment progenitors (perhaps APSC) in both the dorsal and ventral medial pathway. The zebrafish *sox10* gene has been cloned into the same vector and will be tested in due course.

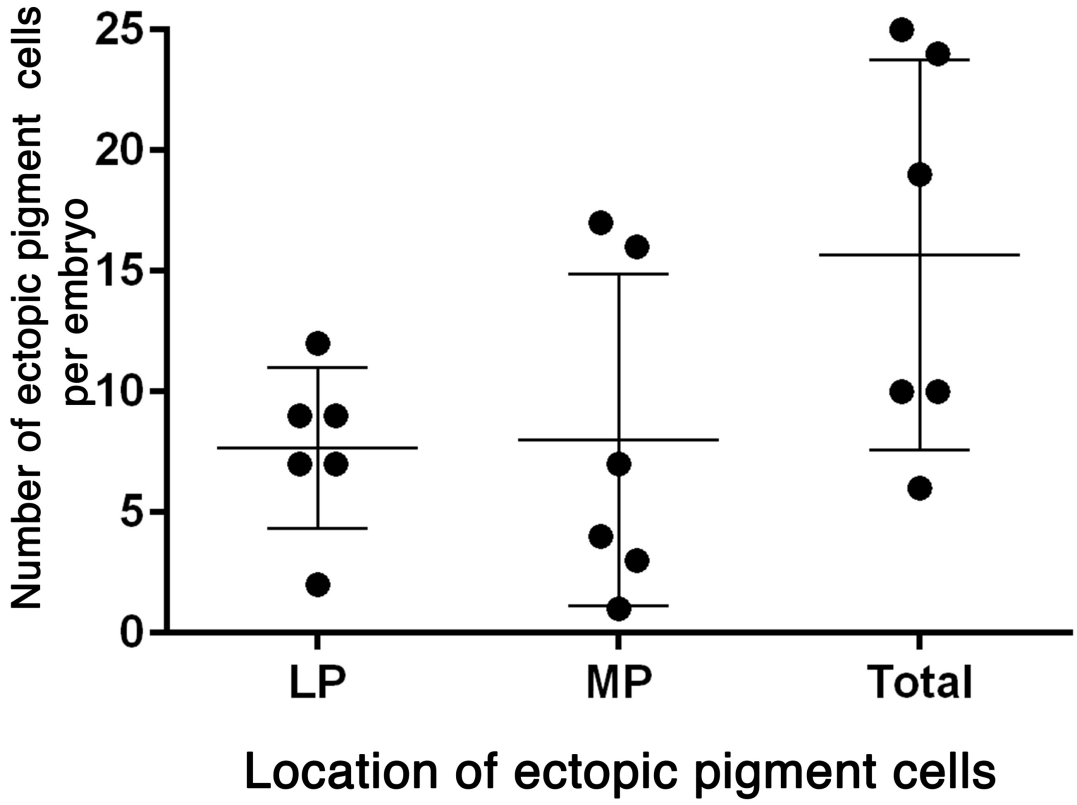

Figure 5.11 Quantitation of ectopic pigment cells in soxE2 overexpression experiment. Dot plot of number of ectopic pigment cells in the lateral (LP m=7.66±1.35) and medial migratory pathway (MP; m=8 ± 2.80) and the total number of ectopic pigment cells (Total; m=15.66±3.29). Each dot corresponds to one embryo.

5.2.3 Pharmacological inhibition of signalling pathways involved in of stem cell regulation.

As we have hypothesised that ectopic pigment cells in *parade* mutant arise from premature activation of APSC, we then tested whether pharmacological inhibition of TGF-β, Wnt and Notch signalling pathways, that have been described to regulate stem cells, phenocopy the *pde* mutant. We expected that treatment with specific chemical inhibitors of such pathways in wild type fish would activate APSCs, resulting in ectopic pigment cell differentiation.

For each inhibitor, we performed at least three independent experiments using batches of embryos from different adult pairs (Fig. 5.12 A; see details on section 2.4). Images of embryos and dot plots correspond to a representative experiment. Briefly, embryos were manually dechorionated and sorted into 12-well plates (6 embryos/well, at least two wells per condition). Control embryos were in all cases sibling embryos treated with embryo medium without methylene blue/DMSO 1% or embryo medium without methylene blue/DMSO 1% + inhibitor. After treatment, embryos were washed three time with fresh embryo medium and the pigment phenotype was examined and imaged at 5 dpf.

To validate the functionality of each inhibitor we performed previously reported experiments and corroborated that we could replicate the reported effect/phenotypes in our hands. We then tested three time windows that overlapped with the different processes of neural crest formation and establishment of APSC. We have previously discussed that establishment of APSC occurs from 9-48 hpf, and more specifically, in the posterior trunk where ectopic cells form in *pde* mutant, establishment of APSC occurs between 18-30 hpf. Thus, we first performed a long treatment from 9-96 hpf (4 dpf) that covers early neural crest formation, pigment cell differentiation and establishment of stem cells and tested at least three different concentrations. Based on the results we selected two concentrations in which embryonic morphology was normal or where changes in morphology allowed a clear interpretation of results. We then tested the selected concentration in two time windows, an early treatment from 18-30 hpf (establishment of APSC) and a late treatment from 24-72 hpf (end of establishment of APSC and after establishment; Fig.5.12 B). For each signalling pathway, the nature and mechanism of action of the inhibitor used, is described in the corresponding section.

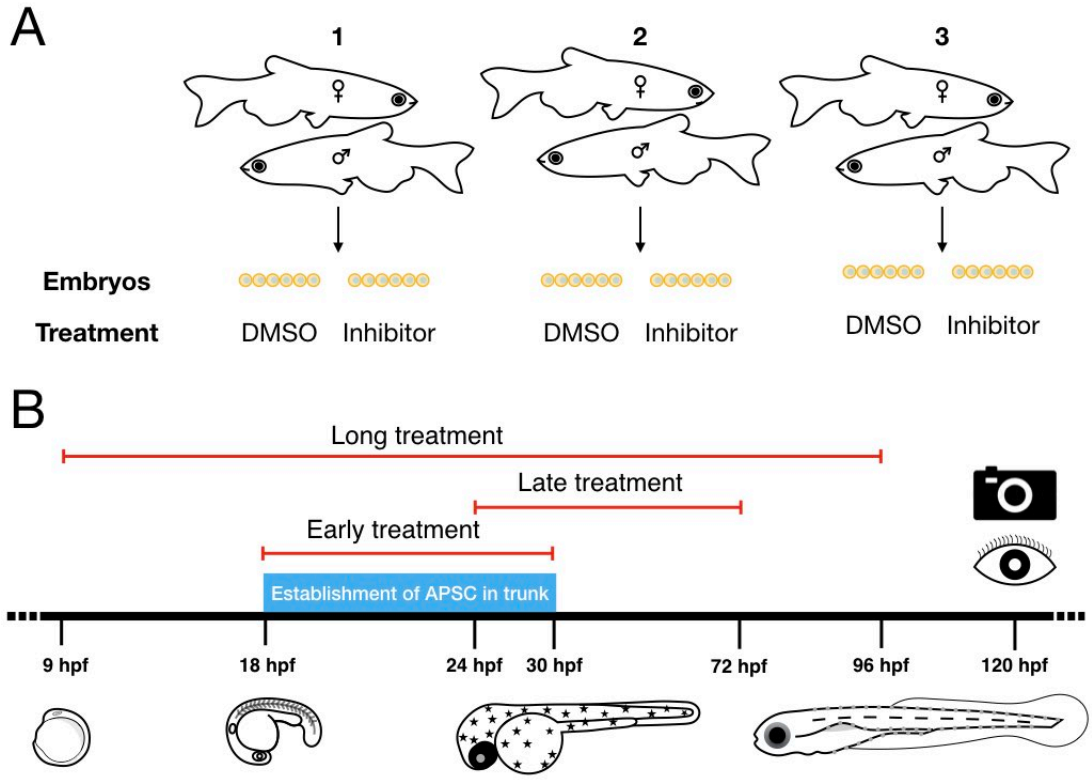

Figure 5.12 Pharmacological treatment of zebrafish embryos. Scheme shows drug treatment experimental design. Embryos from three different crosses (A) were screened into group of six embryos per condition. Three time windows of treatment were tested (red lines; B) 9-96 hpf, 10-30 hpf and 30-72 hpf. Examination (eye cartoon) and imaging (camera cartoon) of embryos was performed at 5 dpf.

5.2.3.1 Single or dual inhibition of transforming growth factor-β and Wnt signalling does not phenocopy the *pde* phenotype.

Transforming growth factors β (TFG-β) are a large superfamily of cytokines that bind simultaneously to two types of receptors: Type I, known as Activin Receptor-Like Kinase (ALK) Receptors 1-7 and the receptors type II: ActRIIB, BMPRII, TGFβRII, and AMHRII. Both, type I and type II receptors are serine/threonine kinases. The known ligands of the TFG-β superfamily are TGF-βs, activins, inhibins, nodals, Growth Differentiation Factors (GDFs), Anti-Mullerian Hormone (AMH), Bone Morphogenic Protein (BMPs) and Glial-derived Neurotrophic Factors (GDNFs; (Massagué 2012). It has been described that the ligands signal via a specific combination of type I and II receptor. TGF-βs signals through TβR-II/ALK5 or ALKI (Piek et al. 1999; Oh et al. 2000); activins signal through ActR-II or ActR-IIB/ALK4; BMPs through ActR-II, ActR-IIB, BMPR-II/ALK2, ALK3, or ALK6 (Piek et al. 1999); AMH signals through a AMHR-II/ALK6 (Gouedard et al. 2000); and nodal through ActR-IIB/ALK7 (Reissmann et al. 2001).

We used a small molecule selective inhibitor (SB-431542) that binds competitively to the ATP binding site of the kinase domain of ALK5 (TFG-β) (Inman et al. 2002), ALK4 (activin) and ALK7 (nodal), blocking the phosphorylation of the downstream effectors Smad2/3. Rigorous tests in zebrafish embryos revealed that Smad2/3 signalling is blocked in embryos exposed to SB-431542 and that embryos treated with 50 μM of SB-431542 (8 cells- 24 hpf) phenocopy the morphological defects seen in *cyclop* (*cyc*) mutants, which are homozugous for a loss of function allele of one of the zebrafish Nodals (Sun et al. 2006).

To validate the functionality of SB-431542 in hour hands, we first treated wild type embryos with 50 μM of SB-431542, which from now on is referred as inhibitor of TGF-β (iTGF-β) from 8 cells-24 hpf. We found that 88% of the embryos ($^{16}/_{18}$) treated with 50 μM of iTGF-β, phenocopied *cyclope* mutants (completely fused eyes: Fig. 5.13 B), while 100% ($^{16}/_{18}$) of the control DMSO treated embryos showed a normal phenotype (Fig. 5.13 B).

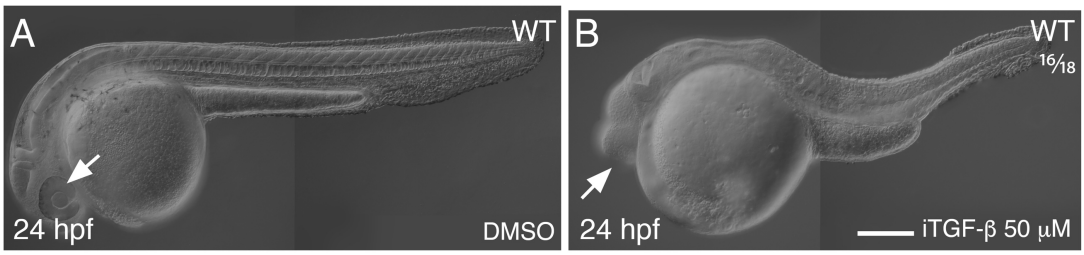

Figure 5.13 Verification of SB-431542 activity as inhibitor of TGF-β signalling. Live DIC imaging of 24 hpf WT embryos treated with DMSO (A) and 50 μM of TGF-β inhibitor (iTGF-β; B) SB-431542 from 8 cells stage - 24 hpf. Eye (white arrow). Scale bar = 50 μm (A and B).

Then we tested three concentrations, 10 μM, 25 μM and 50 μM of iTGF-β from 9 hpf-4 dpf. Examination of embryos at 5 dpf showed a general edema in the heart and yolk sac of the embryos treated with 50 μM of iTGF-β but no pigment cells were found in the ventral medial pathway of any of the embryos treated at any of the tested concentrations. We then decided to test the concentrations 10 μM and 25 μM at the early and later time window treatments, as the embryos treated with 50 μM of iTGF-β were largely deformed. Disappointingly, none of the tested concentration at the time windows 18-30 hpf (Fig. 5.14 A-C) and 24-72hpf (Fig. 5.13 D-F) showed formation of ectopic pigment cells.

Wnt ligands are part of a group of genes known as wingless-type mouse mammary tumour virus (MMTV) integration site (Wnt) gene family. These ligands bind to a wide variety of WNT receptors and co-receptors such as Frizzled (Fz) (van Amerongen 2012); low-density lipoprotein receptor-related protein 6 (LRP6; et al 2004), receptor Tyr kinase-like orphan receptor (ROR) (Minami et al. 2009), protein Tyr kinase 7 (PTK7) (Peradziryi et al. 2012), receptor Tyr kinase (RYK) (Fradkin et al. 2010), muscle skeletal receptor Tyr kinase (MUSK) (Jing et al. 2009) and proteoglycan families (Kikuchi et al. 2011).

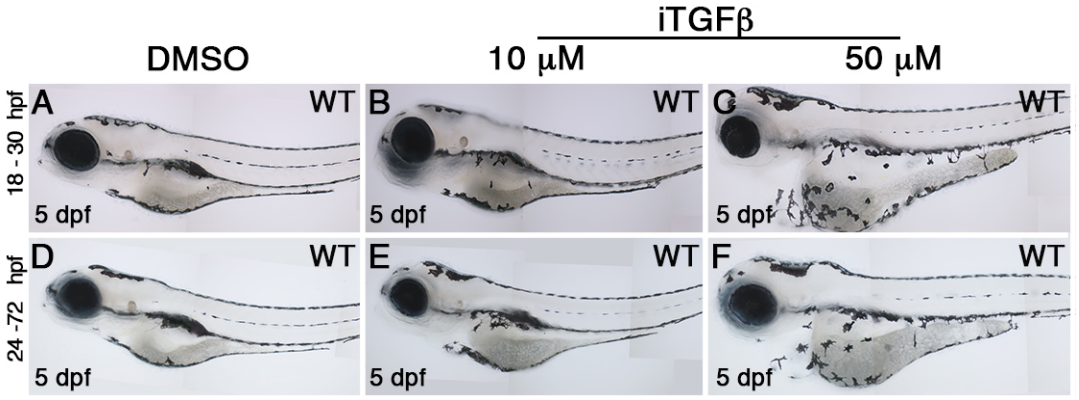

Figure 5.14 Inhibition of TGF-β signalling in WT embryos does not generate ectopic pigment cells in the ventral medial pathway. Bright field imaging of WT embryos fixed at 4 dpf, treated with DMSO (A and D), 10 μM of iTGF-β (B and E) and 50 μM of iTGF-β (C and F) from 9 hpf - 4 dpf (A-C) and 18 hpf - 4 dpf (D-F). Scale bar = 50 μm.

Wnt signalling has been classified into two major pathways, the canonical/β-catenin-dependent and the non-canonical/β-catenin-independent pathways. Amongst the several Wnt ligands that have been identified, some of them preferentially activate one or both pathways. In the Intestine Stem cell niche, Wnt promotes self-renewal via the β-catenin-dependent pathway (Muncan et al. 2006). In the Wnt canonical pathway, in the absence of Wnt ligand, the level of cytoplasmic β-catenin is kept in a low concentration through its phosphorylation and ubiquitination by the 'destruction complex' integrated by the proteins Axin, Adenomatous polyposis coli (Apc), glycogen synthase kinase 3 (Gsk3) and casein kinase 1α (Ck1α), after which β-catenin is degraded by the proteasome (Behrens et al. 1998). Wnt ligands bind to a Fz/LPR5/6 receptor complex, recruiting disheveled (DVL), which is needed for the phosphorylation of the Fz/LPR5/6 receptor complex by Ck1α and Gsk3, resulting in the dissociation of the destruction complex through the recruitment of Axin. Consequently, β-catenin is accumulated in the cytoplasm and then translocated to the nucleus. Nuclear β-catenin dissociates the transducin-like Enhancer (TLE)/Groucho repression complex and forms and active complex with the lymphoid enhancer factor (LEF) and the T-cell factor (TCF), resulting on the initiation of transcription of targeted genes (Behrens et al. 1996)

Association of the destruction complex has been shown to rely on a constant concentration of Axin, which has been identified as the limiting factor of the destruction complex (Spink et al. 2000). Levels of Axin are regulated by the poly-ADP-ribosylating enzymes tankyrase, which role is to promote Axin's degradation through ubiquitination and proteasome degradation (Huang et al. 2009). The small molecule XAV939 selectively inhibits tankyrase, resulting in stabilization of Axin (Callow et al. 2011) and therefore promoting b-catenin degradation and ultimately, WNT signalling inhibition (Behrens et al. 1998).

Wnt signalling has been shown to regulate melanophore differentiation, and specifically, previous work from our lab showed that WNT signalling is required for melanophore development (Vibert et al. 2017). In zebrafish, treatment of embryos of the Wnt reporter line *Tg(TopFlash:GFP)* with XAV939 5 μM, from now on referred as inhibitor of WNT (iWNT), has been shown to reduce GFP signal and cause curvature of the trunk when treated from 4.5 hpf until 24 hpf (Robertson et al. 2014). As part of the work of a Masters student we corroborated the observation: inhibition of WNT signalling with 50 μM iWNT reduces the number of melanophores in the anterior

dorsal head when treated from 15-72 hpf (one-tail unpaired t-test; number of melanophores in anterior dorsal head; DMSO m=22.2 ±1.494, n=11; iWNT 50 μM m=16.1 ± 1.156, n=11; p-value <0.0021; Fig. 5.15; research report Stratfor-Smith, C.). The student tested three concentrations of iWNT, 1 μM, 50 μM and 100 μM. Quantification of the number of melanophores revealed that 1 μM did not have an effect on the number of melanophore while iWNT 100 μM caused strong changes in morphology making the assessment of the pigment phenotype difficult (data not shown). Thus, we decided to perform further experiments using a concentration of 50 μM iWNT.

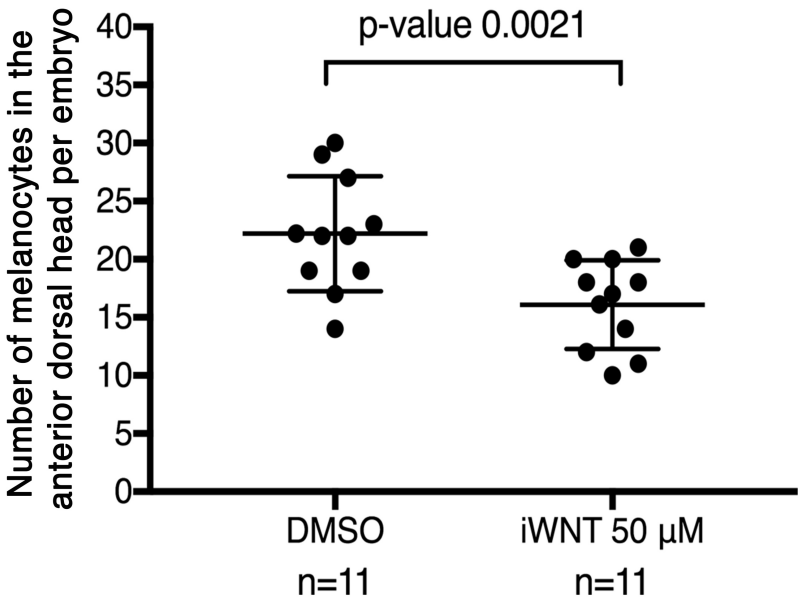

Figure 5.15 Verification of XAV-939 activity as inhibitor of Wnt signalling. Dot plot shows number of melanophores in the dorsal head of embryos treated with DMSO, 10 μM or 50 μM of Wnt inhibitor (iWnt) XAV-939 from 15-72 hpf. Each dot corresponds to one embryo.

Although Wnt signalling is required for melanophore development, we considered that it might also have another role, in differentiation of APSC, at different times or when in combination with TGF-β inhibition. Thus, we first assessed the effect of single inhibition of Wnt signalling. We tested a concentration of 50 μM of iWNT from 18-30 hpf and 24-72 hpf. Examination of embryos at 5 dpf showed no ectopic pigment cells

in the ventral medial pathway of any of the embryos treated neither at the early (Fig. 5.16 A) nor the late (Fig. 5.16 B) time window treatments.

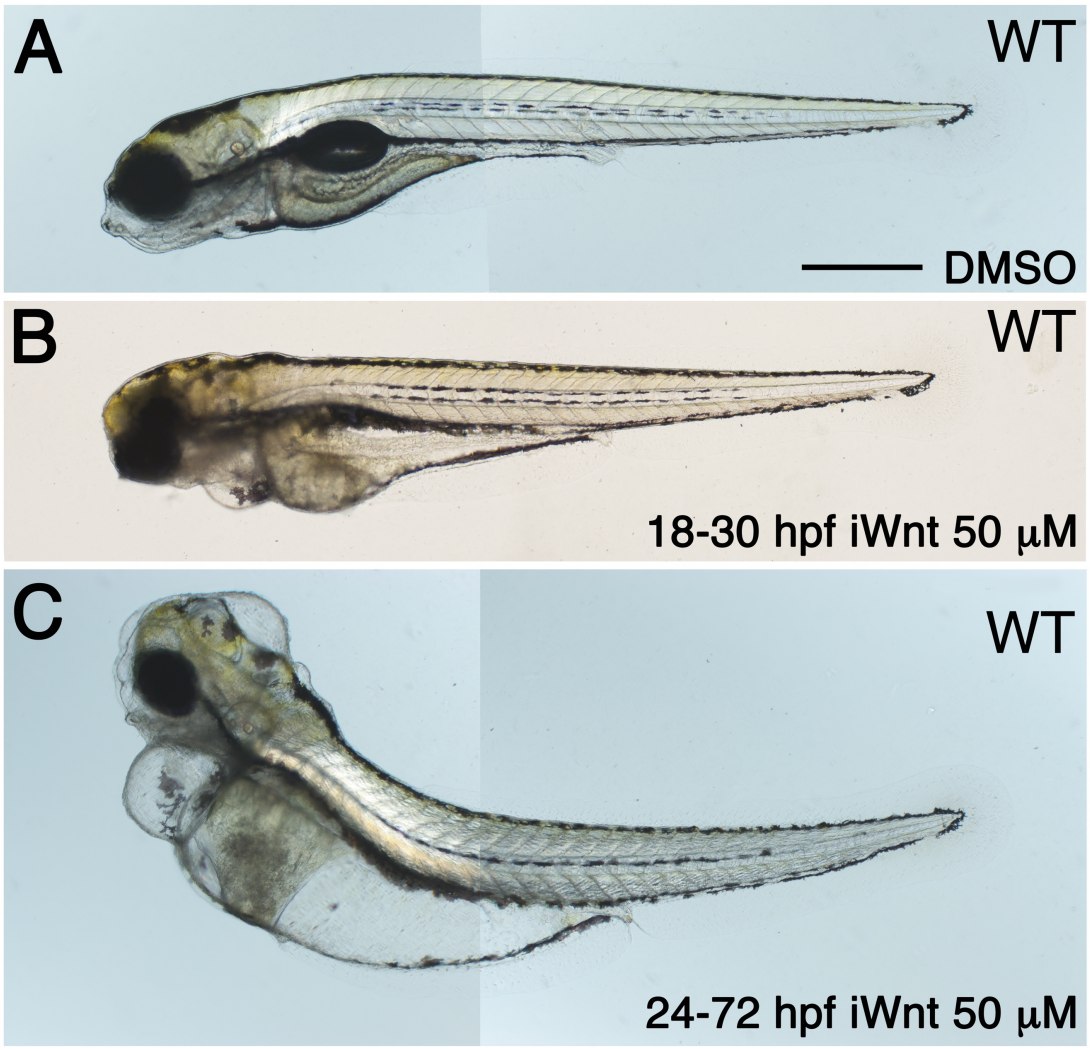

Figure 5.16 Inhibition of Wnt signalling in WT embryos does not generate ectopic pigment cells in the ventral medial pathway. Live bright field imaging of 4 dpf WT embryos treated with DMSO (A) and 50 μM of iWNT from 18-30 hpf (B) and 24-72 hpf (C). Scale bar = 500 μm (A-C).

We then assessed the effect of double inhibition of iTGF-β and iWNT. We treated embryos with a concentration of 25 μM of iTGF-β + 50 μM of iWNT, however similar to the single treatments, neither the double treatment from18-30 hpf (Fig. 5.17 A) nor

from 24-72 hpf (Fig. 5.17 A) induced the formation of ectopic pigment cells in the ventral medial pathway. In all of the tested concentration and time windows the wild type pigment phenotype was largely unaffected. However, we observed changes in morphology. Embryos treated form 18-30 hpf with either iWNT or iTGF-β + iWNT (Fig. 5.16 B and 5.6 B) showed a delayed absorption of the yolk and craniofacial deformities, while embryos treated form 24-72 hpf with either iWNT or iTGF-β + iWNT (Fig. 5.17 B and 5.17 B) showed edema, curved trunk, craniofacial and brain disruption and delayed absorption of the yolk.

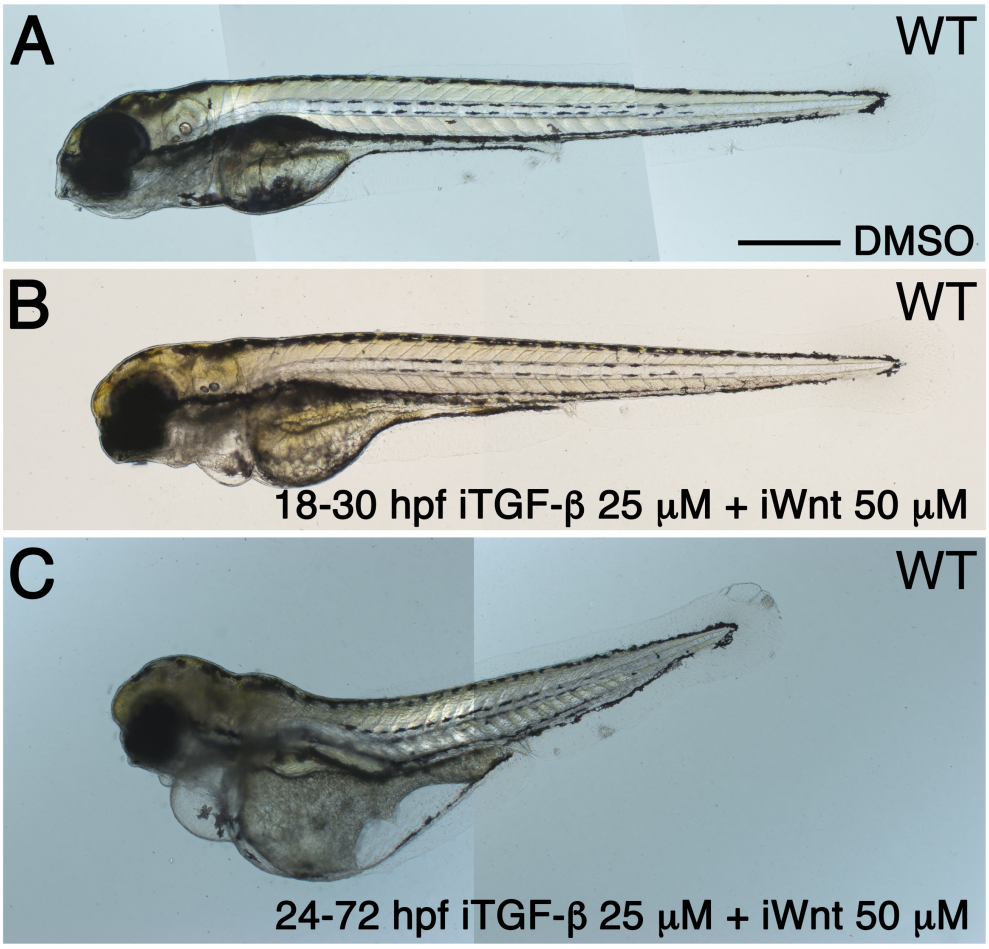

Figure 5.17 Double inhibition of TGF-β and Wnt signalling in WT embryos does not generate ectopic pigment cells in the ventral medial pathway. Live bright field imaging of WT embryos at 4 dpf, treated with DMSO (A), 25 μM of iTGF-β + 50 μM of iWnt from 18-30 hpf (B) and 24-72 hpf (C). Scale bar = 500 μm (A-C).

5.2.3.2 Inhibition of Wnt signalling rescues the *pde* phenotype.

We wanted to test whether in a sensitised background we could enhance the activation of APSC, thus we treated *pde* homozygote mutants with 25 μM of iTGF-β + 50 μM of iWNT from 18-30 hpf, expecting an increase of ectopic pigment cells. However, treated *pde* mutant embryos revealed more severe changes in morphology that in wild type embryos. Thus, we decided to vary the concentration of both inhibitors. Strikingly, we found that embryos treated with 25 μM of iTGF-β + 10 μM of iWNT (Fig. 15.18 B and D) have a reduction of 76.69% of ectopic pigment cells compared to *pde* embryos treated with DMSO (Fig. 15.18 A and C; one-tail Welch's unpaired t-test; number of ectopic pigment cells in the ventral medial pathway per embryo; *pde* + DMSO m=14.55 ± 1.5, n=33; *pde* + 25 μM of iTGF-β + 10 μM of iWNT m=3.391 ± 0.3251, n=23; p-value<0.0001; Fig. 5.18 E). Similar to WT embryos, *pde* embryos treated with iTGF-β + iWNT showed edema, curved trunk, craniofacial and brain disruption, delayed absorption of the yolk but the embryonic pigment pattern was not affected (Fig. 5.18 B).

To identify the contribution of each signalling pathway we performed single treatments of *pde* mutants with 25 μM of iTGF-β or 10 μM of iWNT. Quantification of ectopic pigment cells revealed that the difference between the mean number of ectopic pigment cell in embryos treated with DMSO and embryos treated with 25 μM of iTGF-β is not statistically significant (two-tails unpaired t-test; number of ectopic pigment cells in the ventral medial pathway per embryo; *pde* + DMSO m=15.65 ± 1.613, n=17; *pde* + 25 μM of iTGF-β m=14.44 ± 1.676, n=16; p-value=0.6067; Fig. 5.19). In contrast, iWNT treated embryos showed a reduction of 93.20% compared with DMSO treated siblings (one-tail Welch's unpaired t-test; number of ectopic pigment cells in the ventral medial pathway per embryo; *pde* + DMSO m=15.65 ± 1.613, n=17; *pde* + 10 μM of iWnt m=1.063 ± 0.3223, n=16; p-value<0.0001; Fig. 5.19). Comparison between the number of ectopic pigment cells in embryos treated with 10 μM of iWNT and the sibling embryos treated with 25 μM of iTGF-β + 10 μM of iWNT revealed that there is not significant difference (two-tails unpaired t-test; number of ectopic pigment cells in the ventral medial pathway per embryo; *pde* + iWNT m=1.063 ± 0.3223, n=16; *pde* +25 μM of iTGF-β + 10 μM of iWnt m=1.652 ± 0.3363, n=23; p-value<0.0001; Fig. 5.19).

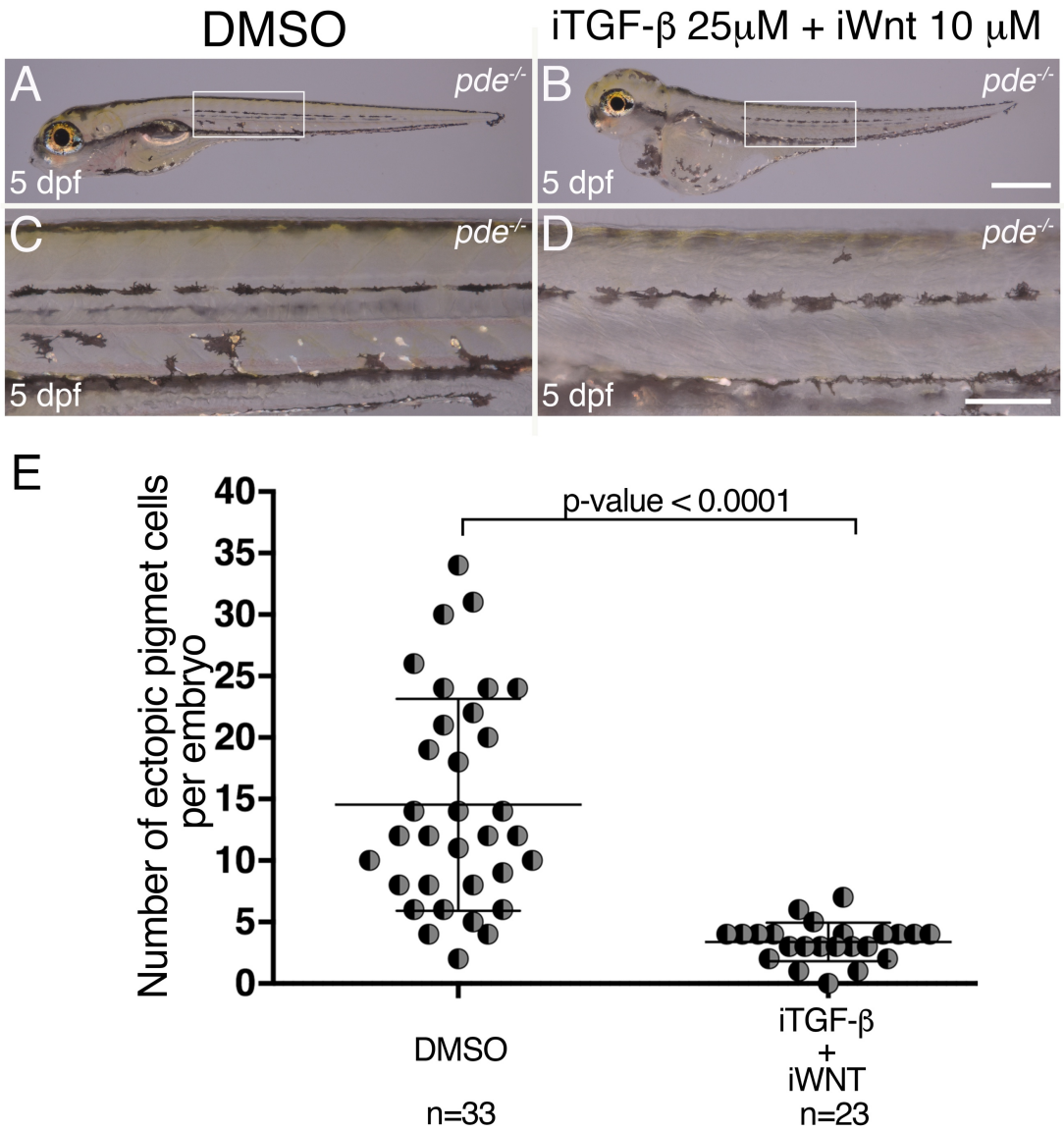

Figure 5.18 Double inhibition of TGF-β and Wnt signalling reduces the number of ectopic pigment cells in the ventral medial pathway of *pde* mutants. Live imaging of 5 dpf *pde* larvae treated with DMSO (A and C) and 25 μM of iTGF-β + 50 μM of iWnt (B and D) from18-30 hpf. Close up of posterior trunk (C and D). Scale bar = 500 μm (A and C) and 100 μm (B and D). Dot plot shows number of ectopic pigment cells in the ventral medial pathway in embryos treated with DMSO, 25 μM of iTGF-β, 50 μM of iWnt and 25 μM of iTGF-β + 50 μM of iWnt. Each dot corresponds to one fish.

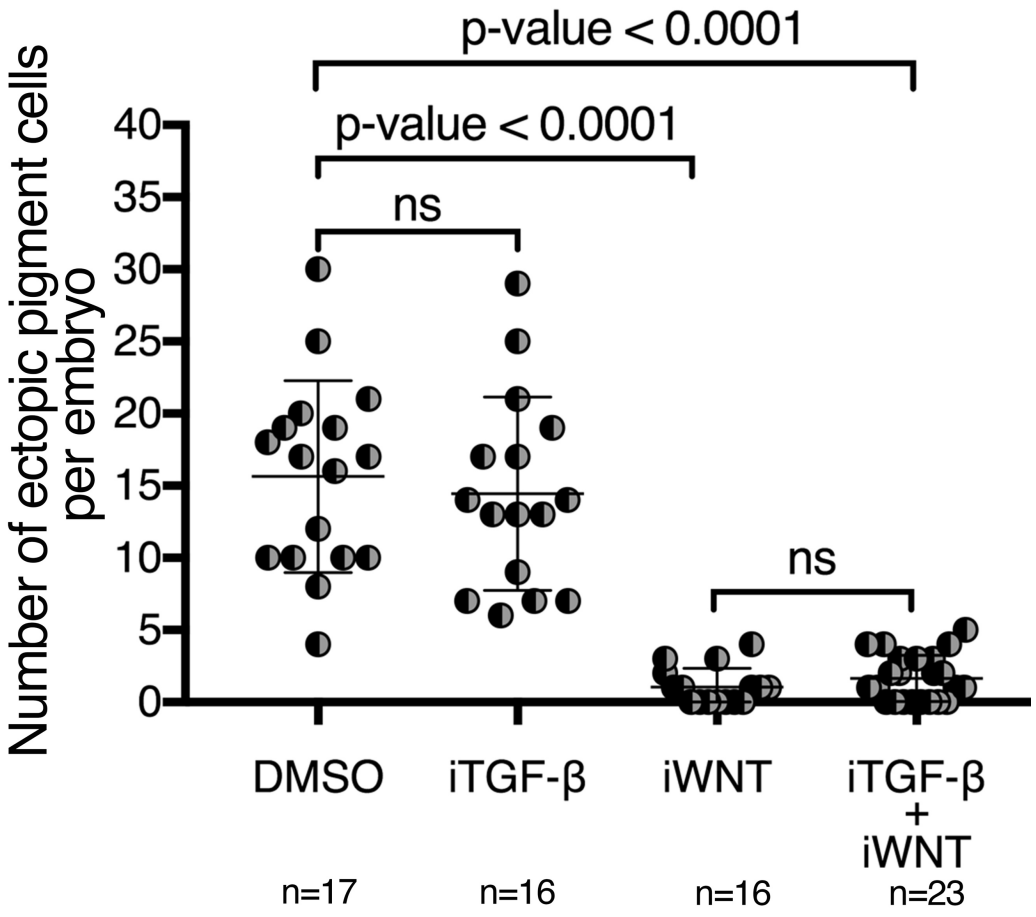

Figure 5.19 Inhibition of Wnt signalling is sufficient to reduces the number of ectopic pigment cells in the ventral medial pathway of *pde* mutants. Dot plot shows number of ectopic pigment cells (melanophores + iridophores) in *pde* embryos treated with DMSO, 25μM of iTGF-β, 10 μM of iWnt or 25μM of iTGF-β + 10 μM of iWnt. Each dot corresponds to one fish. Not significant (ns).

Comparison of number of melanophores and iridophores showed that numbers of both pigment cells type are unchanged in iTGF-β treated embryos when compared to DMSO treated ones (Two-tails unpaired t-test; number of ectopic melanophores in the ventral medial pathway per embryo; *pde* + DMSO m=2.059 ± 1.688, n=17; *pde* + 25 μM of iTGF-β m=1.688 ± 0.3843, n=16; p-value=0.5180; Fig. 5.20 A; Two-tails unpaired t-test; number of ectopic iridophores in the ventral medial pathway per embryo; *pde* + DMSO m=13.59 ± 1.331, n=17; *pde* + 25 μM of iTGF-β m=12.75 ± 1.499, n=16; p-value=0.6779; Fig. 5.20 B).

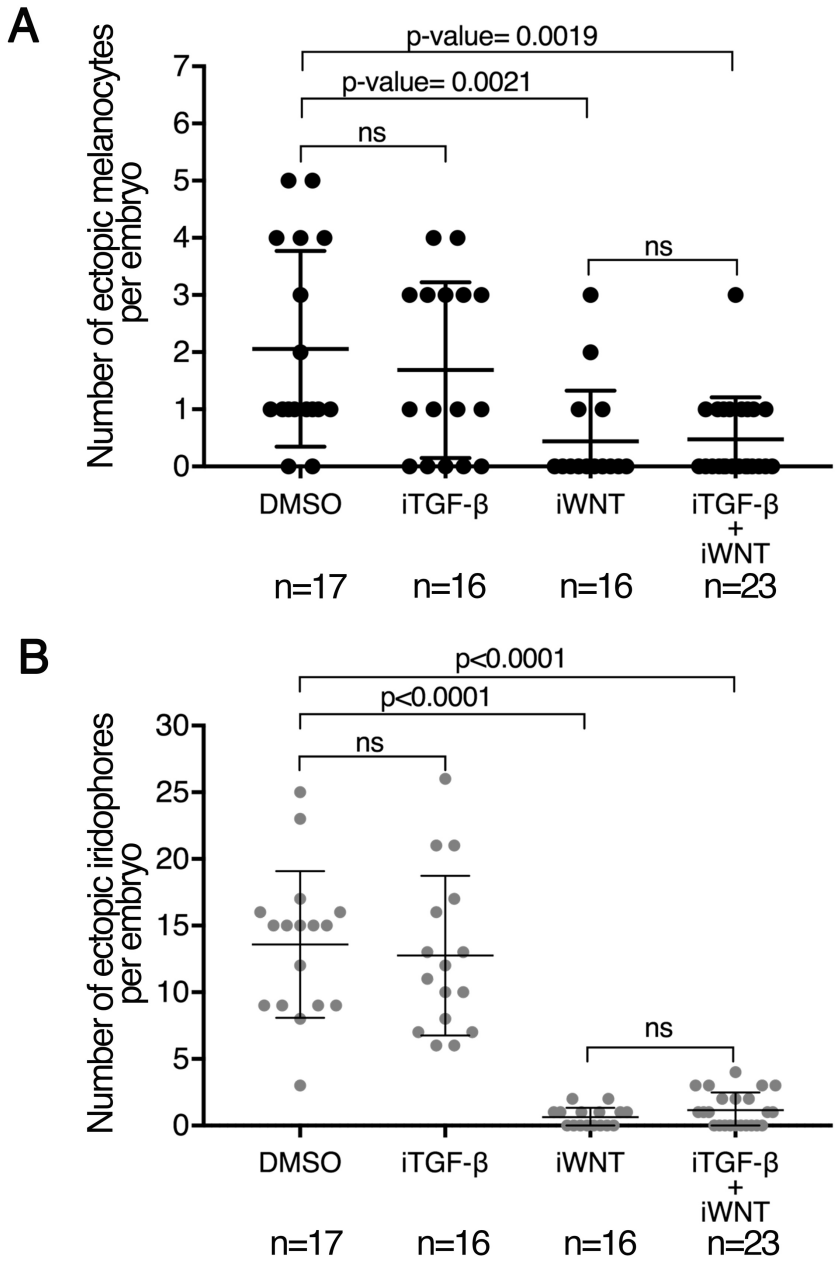

Figure 5.20 Inhibition of Wnt signalling decreases the number of ectopic melanophores and iridophores in the ventral medial pathway of *pde* mutants. Dot plot shows number of ectopic melanophores (A) and iridophores (B) in *pde* embryos treated with DMSO, 25μM of iTGF-β, 10 μM of iWnt or 25μM of iTGF-β + 10 μM of iWnt. Each dot corresponds to one fish. Not significant (ns).

In contrast, treatment with 10μM of iWnt reduces number of melanophores by 78.75% (Two-tails Welch's unpaired t-test; number of ectopic melanophores in the ventral medial pathway per embryo; *pde* + DMSO m=2.059 ± 1.688, n=17; *pde* + 10 μM of iWnt m=0.4375 ± 0.223, n=16; p-value=0.0021; Fig. 5.20 A) while, iridophores are

almost completely depleted, reduction >99.0% (Two-tails Welch's unpaired t-test; number of ectopic iridophores in the ventral medial pathway per embryo; *pde* + DMSO m=13.59 ± 1.331, n=17; *pde* + 10 μM of iWnt m=0.625 ± 0.1797, n=16; p-value<0.0001; Fig. 5.20 B). Double treatment with 25 μM of iTGF-β + 10 μM of iWNT did not shows an effect different to single treatment with iWnt only. (Two-tails unpaired t-test; number of ectopic melanophores in the ventral medial pathway per embryo; *pde* + 10 μM iWnt m=0.4375 ± 0.223, n=17; *pde* + 25 μM of iTGF-β + 10 μM iWnt m=0.4783 ± 0.1523, n=23; p-value=0.4382; Fig. 5.20 A; Two-tails unpaired t-test; number of ectopic iridophores in the ventral medial pathway per embryo; *pde* + 10 μM iWnt m=0.625 ± 0.1797, n=16; *pde* + 25 μM of iTGF-β + 10 μM iWnt, m=1.174 ± 0.2715, n=23; p-value=0.1350; Fig. 5.20 B).

These results show that, while inhibition of TGF-β signalling alone does not affect the formation of ectopic pigment cells in the ventral medial pathway, inhibition of Wnt signalling is sufficient to prevent the formation of ectopic melanophores and iridophores, having a more pronounce effect on iridophores. This was an interesting result, even if it was not the indication that Wnt signalling played a role in maintenance of APSC quiescence.

Note that we did not assessed the effect of these inhibitors on blood vessel. We predict that if the blood vessels are not effect, the rescue of the *pde* phenotype will be due to the effect on Wnt signalling pathway. However, if the blood vessels are affected it would suggest that rescue of the *pde* phenotype is due to the lack of other signals normally provided by the blood vessels.

5.2.3.3 Investigating the role of Notch signalling in the mechanism of the *parade* mutants.

Notch signalling is a system based on ligand-receptor interaction. In humans, there are four paralogues of Notch receptors (1-4) and five ligands, three of them known as Delta-like (DLL1, DLL3 and DLL4) and two of them as Jagged (JAG1 and JAG2). Ligand interaction can be in *cis* (within the same cell) or *trans* (between adjacent cells). Ligand binding in *trans* leads to a series of cleavages of the notch receptor that ends in the release of the Notch intracellular domain (NICD). The NICD is translocated to the nucleus where it regulates gene expression by interacting with other transcriptional complexes such as CBF1/RBPjk/Su(H)/Lag1 (CSL). Cleavage of

the Notch receptor is performed by two proteases. First, the extracellular domain is cleaved by ADAM10 (Bozkulak & Weinmaster 2009) followed by the cleavage within the transmembrane domain by γ-secretase complex, this one being responsible of the release of the NICD. The γ-secretase complex is located at the cell membrane and is comprised of four proteins; Presenilin (PS1/2), Nicastrin (Nct), Anterior pharynx-defective phenotype (Aph-1) also known as Presenilin enhancer (Pen-1) and Pen-2, where Presenilin is responsible for the NICD cleavage (Grotek et al. 2013; De Strooper 2003). Inhibition of notch signalling has been largely accomplished using a compound called N-[N-(3,5-difluorophenacetyl)-l-alanyl]-*S*-phenylglycine *t*-butyl ester (DAPT) that targets Presenilin, therefore preventing cleavage of the NICD and ultimately inhibiting Notch signalling. Despite that γ-secretase complex mediates cleavage of other proteins such as the Amyloid Precursor Protein (APP) (Wolfe & Haass 2001), use of DAPT is widely recognised as a means of inhibiting Notch signalling. Furthermore, previous work has shown that treatment of zebrafish wild type embryos with 100 μM of DAPT from 1-cell stage to 24 hpf, resembles the phenotypes of Notch pathway mutants (Geling et al. 2002). Work in our lab showed that treatment of wild type embryos with 100 μM of DAPT from 30-72 hpf results on decrease number of sensory neurons in the DRGs (Delfino-Machín et al. 2017).

We wanted to test whether inhibition of Notch signalling induced the formation of ectopic pigment cells. In this section, we will describe the results of the experiments performed using DAPT and another inhibitor of the γ-secretase complex known as LY411575 provided by Dr Laure Bally-Cuif; (Fauq et al. 2007). Note that, whereas for all of the previously reported experiments on Wnt and TGFb inhibition results were consistent across all repeats (at least three times with embryos from different crosses each time), for the inhibition of notch signalling, the results were not consistent across all repeats. Thus, we consider the findings presented here preliminary and in need for further investigation and verification.

We first treated wild type embryos with 100 μM of DAPT from 18-30 hpf, using embryos from two crosses, with the experiment being performed in parallel by myself (Cross 1) and a Masters student (Cross 2; Justin Montovio). Solutions were prepared independently and result were discussed only after the statistical analysis was performed. Embryos were treated from 18-30 hpf, then washed three times with fresh embryo medium and incubated until 5 dpf for phenotypical assessment. In both crosses, control embryos treated with DMSO (Fig. 5.21 A and C) did not show ectopic

pigment cells except for one embryo in cross 1 that displayed one ectopic cell and in Cross 2, two embryos displayed a single ectopic cell. In contrast, all of the embryos treated with 100 μM of DAPT displayed several ectopic cells, with between 4 and 20 cells recorded in Cross 1, and between 4 and 18 cells in Cross 2.

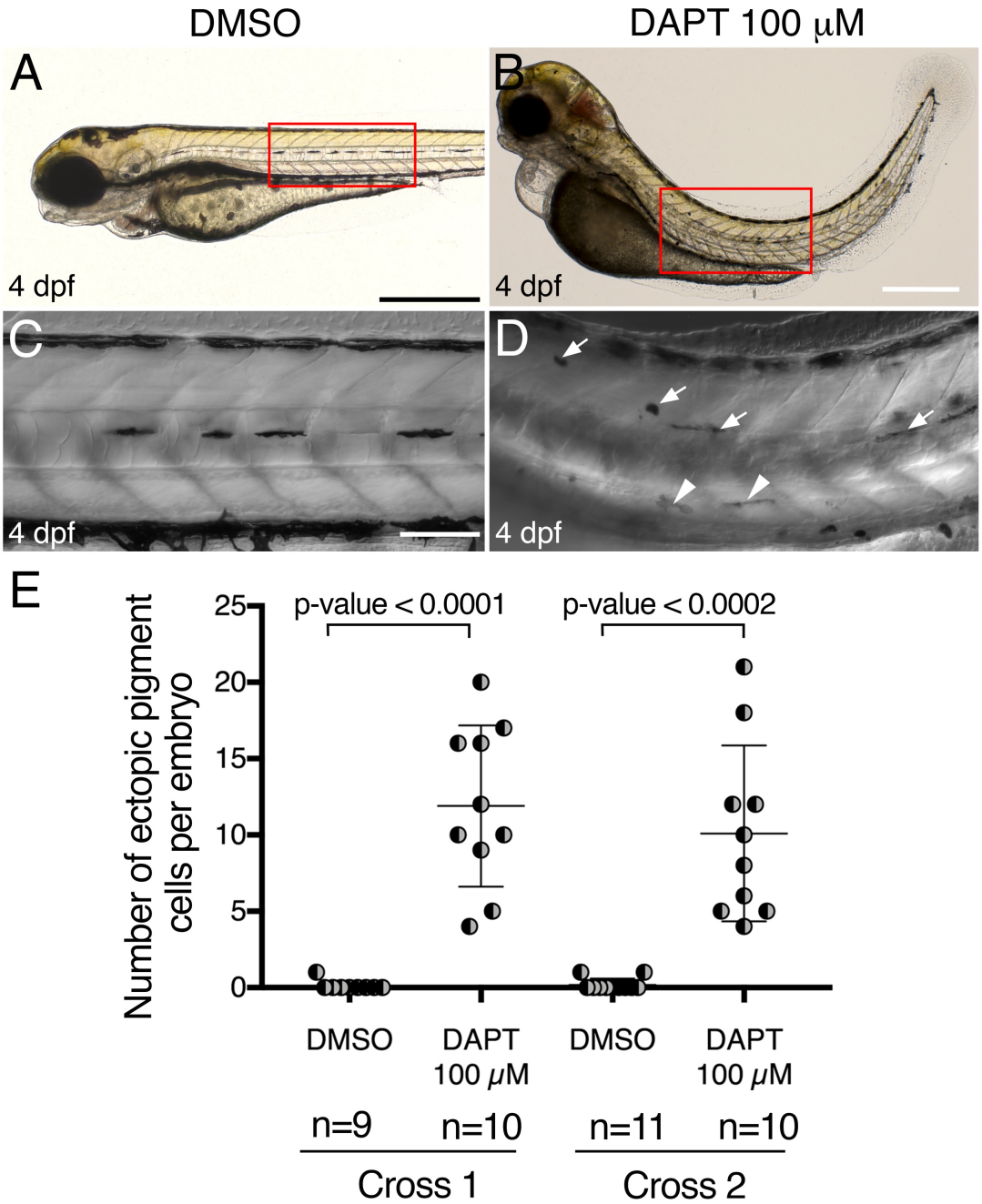

Figure 5.21 Inhibition of Notch signalling with DAPT in WT embryos generates ectopic pigment cells in the dorsal and ventral medial pathway and curved trunks. Live imaging of 4 dpf WT larvae treated with DMSO (A and C) and 100 μM of Notch

inhibitor DAPT (B and D) from18-30 hpf. Close up of posterior trunk shows no ectopic cells in DMSO treated embryos (C) and ectopic pigment cells in the dorsal (white arrows) and ventral (white arrowheads; D) medial pathway. Scale bar = 500 μm (A), 200 μm (B), 100 μm (C and D). Dot plot shows number of ectopic pigment cells in the medial pathway of WT embryos treated with DMSO and DAPT 100 μM. Each dot corresponds to one embryo.

Comparison of the mean number of ectopic pigment cells per embryo between DMSO and DAPT treated embryos revealed a significant difference. Cross 1: one-tail Welch's unpaired t-test; number of ectopic pigment cells in the ventral medial pathway per embryo; WT + DMSO m=0.111 ± 0.1111, n=9; WT + 100 μM of DAPT m=11.9 ± 1.67, n=10; p-value<0.0001(Fig. 5.21 E). Cross 2: one-tail Welch's unpaired t-test; number of ectopic pigment cells in the ventral medial pathway per embryo; WT + DMSO m=0.1818 ± 0.122, n=11; WT + 100 μM of DAPT m=10.1 ± 1.822, n=10; p-value<0.0002 (Fig. 5.21 E). Note that ectopic pigment cells were found both in the dorsal and the ventral medial pathway (Fig. 5.21 D).

Due to the curved trunks in all of the DAPT treated embryos we decided to reduce the concentration to 10 μM of DAPT. The experiment was performed in the same way as previously described, but in a different week. We used embryos from pairs different to the previous experiment, and again, two experiments were performed in parallel by myself (Cross 3) and a Masters student (Cross 4). In this experiment, treatment of embryos with 10 μM of DAPT did not cause curvature of the trunk. In the embryos treated with DMSO (Fig. 5.22 A and C), 6 embryos displayed a single ectopic pigment cell and 2 embryos displayed two ectopic pigment cells in cross 3, whereas in cross 4 none of the embryos displayed a single ectopic pigment cell (Fig. 5.22 E). 70% of the embryos treated with 10 μM of DAPT (Fig. 5.22 B and D) in cross 3, displayed between two and seven ectopic pigment cells and 30% of the embryos did not show ectopic pigment cells at all. In cross 4, only 40% of embryos displayed between one and four ectopic pigment cells (Fig. 5.22 E).

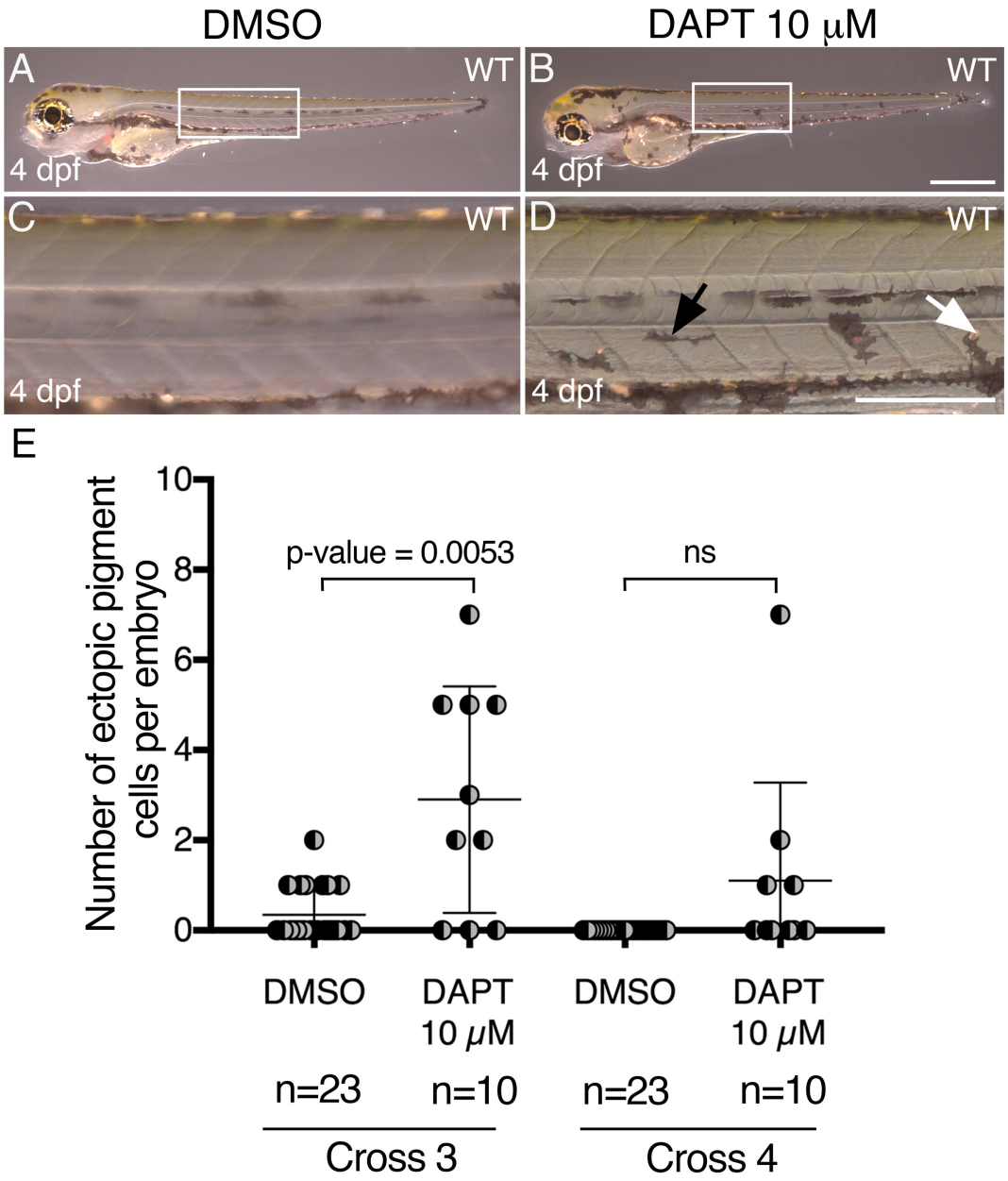

Figure 5.22 Treatment of WT embryos with a lower dose of Notch inhibitor generates ectopic pigment cells in the ventral medial pathway. Live imaging of 4 dpf WT larvae treated with DMSO (A and C) and 10 μM of Notch inhibitor DAPT (B and D) from18-30 hpf. Close up of posterior trunk shows no ectopic cells in DMSO treated embryos (C) and ectopic pigment melanophores (black arrows) and iridophores (white arrows; D) in the ventral medial pathway in treated embryo. Dot plot shows number of ectopic pigment cells in the medial pathway of WT embryos treated with DMSO and DAPT 10 μM. Each dot corresponds to one embryo. Scale bar = 500 μm (A and B) and 200 μm (C-D).

Comparison of the mean number of ectopic pigment cells per embryo between DMSO and DAPT treated embryos in cross 3 revealed a significant difference: one-tail Welch's unpaired t-test; number of ectopic pigment cells in the ventral medial pathway per embryo; WT + DMSO m=0.3478 ± 0.1194, n=23; WT + 10 μM of DAPT m=2.9 ± 0.7951, n=10; p-value<0.0053 (Fig. 5.22E). In contrast, the difference in the mean number of ectopic pigment cells per embryo between DMSO and DAPT treated embryos in cross 4 was not significant. Cross 4: one-tail Welch's unpaired t-test; number of ectopic pigment cells in the ventral medial pathway per embryo; WT + DMSO m=0.0 ± 0.0, n=22; WT + 10 μM of DAPT m=1.1 ± 0.6904, n=10; p-value=0.0728 (Fig. 5.22E). Also, all pigment cells were found exclusively in the ventral medial pathway. Unexpectedly, further repetition of treatments with 100 μM and 10 μM of DAPT did not show a significant difference between the number of ectopic pigment cells in the ventral medial pathway. Although the DAPT stock solution was stored in single use aliquots, we considered the possibility of the drug having lost its activity.

We decided to test another Notch signalling inhibitor, LY411575 (LY), that also targets the γ-secretase complex. An aliquot of LY was kindly provided by Dr Laure Bally-Cuif (Fauq et al. 2007) for us to test. We treated wild type (WT), heterozygote *pde*$^{+/-}$ mutants (Het) and *pde*$^{-/-}$ homozygote mutants (*pde*) with DMSO or with 10 μM of LY. We reasoned that given that disruption of both *ednraa* alleles in *pde* mutants causes the formation of ectopic pigment cells, in heterozygote *pde*$^{+/-}$ embryos, that have only one functional allele of *ednraa*, embryos would be prone to the formation of ectopic pigment cells when Notch signalling is inhibited. Following the same reasoning, we expected that inhibition of Notch signalling in *pde* homozygote mutants would increase the number of ectopic pigment cells. Again, the experiment was performed in parallel by myself and by a Masters student (Justin Montovio) using embryos from different crosses each and results were discussed only after statistical analysis was performed.

Embryos were treated from 18-30 hpf and the phenotype assessed at 5 dpf. WT embryos (Fig. 5.23 A, D and M) and Het (Fig. 5.23 B, E and M) treated with DMSO did not display a single ectopic pigment cell whereas wild type embryos treated with 10 μM of LY, showed between one and six ectopic pigment cells (Fig. 5.23 G, J and M) and Het embryos treated with 10 μM of LY showed between one and four ectopic pigment cells (Fig. 5.23 H, K and M). In both cases, comparison of the number of

ectopic pigment cell between DMSO and LY treated embryos revealed a significant difference. (one-tailed Welch's unpaired t-test; number of ectopic pigment cells in the ventral medial pathway per embryo; WT + DMSO m=0.0 ± 0.0, n=12; WT + 10 μM of LY m=2.133 ± 0.3501, n=15; p-value<0.0001. Het + DMSO m=0.0 ± 0.0, n=12; Het + 10 μM of LY m=2.059 ± 0.3028 n=17; p-value<0.000.1 Fig. 5.23 M). Strikingly, and in contrast to our predictions, *pde* mutants treated with LY (Fig. 5.23 I and L) showed a 87.4% decrease of the number of ectopic pigment cells compared to *pde* mutant treated with DMSO (Fig. 5.23 C and F). Comparison of the number of ectopic pigment cell between DMSO and LY treated embryos revealed a significant difference. (*pde* + DMSO m=19.55 ± 2.918, n=11; *pde* + 10 μM of LY m=2.462 ± 0.5841, n=13; p-value<0.0001; Fig. 5.23 N). This was consistent also with the results obtained by the Masters student, but we only present the data of one experiment. As we had a limited amount of drug, we have not been able to perform this experiment for a third time yet.

In summary, when wild-type embryos were treated with 100 μM (two crosses) or 10 μM (one cross) of DAPT, we found a significant difference in the mean number of ectopic pigments cells per embryos compare to DMSO treated embryos, however, repetition of the experiment in three following occasions did not reproduce the initial results. When embryos were treated with 100 μM DAPT, we found ectopic pigment cells in both the dorsal and the ventral medial pathway, and only in the ventral medial pathway when treated with 10 μM DAPT. When we tested a second Notch inhibitor (LY), we found formation of ectopic pigment cells exclusively in the ventral medial pathway. Strikingly, inhibition of notch signalling in *pde*$^{-/-}$ homozygote mutants, opposite to what we expected, caused a reduction of the number of ectopic pigment cells, suggesting a multiple role of Notch signalling on the formation of ectopic pigment cells in the ventral medial pathway. We will develop in more detail the possible reasons on the variation of the results across experiments in the discussion.

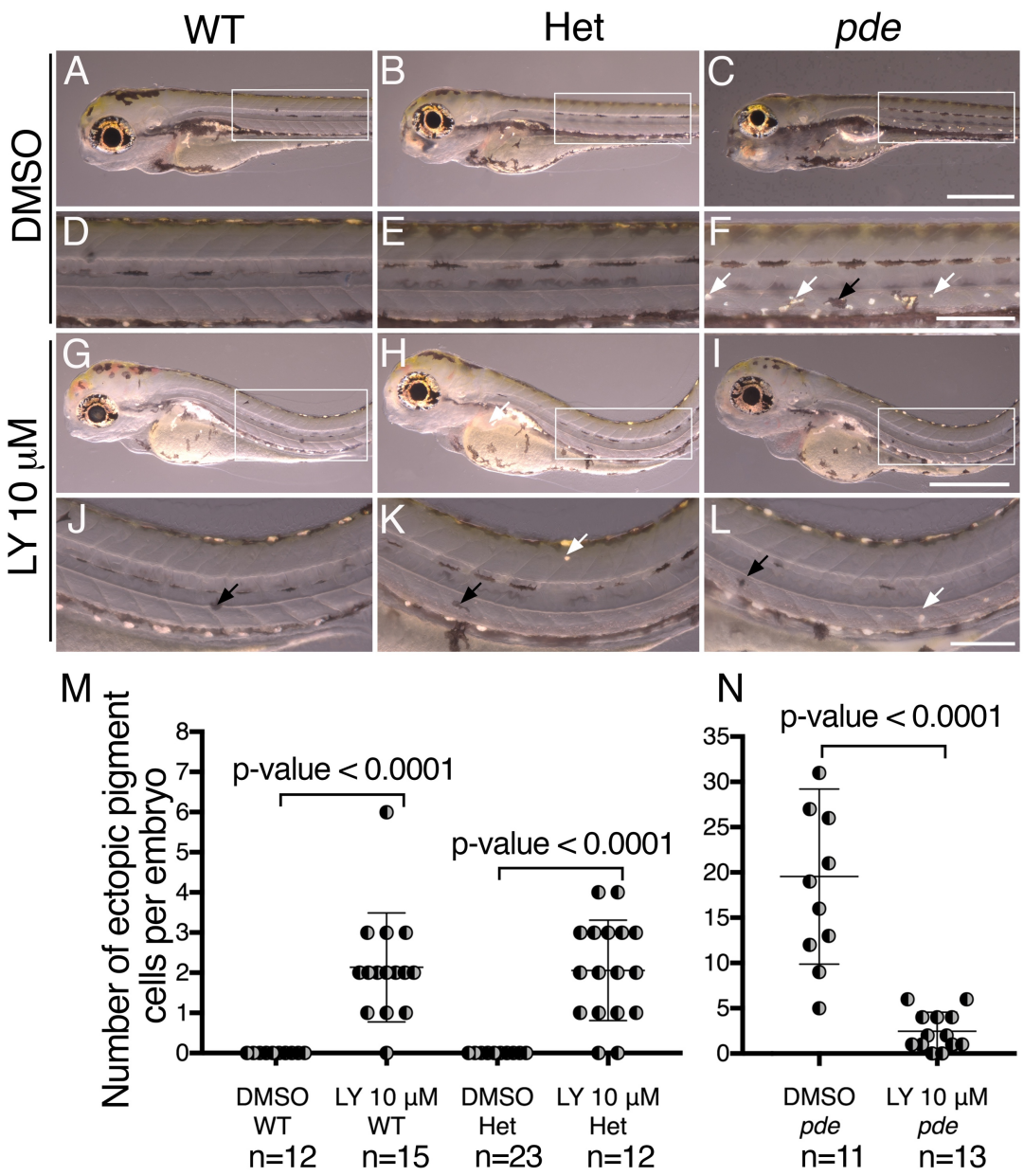

Figure 5.23 Inhibition of Notch signalling with LY decreases the number of ectopic pigment cells in the medial pathway of *pde* embryos, but results in ectopic pigment cells in heterozygotes. Live imaging of WT (A, D, G and J), *pde*$^{+/-}$ (Het; B, E, H and K) and *pde*$^{-/-}$ (C, F, I and L) larvae treated with DMSO (A-F) and 10 μM of notch inhibitor LY. (G-L). Close up of posterior trunk (D-F and J-K) shows ectopic melanophores (black arrows; F, J, K and L) and iridophores (white arrows; F, K and L). Scale bar = 500 μm (A-C and G-I) and 200 μm (D-F and J-L). Dot plot shows number of ectopic pigment cells in the medial pathway of WT and Het embryos (M), and *pde*$^{-/-}$ embryos (N) treated with DMSO and 10 μM of Notch inhibitor LY from15-30 hpf. Each dot corresponds to one embryo.

Note that in order to corroborate that the ectopic cells observed in the embryos treated with either of the Notch Inhibitors are not result of miss placed embryonic pigment cells that did not migrated properly, quantification of the embryonic pigment cell on each stripe is necessary. We predict the number of embryonic pigment cells on each stripe is not different between DMSO treated embryos and embryo treated with the Notch inhibitor.

5.3 Discussion

Based on our previous results, we have hypothesised that disruption of EdnrAa signalling in *pde* mutant allows precocious activation of APSC (proliferation and differentiation), resulting in the formation of ectopic pigment cell in the ventral medial pathway. Thus, we proposed that there is a niche of APSC in the ventral medial pathway and that these APSC are keep quiescent by EdnrAa-dependent signals within the dorsal aorta.

In this chapter, 1) we investigated the ontogeny of ectopic chromatophores in *pde* mutants; 2) we looked for evidence for the existence of pigment progenitor in the ventral medial pathway that could potentially be APSC; and 3) we tested whether signalling pathways that have been previously identified to regulate stem cells in other systems might also be involved in the mechanism of the *parade* phenotype.

5.3.1 The embryonic origin of ectopic pigment cells in *pde* mutants.

To further test our hypothesis that ectopic pigment cells in *pde* mutants do not derive from embryonic pigment cells, we took advantage of the differential molecular requirement between the formation of embryonic melanophores and APSC, where formation of embryonic melanophores requires of *mitfa* expression (Fig. 5.24 A) while APSC formation does not (Fig. 5.24 B). We reasoned that if ectopic melanophores in *pde* mutants derive from embryonic melanophores, ablation of embryonic melanophores by morpholino-knock down of *mitfa* would ablate the ectopic melanophores, but if the ectopic melanophores derive from APSC (Fig. 5.24 C), morpholino-knock down of *mitfa* (Fig. 5.24 D) would not affect them. Our results showed that 60% of the embryos where embryonic melanophores were completely ablated formed ectopic melanophores at 5 dpf. Previous work has shown that regeneration of embryonic melanophores occurs as early as 72 hpf and that the larval melanophore pattern is recovered by 5 dpf. However, in our hands injection of 5 ng of *mitfa*-MO did not generate embryos with an absolute absence of embryonic melanophores; the closest to a complete ablation of embryonic melanophores was embryos with between 1 and 10 melanophores in the DS. Because we wanted to differentiate embryonic melanophores from melanophores derived from APSC, we required complete absence of embryonic melanophores. Thus, only when using 10 ng of *mitfa*-MO could we identify embryos with 0 melanophores. In our experiment, we observed that regeneration of the melanophore larval pattern occurred at 72 hpf

and examination of larvae at 5 dpf revealed that most of the larval melanophore pattern had already regenerated except for small regions in the ventral stripe. Note that although *mitfa* is not required for the establishment of APSC, it is required for the differentiation of regenerating (Fig. 5.24 E). and ectopic melanophores (Fig. 5.24 F). Because we injected a higher amount of morpholino, after the establishment of APSC, residual *mitfa*-MO at 5 dpf could be delaying regeneration of melanophores and differentiation of ectopic melanophores (Fig. 5.24 G). We would expect that if the melanophore larval pattern is completely regenerated then the embryos that at 5 dpf did not present ectopic melanophores would develop them after 5 dpf.

Thus, formation of ectopic pigment cells in *pde* mutants shares two features with APSC formation: requirement for ErbB signalling and independency from *mitfa* early activity. This provides strong independent support for our hypothesis that ectopic pigment cells in *pde* mutants derive from APSC (Fig. 5.24 H).

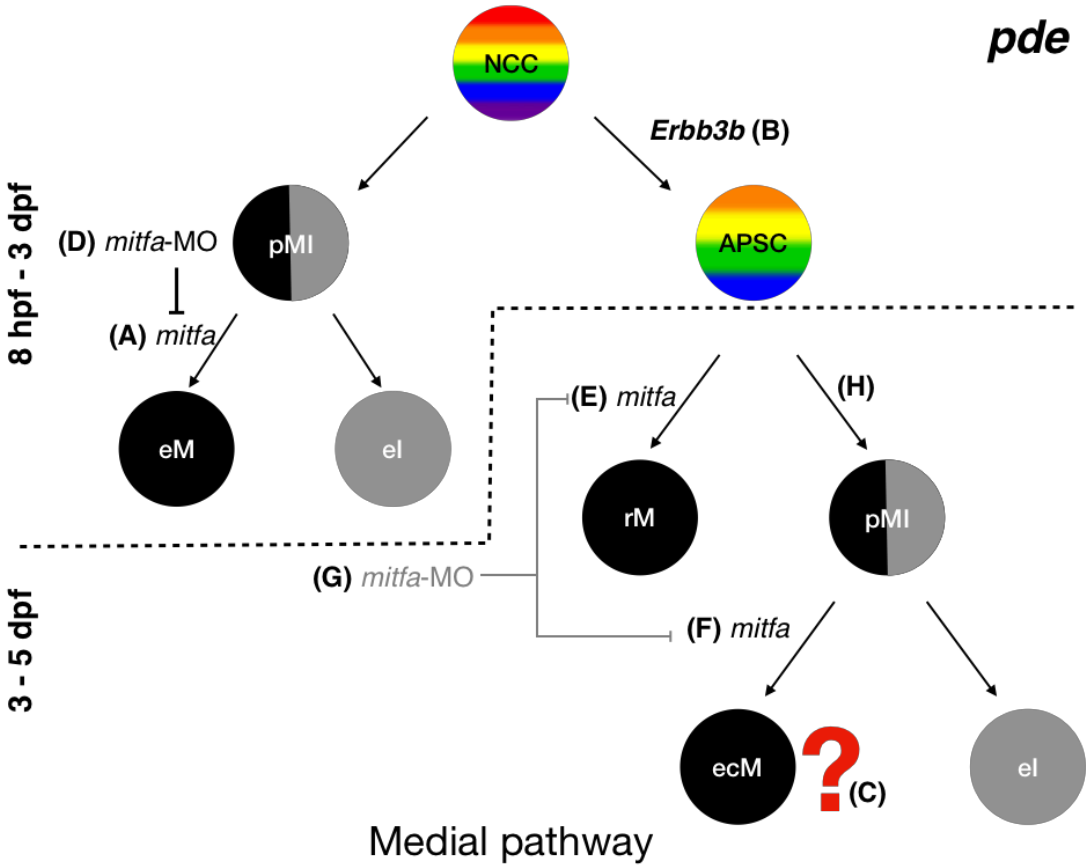

Figure 5.24 Ectopic melanophores in *pde* mutants do not derive from embryonic melanophores. Scheme shows multipotent neural crest cell (NCC), from which embryonic melanophores (eM) differentiate in a *mitfa* dependent manner, from pigment progenitors (pMI) which also embryonic iridophores (eI) differentiate. (A). The NCC also generate adult pigment stem cells (APSC) in a Erbb3b dependant manner (B). Our model proposes that in *pde* mutants, activation of APSC generates pigment progenitors (pMI) from which ectopic melanophores (ecM; C) form. Knock down of *mitfa* by injection of a *mitfa*-MO (D), prevents formation of eM. Residual mitfa-MO (G), delays regenerating melanophores (rM; E) and ecM formation (F).

5.3.2 Evidence of pigment progenitors in the ventral medial pathway.

Our confocal imaging of *moonstone* (*mne)* mutants (Fig. 5.8E), revealed that ectopic iridophores are placed in defined positions along the medial pathway; in particular we observed that dorsal ectopic iridophores are near the position of DRGs, while ventral

ectopic iridophores are located under the dorsal aorta, close to the ventral nerve projections that emerge from the DRGs, just as in *pde* mutants. Additionally, ectopic pigment cells induced by the overexpression of the *Petromyzon marinus sox10* orthologue *SoxE2* in WT embryos, were located near the DRG and under the dorsal aorta. The reproducible position where ectopic pigment cells form in these diverse experiments is very intriguing. We now have available the zebrafish *sox10* gene in the same vector used in this experiment. It is crucial to corroborate that formation of ectopic pigment cells is achieved also by over expression of the zebrafish *sox10* and so not only a characteristic unique to the lamprey *SoxE2*. In the neural rest, *sox10* is required to trigger a series of genetic programs that results in specification and differentiation of neural crest derivatives such as, glia (Britsch et al. 2001), melanophore specification (Greenhill et al. 2011), sensory neuron specification (Ma et al. 1996; Carney et al. 2006) and iridophore development (Petratou et al. 2018). However, the genetic program of APSC maintenance is unknown. It is likely that overexpression of *sox10* triggers the initiation of the specification and differentiation programs for melanophores and iridophores that would normally be silenced on APSC until metamorphosis.

The ectopic position of the induced pigment cells, could be attributed to misplaced embryonic pigment cells. However, as we showed in chapter 3, migration of neural crest-derived cells in the medial pathway of *pde* mutants is normal, furthermore, embryonic melanophores and iridophores successfully reach their position in both the ventral and yolk sac stripes. Because *pde* mutants have supernumerary iridophores in the ventral stripe, it is reasonable to think that the ventral stripe can host a limited number of iridophores and melanophores and that the excess of pigment cells are left in the ventral trunk. However, in the ENU mutagenesis screening of 1996 performed in the Max-Plank Institute for Developmental Biology by the research group of Prof. Christiane Nüsslein-Volhard, in addition to the isolation of the *pde* alleles, a mutant called *moonshine* showing supernumerary iridophores was isolated (Kelsh et al. 1996). In this mutant, the extra iridophores are restricted to the dorsal, post anal, ventral and the yolk sac stripes, interestingly this mutant does not present ectopic iridophores, suggesting that overproduction of pigment cells does not necessarily result in ectopic pigment cells in the ventral medial pathway.

All this evidence supports the idea of pigment progenitors located in two specific positions of the medial pathway, but that in *pde* mutants only a specific set of those pigment progenitors differentiate. This reinforces the idea of the presence of a set of

pigment progenitors in the ventral medial pathway and their specific control by *ednraa*. Consistent with this, disruption of *ednraa* in *mne* mutants showed a striking formation of a continuous chain of iridophores in the ventral medial pathway (Fig. 5.8 F). Although we observed a barely significant increased ectopic iridophores in the dorsal side of the medial pathway, at least 3 times more iridophores were found in the ventral medial pathway, highlighting the spatially restricted role of *ednraa*.

5.3.3 Requirement of Wnt and Notch signalling in the formation of ectopic pigment cells.

Regulation of stem cells requires the orchestration of cycles of quiescence (Fig. 25 A) and activation (Fig. 25 B) in which stem cells self-renew (Fig. 25 C) and generate progenitors that proliferate (Fig. 25 D) and generate differentiated cells, i.e. in the case of APSC, pigment cells at the onset of metamorphosis (Fig. 25 E). This balance is regulated by the niche (environment) in which stem cells reside.

In zebrafish, one niche described for adult pigment stem cells has been suggested within the DRG (Dooley et al. 2013; Singh et al. 2016). However, our data indicate that from a time early in development, pigment progenitors also reside in the ventral region of the medial pathway, below the dorsal aorta (DA). Based on our studies of the properties of these progenitors, they appear to be very similar or identical to those of APSCs characterised in the DRG, leading us to propose that *bona fide* APSCs reside both in the DRGs and in the ventral medial pathway, near the dorsal aorta. Although the molecular mechanism by which pigment cells differentiate has been studied (Parichy & Spiewak 2015), we do not know which signalling pathways control APSC activation. Our studies on the *pde/ednraa* mutant suggest that EdnrAa (Fig. 25 F) signalling in the DA is a key regulator of signals controlling the quiescence of APSCs located in the ventral region of the medial pathway.

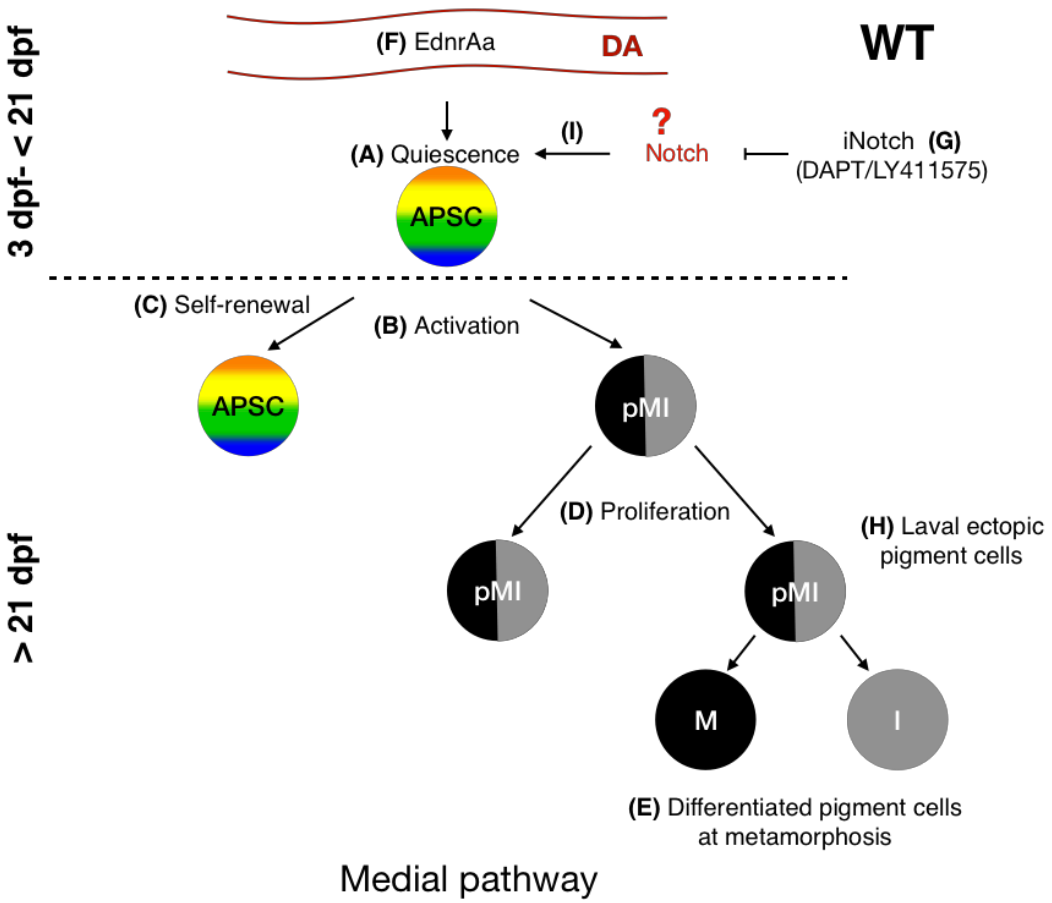

Figure 5.25 Inhibition of notch signalling induce formation of ectopic pigment cells in WT larvae. Scheme shows quiescent APSC (A) that after activation (B) self-renews (C) and generates pigment progenitors (pMI) that proliferate (D) and generate pigment cells at the onset of metamorphosis (E). We hypothesize that Ednraa in the dorsal aorta (DA; F) keeps APSC quiescence, likely via maintenance of quiescence signals in the niche. Inhibition of Notch signalling with DAPT or LY411575 (iNotch; G). Formation of larval ectopic pigment cells (H).

After reviewing the different signalling pathways that have been shown to regulate adult stem quiescence and particularly that of melanophores stem cells (McSC) in the hair follicle, we tested whether these signalling pathways have a role on APSC regulation. For instance, TGF-β has been shown to promote quiescence of McSC (Nishimura et al. 2002; Nishimura et al. 2010), while Notch signalling is required for maintenance of McSC (Kumano et al. 2008). In other stem cells systems, like in

intestinal stem cells (ISC), canonical Wnt signalling is known to promote self-renewal (Flanagan et al. 2018) and Notch signalling has reported to be required to keep NSC in a quiescent state, as loss of function of *Notch2* results in activation of quiescent NSC, accelerated neurogenesis and early exhaustion of the NSC reservoir (Imayoshi et al. 2010). In a wild type background, our results showed that neither single nor dual inhibition of TGF-β nor Wnt signalling induced formation of ectopic pigment cells. In contrast, although aware of the inconsistencies between experiment, inhibition of Notch signalling (Fig. 25 G) induced the formation of ectopic pigment cells (Fig. 25 H). Thus, we hypothesized that inhibition of Notch signalling (F) in wild type embryos, allows APSC activation (Fig. 25 I), their proliferation (Fig. 25 D) and premature differentiation of pigment cells seen ectopically in the ventral medial pathway (Fig. 25 H).

Surprisingly, expecting to enhance activation of APSC in a *pde* background by inhibition TGF-β, Wnt or Notch signalling, we observed unexpected results. In the absence of EdnrAa signalling (Fig. 26 A), APSC that normally are quiescent (Fig. 26 B), are activated (Fig. 26 C) but not depleted, resulting in proliferation (Fig. 26 D) and premature differentiation of the ectopic pigment cells in the ventral medial pathway seen in *pde* mutants (Fig. 26 E). Our results show that inhibition of TGF-β signalling does not affect the number of ectopic pigment cells in *pde* mutants while inhibition of Wnt signalling, decreased the number of both melanophores and iridophores. Wnt signalling has been well characterised to promote self-renewal of intestinal stem cell via β-catenin (Valenta et al. 2016), but also required to promote proliferation of transient amplifier progenitors derived from ISC (Kuhnert et al. 2004). In the McSC context, Wnt signalling promotes proliferation of activated McSC. Thus, it is likely that in *pde* mutants, inhibition of Wnt signalling (Fig. 26 F-H) not only prevents self-renewal (Fig. 26 I), but at the same time prevents proliferation (Fig. 26 D; Ref) and differentiation of the pigment progenitor derived from APSC (Fig. 26 J), resulting in the reduced number of ectopic pigment cells (Fig. 26 E). Although in zebrafish Wnt signalling has been shown to be required in melanophore development (Vibert et al. 2017), we observed that reduction of the number of ectopic iridophores was larger than melanophores.

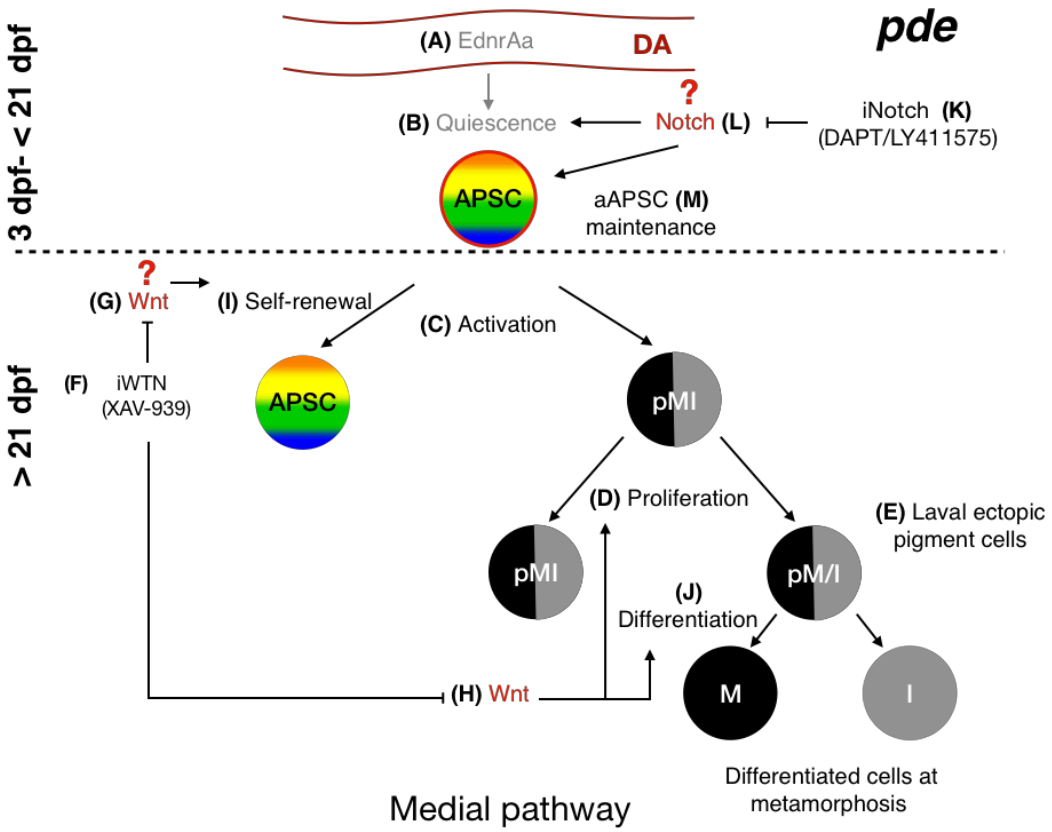

Figure 5.26 Inhibition of notch signalling reduce the number of ectopic pigment cells in *pde* larvae. Scheme shows disruption of EdnrAa signalling in the dorsal aorta (DA; A) that normally keep APSC quiescent (B). Activation and of APSC (C), giving rise to pigment progenitors (pMI) that proliferates (D) and differentiate into ectopic larval pigment cells (E). Inhibition of Wnt signalling with XAV-939 (iWnt; F-H) prevents self-renewal (I) of APSC, proliferation of pigment progenitor (D) and differentiation of melanophores (J) Inhibition of Notch signalling with DAPT or LY411575 (iNotch; K and L), disrupts maintenance of active APSC (aAPSC; M).

Requirement of Wnt signalling pathway in iridophore development has not been previously reported. In our experiments, embryonic pigment pattern looked largely normal. However, we did not quantify the number of embryonic iridophores; this data would reveal whether Wnt signalling is required for iridophore development in general. Otherwise, if embryonic iridophores are not affected, our results would suggest that proliferation of pigment progenitors may be being prevented. To test this

hypothesis, we could perform quantification of proliferative neural crest cells in the ventral media pathway of *pde* mutants treated with Wnt inhibitor.

Similarly, decrease numbers of ectopic pigment cells in *pde* mutant (Engler et al. 2018) treated with Notch inhibitor (Fig. 26 K and L) was not immediately expected. However, Notch signalling in mouse NSC has a dual role, one is to keep NSC quiescent through Notch 2 (Engler et al. 2018), and to maintain activated NSC via Notch 1 (Basak et al. 2012). Furthermore, in zebrafish, a similar role between Notch 3 (maintenance of quiescence) and Notch 1 (prevents differentiation of activated NSC) on NSC has been reported (Alunni et al. 2013). Thus, we hypothesised that Inhibition of Notch signalling in *pde* mutants disrupt maintenance of active APSC (Fig. 26 M), resulting in the reduced number of ectopic pigment cells.

Further experiments would require individual assessment of each zebrafish Notch receptor, whether by morpholino mediated knock down or generation of mutants.

Both Wnt and Notch signalling have dual, and opposing, roles in melanophore stem cells regulation. They are required for maintenance of stem cell quiescence, but also for proliferation of active stem cells. The time windows we tested here could be overlapping both processes, thus confounding the results obtained. Shorter and higher dose treatments with Wnt and Notch inhibitors may help to dissect this, but also cell-autonomous activation of these signals in a more finely-controlled manner may be necessary to dissect the precise roles of these signals in APSC development.

CHAPTER 6

CHAPTER 6 General discussion.

In this work, we use the zebrafish *Danio rerio* as a model for the study of embryonic and adult pigment development. We focus mainly on the characterisation of a mutant of Endothelin receptor Aa (*ednraa*/*pde*) in which we propose regulation of adult pigment stem cells is affected.

We will discuss in this section the key findings that lead us to an initial model explaining the *ednraa/pde* mutant phenotype. We will then integrate our further data, showing how these support that model, before discussing approaches we would like to follow, and some preliminary data we have obtained to further test that model. Finally, we will present a refined version of our model.

6.1 The *parade* mutation does not affect embryonic pigment development.

Here we present further cellular and molecular characterisation of a mutant called *parade* that was isolated in the ENU mutagenesis screening in 1996 (Kelsh et al. 1996). Previous work in the Kelsh lab (Colanesi; Mueller PhD theses) identified that the gene affected in the *parade* mutant encodes the Endothelin receptor Aa (EdnrAa; Colanesi; Mueller PhD theses; Camargo-Sosa., et al 2018). At around 4 dpf, this mutant displays a very interesting larval phenotype, in which in addition to the wild type pigment phenotype, a group of melanophores and iridophores appear in a very restricted area of ventral medial pathway of the posterior trunk, just below the dorsal aorta. One of the interesting futures of this mutants is that expression of *ednraa* by *in situ* hybridization is not detected in neural rest cells in the trunk but in developing blood vessels from 22 hpf until 72 hpf, specifically in the dorsal aorta, posterior cardinal vein and the intersegmental vessels. Our data is consistent with previous work that reported *ednraa* as strongly expressed in the cranial neural crest, specifically in the branchial arches, but not in the neural crest of the trunk, instead, detection of *endraa* was found in the vasculature of the trunk at 24 hpf (Nair et al. 2007).

The endothelin system is well known for its role in regulation of blood pressure (Haynes and Webb, 1994), but work on mice identified new roles of endothelins on craniofacial (Ruest et al. 2004) and enteric and melanophore development (Kurihara et al. 1999). In mice, there are two types of endothelin receptors, EdnrA and EdnrB. Mutants of *EdnrB* lack epidermal melanophores (Hosoda et al. 1994; Shin et al. 1999), while mutants of *EdnrA* do not display any pigment phenotype. In contrast, zebrafish has two orthologues genes of each type of receptor, *ednraa*, *ednrab*, *ednrba* and *ednrbb*. Mutants of *ednrba* display disruption of the adult pigment phenotype and reduced melanophores and iridophores (Parichy et al. 2000). In

agreement with the observed phenotypes of above mentioned mutant, in mice, *EdnrA* and *EdnrB*, both are expressed in the cranial neural crest or the hair follicle, while in zebrafish *ednrba* is also expressed in the neural crest and iridophores.

In zebrafish, *ednraa* is not expressed in the neural crest of the trunk, but in the developing blood vessels. Thus, the mechanism by which of EdnrAa signalling in the dorsal aorta affects neural crest in the trunk, in particular the chromatophores lineage, seem to be indirect and no similar role of EdnrA on pigmentation has been noticed before. The previous work in the Kelsh lab (Colanesi; Mueller PhD theses) and this work, approached the study of the cellular mechanism underlying the *parade* phenotype based upon disruption of embryonic pigment development.

The position of the ectopic pigment cells in the ventral medial pathway resembles that of the developing sympathetic ganglia, so that one of the models we considered centred on a switch of fate of sympathetic neurons towards pigment cells. However, as shown here, our data is inconsistent with this model – 1) the number of sympathetic neurons is not reduced in *pde* mutants; and 2) prevention of formation of sympathetic neuron in *pde* mutants does not lead to an increase in the number of ectopic pigment cells. For these reasons, we, discarded this fate transformation model. Our alternative hypothesis considered that presence of the ectopic pigment cells is due to failure of neural crest cells migration towards the ventral region. However, assessment of migration of fluorescently labelled neural crest cells through the medial pathway showed that this process is not affected at any time point between 30 hpf and 5 dpf. Furthermore, the ventral and yolk sac stripes are properly formed, with the ventral stripe presenting supernumerary iridophores but not melanophores, indicating that neural crest migration occurs.

Although the earliest we can distinguish the ectopic cells in *pde* mutants is at 3 dpf, previous work in the lab, together with this work identified increased numbers of cells expressing the melanophore marker *dct* and the iridophore marker *ltk* in the ventral medial pathway of the posterior trunk as early as 35 hpf (Colanesi, S., PhD thesis and this work), thus, suggesting that the processes affected in *pde* mutants occur earlier in development than realised before. We quantified the numbers of proliferating neural crest cells, showing that these were increased in *pde* mutants compared to their WT siblings. Strikingly, the increase in proliferating cells was almost exclusively restricted to the ventral region of the neural crest medial migratory pathway, indicating

that the disrupted signalling of EdnrAa has a local effect on the cells in the vicinity of the dorsal aorta.

We considered the hypothesis that the Ventral Stripe can host only a limited amount of iridophores and melanophores, so that the excess of pigment cells in the ventral trunk might be misplaced pigment cells that could not fit in the ventral stripe. However, evidence from a mutant called *moonshine* showing supernumerary iridophores in the dorsal, post anal, ventral and the yolk sac stripes, but without ectopic iridophores (Kelsh et al. 1996), suggesting that overproduction of pigment cells is unlikely to be the cause of the ectopic location of pigment cells.

What changed our approach to the study of the mechanism of the *pde* phenotype was the screening of almost 1400 small molecules performed by Sarah Colanesi. Her work showed that a specific EGFR inhibitor, AG1478, recued the *pde* phenotype (no ectopic pigment cells were formed) when embryos were treated from 4 hpf to 96 hpf with a concentration of 10 μM. Strikingly, this small molecule has been used as a inhibitor of the Erb signalling pathway, which in zebrafish is required for the establishment of adult pigment stem cells (APSC) in development (Budi et al. 2008).

6.2 Shared molecular requirements for the formation of ectopic pigment cells in *pde* mutants and formation of APSC.

APSC are responsible for the generation of newly differentiated pigment cells that will form the adult pigment pattern at the onset of metamorphosis. APSC derive from the neural crest in a process that requires the *epidermal growth factor receptor (EGFR)-like tyrosine kinase* Erbb3b (Budi et al. 2008). In contrast, the pigment cells that form the embryonic pigment pattern differentiate directly from the neural crest and their formation does not require of Erb signalling, since both *erbb3b* mutants and WT embryos exposed to Erb inhibitor from 9-48 hpf, display a normal larval pigment phenotype. Building on the results of the small molecule screen, we predicted that if the ectopic pigment cells derive from APSC, treatment of embryos from 9-48 hpf would prevent the formation of ectopic pigment cells. Our results show that treatment of *pde* mutant embryos with either of two ErbB inhibitors, AG1478 or PD158780, from 9-48 hpf prevents the formation of ectopic pigment cells. This proves that there is not only a shared molecular requirement, but also that it has shared temporal requirements, between formation of the ectopic pigment stem cells in *pde* mutants to that of APSC.

Hultman., et al 2009, determined that APSC are responsible of melanophore regeneration. By chemically ablating embryonic melanophores, they showed that establishment of APSC occurs from anterior to posterior, as embryos exposed to Erb inhibitor from 14-24 hpf do not regenerate melanophores in the region of somites 5-12, while embryos treated from 30-48 hpf do not regenerate melanophores between somites 16-21.

Ectopic pigment cells in *pde* mutants are distributed between the 8 and the 16 somites. By testing Erb inhibitor treatment of *pde* embryos during a series of treatment time windows, we showed that inhibition of Erb signalling in a narrow window of time from 19-30 hpf prevents the formation of ectopic pigment cells. In contrast, embryos treated from 24-32 hpf display normal numbers of ectopic pigment cells. Thus, formation of ectopic pigment cells in *pde* mutants come from a population of cells that follows the same temporal and molecular requirement to that of APSC formation.

Using a transgenic line that labels all neural crest derivatives, we were able to show that the ectopic pigment cells in *pde* mutants are always in very close association with the nerve projections that emerge from the DRG, and on some occasions, are associated with the sympathetic ganglia. Previous work has suggested the existence of a niche of APSC within the dorsal root ganglion (DRG) (Dooley et al. 2013). However, those studies exclusively focused on tracking cells within the DRGs, without assessing the contribution of cells located in other regions of the fish. Thus, it is possible that there is more than one niche of stem cells within the fish body.

Thus, based on these observations we generated our first model in which, EdnrAa signalling in the dorsal aorta regulates a second niche of APSC in the ventral medial pathway and keeps them in a quiescent state (Fig. 6.1 A), whereas in *pde* mutants, disruption of EdnrAa (Fig. 6.1 B) allows premature activation of APSC and subsequent differentiation resulting in the *pde* phenotype (Fig. 6.1 C).

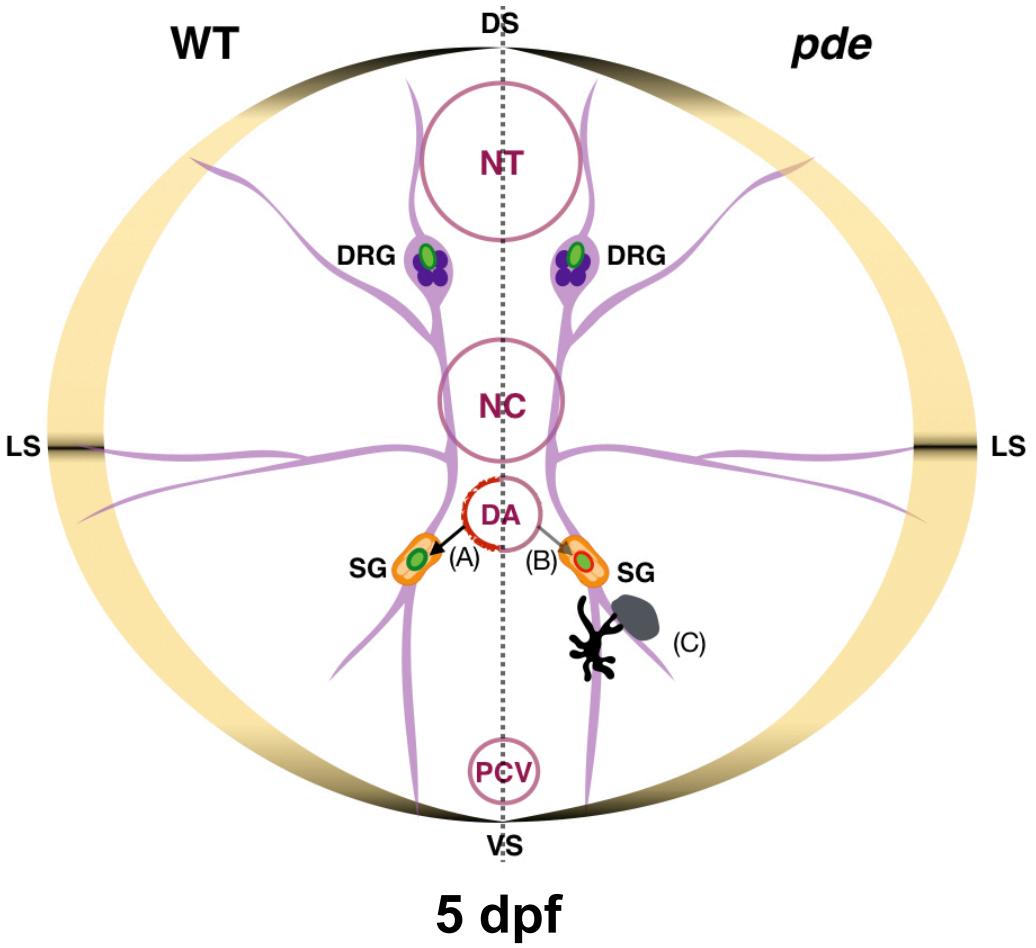

Figure 6.1 APSC model to explain the *parade* phenotype. Schematic showing a transversal view of a 5 dpf zebrafish anterior trunk. The left segment represents the WT context and the right segment the *pde* background. In the most outer layer we indicate the position of the dorsal, lateral and ventral stripes (DS, LS, and VS correspondingly. Centrally are indicated the neural tube (NT), notochord (NC), dorsal aorta (DA) and posterior cardinal vein (PCV). Dorsal root ganglia (DRG) and nerve projections are shown in purple while Sympathetic ganglia (SG) are shown in orange. APSC are shown in green. In the WT panel, EdnrAa signaling in the DA results in the production of signals(s) (shown in red), that influences the neighbouring APSC (A). Loss of EdnrAa signalling in *pde* mutants results in premature activation of APSCs causing precocious differentiation of ectopic pigment cells (C).

To further test our hypothesis that ectopic pigment cells in *pde* mutants do not derive from embryonic pigment cells but APSC, we took advantage of a second molecular difference between embryonic melanophores and APSC formation. It has been

shown that formation of embryonic melanophores requires early activity of *mitfa*, while formation of APSC does not (Dooley et al. 2013). In the present work, we show that prevention of formation of embryonic melanophores by morpholino mediated-knock down of *mitfa* in *pde* embryos, does not affect the formation of ectopic melanophores. Thus, formation of ectopic melanophores in *pde* mutants does not depend on early embryonic *mitfa* activity, again consistent with their not being derived from embryonic melanophores.

Thus, we have strong evidence that supports the proposal that ectopic chromatophores in *pde* mutants derive from a population of cells with similar molecular requirements of that of APSC: Erb signalling dependency in the same time window of development and independence from early activity of *mitfa*.

6.3 Location of ectopic pigment cells in the ventral medial pathway suggest a second niche of APSC.

Our model, proposes a second niche of APSC located within the ventral medial pathway. We showed evidence of another zebrafish mutant, *ltk*^{mne} that displays ectopic iridophores in the medial pathway (Fadeev et al. 2016), not only ventrally but also dorsally. Similar to *pde* mutant, ectopic iridophores in the ventral region are closely associated to the ventral projection of the nerve that emerge from the DRGs and are located under the dorsal aorta. Strikingly, disruption of *ednraa* in *ltk*^{mn} strongly enhances the formation of these ectopic iridophores in the ventral medial pathway. This data, together with the local increased proliferation observed in *pde* mutants, support the idea that EdnrAa has a restricted effect on pigment progenitors exclusively located in ventral regions. Furthermore, this idea is reinforced by the observed induced ectopic pigment cells after over expression of the *Petromyzon marinus sox10* orthologue *SoxE2* in WT *soxE2* in WT embryo. Together, this evidence favours our model of the embryo hosting pigment progenitors, perhaps APSC, in at least two locations of the medial pathway.

As part of our future work, we aim to test our model by asking whether 1) in a wild type background there are pigment progenitors or APSC in the ventral medial pathway that contribute to the formation of the adult pigment pattern.; and 2) in a *pde* background, clones labelled at 30 hpf generate both ectopic pigment cells and adult pigment cells.

6.3.1 Validation of a second niche of APSC.

Previous work using clonal analysis demonstrated that cells within the DRGs contribute to the adult pigment pattern (Singh et al. 2016). This technique consists of using a transgenic line with an inducible Cre recombinase transgene driven by the promotor of the neural crest marker *sox10* (*sox10:creER*^{T2}) in combination with a fluorescent flox responder transgene (*actin-β:loxp-STOP-loxp-DsRed*) .

We have preliminary data generated in the lab of Prof. Christiane Nüsslein-Volhard, in which we labelled single clones by inducing recombination at 30 hpf with a low dose and short treatment of 4-OHT (5 μM for 1 h). We allowed expression of DsRed for 12 hours before screening for embryos with single cells at 42 hpf. Initially, we induced recombination in 400 embryos and we screened one by one through both sides of the embryo using a 20x lens. We found that 102/400 embryos had at least one labelled clone, from which 87/102 embryos had one labelled clone, 9/102 embryos had two distinguishable (i.e distant from each other, head and tail) labelled clones and 3/102 embryos had three distinguishable labelled clones. From the 87 embryos with singles clones 26/87 (Fig. 6.2 A and B) embryos had a single clone in the medial pathway and only in 4/26 embryos was the labelled clone located in the ventral medial pathway (Fig. 6.2 C). Thus, 1% of our initial number of induced embryos showed a clone in the area of interest. In this first experiment, we attempted to systematically image the 26 clones located in the medial pathway on a daily basis until metamorphosis.

However, we encounter several methodological challenges. Imaging of the embryos requires mounting them on low melting point agarose, thus daily manipulation of the embryo resulted in the loss of a subset of embryos. Also, we found that from around 12 dpf, recovery from anaesthesia was impaired, so that most of the clones could not be tracked beyond 12 dpf. We have an example of a clone screened at 2 dpf (Fig. 6.2 C) and imaged at 24 dpf (Fig. 6.2 D) in which xanthophores and other unidentified cell types, but presumably glial cells based on their position and morphology, are fluorescently labelled. This data suggests that there are pigment progenitors in the ventral medial pathway that contribute to adult pigment pattern. We will repeat this experiment and increase the number of analysed and recorded clones in the ventral medial pathway.

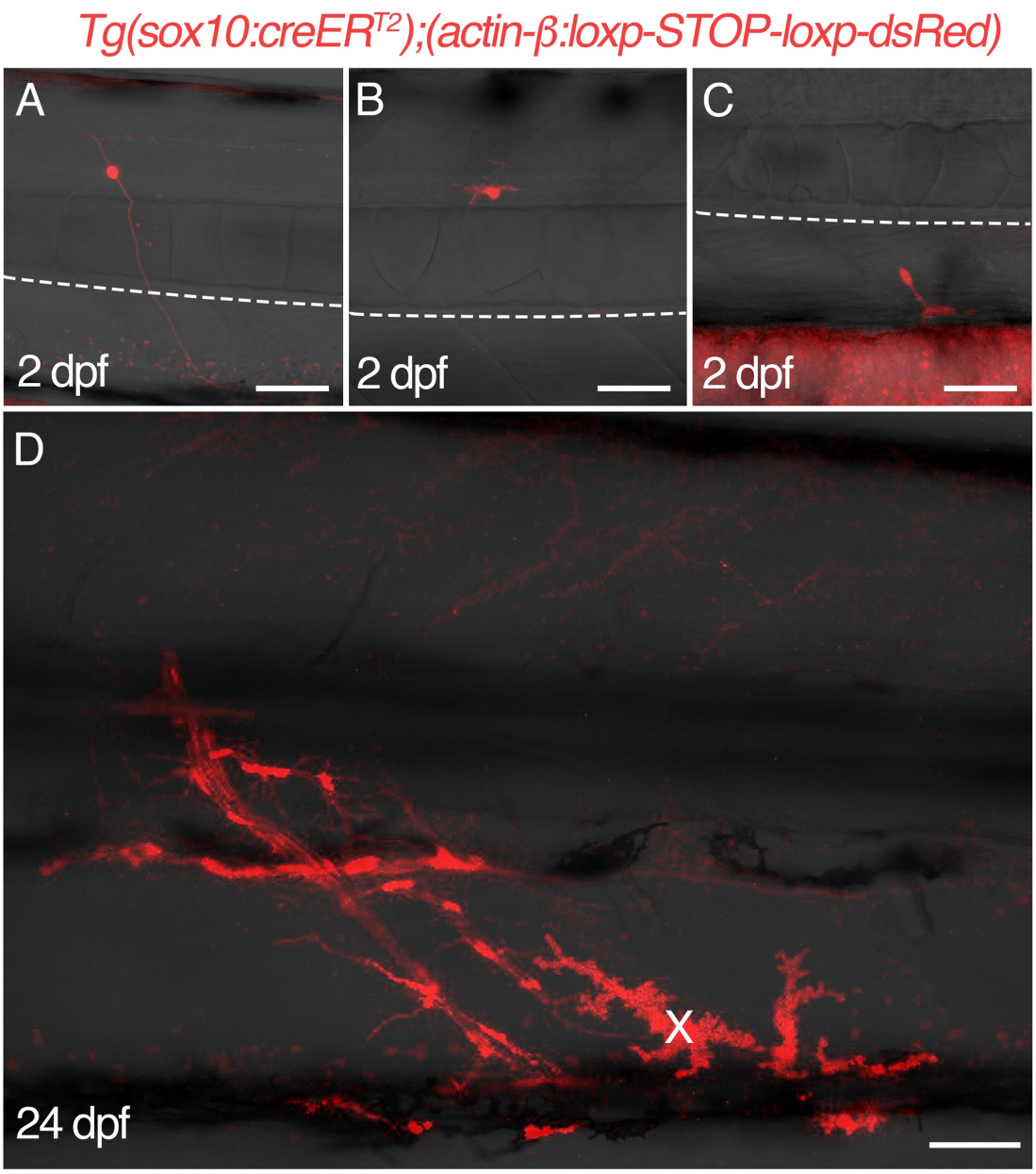

Figure 6.2 Clonal analysis of neural crest derived cells located in the ventral medial pathway. Confocal imaging of fluorescently labelled clones in wildtype fish carrying the transgenes *sox10:creER^{T2};* (*actin-β:loxp-STOP-loxp-DsRed*. Induction was performed at 30 hpf and, single cell clones were screened at 42 hpf. Overlapping images of DsRed and DIC channels of single cell clones at 50 hpf (A-C). D) Clone in panel C was imaged at 22 dpf. Xanthophores = X: Scale bar = 50 μm.

We have now successfully standardized a protocol for repeated anaesthesia of larvae and fish with both transgenes (*sox10:creER^{T2}*; *actin-β:loxp-STOP-loxp-DsRed*) are now available in the facility at the University of Bath. We are currently breeding both

transgenes into a *pde* background in order to test whether ectopic pigment cells and adult pigment cells in *pde* mutants have a common cellular origin.

6.4 Regulation of adult pigment stem cells.

Since our model proposes that ectopic pigment cells in *parade* mutants arise from premature activation of APSC, we tested whether chemical manipulation of signalling pathways involved in stem cells regulation could induce the formation of ectopic pigment cells. We made a comprehensive review to identify potential candidates. In this work, we targeted three signalling pathways, TGF-β, Wnt and Notch signalling. These signalling pathways have been described as having a role in maintaining stem cell quiescence in different stem cell models such as, intestinal stem cells (ISC) (Valenta et al. 2016; Barker et al. 2007), and Neural stem cells (NSC) (Engler et al. 2018; Basak et al. 2012) but also in the maintenance of melanophore stem cells niche in the mouse hair follicle (McSC) (Nishimura et al. 2002; Kumano et al. 2008; Rabbani et al. 2011). Wnt signalling is required for the maintenance of the ISC niche is well known, specifically in the promotion of self- renewal (Valenta et al. 2016) and prevention of proliferation (Kabiri et al. 2018) and terminal differentiation (Korinek et al. 1998; Fevr et al. 2007).

Our initial reasoning was that chemical inhibition of such pathways would allow the premature activation of APSC and induce the formation of ectopic pigment cells, mimicking the *parade* mutant. Thus, our first prediction was that inhibition of Wnt signalling might promote activation of APSC, and thus differentiation of pigment cells, in a wild type background. However, we did not observe such result. Furthermore, we also tested these inhibitors on *pde* mutants, asking if they might enhance the pigment phenotype. However, when Wnt signalling was inhibited in *pde* mutants, we observed a strong reduction of both ectopic melanophore and iridophores, with the latter being more reduced. This suggests that Wnt signalling is required for melanophore and iridophore specification. Requirement of Wnt signalling on embryonic melanophore differentiation and regenerating melanophores has been described (Vibert et al. 2017; Iyengar et al. 2015), so this is perhaps not unexpected. However, a role for Wnt signalling in iridophore development has not previously been identified. This raises two possible scenarios. 1) Wnt signalling is necessary for differentiation of both chromatophores. This could be easily tested by quantifying the formation of embryonic iridophores, which would test whether Wnt signalling is required for iridophores formation, in addition to its role in melanophore development. We note

that in this scenario, our experiment would not be expected to allow assessment of the role of Wnt signalling in maintenance of APSC quiescence, since the cells' activation would be masked by the subsequent role in pigment cell specification. On the other hand, it has been reported that activation of canonical Wnt signalling within the hair follicle niche is required for proliferation and differentiation of McSC in mammals. Thus, an alternative scenario is that 2) inhibition of Wnt signalling prevents proliferation of pigment progenitors derived from the activated APSC. In which case, only if Wnt signalling does not have a role in iridophores development we would again expect that proliferation of NC-derived cells of *pde* mutants treated with Wnt inhibitor is reduced.

Regarding the role of Notch signalling, the results obtained in our inhibitor experiments were inconclusive. We observed opposite effects when inhibition of Notch signalling was performed in a wild type and a *pde* mutant background. In mice and zebrafish, Notch2 and Notch3, correspondingly, have a role in keeping non-cycling NSC in a quiescent state. By analogy, we might expect inhibition of Notch signalling to result in premature activation of APSCs, and consistent with this, wild type embryos treated with either of the two tested Notch inhibitors (DAPT) displayed ectopic pigment cells in the medial pathway, on three of 5 experiments. Testing of a second Notch inhibitor (LY), produces very few ectopic cells.

Given this result, we expected that *pde* mutants treated with Notch inhibitors might display an enhancement of the ectopic pigment cell phenotype; instead, they showed a reduction in the number of ectopic pigment cells. However, Notch signalling in mouse and zebrafish NSC has a complex dual role, both to keep non-cycling NSC quiescent (Notch2 and Notch 3 dependent) (Engler et al. 2018; Alunni et al. 2013), and to maintain activated NSC (via Notch1 and Notch 1b) (Basak et al. 2012). Indeed, in mice and zebrafish, loss of function of Notch1 and Notch1b, respectively, results in differentiation of active NSC at the expense of maintenance of active NSC. So, we can perhaps reconcile the results from both WT and *pde* mutants by postulating that Notch signalling, likely mediated by different Notch receptors, might have different roles in both maintenance of quiescence in APSCs, and in other aspects of their biology. Perhaps the effect in WT embryos treated with Notch inhibitors (weak increase in ectopic pigment cells) predominantly reflects inhibition of the role in APSC quiescence, whereas that in *pde* mutants (where the APSCs are likely already activated), perhaps predominantly reflects inhibition of the role in maintenance of an activated APSC, giving decreased numbers of differentiated ectopic cells.

Clearly there is further work required to dissect what may be a complex mesh of APSC regulation. Our data demonstrate the limitations of chemical inhibition studies where there are pleiotropic and opposing roles of each of Wnt and Notch signalling on stem cell regulation. One way to overcome this limitation is by performing shorter and higher dose treatment of Wnt and Notch inhibitions. However, a better approach would likely be through cell-specific activation of each pathway to help dissect the specific roles of each signal on APSC regulation. Furthermore, these data made clear that we require an independent approach to try to identify the signalling pathways that may be most relevant here.

6.4.1 On the search for more candidates behind the mechanism of the *pde* mutant.

As a complementary approach, we propose a direct assessment of the changes in blood vessel signalling pathways in *pde* mutants compare to their WT siblings. Thus, we have bred the combination of three transgenes *Tg(fli:EGFP); Tg(sox10:cre); Tg(hsp70:loxp-dsRed-loxp-EGFP* onto a *pde* background (Fig. 6.3 A). This will allow us to independently isolate blood vessel cells and neural crest-derived cells in order to perform RNAseq in both WT and *pde* mutant backgrounds.

This combination allows the labelling of blood vessels (Fig. 6.3 B; *Tg(fli:EGFP)*), followed by screening of embryos negative for this first transgene, and further heat-shock to label neural crest-derived cells in the remaining embryos that contain the other two transgenes (Fig. 6.3 C; *Tg(sox10:cre; hsp70:loxp-dsRed-loxp-EGFP)*. Embryos lacking all transgenes will constitute a background control. Note that all samples will be derived from embryos of the same cross. Because *ednraa* is expressed in the cranial neural crest, we will dissect off the posterior trunk and tail of all embryos and process the samples to obtain single cell suspensions of blood vessel cells, NC, and general trunk/tail cells respectively. Finally, through staining using Hoechst (see section 2.5), we will be able to exclude dead and dying cells.

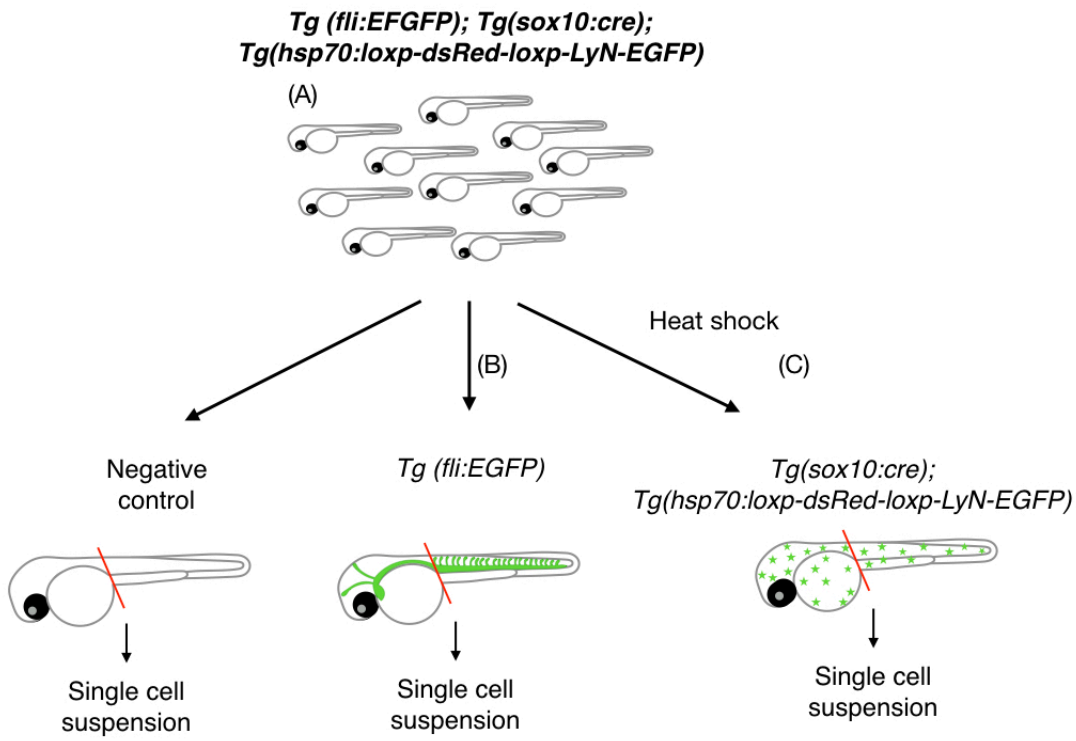

Figure 6.3 Methodology for single cell suspension of GFP labelled blood vessel and neural crest cells. Embryos carrying the transgene *Tg(fli:EGFP)* were out crossed to embryos carrying the transgenes *Tg(sox10:cre); Tg(hsp70:EGFP)* (A). Embryos positive for *Tg(fli:EGFP)* (B) were screened, the remaining embryos were heat-shocked and embryos positive for *Tg(sox10:cre); Tg(hsp70:EGFP)* were screened (C). The embryos negative for all of the transgenes were used as negative control. Embryos were independently processed to obtain a single cell suspension.

We performed Fluorescence Activated Cell Sorting (FACS), using sibling embryos negative for all transgenes (Fig. 6.4 A and B) to establish the negative and positive quadrant thresholds for sorting of the GFP+ cell populations. By plotting of the forward scatter (FSC) against the side scatter (SSC), we delimited a first main population of cells (P1), from which we plotted the GFP and Hoechst channels, and sorted cells negative for Hoechst and positive for GFP (P2) from a single cell suspension sample of embryos positive for *Tg(fli:EGFP)* (Fig. 6.4 C and D) and embryos positive for *Tg(sox10:cre; hsp70:loxp-dsRed-loxp-EGFP)* (Fig. 6.4 E and F). We corroborated in a epifluorescente compound microscope that cell form both samples (Fig. 6.4 D' and F') were in fact positive for GFP and negative for Hoechst.

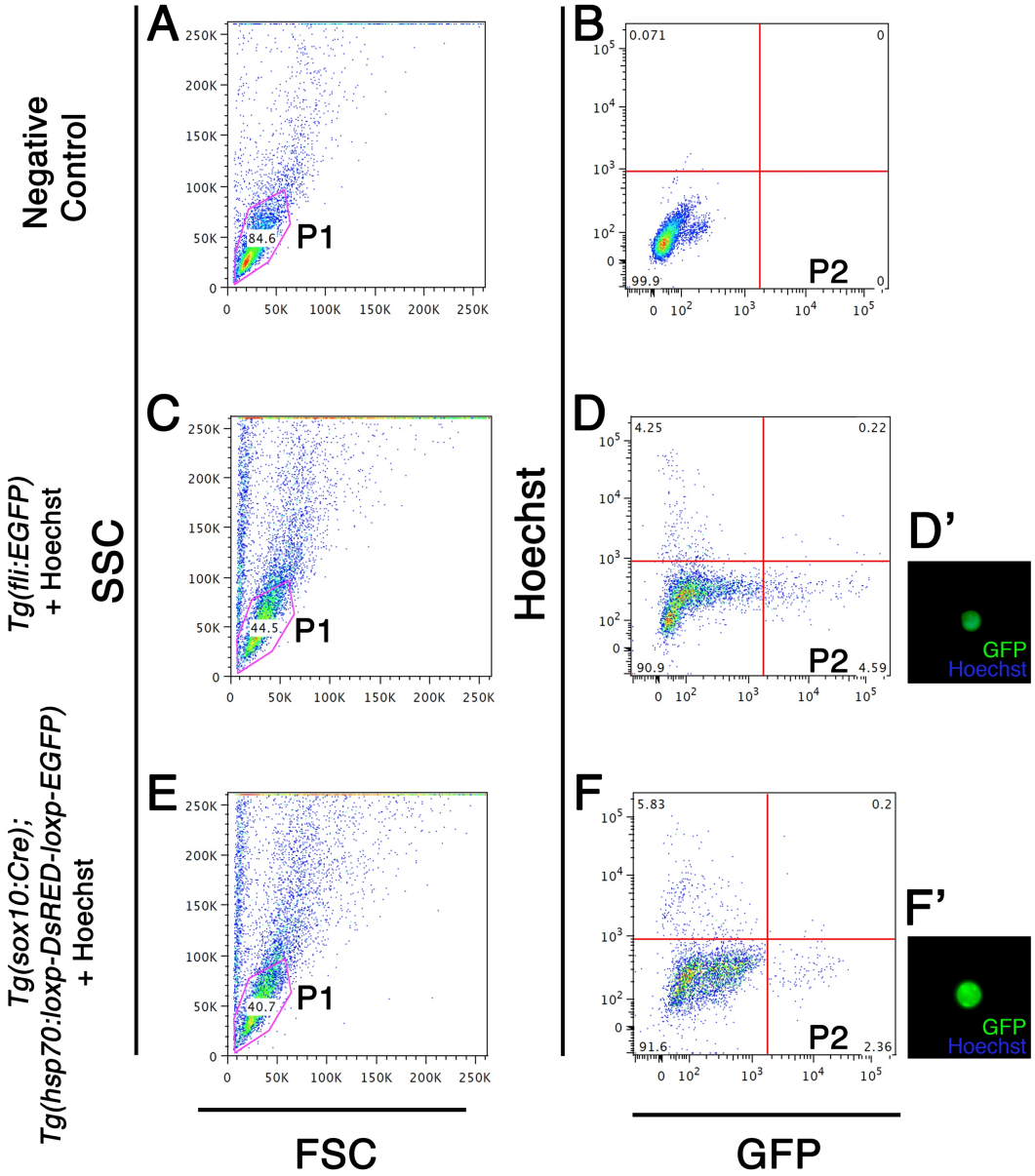

Figure 6.4 Sorting of blood vessel cells and neural crest cells. Dot plots of single cell suspension from WT fish (A and B), *Tg(fli:EGFP)* + Hoechst (C and D) and *Tg(sox10:cre); Tg(hsp70:EGFP)* + Hoechst (E and F). A first population (P1) was selected from the dot plot of the forward scatter (FSC) against the side scatter (SSC; A, C and E). Cells from P1 were displayed in a dot plot of GFP against Hoechst (B, D and F). Thresholds (red lines) were established based on the WT sample negative for both GFP and Hoechst (B). From the samples *Tg(fli:EGFP)* + Hoechst (D) and *Tg(sox10:cre); Tg(hsp70:EGFP)* + Hoechst (F), a second population of cells (P2) positive for GFP and negative for Hoechst was sorted. Fluorescent signal for GFP and Hoechst was assessed and imaged (D' and F').

We have successfully standardised this methodology and calculated that per 100 dissected trunks and tails we can isolate 10,000 cells from which we are able to extract approximately 100 ng of total RNA using a RNeasy Plus Micro Kit. We corroborated the quality of the RNA in a bleached gel (Fig. 6.5 A) by loading 100 ng of RNA and used the same amount of RNA to make cDNA. We took the opportunity to direct test the expression of *ednraa* by RT-PCR; we see *ednraa* is only detected in blood vessel (BV) cells and not in neural crest derived (NC) cells (Fig. 6.5 B). Expression of house-keeping genes (actin-β2 and ef1α) was detected through all sample (Fig. 6.5 C). We are currently in the process of obtaining multiple biological replicates for RNA-seq. Analysis of GO term enrichment on the RNA-seq data will be used to identify signalling pathways showing differences between WT and *pde* mutant blood vessels. Subsequent validation of the RNA-seq analysis can be performed through qPCR suing samples obtained in this way.

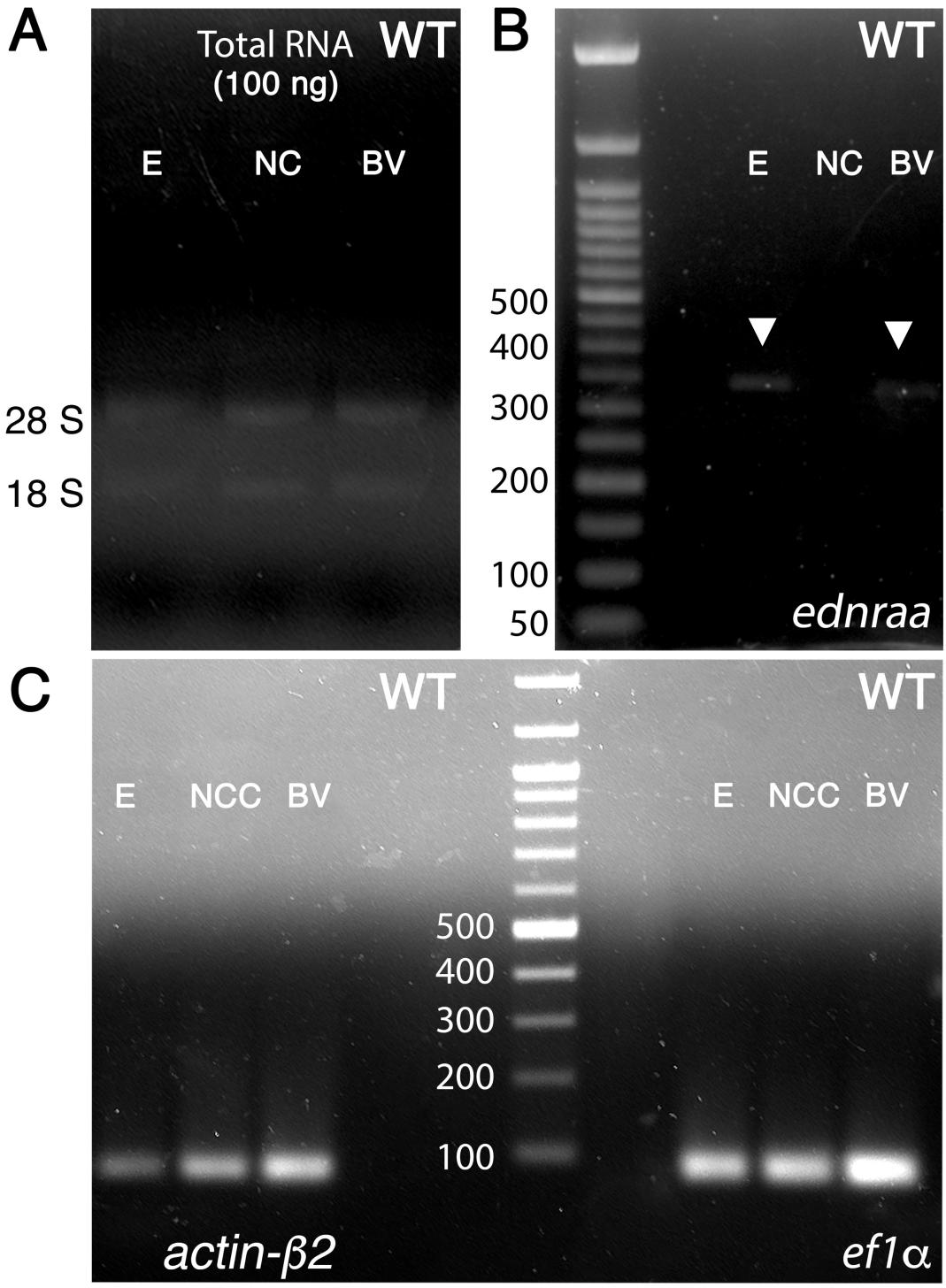

Figure 6.5 Expression of *ednraa* is not detected in neural crest. Visualisation of RNA integrity (A) in a single 35 hpf embryo (E), neural crest cells (NC) and blood vessels cells (BV). Detection of *ednraa* expression (white arrowheads; B) and house-keeping genes actin-β2 and ef1α(C).

6.5 New roles of the endothelin system in embryonic and adult pigment development and ventral craniofacial cartilages.

Analysis of the zebrafish genome identifies twelve genes that encode the elements of the endothelin signalling system: Six ligands, Edn1, Edn2a, Edn2b Edn3a, Edn3b and Edn4; four receptors, Ednraa, Ednrab, Ednrba and Ednrbb; and three Endothelin Converting Enzymes, Ece1, Ece2a, Ece2b that activate the ligands (Braasch et al. 2009). In this work, we present the characterisation of seven mutants (*edn1, edn2a, edn3a, edn3b, ednraa, ednrab,* and *ece1*) of the zebrafish endothelin system. These mutants were generated using CRISPR/Cas9 targeted mutagenesis. Our main objective was to identify the other components, including the key ligand of the EdnrAa signalling pathway, affecting pigment cell development.

6.5.1 *end1*, *edn2* and *ednrab* have a role on embryonic iridophore development.

Since Edn1/EdnrA work together in mice, (Kurihara et al. 1994; Clouthier et al. 1998), we hypothesised that Edn1 was the most likely ligand for EdnrAa in zebrafish and hence predicted that mutants for *edn1* would display ectopic pigment cell in the ventral medial pathway. Although a mutant on *edn1* had been previously characterised (Nair et al. 2007), the authors did not asses the pigment phenotype. Unexpectedly, we did not observe an ectopic pigment cell phenotype. Instead, we observed an absence of iridophores in the dorsal stripe and a strong reduction of iridophores in the ventral stripe, while the embryonic melanophore pattern appeared normal. We then generated a mutant of *edn2a* and we found that similar to *edn1* mutants, ectopic pigment cells were absent. Surprisingly we also observed absence of iridophores in the dorsal and ventral stripes but also no iridophores above the swim bladder. Finally, we showed that mutants of *ednrab* display a similar iridophore phenotype to that of *edn1* mutants, absence of iridophores in the dorsal stripe and reduced iridophores in the ventral stripe. This mutant did form iridophores above the swim bladder.

To test whether the EdnrAa interacts with EdnrAb on the formation the *pde* phenotype we bred double mutants of *ednraa* and *ednrab*. The pigment phenotype was rather intriguing as double homozygote mutants did not display ectopic menlanocytes nor iridophores and showed reduced number of embryonic iridophores in both the dorsal and ventral stripes. Our model proposes that EdnrAa is a key signal in the regulation of APSC (Fig. 6.6 A). Based on the double mutant phenotype, we hypothesised that EdnrAb has an additional role, beyond that in iridophore development (Fig. 6.6 B) shown by the single mutant. For instance, EdnrAb may be required for regulation or establishment of APSC (Fig. 6.6 C) or the progenitors derived from APSC, in which case we expect that adult homozygous mutants for *ednrab* would show disrupted adult pigmentation. In contrast, if *ednrab* only has a role in embryonic iridophore maintenance the phenotype would be normal, in which case we will need to revise our model.

This model explains the premature differentiation of pigment cells however does not explain their ectopic location. We hypothesized that the location of the ectopic melanophores and iridophores in *ednraa* mutants reveals the location of the niche of stem cells. The consistent position at the level of the DRG's and sympathetic ganglia of the ectopic melanophores and iridophores observed in the *moonstone* mutants and the ectopic pigment cells induced by the overexpression of the lamprey sox10 in WT zebrafish embryos, suggest that premature differentiation occurs *in situ*. Furthermore, the morphology of the ectopic melanophores, is always shown as stationary (large cytoplasm and wide spread dendritic cells), suggest that thiese cells are no migrating.

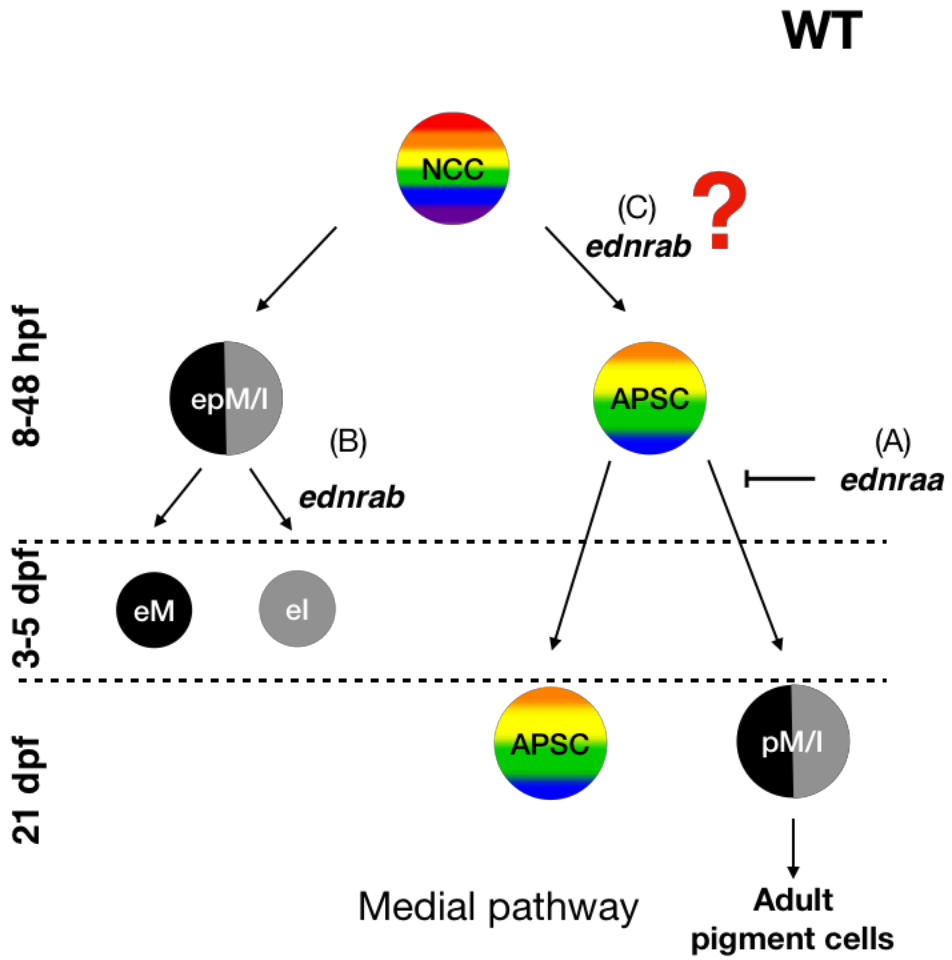

Figure 6.6 Role of *ednraa* and *ednrab* on the regulation of adult pigment stem cells, based on single and double mutant phenotypes. Scheme shows neural crest cells (NCCs) give rise to embryonic pigment progenitors (epM/I) and adult pigment stem cells (APSC) between 8-48 hpf. Production of adult pigment cells from adult pigment stem cells (APSCs) is regulated by *ednraa* (A). epM/I produce melanophore and iridophores from 3-5 dpf, with iridophore differentiation requiring *ednrab* (B). Hypothetical requirement of *ednrab* (C) for the establishment of APSC that give rise to adult pigment cells that activate around 21 dpf.

6.5.2 *end1*, *edn2, endraa* and *ednrab* have a role on ventral craniofacial patterning.

Previous work showed that the *edn1*/*sucker* mutant (Nair et al. 2007), does not form ventral craniofacial cartilages (jaw). In agreement with this, the new null mutant allele of *edn1* that is described in this work does not form the jaw. Surprisingly, *edn2a* mutants also did not form a jaw, suggesting a coordinated role together with *edn1* in jaw formation. Nair., et al also reported that *ednraa* and *ednrab* single morphants display a larger and shorter jaw, correspondingly, however, our null mutant alleles did not show any obvious difference compared to wild type siblings. In contrast, our double homozygote mutant for *ednraa* and *ednrab* did not form a jaw, a feature shown in the double *ednraa*; *ednrab* morphant reported by Nair., et al. These results suggest that EdnrAa and EdnrAb in coordination with Edn1 and Edn2 regulate ventral craniofacial patterning, while none of the other mutants (*edn3a*, *edn3b* and *ece1*) appeared to have a role on it. A very elegant study compared the phenotypes of mutants and morphants of two genes, *egfl7* and *vegfaa*. Their work revealed that mutants did not resemble the previously reported phenotypes of the morphants of egfl7 (severe vascular defects), transcriptomic and proteomic analysis revealed that mutants displayed activation of a set of genes that rescued the morphant phenotype, and that were not activated in the morphants. In the case of the *vegfaa* mutant, upregulation of *vegfab* was identified but not in *vegfab* morphants. Thus, deleterious mutations activate compensatory gene programmes not observed in translational or transcriptional knockdown (Rossi et al. 2015). This could explain the difference in the craniofacial phenotypes of *ednraa* and *ednrab*.

6.5.3 Adult pattern phenotypes of mutants of the endothelin system.

Previously, the coordinated role of EdnrBa (Parichy et al. 2000) and Ece2b (Krauss et al. 2014) on adult pigment pattern formation had been already identified, as both adult mutants display reduced melanophores and iridophores. The *edn3b* null mutant generated by the Nüsslein-Volhard lab revealed a similar phenotype. Thus, suggesting that Ece2b cleaves the precursor of Edn3b and then Edn3b signals through EdnrBa.

The lack of jaw in *edn1* and *edn2* single mutants and the double mutant for *ednraa*; *ednrab* mutants, does not allow the assessment of the adult pigment phenotype in these mutants, since the mutant larvae do not survive to adulthood. The adult pigment phenotype in *ece1* mutants was normal while *edn3a* homozygote mutants are not viable. As part of our further studies we will grow homozygote mutants for *ednrab* to assess the adult pigment phenotype.

Since we proposed that the ectopic pigment cells in the ventral medial pathway of *parade* mutants results from premature activation of APSC, we would expect that the adult pigment pattern of such mutants was affected. However, the adult pigment pattern appears completely normal. This might be reconciled with our model if we assume that formation of the ectopic pigment cells is not at the expense of APSC self-renewal, so that the pool of stem cells is not depleted. We also considered that the population of APSC from which the ectopic pigment cells in *parade* mutants derive might not contribute to the adult pigment pattern of the skin, but to visceral pigmentation (Fig. 6.7 A). We showed that formation of the ectopic cells depends on Erb signalling, however, *erbb3b* mutants have normal visceral pigmentation (Fig. 6.7 B), thus, formation of visceral pigmentation does not require of Erb signalling, suggesting that ectopic pigment cells in *pde* mutants and visceral pigmentation do not derive from the same cellular source.

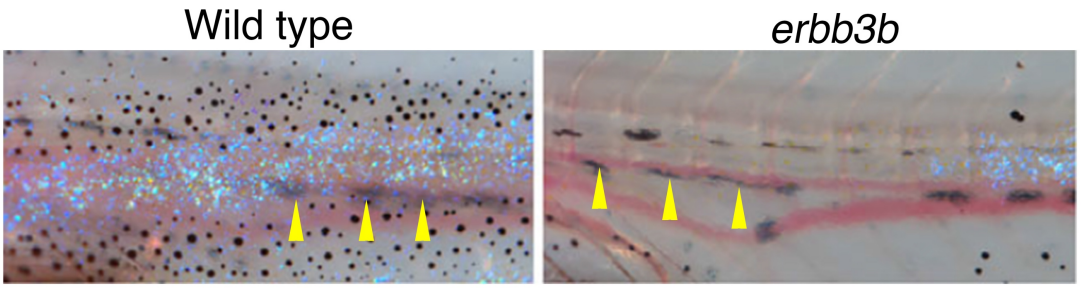

Figure 6.7 Visceral pigmentation does not require Erb signalling. Metamorphic wild-type shows normal pigmentation in the skin but. Visceral pigmentation can be noticed as black shadows pointed with yellow arrowhead (A). *erbb3b* mutant does not form pigmentation in the skin, however, visceral pigmentation is unaffected (yellow arrowheads; B). Modified from Parichy, M. D., 2014. Scales are not specified.

6.6 Revised model of the *pde* mutant phenotype.

Our first model proposed that EdnrAa signalling in the dorsal aorta regulates a second niche of APSC in the ventral medial pathway and keeps them in a quiescent state (Fig. 6.1 A), whereas in *pde* mutants, disruption of EdnrAa (Fig. 6.1 B) allows premature activation of APSC and subsequent differentiation resulting in the *pde* phenotype (Fig. 6.1 C). As previous studies have suggested a niche for APSC within the DRGs (Dooley., 2018; Sigh, 2016), based on the position of the ectopic pigment cells in *pde* mutants we originally considered that this second APSC niche in the ventral medial pathway would likely be located within the sympathetic ganglia. However, our confocal imaging of GFP labelled neural crest derivatives in *pde* mutants (Fig. 3.S3) revealed that ectopic pigment cells do not always coincide with sympathetic neurons, but they always appear to be associated with the ventral nerve projections, the spinal nerves. A similar pattern was also observed in the increased formation of iridophore clusters due to disruption of *ednraa* in *ltk*^{mne} mutants (Fig. 5.8). Thus, we now consider that the APSC niche in the ventral medial pathway is more likely to be within the ventral nerve projections.

Dooley, et al, 2013, used a transgenic line *Tg(mitfa:gfp)* to shows that GFP positive cells within the DRG are responsible for melanophore regeneration. We first tested whether using a *Tg(mitfa:gfp)* line we could find GFP positive cells in the ventral medial pathway in the early larvae. Our original model (Fig. 6.1 A and B) proposed that APSC in the medial pathway are located within the sympathetic ganglions. Given that sympathetic ganglia start developing as early as 5 dpf but are more abundant at 8 dpf, we performed immunodetection of GFP and the early neuronal marker Elav/HuC (Hu) at (8 dpf) in WT larvae in order to be able to correlate the presence of *Tg(mitfa:gfp)* positive cells with respect to the position of the sympathetic ganglia.

In agreement with their findings, we identified the presence of multiple GFP$^+$ cells within the DRGs (Fig. 6.8 C and E) but also along the medial pathway (Fig. 6.8 C). In order to identify the position of the GFP$^+$ labelled cells within the nerve projections, we labelled glial cells through the immunodetection of the transcription factor Sox10.

Early expression of *mitfa* (15 hpf-24 hpf) in the embryo corresponds to undifferentiated but partially restricted cells chromatoglioblast lineages. However, its later expression (3-5 dpf) is restricted to the melanocytic lineage and at 5 dpf is expressed in differentiated/pigmented melanophores.

The presence of unpigmented *mitfa:gfp* positive cells at 8 dpf in the medial pathway, suggests the existence of partially undifferentiated cells restricted to the chromatioglia lineage. Furthermore these *mitfa:gfp* positive cells are not exclusive of the dorsal medial pathway as are also found in the ventral medial pathway. Supporting the hypothesis of a second niche of APSC in the ventral medial pathway of the posterior trunk.

Close up of the dorsal (Fig. 6.9) and ventral (Fig. 6.10) regions revealed that in the 6 DRGs there was a mean of 3.8 GFP^+ per DRG (Fig. 6.9 C), from which 1 GFP^+ positive cell per every pair of DRGs in one segment, is double labelled with sox10 (Fig. 6.9 F, G, K and P). We also found that most GFP^+ in the DRG (m=3.1cell/ DRG) are double labelled with Hu (Fig. 6.9 C, E, F, H, M-P). Only in one out of 6 DRGs we found a GFP^+ $sox10^-$ cell (Fig. 6.9 F-H, K, L, O and P).

In contrast, in the ventral region, all GFP^+ cells along the (Fig. 6.10 C, E, M and N) nerve projections (n=4 nerves) were double labelled with sox10 (4 cells/ nerve). While all sympathetic neurons, similar to sensory neurons in the DRGs, were double GFP^+ Hu^+ labelled (Fig. 6.10 C, E, H and I).

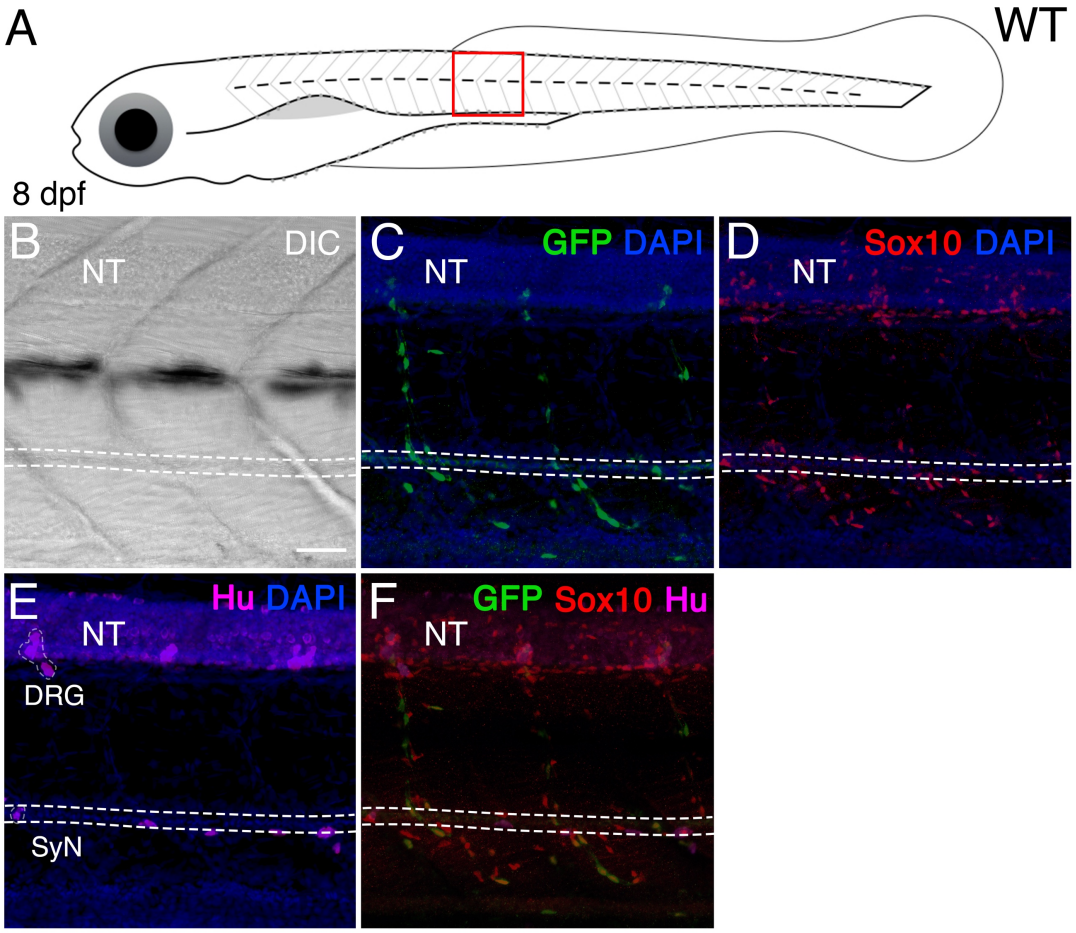

Figure 6.8 *mitfa:EGFP* labelled cells are found along the medial pathway. Scheme shows imaged area (red box) of 8 dpf *Tg(mitfa:gfp)* larvae (A). DIC of medial pathway (B) shows neural tube (NT) and borders of dorsal aorta (DA) lined byt white dashed line. Stack projection of medial pathway counterstained with DAPI (C-E) and immunodetection of GFP (C), Sox10 (D) and Hu (E). Dorsal root ganglia (DRGs) and sympathetic neurons (SyN). Overlapping of GFP, Sox10 and Hu (F). Scale bar = 40 µm (B-F).

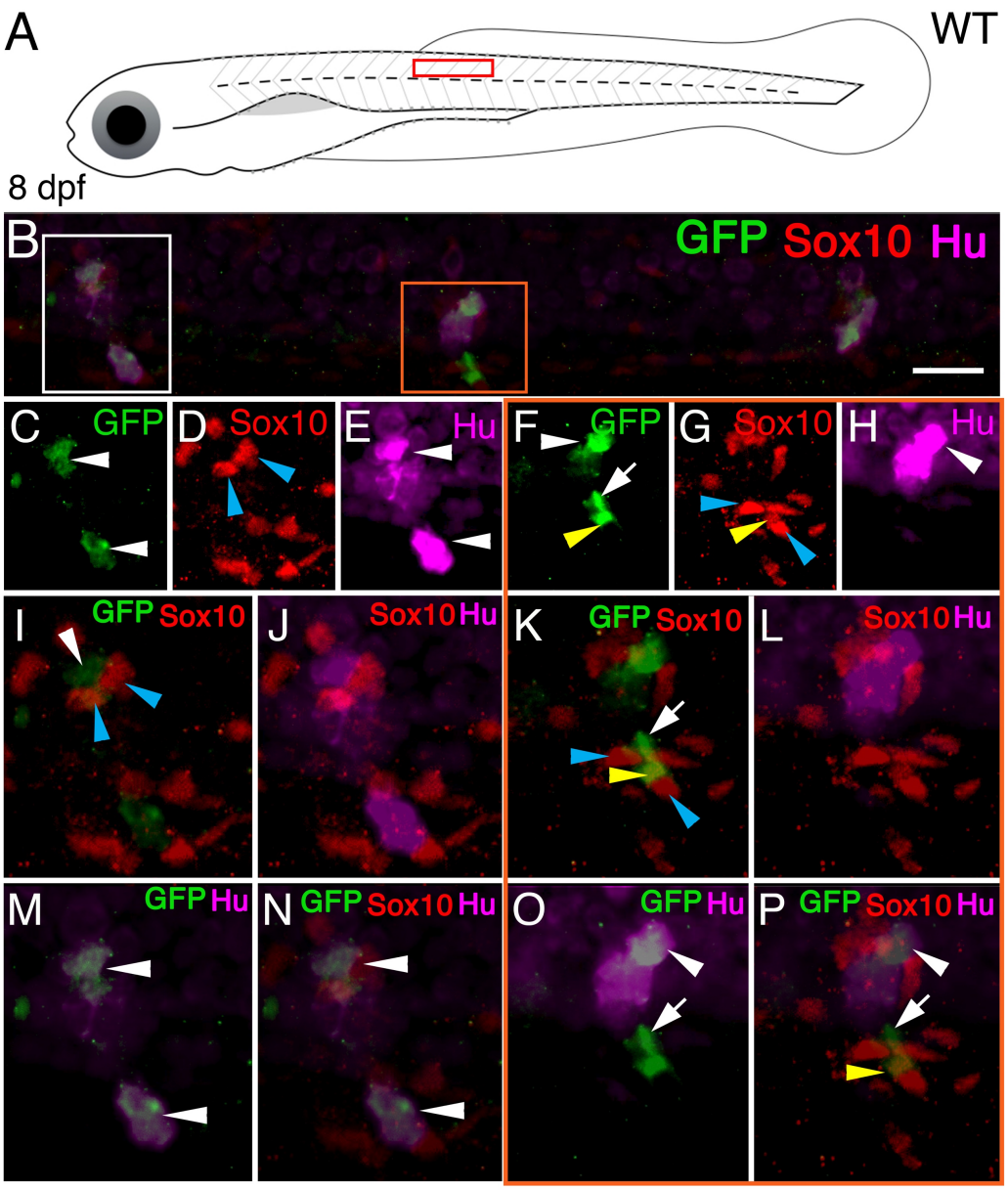

Figure 6.9 *mitfa:EGFP*; Sox10 labelled cells are localised in the dorsal medial pathway. Scheme shows close up of imaged area (red box) of 8 dpf *Tg(mitfa:gfp)* (GFP) larvae (A). Single focal plane of dorsal medial pathway shows immunodetection of GFP, Hu and Sox10 in DRGs (B). Magnified areas in white box in panel B is shown in C-E, I, J, M and N, while magnification of area in orange box in panel B is shown in F-H, K, L, O and P. GFP (C and F), Sox10 (D and G) and Hu (E and H) labelled cells. GFP-only labelled cell (white arrow; F, K, O and P). Sox10 labelled cells (blue arrows; D and I and G and K) close to GFP labelled cells (white arrowheads C and I; white arrow and yellow arrowhead F and K). Doubled GFP (yellow arrowhead; F, K and P) and Sox10 (yellow arrowhead; G, K and P) labelled cell. Double GFP labelled cells (white arrowhead; C, F and M-P) and Hu (white arrowheads; E, H, M-P) labelled cells (red arrowheads; M-P). Scale bar = 40 μm.

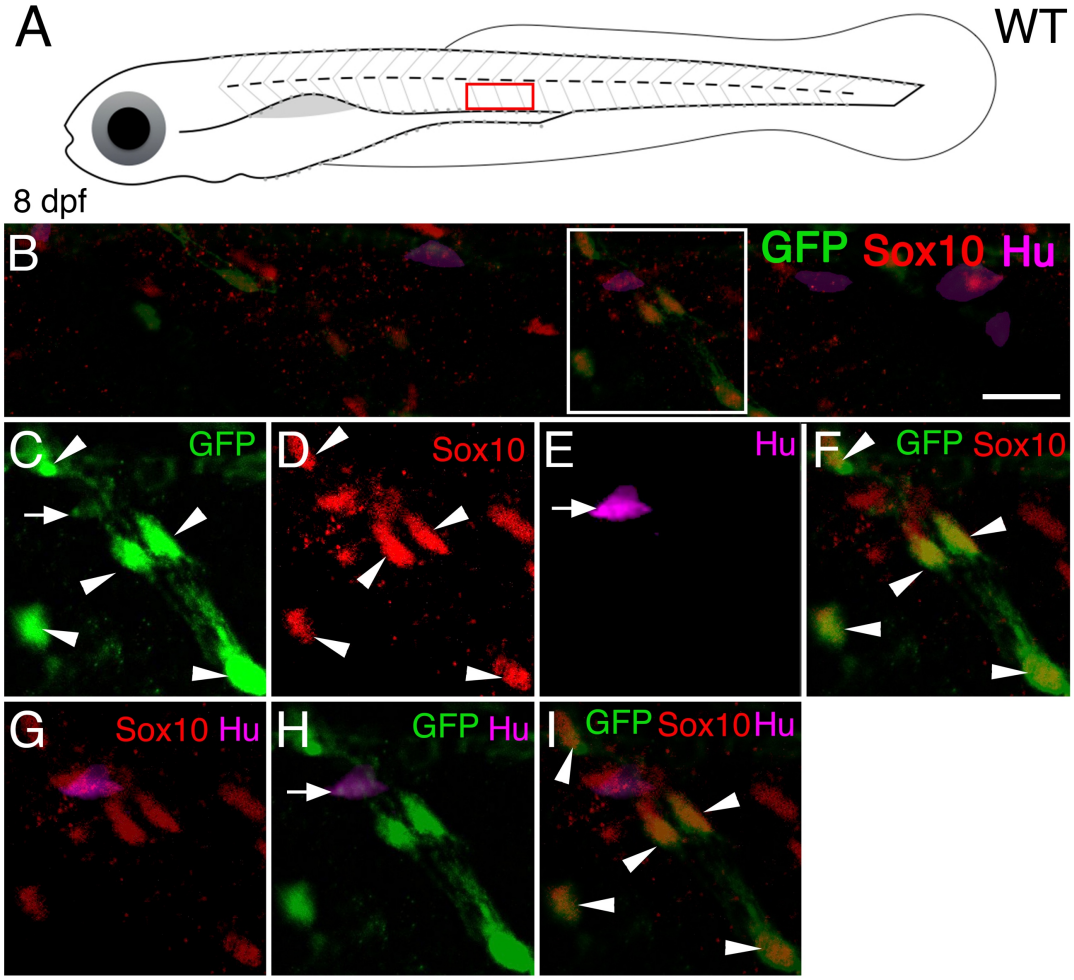

Figure 6.10 *mitfa:EGFP*; Sox10 labelled cells in the ventral medial pathway. Scheme shows imaged (red box) area of 8 dpf *Tg(mitfa:gfp)* larvae (A). Single focal plane of ventral medial pathway shows immunodetection of GFP, Hu and Sox10 (B). Magnification of area in white box in panel B in C-I. Double GFP (white arrowheads; C, F and I) and Sox10 (white arrowheads; D, F and I) labelled cells. Double GFP (white arrow; C and H) and Hu (white arrow; E and H). Scale bar = 40 μm.

		No. Cells	
	Marker	**DRG**	**VN**
Single labelled	**GFP**	0.2	0
	Sox10	5.7	3
	Hu	0	1
Double labelled	**GFP/Sox10**	0.5	4
	Sox10/Hu	0	0
	GFP/Hu	3.2	1
Triple labelled	**GFP/Sox10/Hu**	0	0
Total per marker	**GFP**	3.8	4
	Sox10	6.3	3
	Hu	3.2	1

Table 8 .1 Average number of labelled cells for the immune detection of GFP Sox10 Hu in WT larvae at 8 dpf.

In both regions, double GFP^+ Hu^+ labelled cells were not expected. However, it could be easily explained as residual GFP form recently differentiated neurons. In contrast, all double *mitfa:gfp* and Sox10 labelled cells, suggest a bipotent pigment progenitor (Petratou et al. 2018). An interesting feature to look into is the lower number of double GFP^+ $Sox10^+$ labelled cells in the dorsal compared to the ventral regions. It is possible that in *pde* mutants the number of double labelled cells is reduced.

In mice and chick embryos, developing nerve projections that emerge from the DRG, have been suggested as a niche containing Schwann (glia) cell precursors that are the cellular origin that contribute to skin pigmentation (Adameyko et al. 2009). Thus, our observations agree with a model in which in zebrafish, either multipotent progenitor are associated with the peripheral nerve projections.

Our revised model proposes that in addition to the niche of APSC in the DRGs (Fig. 6.11 A), a second niche of APSC associated with the ventral nerve projections (Fig. 6.11 B). is regulated (indirectly) through *ednraa* signalling from the dorsal aorta (Fig. 6.11 C). The results of our pharmacological treatments, suggest that Notch signalling is required to keep APSC inactive (Fig. 6.11 D). In contrast, disruption of *ednraa* (Fig. 6.11 E) in *pde* mutants, allows the premature activation (Fig. 6.11 F) and differentiation of ventral APSC resulting in the *pde* phenotype (Fig. 6.11 G), a process that requires Wnt and Notch signalling (Fig. 6.11 H).

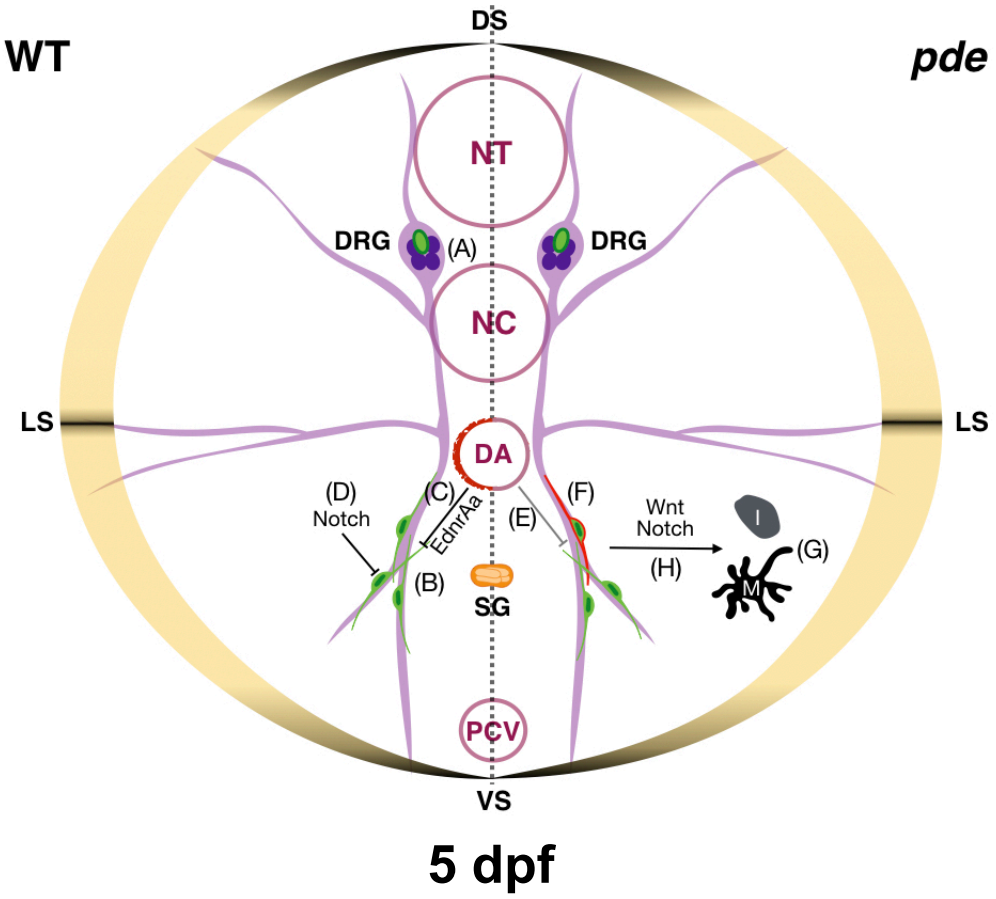

Figure 6.11 New model for the mechanism of the *parade* phenotype. Scheme shows, a transversal view of a 5 dpf zebrafish anterior trunk. The left segment represents the WT context and the right the *pde* background. In the most outer layer we indicate the position of the dorsal, lateral and ventral stripes (DS, LS, and VS correspondingly). In the middle indicated are the neural tube (NT), notochord (NC), dorsal aorta (DA) and posterior cardinal vein (PCV). Dorsal root ganglia (DRG) and nerve projections are shown in purple while Sympathetic ganglia (SG) are shown in orange. APSC at the DRGs (round green cells; A), APSC in the ventral region (elongated green cells; B). EdnrAa signaling in the DA results in the production of signals(s) (shown in red), that influences the neighbouring APSC (DA; C) keeps APSC inactive together with Notch signalling (D). In *pde* mutants, disrupted signalling from EdnrAa (E) allows APSCs to activate (red contoured elongated green cell; F) and prematurely differentiate into ectopic pigment cells (G), a process that requires Wnt and Notch signalling (H).

We found in the *pde* mutant an exciting opportunity for *in vivo* study of the biology adult pigment stem cells

REFERENCES

Adameyko, I. et al., 2009. Schwann Cell Precursors from Nerve Innervation Are a Cellular Origin of Melanocytes in Skin. *Cell*, 139(2), pp.366–379.

Adameyko, I. & Lallemend, F., 2010. Glial versus melanocyte cell fate choice: Schwann cell precursors as a cellular origin of melanocytes. *Cellular and Molecular Life Sciences*, 67(18), pp.3037–3055.

Alunni, A. et al., 2013. Notch3 signaling gates cell cycle entry and limits neural stem cell amplification in the adult pallium. *Development*, 140(16), pp.3335–3347.

van Amerongen, R., 2012. Alternative Wnt pathways and receptors. *Cold Spring Harbor perspectives in biology*, 4(10).

An, M., Luo, R. & Henion, P.D., 2002. Differentiation and maturation of zebrafish dorsal root and sympathetic ganglion neurons. *The Journal of comparative neurology*, 446(3), pp.267–275.

Aranda, P.S., LaJoie, D.M. & Jorcyk, C.L., 2012. NIH Public Access. *NAtional Institutes Health*, 33(2), pp.366–369.

Arduini, B.L., Bosse, K.M. & Henion, P.D., 2009. Genetic ablation of neural crest cell diversification. *Development (Cambridge, England)*, 136(12), pp.1987–94.

Bagnara, J.T. et al., 1979. Common origin of pigment cells. *Science (New York, N.Y.)*, 203(4379), pp.410–5.

Bagnara, J.T., Fernandez, P.J. & Fujii, R., 2007. On the blue coloration of vertebrates. *Pigment Cell Research*, 20(1), pp.14–26.

Bagnara, J.T. & Matsumoto, J., 2006. Comparative Anatomy and Physiology of Pigment Cells in Nonmammalian Tissues. In *The Pigmentary System*. Oxford, UK: Blackwell Publishing Ltd, pp. 11–59.

Barker, N. et al., 2007. Identification of stem cells in small intestine and colon by marker gene Lgr5. *Nature*, 449(7165), pp.1003–1007.

Basak, O. et al., 2012. Neurogenic Subventricular Zone Stem/Progenitor Cells Are Notch1-Dependent in Their Active But Not Quiescent State. *Journal of Neuroscience*, 32(16), pp.5654–5666.

Baynash, A.G. et al., 1994. Interaction of endothelin-3 with endothelin-B receptor is essential for development of epidermal melanocytes and enteric neurons. *Cell*, 79(7), pp.1277–1285.

Behrens, J. et al., 1998. Functional interaction of an axin homolog, conductin, with beta-catenin, APC, and GSK3beta. *Science (New York, N.Y.)*, 280(5363), pp.596–9.

Behrens, J. et al., 1996. Functional interaction of β-catenin with the transcription factor LEF-1. *Nature*, 382(6592), pp.638–642.

Bertrand, J.Y. et al., 2010. Haematopoietic stem cells derive directly from aortic endothelium during development. *Nature*, 464(7285), pp.108–111.

Besmer, P. et al., 1993. The kit-ligand (steel factor) and its receptor c-kit/W: pleiotropic roles in gametogenesis and melanogenesis. *Development (Cambridge, England). Supplement*, pp.125–37.

Bond, A.M., Ming, G.L. & Song, H., 2015. Adult Mammalian Neural Stem Cells and Neurogenesis: Five Decades Later. *Cell Stem Cell*, 17(4), pp.385–395.

Bourgeois, C. et al., 1997. Endothelin-1 and ETA Receptor Expression in Vascular Smooth Muscle Cells from Human Placenta: A New ETA Receptor Messenger Ribonucleic Acid Is Generated by Alternative Splicing of Exon 3. *The Journal of Clinical Endocrinology & Metabolism*, 82(9), pp.3116–3123.

Bozkulak, E.C. & Weinmaster, G., 2009. Selective Use of ADAM10 and ADAM17 in Activation of Notch1 Signaling. *Molecular and Cellular Biology*, 29(21), pp.5679–5695.

Braasch, I., Volff, J.N. & Schartl, M., 2009. The endothelin system: Evolution of vertebrate-specific ligand-receptor interactions by three rounds of genome duplication. *Molecular Biology and Evolution*, 26(4), pp.783–799.

Brenner, M. & Hearing, V.J., 2008. The protective role of melanin against UV damage in human skin. *Photochemistry and photobiology*, 84(3), pp.539–49.

Britsch, S. et al., 2001. The transcription factor Sox10 is a key regulator of peripheral glial development. *Genes & development*, 15(1), pp.66–78.

Bronner-Fraser, M. & Fraser, S., 1989. Developmental potential of avian trunk neural crest cells in situ. *Neuron*, 3(6), pp.755–766.

Bronner-Fraser, M. & Fraser, S.E., 1991. *Cell lineage analysis of the avian neural crest*,

Bronner-Fraser, M. & Fraser, S.E., 1988. Cell lineage analysis reveals multipotency of some avian neural crest cells. *Nature*, 335(6186), pp.161–164.

Bronner, M.E. & LeDouarin, N.M., 2012. Development and evolution of the neural crest: An overview. *Developmental Biology*, 366(1), pp.2–9.

Brons, I.G.M. et al., 2007. Derivation of pluripotent epiblast stem cells from mammalian embryos. *Nature*, 448(7150), pp.191–195.

Budi, E.H., Patterson, L.B. & Parichy, D.M., 2008. Embryonic requirements for ErbB signaling in neural crest development and adult pigment pattern formation. *Development (Cambridge, England)*, 135(15), pp.2603–2614.

Budi, E.H., Patterson, L.B. & Parichy, D.M., 2011. Post-embryonic nerve-associated precursors to adult pigment cells: Genetic requirements and dynamics of morphogenesis and differentiation. *PLoS Genetics*, 7(5).

Cacioppo, J.A. et al., 2015. Generation and characterization of an endothelin-2 iCre mouse. *Genesis*, 53(2), pp.245–256.

Callow, M.G. et al., 2011. Ubiquitin ligase RNF146 regulates tankyrase and Axin to promote Wnt signaling. *PloS one*, 6(7), p.e22595.

Carney, T.J. et al., 2006. A direct role for Sox10 in specification of neural crest-derived sensory neurons. *Development*, 133(23), pp.4619–4630.

Chang, I. et al., 2013. Endothelin-2 deficiency causes growth retardation, hypothermia, and emphysema in mice. *Journal of Clinical Investigation*, 123(6), pp.2643–2653.

Clouthier, D.E. et al., 1998. Cranial and cardiac neural crest defects in endothelin-A receptor-deficient mice. *Development (Cambridge, England)*, 125(5), pp.813–24.

Collazo, A., Bronner-Fraser, M. & Fraser, S.E., 1993. Vital dye labelling of Xenopus laevis trunk neural crest reveals multipotency and novel pathways of migration. *Development (Cambridge, England)*, 118(2), pp.363–76.

Coller, H.A., 2011. The Essence of Quiescence HHS Public Access. *Science*, 334(6059), pp.1074–1075.

Crane, G.M., Jeffery, E. & Morrison, S.J., 2017. Adult haematopoietic stem cell niches.

Curran, K. et al., 2010. Interplay between Foxd3 and Mitf regulates cell fate plasticity in the zebrafish neural crest. *Developmental Biology*, 344(1), pp.107–118.

Davenport, A.P. & Kuc, R.E., 2000. Cellular expression of isoforms of endothelin-converting enzyme-1 (ECE-1c, ECE-1b and ECE-1a) and endothelin-converting enzyme-2. *Journal of cardiovascular pharmacology*, 36(5 Suppl 1), pp.S12-4.

Davenport et al., 1998. Endothelin-converting enzyme in human tissues. *The Histochemical Journal*, 30(5), pp.359–374.

Delfino-Machín, M. et al., 2017. Sox10 contributes to the balance of fate choice in dorsal root ganglion progenitors. *PLoS ONE*, 12(3), pp.1–29.

Donovan, P.J. & de Miguel, M.P., 2003. Turning germ cells into stem cells. *Current opinion in genetics & development*, 13(5), pp.463–471.

Dooley, C.M. et al., 2013. On the embryonic origin of adult melanophores: the role of ErbB and Kit signalling in establishing melanophore stem cells in zebrafish. *Development (Cambridge, England)*, 140(5), pp.1003–13.

Le Douarin, N. & Kalcheim, C., 1999. *The neural crest*, Cambridge University Press.

Le Douarin, N.M., Calloni, G.W. & Dupin, E., 2008. The stem cells of the neural crest. *Cell Cycle*, 7(8), pp.1013–1019.

Le Douarin, N.M. & Teillet, M.A., 1973. The migration of neural crest cells to the wall

of the digestive tract in avian embryo. *Journal of embryology and experimental morphology*, 30(1), pp.31–48.

Driever, W. et al., 1996. A genetic screen for mutations affecting embryogenesis in zebrafish. *Development (Cambridge, England)*, 123, pp.37–46.

Dutton, K.A. et al., 2001. Zebrafish colourless encodes sox10 and specifies non-ectomesenchymal neural crest fates. *Development (Cambridge, England)*, 128(21), pp.4113–25.

Dzierzak, E. & Speck, N. a, 2008. Of lineage and legacy: the development of mammalian hematopoietic stem cells. *Nature Immunology*, 9(2), pp.129–136.

Engler, A. et al., 2018. Notch2 Signaling Maintains NSC Quiescence in the Murine Ventricular-Subventricular Zone. *Cell Reports*, 22(4), pp.992–1002.

van Es, J.H. et al., 2005. Notch/γ-secretase inhibition turns proliferative cells in intestinal crypts and adenomas into goblet cells. *Nature*, 435(7044), pp.959–963.

Evans, M.J. & Kaufman, M.H., 1981. Establishment in culture of pluripotential cells from mouse embryos. *Nature*, 292(5819), pp.154–6.

Evans, N.J. & Walker, J.W., 2008. Endothelin receptor dimers evaluated by FRET, ligand binding, and calcium mobilization. *Biophysical journal*, 95(1), pp.483–92.

Fadeev, A. et al., 2016. Zebrafish Leucocyte tyrosine kinase controls iridophore establishment, proliferation and survival. *Pigment Cell and Melanoma Research*, 29(3), pp.284–296.

Fauq, A.H. et al., 2007. A multigram chemical synthesis of the γ-secretase inhibitor LY411575 and its diastereoisomers. *Bioorganic and Medicinal Chemistry Letters*, 17(22), pp.6392–6395.

Fevr, T. et al., 2007. Wnt/ -Catenin Is Essential for Intestinal Homeostasis and Maintenance of Intestinal Stem Cells. *Molecular and Cellular Biology*, 27(21), pp.7551–7559.

Flanagan, D.J. et al., 2018. Wnt signalling in gastrointestinal epithelial stem cells. *Genes*, 9(4).

Fradkin, L.G., Dura, J.-M. & Noordermeer, J.N., 2010. Ryks: new partners for Wnts in the developing and regenerating nervous system. *Trends in Neurosciences*, 33(2), pp.84–92.

Frank, E. & Sanes, J.R., 1991. Lineage of neurons and glia in chick dorsal root ganglia: analysis in vivo with a recombinant retrovirus. *Development (Cambridge, England)*, 111(4), pp.895–908.

Garcia, R.J. et al., 2008. Endothelin 3 induces skin pigmentation in a keratin-driven inducible mouse model. *Journal of Investigative Dermatology*, 128(1), pp.131–

142.
Geling, A. et al., 2002. A γ-secretase inhibitor blocks Notch signaling in vivo and causes a severe neurogenic phenotype in zebrafish. *EMBO Reports*, 3(7), pp.688–694.
Giaid, A. et al., 1991. Topographical localisation of endothelin mRNA and peptide immunoreactivity in neurones of the human brain. *Histochemistry*, 95(3), pp.303–14.
Gouedard, L. et al., 2000. Engagement of bone morphogenetic protein type IB receptor and Smad1 signaling by anti-Mullerian hormone and its type II receptor. *Journal of Biological Chemistry*, 275(36), pp.27973–8.
Greenhill, E.R. et al., 2011. An iterative genetic and dynamical modelling approach identifies novel features of the gene regulatory network underlying melanocyte development M. C. Mullins, ed. *PLoS Genetics*, 7(9), p.e1002265.
Grotek, B., Wehner, D. & Weidinger, G., 2013. Notch signaling coordinates cellular proliferation with differentiation during zebrafish fin regeneration. *Development*, 140(7), pp.1412–1423.
Le Guellec, D., Morvan-Dubois, G. & Sire, J.-Y., 2004. Skin development in bony fish with particular emphasis on collagen deposition in the dermis of the zebrafish (Danio rerio). *The International journal of developmental biology*, 48(2–3), pp.217–31.
Hans, S. et al., 2009. Temporally-controlled site-specific recombination in zebrafish. *PloS one*, 4(2), p.e4640.
Harland, S.P. et al., 1995. Characterization of endothelin receptors in human brain cortex, gliomas, and meningiomas. *Journal of cardiovascular pharmacology*, 26 Suppl 3, pp.S408-11.
Hashido, K. et al., 1992. Truncation of N-terminal extracellular or C-terminal intracellular domains of human ETA receptor abrogated the binding activity to ET-1. *Biochemical and biophysical research communications*, 187(3), pp.1241–8.
Hawkes, J.W., 1974. The structure of fish skin. I. General organization. *Cell and tissue research*, 149(2), pp.147–58.
Haynes, W.G. & Webb, D.J., 1994. Contribution of endogenous generation of endothelin-1 to basal vascular tone. *Lancet (London, England)*, 344(8926), pp.852–4.
Hearing, V.J., 2011. Milestones in Melanocytes/Melanogenesis. *Journal of Investigative Dermatology*, 131(E1), p.E1.
Henion, P.D. & Weston, J.A., 1997. Timing and pattern of cell fate restrictions in the

neural crest lineage. *Development (Cambridge, England)*, 124(21), pp.4351–9.

Hickey, K.A. et al., 1985. Characterization of a coronary vasoconstrictor produced by cultured endothelial cells. *The American journal of physiology*, 248(5 Pt 1), pp.C550-6.

Hirata, M. et al., 2003. Pigment cell organization in the hypodermis of zebrafish. *Developmental Dynamics*, 227(4), pp.497–503.

Hosoda, K. et al., 1994. Targeted and natural (piebald-lethal) mutations of endothelin-B receptor gene produce megacolon associated with spotted coat color in mice. *Cell*, 79(7), pp.1267–1276.

Howe, K. et al., 2013. The zebrafish reference genome sequence and its relationship to the human genome.

Huang, S.M.A. et al., 2009. Tankyrase inhibition stabilizes axin and antagonizes Wnt signalling. *Nature*, 461(7264), pp.614–620.

Huggins, J.P., Pelton, J.T. & Miller, R.C., 1993. The structure and specificity of endothelin receptors: Their importance in physiology and medicine. *Pharmacology & Therapeutics*, 59(1), pp.55–123.

Hultman, K.A. et al., 2009. Defects in ErbB-dependent establishment of adult melanocyte stem cells reveal independent origins for embryonic and regeneration melanocytes. *PLoS Genetics*, 5(7).

Imayoshi, I. et al., 2010. Essential Roles of Notch Signaling in Maintenance of Neural Stem Cells in Developing and Adult Brains. *Journal of Neuroscience*, 30(9), pp.3489–3498.

Inman, G.J. et al., 2002. SB-431542 Is a Potent and Specific Inhibitor of Transforming Growth Factor-beta Superfamily Type I Activin Receptor-Like Kinase (ALK) Receptors ALK4, ALK5, and ALK7. *Molecular Pharmacology*, 62(1), pp.65–74.

Iyengar, S., Kasheta, M. & Ceol, C.J., 2015. Poised Regeneration of Zebrafish Melanocytes Involves Direct Differentiation and Concurrent Replenishment of Tissue-Resident Progenitor Cells. *Developmental Cell*, 33(6), pp.631–643.

Janes, R.W., Peapus, D.H. & Wallace, B.A., 1994. The crystal structure of human endothelin. *Nature structural biology*, 1(5), pp.311–9.

JF, W., 1999. Larvae in fish develop- ment and evolution. In E. In: Hall BK, Wake MH, ed. *The origin and evolution of larval forms.* New York: Academic Press., p. p 109–158.

Jing, L. et al., 2009. Wnt Signals Organize Synaptic Prepattern and Axon Guidance through the Zebrafish unplugged/MuSK Receptor. *Neuron*, 61(5), pp.721–733.

Kabiri, Z. et al., 2018. Wnt signaling suppresses MAPK-driven proliferation of intestinal stem cells. *Journal of Clinical Investigation*, 128(9), pp.3806–3812.

Kasai, A. & Oshima, N., 2006. Light-sensitive Motile Iridophores and Visual Pigments in the Neon Tetra, Paracheirodon innesi. *Zoological Science*, 23(9), pp.815–819.

Kelsh, R.N., 2004. Genetics and evolution of pigment patterns in fish. *Pigment cell research / sponsored by the European Society for Pigment Cell Research and the International Pigment Cell Society*, 17(4), pp.326–36.

Kelsh, R.N. et al., 2009. Stripes and belly-spots—A review of pigment cell morphogenesis in vertebrates. *Seminars in Cell & Developmental Biology*, 20(1), pp.90–104.

Kelsh, R.N. et al., 1996. Zebrafish pigmentation mutations and the processes of neural crest development. *Development (Cambridge, England)*, 123, pp.369–389.

Kelsh, R.N. & Eisen, J.S., 2000. The zebrafish colourless gene regulates development of non-ectomesenchymal neural crest derivatives. *Development (Cambridge, England)*, 127(3), pp.515–25.

Kikuchi, K. et al., 2011. Retinoic acid production by endocardium and epicardium is an injury response essential for zebrafish heart regeneration. *Developmental cell*, 20(3), pp.397–404.

Kimmel, C.B. et al., 1995. Stages of embryonic development of the zebrafish. *Developmental dynamics : an official publication of the American Association of Anatomists*, 203(3), pp.253–310.

Kirschbaum, F., 1975. Studies on the color pattern of the zebra barb, Brachydanio rerio (Cyprinidae, Teleostei). *Wilhelm Roux's Archives of Developmental Biology*, 177(2), pp.129–152.

Ko, C., Meidan, R. & Bridges, P.J., 2012. Why two endothelins and two receptors for ovulation and luteal regulation? *Life Sciences*, 91(13–14), pp.501–506.

Korinek, V. et al., 1998. Depletion of epithelial stem-cell compartments in the small intestine of mice lacking Tcf-4. *Nature Genetics*, 19(4), pp.379–383.

Krauss, J. et al., 2014. Endothelin signalling in iridophore development and stripe pattern formation of zebrafish. *Biology open*, 3(6), pp.503–9.

Krauss, S., Concordet, J.P. & Ingham, P.W., 1993. A functionally conserved homolog of the Drosophila segment polarity gene hh is expressed in tissues with polarizing activity in zebrafish embryos. *Cell*, 75(7), pp.1431–44.

Kühn, R., Wurst, W. & Wefers, B., 2016. *TALENs Methods and Protocols Methods in Molecular Biology 1338* R. Kühn, ed., New Yotk: Humana Press.

Kuhnert, F. et al., 2004. Essential requirement for Wnt signaling in proliferation of adult small intestine and colon revealed by adenoviral expression of Dickkopf-1. *Proceedings of the National Academy of Sciences*, 101(1), pp.266–271.

Kumano, K. et al., 2008. Both Notch1 and Notch2 contribute to the regulation of melanocyte homeostasis. *Pigment Cell and Melanoma Research*, 21(1), pp.70–78.

Kurihara, H. et al., 1999. Endothelin and neural crest development. *Cellular and molecular biology (Noisy-le-Grand, France)*, 45(5), pp.639–51.

Kurihara, Y. et al., 1994. Elevated blood pressure and craniofacial abnormalities in mice deficient in endothelin-1. *Nature*, 368(6473), pp.703–10.

Kuwaki, T. et al., 2002. Blood pressure of endothelin-3 null (-/-) knockout mice and endothelin A receptor null (-/-) knockout mice under anaesthesia. *Clinical Science*, 103(s2002), p.48S–52S.

Lacroix, L. et al., 2000. Pyrimidine Morpholino Oligonucleotides Form a Stable Triple Helix in the Absence of Magnesium Ions.

Land, M.F., 1972. The physics and biology of animal reflectors. *Progress in Biophysics and Molecular Biology*, 24, pp.75–106.

Lang, M.R. et al., 2009. Basonuclin-2 Requirements for Zebrafish Adult Pigment Pattern Development and Female Fertility G. S. Barsh, ed. *PLoS Genetics*, 5(11), p.e1000744.

Langworthy, M.M. & Appel, B., 2012. Schwann cell myelination requires Dynein function. *Neural Development*, 7(1), p.37.

Lawson, N.D. & Weinstein, B.M., 2002. In vivo imaging of embryonic vascular development using transgenic zebrafish. *Developmental biology*, 248(2), pp.307–318.

Lee, E.M. et al., 2016. Functional constraints on SoxE proteins in neural crest development: The importance of differential expression for evolution of protein activity. *Developmental Biology*, 418(1), pp.166–178.

Li, Y.-X. et al., 2003. Cardiac neural crest in zebrafish embryos contributes to myocardial cell lineage and early heart function. *Developmental Dynamics*, 226(3), pp.540–550.

Lim, X. et al., 2016. Axin2 marks quiescent hair follicle bulge stem cells that are maintained by autocrine Wnt/β-catenin signaling. *Proceedings of the National Academy of Sciences of the United States of America*, 113(11), pp.E1498-505.

Ling, L., Maguire, J.J. & Davenport, A.P., 2013. Endothelin-2, the forgotten isoform: emerging role in the cardiovascular system, ovarian development, immunology and cancer. *British journal of pharmacology*, 168(2), pp.283–95.

Linney, E. et al., 1999. Transgene Expression in Zebrafish: A Comparison of Retroviral-Vector and DNA-Injection Approaches. *Developmental Biology*, 213(1), pp.207–216.

Lopes, S.S. et al., 2008. Leukocyte tyrosine kinase functions in pigment cell development. *PLoS genetics*, 4(3), p.e1000026.

Lowry, W.E. et al., 2005. Defining the impact of -catenin/Tcf transactivation on epithelial stem cells. *Genes & Development*, 19(13), pp.1596–1611.

Lumsden, A., Sprawson, N. & Graham, A., 1991. Segmental origin and migration of neural crest cells in the hindbrain region of the chick embryo. *Development (Cambridge, England)*, 113(4), pp.1281–91.

Lyons, D.A. et al., 2005. erbb3 and erbb2 are essential for schwann cell migration and myelination in zebrafish. *Current biology : CB*, 15(6), pp.513–24.

Lytle, N.K., Barber, A.G. & Reya, T., 2018. Stem cell fate in cancer growth, progression and therapy resistance. *Nature Reviews Cancer*, p.1.

Ma, Q., Kintner, C. & Anderson, D.J., 1996. Identification of neurogenin, a vertebrate neuronal determination gene. *Cell*, 87(1), pp.43–52.

Mahalwar, P. et al., 2014. Local reorganization of xanthophores fine-tunes and colors the striped pattern of zebrafish. *Science (New York, N.Y.)*, 345(6202), pp.1362–4.

Massagué, J., 2012. TGFβ signalling in context. *Nature Reviews Molecular Cell Biology*, 13(10), pp.616–630.

McMenamin, S.K. et al., 2014. Thyroid hormone-dependent adult pigment cell lineage and pattern in zebrafish. *Science (New York, N.Y.)*, 345(6202), pp.1358–61.

Mcmenamin, S.K. & Parichy, D.M., 2017. *Metamorphosis in Teleosts*,

Meidan, R. & Levy, N., 2007. The ovarian endothelin network: an evolving story. *Trends in endocrinology and metabolism: TEM*, 18(10), pp.379–85.

Mellgren, E.M. & Johnson, S.L., 2004. A requirement for kit in embryonic zebrafish melanocyte differentiation is revealed by melanoblast delay. *Development Genes and Evolution*, 214(10), pp.493–502.

Metral, E. et al., 2018. Keratinocyte stem cells are more resistant to UVA radiation than their direct progeny.

Minami, Y. et al., 2009. Ror-family receptor tyrosine kinases in noncanonical Wnt signaling: Their implications in developmental morphogenesis and human diseases. *Developmental Dynamics*, 239(1), p.NA-NA.

Mirzadeh, Z. et al., 2008. Neural stem cells confer unique pinwheel architecture to the ventricular surface in neurogenic regions of the adult brain. *Cell Stem Cell*, 11(3(3)), pp.265–278.

Miyamoto, Y. et al., 1996. Alternative RNA splicing of the human endothelin-A receptor generates multiple transcripts. *The Biochemical journal*, 313 (Pt 3(Pt 3), pp.795–801.

Mongera, A. et al., 2013. Genetic lineage labeling in zebrafish uncovers novel neural crest contributions to the head, including gill pillar cells. *Development*, 140(4), pp.916–925.

Moore, K. a & Lemischka, I.R., 2006. Stem cells and their niches. *Science (New York, N.Y.)*, 311(5769), pp.1880–1885.

Morrison, S.J., Shah, N.M. & Anderson, D.J., 1997. Regulatory mechanisms in stem cell biology. *Cell*, 88(3), pp.287–98.

Muncan, V. et al., 2006. Rapid loss of intestinal crypts upon conditional deletion of the Wnt/Tcf-4 target gene c-Myc. *Molecular and cellular biology*, 26(22), pp.8418–26.

Nair, S. et al., 2007. Requirements for Endothelin type-A receptors and Endothelin-1 signaling in the facial ectoderm for the patterning of skeletogenic neural crest cells in zebrafish. *Development*, 134(2), pp.335–45.

Nishimura, E.K. et al., 2002. Dominant role of the niche in melanocyte stem-cell fate determination. *Nature*, 416(6883), pp.854–860.

Nishimura, E.K. et al., 2010. Key Roles for Transforming Growth Factor β in Melanocyte Stem Cell Maintenance. *Cell Stem Cell*, 6(2), pp.130–140.

Obika, M. & Fukuzawa, T., 1993. Cytoskeletal architecture of dermal chromatophores of the freshwater teleost Oryzias latipes. *Pigment cell research*, 6(6), pp.417–22.

Odenthal, J. et al., 1996. Mutations affecting xanthophore pigmentation in the zebrafish, Danio rerio. *Development (Cambridge, England)*, 123, pp.391–8.

Oh, S.P. et al., 2000. Activin receptor-like kinase 1 modulates transforming growth factor-beta 1 signaling in the regulation of angiogenesis. *Proceedings of the National Academy of Sciences of the United States of America*, 97(6), pp.2626–31.

Opdecamp, K. et al., 1997. Melanocyte development in vivo and in neural crest cell cultures: crucial dependence on the Mitf basic-helix-loop-helix-zipper transcription factor. *Development (Cambridge, England)*, 124(12), pp.2377–86.

Orry, A.J.W. & Wallace, B.A., 2000. Modeling and Docking the Endothelin G-Protein-Coupled Receptor. *Biophysical Journal*, 79(6), pp.3083–3094.

Ota, S. et al., 2014. Multiple genome modifications by the CRISPR/Cas9 system in zebrafish. *Genes to Cells*, 19(7), pp.555–564.

Pándy-Szekeres, G. et al., 2018. GPCRdb in 2018: adding GPCR structure models and ligands. *Nucleic acids research*, 46(D1), pp.D440–D446.

Parichy et al., 2000. Mutational analysis of endothelin receptor b1 (rose) during neural crest and pigment pattern development in the zebrafish Danio rerio.

Developmental biology, 227(2), pp.294–306.

Parichy, D.M. et al., 2009. Normal table of postembryonic zebrafish development: Staging by externally visible anatomy of the living fish. *Developmental Dynamics*, 238(12), pp.2975–3015.

Parichy, D.M. & Spiewak, J.E., 2015. Origins of adult pigmentation: Diversity in pigment stem cell lineages and implications for pattern evolution. *Pigment Cell and Melanoma Research*, 28(1), pp.31–50.

Peradziryi, H., Tolwinski, N.S. & Borchers, A., 2012. The many roles of PTK7: A versatile regulator of cell–cell communication. *Archives of Biochemistry and Biophysics*, 524(1), pp.71–76.

Petratou, K. et al., 2018. A systems biology approach uncovers the core gene regulatory network governing iridophore fate choice from the neural crest. D. M. Parichy, ed. *PLoS genetics*, 14(10), p.e1007402.

Phinney, D.G. & Prockop, D.J., 2007. Concise review: mesenchymal stem/multipotent stromal cells: the state of transdifferentiation and modes of tissue repair--current views. *Stem cells (Dayton, Ohio)*, 25(11), pp.2896–902.

Piek, E. et al., 1999. Expression of transforming-growth-factor (TGF)-beta receptors and Smad proteins in glioblastoma cell lines with distinct responses to TGF-beta1. *International journal of cancer*, 80(5), pp.756–63.

Plumpton, C. et al., 1993. Characterization of endothelin isoforms in human heart: endothelin-2 demonstrated. *Journal of cardiovascular pharmacology*, 22 Suppl 8, pp.S26-8.

Prendergast, A. & Raible, D.W., 2014. Neural Crest Cells and Peripheral Nervous System Development. *Neural Crest Cells*, pp.255–286.

Qiu, J.M., Roberts, S.A. & Potten, C.S., 1994. Cell migration in the small and large bowel shows a strong circadian rhythm. *Epithelial cell biology*, 3(4), pp.137–48.

Quigley, I.K. & Parichy, D.M., 2002. Pigment pattern formation in zebrafish: a model for developmental genetics and the evolution of form. *Microscopy research and technique*, 58(6), pp.442–55.

Rabbani, P. et al., 2011. Coordinated activation of wnt in epithelial and melanocyte stem cells initiates pigmented hair regeneration. *Cell*, 145(6), pp.941–955.

Raible, D.W. et al., 1992. Segregation and early dispersal of neural crest cells in the embryonic zebrafish. *Developmental Dynamics*, 195(1), pp.29–42.

Raible, D.W. & Eisen, J.S., 1994. Restriction of neural crest cell fate in the trunk of the embryonic zebrafish. *Development (Cambridge, England)*, 120(3), pp.495–503.

Raible, D.W. & Ungos, J.M., 2006. Specification of Sensory Neuron Cell Fate from

the Neural Crest. In *Neural Crest Induction and Differentiation*. Boston, MA: Springer US, pp. 170–180.

Rakers, S. et al., 2010. 'Fish matters': the relevance of fish skin biology to investigative dermatology. *Experimental Dermatology*, 19(4), pp.313–324.

Ransom, D.G. et al., 1996. Characterization of zebrafish mutants with defects in embryonic hematopoiesis. *Development (Cambridge, England)*, 123, pp.311–319.

Regard, J.B., Sato, I.T. & Coughlin, S.R., 2008. Anatomical Profiling of G Protein-Coupled Receptor Expression. *Cell*, 135(3), pp.561–571.

Reid, K. et al., 1996. Multiple roles for endothelin in melanocyte development: regulation of progenitor number and stimulation of differentiation. *Development (Cambridge, England)*, 122(12), pp.3911–3919.

Reissmann, E. et al., 2001. The orphan receptor ALK7 and the Activin receptor ALK4 mediate signaling by Nodal proteins during vertebrate development. *Genes & Development*, 15(15), pp.2010–2022.

Reya, T. et al., 2001. Stem cells, cancer, and cancer stem cells. *Nature*, 414(6859), pp.105–11. Available at: http://dx.doi.org/10.1038/35102167 [Accessed May 22, 2013].

Robertson, J.K. et al., 2014. Targeting the Wnt pathway in zebrafish as a screening method to identify novel therapeutic compounds. *Experimental Biology and Medicine*, 239(2), pp.169–176.

Rodrigues, F.S.L.M. et al., 2012. A novel transgenic line using the Cre-lox system to allow permanent lineage-labeling of the zebrafish neural crest. *Genesis*, 50(10), pp.750–757.

Rossi, A. et al., 2015. Genetic compensation induced by deleterious mutations but not gene knockdowns. *Nature*, 524(7564), pp.230–233.

Rossi, G.P. et al., 1995. Expression of the Endothelin-Converting Enzyme Gene in Human Tissues. *Biochemical and Biophysical Research Communications*, 211(1), pp.249–253.

Ruest, L.-B.L.-B. et al., 2004. Endothelin-A receptor-dependent and -independent signaling pathways in establishing mandibular identity. *Development*, 131(18), pp.4413–4423.

Schartl, M. et al., 2016. What is a vertebrate pigment cell? *Pigment Cell & Melanoma Research*, 29(1), pp.8–14.

Schilling, T.F. & Kimmel, C.B., 1994. Segment and cell type lineage restrictions during pharyngeal arch development in the zebrafish embryo. *Development (Cambridge, England)*, 120(3), pp.483–94.

Schofield, R., 1978. The relationship between the spleen colony-forming cell and the haemopoietic stem cell. *Blood cells*, 4(1–2), pp.7–25.

Serbedzija, G.N., Fraser, S.E. & Bronner-Fraser, M., 1990. Pathways of trunk neural crest cell migration in the mouse embryo as revealed by vital dye labelling. *Development (Cambridge, England)*, 108(4), pp.605–12.

Shin, M.K. et al., 1999. The temporal requirement for endothelin receptor-B signalling during neural crest development. *Nature*, 402(6761), pp.496–501.

Shinmi, O. et al., 1993. Endothelin-2-converting enzyme from human renal adenocarcinoma cells is a phosphoramidon-sensitive, membrane-bound metalloprotease. *Journal of cardiovascular pharmacology*, 22 Suppl 8, pp.S61-4.

Singh, A.P. et al., 2016. Pigment Cell Progenitors in Zebrafish Remain Multipotent through Metamorphosis. *Developmental Cell*, 38(3), pp.316–330.

Singh, A.P., Schach, U. & Nüsslein-Volhard, C., 2014. Proliferation, dispersal and patterned aggregation of iridophores in the skin prefigure striped colouration of zebrafish. *Nature cell biology*, 16(6), pp.607–14.

Smollich, M. et al., 2007. On the role of endothelin-converting enzyme-1 (ECE-1) and neprilysin in human breast cancer. *Breast Cancer Research and Treatment*, 106(3), pp.361–369.

Snell, R.S., 1963. A study of the melanocytes and melanin in a healing deep wound. *Journal of anatomy*, 97(Pt 2), pp.243–53.

Spink, K.E., Polakis, P. & Weis, W.I., 2000. Structural basis of the Axin–adenomatous polyposis coli interaction. *The EMBO Journal*, 19(10), pp.2270–2279.

Stemple', D.L. et al., 1992. Isolation of a stem cell for neurons and glia from the mammalian neural crest. *Cell*, 71(6), pp.973–985.

Stoller, J.Z. & Epstein, J.A., 2005. Cardiac neural crest. *Seminars in Cell & Developmental Biology*, 16(6), pp.704–715.

De Strooper, B., 2003. Aph-1, Pen-2, and Nicastrin with Presenilin generate an active gamma-Secretase complex. *Neuron*, 38(1), pp.9–12.

Sun, Z. et al., 2006. Activation and roles of ALK4/ALK7-mediated maternal TGFβ signals in zebrafish embryo. *Biochemical and Biophysical Research Communications*, 345(2), pp.694–703.

Suzuki, T. & Chiba, S., 2005. Notch Signaling in Hematopoietic Stem Cells. *International Journal of Hematology*, 82(4), pp.285–294.

Takahashi, K. & Yamanaka, S., 2006. Induction of pluripotent stem cells from mouse embryonic and adult fibroblast cultures by defined factors. *Cell*, 126(4), pp.663–76.

Takeo, M. et al., 2016. EdnrB Governs Regenerative Response of Melanocyte Stem Cells by Crosstalk with Wnt Signaling. *Cell Reports*, 15.

Takeshi, S., Masashi, Y. & Tomoh, M., 1992. Molecular characterization of endothelin receptors. *Trends in Pharmacological Sciences*, 13, pp.103–108.

Tanese, K. et al., 2010. Endothelin-2 is upregulated in basal cell carcinoma under control of Hedgehog signaling pathway. *Biochemical and Biophysical Research Communications*, 391(1), pp.486–491.

Tesar, P.J. et al., 2007. New cell lines from mouse epiblast share defining features with human embryonic stem cells. *Nature*, 448(7150), pp.196–202.

Than-Trong, E. et al., 2018. Neural stem cell quiescence and stemness are molecularly distinct outputs of the Notch3 signalling cascade in the vertebrate adult brain. *Development*, 145(10), p.dev161034.

Theveneau, E. & Mayor, R., 2012. Neural crest migration: interplay between chemorepellents, chemoattractants, contact inhibition, epithelial-mesenchymal transition, and collective cell migration. *Wiley Interdisciplinary Reviews: Developmental Biology*, 1(3), pp.435–445.

Thisse, C. & Thisse, B., 2005. High throughput expression analysis of ZF-models consortium clones. ZFIN direct data submission.

Thomas, A.J. & Erickson, C.A., 2009. FOXD3 regulates the lineage switch between neural crest-derived glial cells and pigment cells by repressing MITF through a non-canonical mechanism. *Development*, 136(11), pp.1849–1858.

Till, J.E. & McCulloch, E.A., 1961. A direct measurement of the radiation sensitivity of normal mouse bone marrow cells. *Radiation research*, 14, pp.213–22.

Till, J.E. & McCulloch, E.A., 1980. Hemopoietic stem cell differentiation. *Biochimica et biophysica acta*, 605(4), pp.431–59.

Tryon, R.C., Higdon, C.W. & Johnson, S.L., 2011. Lineage Relationship of Direct-Developing Melanocytes and Melanocyte Stem Cells in the Zebrafish B. Riley, ed. *PLoS ONE*, 6(6), p.e21010.

Tu, S. & Johnson, S.L., 2011. Fate restriction in the growing and regenerating zebrafish fin. *Developmental cell*, 20(5), pp.725–32.

Tumbar, T., Guasch, G. & Greco, V., 2014. Defining the Epithelial Stem Cell. , 359(January), pp.359–364.

Valenta, T. et al., 2016. Wnt Ligands Secreted by Subepithelial Mesenchymal Cells Are Essential for the Survival of Intestinal Stem Cells and Gut Homeostasis. *Cell Reports*, 15(5), pp.911–918.

Vibert, L. et al., 2017. An ongoing role for Wnt signaling in differentiating melanocytes in vivo. *Pigment Cell and Melanoma Research*, 30(2), pp.219–232.

Vries, R.G.J., Huch, M. & Clevers, H., 2010. Stem cells and cancer of the stomach and intestine Stochastic model Gastrointestinal cancer Stem cell WNT.

Wang, W. Der et al., 2011. Tfap2a and Foxd3 regulate early steps in the development of the neural crest progenitor population. *Developmental Biology*, 360(1), pp.173–185.

Weston, J.A., 1991. Sequential segregation and fate of developmentally restricted intermediate cell populations in the neural crest lineage. *Current topics in developmental biology*, 25, pp.133–53.

Whyteside, A.R., Turner, A.J. & Lambert, D.W., 2014. Endothelin-Converting Enzyme-1 (ECE-1) is post- transcriptionally regulated by alternative polyadenylation. *PLoS ONE*, 9(1).

Wixon, J., 2000. Danio rerio, the zebrafish. *Yeast*, 17(3), pp.225–231.

Wolfe, M.S. & Haass, C., 2001. The Role of presenilins in gamma-secretase activity. *The Journal of biological chemistry*, 276(8), pp.5413–6.

Woodhoo, A. & Sommer, L., 2008. Development of the Schwann cell lineage: From the neural crest to the myelinated nerve. *Glia*, 56(14), pp.1481–1490.

Yan, Y.-L. et al., 1998. Mutant Rescue by BAC Clone Injection in Zebrafish. *Genomics*, 50(2), pp.287–289.

Yanagisawa, H. et al., 2000. Disruption of ECE-1 and ECE-2 reveals a role for endothelin-converting enzyme-2 in murine cardiac development. *The Journal of clinical investigation*, 105(10), pp.1373–82.

Yanagisawa, H., Yanagisawa, M., et al., 1998. Dual genetic pathways of endothelin-mediated intercellular signaling revealed by targeted disruption of endothelin converting enzyme-1 gene. *Development (Cambridge, England)*, 125(5), pp.825–836.

Yanagisawa, H., Hammer, R.E., et al., 1998. Role of Endothelin-1/Endothelin-A receptor-mediated signaling pathway in the aortic arch patterning in mice. *The Journal of clinical investigation*, 102(1), pp.22–33.

Yanagisawa, M. et al., 1988. A novel potent vasoconstrictor peptide produced by vascular endothelial cells. *Nature*, 332(6163), pp.411–415.

Yang, C.-T. & Johnson, S.L., 2006. Small molecule-induced ablation and subsequent regeneration of larval zebrafish melanocytes. *Development*, 133(18), pp.3563–3573.

Yorimitsu, K. et al., 1992. Effect of phosphoramidon on big endothelin-2 conversion into endothelin-2 in human renal adenocarcinoma (ACHN) cells. Analysis of endothelin-2 biosynthetic pathway. *FEBS letters*, 314(3), pp.395–8.

Zhang, Y.F. et al., 1998. Truncated human endothelin receptor A produced by

alternative splicing and its expression in melanoma. *British journal of cancer*, 78(9), pp.1141–6.

Ziegler, I., 2003. The pteridine pathway in zebrafish: regulation and specification during the determination of neural crest cell-fate. *Pigment cell research*, 16(3), pp.172–82.

APPENDICES

A. Primers

Name	Sequence 5'-3'
T1732	ATTGGGGGGAAATACAGGGG
T1733	CCAGTAGTAGTCCAGTAAAACAG
T1734	TGCATCACTTGAGGAACTTG
T1735	GAATGATAGGCTGTCACATCAG
edn2Fw1	CTACCCTATGTGTCCTGCAGC
edn2Fw2	AGCATCTAGCAATCCACCTGC
edn2Rv2	ACATTCCTCATGGCTACATCTTGC
T1455	TGGCAAATGTAGATTCCAGC
T1363	CCAAATGGAACCTTTCTTCTGG
ednraaFw1	CTGCAATGGCCATTACGACG
ednraaFwWT	GCCACTGGTGGATTATGTCTGATAA
ednraaFwMT	TGATGTAAATGAGGTCTCCAAGAGC
ednrabFw2	ATGATGACCTCATCCTGCCTG
ednrabFwWT	TGACCTCTGACCTGCGTGCG
ednrabFwMT	TGACCTCTGACCTGCGCGAC
ednrabRv2	TTCCTCATGCTCCTGTTCTGG
ednrabRv2.1	CCGTTCCTCATGCTCCTGTTCTGG
ednraaRv2	TGATGTAAATGAGGTCTCCAAGAGC
actb2Fw1	CGAGCTGTCTTCCCATCCA
actb2Rv2	CCAACGTAGCTGTCTTTCTG
EF1aFw1	CTGGAGGCCAGCTCAAACAT
EF1aRw1	ATCAAGAAGAGTAGTACCGCTAGCATTAC

Table 7.1 Primer sequences.

B. Antibodies

Company	Antibody	Dilution
Millipore	Mouse α -TH	1:200
Santa Cruz	Rabbit α -Sox10	1:100
ThermoFisher Scientific	Mouse α -Hu	1:400
	Mouse α -PH3	1:500
	Rabbit α -PH3	1:500
	Mouse α -GFP	1:750
	Rabbit α -GFP	1:750
	Chicken α -GFP	1:500
	Goat α -Mouse AF488	1:750
	Goat α -Mouse AF546	1:750
	Goat α -Rabbit AF488	1:750
	Goat α - Rabbit AF546	1:750
	Goat α -Chicken AF 633	1:500

Table 7.2 Antibody working concentrations.

C. Chemical inhibitors

Name	Target	Company	Cat No
AG1478	MAPK/ERK	Sigma	175178-82-2
PD158780	MEK1/2		7063
XAV939	Wnt		X3004-5MG
Dorsomorphin	BMP		P5499-5MG
SB-431542	TGF-b		S4317
DAPT	Notch		D5942
LY411575	Notch		SML0506

Table 7.3 Chemacal inhibitor details.